Streaming induced by high amplitude acoustic pulses and its implications

Starritt, Hazel Catherine

Award date:
1990

Awarding institution:
University of Bath

STREAMING INDUCED BY HIGH AMPLITUDE ACOUSTIC PULSES AND ITS IMPLICATIONS

Submitted by Hazel Catherine Starritt

for the degree of PhD

of the University of Bath

1990

ProQuest LLC
789 East Eisenhower Parkway
P.O. Box 1346
Ann Arbor, MI 48106-1346

CONTENTS

ABSTRACT

This thesis investigates some aspects of the nonlinear propagation of high amplitude ultrasound in the context of medical diagnostic applications. Nonlinear propagation occurring in focused diagnostic fields is shown to enhance acoustic streaming in water due to the increased absorption of the high frequency components in the distorted wave. The results of an extensive experimental investigation of streaming in water are presented. The streaming velocities were measured using the technique of hot film anemometry and were found to vary with total acoustic power, pulse repetition frequency, pulse duration and pulse pressure amplitude. The velocity in a high amplitude beam was shown to be enhanced typically by a factor of 5 compared with that in a low amplitude beam of the same acoustic power. Measurements of acoustic parameters were made for comparison. The results showed that in a nonlinear field absorption is enhanced in the region immediately on the transducer side of the focus and this region is shown to act as the "source pump" for the stream.

The maximum streaming velocities generated by commercial ultrasonic equipment were measured in the fields of pulsed Doppler units, with maximum velocities generated in the fields of scanned imaging beams being an order of magnitude lower. Streams in stationary beams were observed to become established in time periods which are short compared with the "dwell time" of the transducer at a single location in clinical use.

The implications of acoustic streaming and the forces associated with it are discussed in the context of the current diagnostic usage of ultrasound. In particular, obstetric applications are considered where the fetus is scanned through a low loss fluid path in which nonlinear propagation and acoustic streaming may occur.

CHAPTER 1

INTRODUCTION

1.1 BACKGROUND

In the present day ultrasound is used extensively in medicine for a range of diverse applications in both diagnosis and therapy. Safety must be an important consideration for each application since exposure parameters vary and organs differ in their susceptibility to damage. It is clear that ultrasound can produce damage in tissue, and indeed it is used not only as a diagnostic tool but also as a surgical tool. In the first case there is the assumption that no biological change is induced during the ultrasonic exposure, while in the second case destruction of tissue is deliberate. In therapeutic applications ultrasound is believed to interact with human tissue in a beneficial way which can promote healing. For diagnostic ultrasound therefore the question must be asked at what level of exposure can it be assumed that no adverse effects will result from the interaction of the acoustic beam with tissue.

The question of safety is of particular concern for ultrasonic examination of the fetus. A large proportion of the population is now exposed to ultrasound by such an examination and it is likely that this will increase as more general practitioners purchase diagnostic ultrasound units and carry out obstetric scanning. The fetus is known to be susceptible to thermal damage (see Section 2.4.2) but its susceptibility to nonthermal mechanisms is not well understood, although it is thought that a developing organism may be at greater risk than mature tissue.

An extensive bioeffects literature reflects the considerable work which

has been undertaken in the field of ultrasound safety, only a small proportion of which has addressed the question of the safety of pulsed diagnostic ultrasound. There are two approaches to the question of ultrasound safety; the mechanistic approach and the empirical approach. In the first case a physical mechanism is identified by which ultrasound potentially may modify or damage a biological system, for example by heating it. In the empirical approach there is an attempt to produce experimentally an observable change in a biological system which correlates in some way with changes in exposure parameters. Only after this has occurred is the mechanism producing the effect considered. Acoustic bioeffects are normally classed as "thermal", "cavitational" or "other".

The aim of this thesis has been to investigate some aspects of the interactions of high amplitude ultrasound, particularly diagnostic pulses, with tissue. For high amplitude pulsed beams nonlinear propagation can result in the enhancement of mechanisms such as heating and acoustic streaming. The experimental work presented here is an investigation of acoustic streaming, principally in pulsed diagnostic fields. Extensive measurements of the acoustic streams generated in water are described, for focused diagnostic ultrasound beams employing microsecond pulses and pulse repetition rates of the order of a kHz. It is shown that streaming is enhanced in high amplitude fields in which nonlinear distortion occurs and for this reason the acoustic fields employed are quantified in considerable detail in terms of shock formation and energy loss. The forces associated with acoustic streaming provide a nonthermal, noncavitational mechanism of interaction between pulsed acoustic ultrasound beams and biological systems.

1.2 APPLICATIONS OF MEDICAL ULTRASOUND

In view of the wide range of applications of ultrasound in medicine only a brief review of the various clinical uses is presented here.

Diagnostic ultrasound

The greatest single use of diagnostic ultrasound is in obstetric scanning where the main applications include estimation of fetal maturity, placental localisation and the diagnosis of early and multiple pregnancies (NCRP, 1983). In the diagnosis of an early pregnancy the fetus is scanned through a full bladder which forms a low loss acoustic path. Increasingly Doppler ultrasound is used in obstetric medicine in order to assess utero-placental blood flow, and currently in experimental studies to investigate flow in fetal arteries (such as the fetal aorta, carotids and mesenteric artery). Continuous wave fetal monitors are low output power devices which remain on the maternal abdomen for many hours in order to monitor the fetal heart rate during labour.

Amongst other applications ultrasonic imaging is also of value in the diagnosis of renal tumours and cysts, thyroid cysts, liver disease and breast tumours. In ophthamology ultrasound is used in the diagnosis of ocular pathology, for example retinal detachments and tumours, and in the measurement of axial length and intraocular biometry.

Doppler ultrasound is currently a rapidly developing field due to the development of colour flow mapping. Its obstetric applications have already been discussed and two other main areas of use are in cardiology and in peripheral vascular assessment. Cardiology applications include evaluation of mitral stenosis and determination of the left ventricular stroke output. Applications to the peripheral vascular system include detection of arterial

occlusions and stenoses particularly in carotid arteries and in the arteries of the leg, detection of deep venous thromboses and measurement of blood volume flow.

Therapeutic ultrasound

Ultrasound is widely used in physiotherapy for the treatment of soft tissue injuries such as torn and strained ligaments and tendons, torn muscles and local oedema among many others. Dyson and Brooks (1982) reported that ultrasonic treatment during the first two weeks following an injury accelerated the rate of bone repair. In a 1985 survey of the use of ultrasound in physiotherapy (reported by ter Haar, 1987) it was found that 20% of all treatments in National Health Service hospital physiotherapy departments and 54% of treatments performed by private practitioners involved ultrasound.

Extracorporeal shockwave lithotripsy is becoming widely used in the treatment of renal calculi (Chaussy *et al.*, 1986). In one type of equipment shock waves are generated by a spark discharge at one focus of an eliptical reflector. The patient is positioned so that the stone is located at the second focus and shock waves are directed onto the stone until it disintegrates. The positioning may be determined by ultrasonic or x-ray imaging.

Other therapeutic applications of ultrasound, less relevant to this thesis, include the use of ultrasonic descalers which are widely used in dentistry (Walmsley, 1988). In this case a small scraping tool, the tip of which is water cooled, is driven at frequencies in the range 18 - 42 kHz and held in contact with the tooth surface. Ultrasound is also used in the treatment of Menières disease, a disorder of the inner ear. This treatment involves the use of a narrow ultrasound beam of high intensity to destroy the sensory

neuroepithelium of the cristae and maculae in the labyrinth of the ear. Ultrasonic beam surgery has been used in the eye (Kelman, 1964, Burgess *et al.*, 1986) and in neurosurgery and experimental work is in progress using highly focused ultrasonic beams which has resulted in the production of lesions in the liver of rats *in vivo* (ter Haar *et al.*, 1989). Ultrasound induced hyperthermia has been investigated as an adjunct to chemotherapy or radiotherapy in the treatment of cancer (for example Lele, 1987).

1.3 EXPOSURE PARAMETERS FOR DIAGNOSTIC APPLICATIONS

In subsequent chapters a distinction is made between diagnostic acoustic beams and therapy beams and also between imaging (scanned) beams and Doppler (stationary) beams. The main features of each of these beams are reviewed here since they have implications for the generation of acoustic streaming. Acoustic parameters quoted below are taken from recent measurement surveys of the output powers and intensities of commercial ultrasound units (Duck and Martin, 1986, Duck *et al.*, 1987).

Stationary beams such as M-mode or pulsed Doppler beams are generally weakly focused and narrow, with focal beam widths of the order of a few millimetres. In contrast the scanned beam from a linear array for example, may have a scan width of many centimetres, while in the perpendicular direction the beam width is equivalent to that of a stationary beam. Focusing of an array is achieved electronically in one direction and physically, by the use of a lens for example, in the other direction. Much of the experimental work described in Chapter 6 of this thesis was carried out using a single element transducer although measurements were also made on some commercial systems including a number of linear array scanheads operating in imaging mode.

Typical acoustic parameters for imaging and Doppler systems are

presented below.

Acoustic parameter	Range
Frequency (MHz)	2.0 - 7.5
Pulse length (μs)	0.15 - 1.85
Pulse repetition frequency (kHz)	0.5 - 4.0
Scan repetition frequency (Hz)	1.4 - 56.2
Beam diameter (mm)	0.5 - 3.0
Focal gain	2.2 - 10.8
Maximum positive pressure (MPa)	7.4
Maximum negative pressure (MPa)	-3.4
Maximum I_{spta}, scanning (mW cm^{-2})	40

Table 1.1 Diagnostic imaging equipment; survey of acoustic parameters. (I_{spta} is the spatial peak temporal average intensity.)

Acoustic parameter	Range
Frequency (MHz)	2.0 - 5.0
Pulse length (μs)	0.3 - 11.3
Pulse repetition frequency (kHz)	1.6 - 18.9
Peak positive pressure (MPa)	0.1 - 5.4
Peak negative pressure (MPa)	-0.1 - -2.6
I_{spta} (mW cm^{-2})	36.0 - 825
I_{sppa} (W cm^{-2})	0.2 - 310

Table 1.2 Pulsed Doppler systems; survey of acoustic parameters. (I_{sppa} is the spatial peak pulse average intensity.)

Table 1.1 shows data taken from a survey by Duck and Martin (1986) of 23 diagnostic imaging transducers and Table 1.2 gives equivalent results from a

survey of commercial pulsed Doppler equipment (Duck *et al.*, 1987).

It can be seen that while the peak positive pressures are comparable in imaging and Doppler beams, the spatial peak temporal average intensity in a Doppler beam is generally considerably greater than in a scanned beam due to the higher pulse repetition frequencies employed in Doppler equipment.

The intensities used in physiotherapy units range from 0.1 to 3.0 W cm^{-2} (spatial average temporal average) at frequencies between 0.75 and 3 MHz (ter Haar, 1987). Beams are generally unfocused and commonly generated by a transducer 2.5 cm in diameter. Exposures can be pulsed in bursts of 1 or 2 ms duration at mark–to–space ratios of 1:1, 1:2 or 1:7 typically. Peak positive pressures generated at maximum intensities are of the order of 0.5 MPa (DHSS, 1977, Starritt *et al.*, 1986). These are significantly lower than the pressures encountered in diagnostic applications.

Measurements of acoustic parameters in lithotripsy fields have been reported by Coleman and Saunders (1989). Peak positive pressures of over 100 MPa and peak negative pressures of 10 MPa were measured in water. Acoustic pulse lengths were typically in the range 0.3 to 10 μs while pulse repetition frequencies were much lower than those used in diagnostic ultrasound, at maximum 100 Hz.

1.4 MODERN TRENDS IN DIAGNOSTIC ULTRASOUND

Comparison of a range of acoustic parameters surveyed in 1985 and again after 1987 showed a general increase in the measured values (Duck, 1989). For example the mean spatial peak temporal average intensity for pulsed Doppler equipment was observed to have increased by a factor of almost 5. Modern equipment also shows a trend towards the use of higher frequency ultrasound beams which are more tightly focused. As a

result the degree of nonlinear distortion, which is dependent on system parameters such as intensity, frequency and focal gain will be increased, although this increase is balanced to some extent by an increased attenuation at the higher frequencies employed.

Recent developments in obstetric ultrasound include transvaginal scanning which enables the transducer to be located much closer to the fetus than is possible in skin contact scanning. This has allowed ultrasound to be used increasingly in investigations of infertility and of early fetal development, particularly during the first trimester. Pulsed Doppler and colour flow modes of operation are also available with vaginal transducers and applications include flow assessment on the uterine and fetal arteries. Measurement of blood flow in the neonatal brain is also possible using modern Doppler equipment.

It is clear that the question of adverse effects on the fetus resulting from ultrasound exposure needs to be reassessed in this situation and this is discussed further in Chapter 7.

1.5 THE BIOEFFECTS LITERATURE

There is a large body of literature relating to acoustic bioeffects which may be subdivided in a number of ways. The most important division, for this thesis, is between those papers reporting effects due to continuous wave ultrasound and those investigating effects in pulsed ultrasound fields. In fact very few studies have been reported in pulsed diagnostic type fields in comparison with the large number relating to continuous wave exposures. Reviews of bioeffects compiled by Williams (1983), Repacholi *et al.*, (1987) and Wells (1987) have grouped results according to the organ or organism affected. A further classification can be made according to the mechanism of interaction between the acoustic beam and the biological system, although

it is not always clear what mechanism is responsible for an observed effect and the chance of more than one mechanism occurring under given experimental conditions may exist. Most of the work to date has concentrated on mechanisms involving heating and cavitation.

Some reports, particularly earlier ones, may be criticised for not quoting the exposure conditions fully or for the use of inadequate controls. Even where no such criticism can be levelled at a report of positive bioeffects it has sometimes been impossible for other workers to reproduce the effect. This can be a particular problem when effects result from a cavitational mechanism.

A brief review of recent literature involving pulsed ultrasound is given below. One area in which a nonthermal mechanism is believed to operate and in which acoustic streaming or the forces associated with streaming may be important, is in modifying the plasma membrane of a cell. Dinno *et al.* (1989) argued (perhaps erroneously) that cellular changes induced by low intensities of therapeutic ultrasound were primarily non-thermal in nature and appeared to be associated with changes in the permeability of the cell membrane and in the transport of ions and molecules across it. If therapeutic beams can modify the membrane of a cell in this way then the concern is that diagnostic beams used in obstetric scanning may adversely affect cell development. This is of most significance when considering the exposure of a developing embryo where differentiation of cells is occurring; particular care in the use of ultrasound during the first eight weeks of embryonic development is recommended. In addition it is reported that prolonged changes in membrane permeability, particularly to calcium ions, could effect late pre-natal and post-natal development. Dyson (1985) suggested that the forces involved in acoustic streaming could produce changes in the membrane of a cell.

Siegel *et al.* (1979) reported a reduction in cell attachment for a

variety of cultured human cells following 30 seconds exposure to a 2.25 MHz ultrasound beam at a total power of 1.8 mW. They suggested that this result may have been due to modification of the cell membrane. However the possibility of the change being induced as a result of thermal effects was not eliminated. Modification of the erythrocyte membrane was reported by Pinamonti *et al.* (1982) following pulsed exposure of whole blood using an 8 MHz ultrasound beam. Ultrasound was delivered in short pulses, 0.5 μs in duration, at a pulse repetition frequency of 0.74 kHz. The total acoustic power was 0.4 mW and the spatial average pulse average intensity was 56 mW cm^{-2}.

An experimental arrangement allowing nonthermal interactions of ultrasound with early embryonic tissue to be studied was described by Barnett *et al.* (1990). This system was employed to investigate pulsed exposures to whole rat embryos *in vitro* using exposure conditions similar to those used in pulsed Doppler applications and the authors conclude that high pulse average intensity ultrasound had a minimal effect on the developing embryo provided that a temperature increase is avoided.

1.6 EPIDEMIOLOGY

The ultimate test of ultrasound safety is its effect on the human population. To date no epidemiological study has produced evidence of any adverse effect resulting from exposure to diagnostic ultrasound (Ziskin and Petitti, 1988). However it cannot therefore be assumed that no such effect exists. A number of problems surround the design of retrospective epidemiological surveys. One problem is that factors other than ultrasonic exposure may affect the outcome. For example if birthweight following *in utero* exposure is considered, it is possible that infants exposed to ultrasound may already have been at a higher risk of being growth retarded, which

resulted in them receiving the exposure. Lack of detailed clinical information makes it difficult in retrospect to find a suitably matched, unexposed control population which would permit direct comparison of the results. Indeed ultrasound scanning during pregnancy is now so widespread that is is difficult to find a suitable unexposed population for any clinical trial. Information which would permit the ultrasonic exposure to be quantified is generally not available.

A retrospective study does not nececessarily provide information relevant to the current use of ultrasound. In the past, ultrasonic exposure of the fetus has tended to occur after the gestational period associated with organogenesis and this has decreased the risk of fetal abnormalities. However interest in the study of early fetal development using ultrasound is increasing. The highest intensities currently seen are associated with pulsed Doppler transducers but to date no epidemiological study concentrating on this application has been reported.

Even with large population studies it is difficult to identify a small increase in the rate of a commonly occurring event and it is possible therefore that small changes in neurological function affecting long term development and behaviour may not be detected (Ziskin and Petitti, 1988).

1.7 CONTENT OF THE THESIS

In outline the content of the thesis is as follows. This chapter has formed an introduction to the use of ultrasound in medicine and the exposure parameters associated with diagnostic applications in particular. The bioeffects literature has been briefly reviewed although no attempt was made to present a full systematic survey since the emphasis throughout is on bioeffects occurring in diagnostic beams. Chapter 2 considers the thermal interaction of ultrasound with tissue and discusses the absorption of

ultrasound which is also very relevant to acoustic streaming. Mechanical interactions of ultrasound such as cavitational effects, acoustic microstreaming and shock formation, are discussed in Chapter 3. Chapter 4 is divided into two parts, the first of which discusses theoretically nonlinear propagation and shock formation. The second part presents standard theory for acoustic streaming in a liquid medium. Experimental work carried out to investigate acoustic streaming in water for a variety of acoustic and physical parameters is then described in the following two chapters. Chapter 5 details the experimental procedures and equipment employed while the results are presented in Chapter 6. Chapter 7 discusses the conclusions and implications of this work and contains some suggestions for future work. In addition there are three appendices, the first of which contains a definition of derived acoustic parameters frequently used in this thesis. Appendix 2 contains a calculation of the degree of enhancement of attenuation coefficient which might be expected to occur for a sawtooth wave propagating in water, amniotic fluid and soft tissue. Finally, Appendix 3 contains three published papers containing some of the material presented in this thesis.

CHAPTER 2

THERMAL EFFECTS OF ULTRASOUND

2.1 INTRODUCTION

This chapter discusses the physical mechanism which is generally considered to be the most significant in current bioeffects literature, that of the thermal interaction of ultrasound with tissue. The following chapters deal with other potential mechanisms.

There is a large body of literature concerned with the effects of ultrasonically produced heating on biological systems. This is almost entirely concerned with therapeutic or surgical ultrasound, using either continuous wave exposures at levels typical of physiotherapy use, or highly focused, high level exposures typically of those used to purposely destroy tissue (as a possible means of cancer therapy for example). The discussion in this chapter excludes the situation in which ultrasound is used deliberately to cause tissue ablation.

Ultrasonic absorption is the underlying mechanism which causes not only thermal effects but also acoustic streaming which is described in later chapters. Much of the material in the following section on absorption is therefore also relevant to studies of streaming.

2.2 ABSORPTION OF ULTRASOUND

As an ultrasonic wave propagates through an absorbing medium some energy associated with the wave is converted into heat and this results in an increase in the temperature of the medium. Loss of energy from the beam

may occur as a result both of absorption and of scattering and the combined effect produces attenuation of the beam. An early study by Pauli and Schwan (1971) investigated losses in homogenated liver and found that the contribution to attenuation due to scattering was no more than 30%. More recent work (Parker, 1983) has shown that in the low megahertz range the scattering component in soft tissue accounts only for about 10% to 15% of the total attenuation. Thus attenuation is dominated by the absorption component. For water and homogenous solutions of simple chemical compounds containing no scatterers, attenuation is wholly due to absorption. Cells however cause scattering of ultrasound as well as absorption.

Acoustic energy is converted to heat by viscous loss and relaxation processes. In each case the periodic motion of particles in the wave is opposed by frictional forces in the medium and this results in a time delay between the instantaneous pressure change in the wave and the resultant change in the density of the medium.

If viscosity is the only mechanism involved the absorption coefficient, α, is related to the shear viscosity of the fluid, μ, by (Kinsler *et al.*, 1982)

$$\alpha = \frac{2\mu\omega^2}{3\rho_0 c^3} \qquad 2.1$$

where ρ_0 is the density, c the speed of sound and ω the angular frequency. The proportionality between absorption and (frequency)^2 holds for water in the range 3 MHz to 70 MHz but not for absorption in biological tissues. Experimentally, it has been shown that absorption in tissue has a power dependence in the range 1 to 1.5. The frequency dependence of measured ultrasonic absorption can be characterised by

$$\alpha = af^b \qquad 2.2$$

where a is a constant, f is the acoustic frequency and b is a number usually in the range 1 to 1.5.

In biological systems relaxation processes not viscosity are considered to

determine the absorption (Wells, 1977). A description of a relaxation process may be obtained by considering the ways in which energy can be distributed within a system. A number of different energy-containing compartments may exist, for example energy may be shared as lattice vibrational energy, or translational energy. The various forms of energy are coupled and an increase in one form of energy, due to the passage of an ultrasound wave, may subsequently be redistributed among the other forms. This process occurs over a finite time with the result that energy returned to the wave during a decompressional cycle is out of phase with the travelling wave. Absorption will thus have occurred.

In gases, thermal relaxation occurs associated with the temperature rise accompanying adiabatic compression. In liquids on the other hand structural relaxation is more important. Absorption occurs due to volume changes in the packing density of the liquid 'lattice'.

In simple fluids which have a single relaxation process the absorption at frequency, f, is characterised by the equation (Wells, 1977)

$$\frac{\alpha}{f^2} = \frac{(\alpha\lambda)_{max}}{cf_r} \quad \frac{1}{(1 + f/f_r)^2} \qquad 2.3$$

where $(\alpha\lambda)_{max}$ is the maximum value of absorption per cycle, c is the velocity and f_r is the relaxation frequency.

In practice however neither viscous absorption nor the presence of a single relaxation process explains the observed variation of absorption coefficient with frequency in tissue. The desired result can be predicted by considering a number of relaxations occurring at a range of frequencies as discussed for liver by Pauli and Schwan (1971).

Values of attenuation coefficient and frequency exponent for various biological tissue and fluids are shown in Table 2.1.

Tissue	Temp °C	Freq MHz	α dB cm^{-1}	a	b	Reference
Amniotic fluid	22	2	0.045			Zana and Lang 1974
Blood	25	1	0.021			Carstensen and Schwan 1959
Plasma	25	1	0.069			Carstensen and Schwan 1959
Brain						
whole	25	1	0.6			Kremkau *et al* 1981
white	37	2.2	1.05			"
infant	37	1	0.16			"
Bone						
adult	37	1	22			Fry and Barger 1978
infant	37	1	6.1			"
Liver	*in vivo*	2–5		0.45	1.05	Parker *et al* 1988
Uterus	*in vivo*	3.5		0.89	1	Masaoka *et al* 1987
Brain						
whole	room	1–6		0.58	1.3	Bamber *et al* 1981
white	room	1–6		0.80	1.1	"

Table 2.1 Ultrasound attenuation coefficients for human tissues (data taken from Duck, 1990). The coefficients a and b, are those obtained by assuming the relationship $\alpha = af^b$ and the units of a are dB cm^{-1} MHz^{-b}.

The attenuation of fetal tissue is likely to vary with its stage of development. For example fetal bone is initially uncalcified. In addition the proportion of total body water decreases as a percentage of fetal weight from approximately 94% at 0.1 kg to 70% at 3.5 kg (ICRP, 1975). There are almost no experimental measurements of the attenuation of fetal tissues available in the literature.

2.3 NONLINEARITY AND ABSORPTION

A high amplitude wave undergoes progressive waveform distortion as nonlinear propagation occurs. This results in a wave which contains higher harmonic components of the fundamental frequency (Muir and Carstensen, 1980). These harmonics will in general be absorbed more strongly than the fundamental, resulting in an increased loss of energy from the wave (Duck and Perkins, 1988). In these circumstances the absorption coefficient at the fundamental frequency will underestimate the degree of absorption occurring since absorption in a particular tissue will depend on both the frequency of the ultrasonic beam and on the pulse amplitude. This will lead in turn to an underestimate of the likely temperature rise. In an experiment designed to model a diagnostic type exposure, Bacon and Carstensen (1990) measured heating rates in tissue mimicking gels. When nonlinear distortion was present, heating rates up to three times greater than those obtained in a linear field were observed. Swindell (1985) has predicted enhanced heating ratios in the range 1.5 to 2 near the focus of a 1 MHz beam.

As part of the investigation reported in this thesis a simple calculation was carried out to estimate the effect of nonlinear wave propagation on absorption coefficient. An initially fully distorted 3.5 MHz wave was assumed to propagate through 1 cm of water without regeneration of the harmonics. The effective absorption in the water was calculated, including

the effects of the high frequency components in the wave and the transmitted intensity was then obtained by summing the intensity in each frequency component for the first 20 harmonics. It was found that the resulting effective absorption coefficient was a factor of 10 greater than the absorption coefficient at the fundamental frequency. This is likely to be an underestimate of the true enhancement factor since regeneration of the harmonic components was neglected and the intensity summation was truncated after 20 harmonics. Details of this calculation are given in Appendix 2 and an experimental measurement of enhanced absorption in water is described in Section 6.7. This result is also of importance in the discussion of streaming.

2.4 EFFECTS OF TEMPERATURE ELEVATION IN TISSUE

2.4.1 Background

The biological consequences of temperature elevation have been thoroughly reviewed by Edwards (1986) and Miller and Ziskin (1989) and the main points are summarised here. The temperature of the human body is maintained at a nearly constant level with any variation being limited to a relatively small range between 36 ^{0}C and 40 ^{0}C. Outside this range thermal damage may occur. The sensitivity of different organs to thermal damage varies. The skin for example has a relatively low thermal sensitivity while the fetus *in vivo* is believed to be much more sensitive to thermal damage. Table 2.2 shows how body temperature can vary with the health of an individual. Diurnal variations of 1 ^{0}C have been observed in normal individuals (Mellette, 1951).

State of health	Oral temp. °C	Elevation °C
Normal	37	-
Mild fever	38.5	1.5
High fever	40.5	3.5
Severe fever	42+	5.0

Table 2.2 Temperature elevations associated with fever

Thermal interactions in a biological system produce different effects depending on the resultant temperature elevation, the duration and the thermal susceptibility of the tissues involved. If the temperature of an organ is elevated there are three possible outcomes: there will be no permanent change, or there will be moderate to severe long term effects, or immediate cellular destruction (ablation) will occur. Damage occurs at intermediate temperatures due to changes in rates of fluid flow, molecular diffusion and biochemical reaction rates which can result in irreversible damage, while at approximately 50 °C the protein constituents of enzymes became degraded. For diagnostic ultrasound the first outcome is the most probable.

2.4.2 Thermal interactions with the fetus

When the fetus is small it may be entirely encompassed within the acoustic beam of an imaging transducer. The temperature dissipation mechanism of the fetus is less efficient than that of the mother with the main heat 'sink' being the umbilical blood flow (Creasy and Resnik, 1984). These two factors are likely to result in higher temperatures being reached throughout the fetus than in other soft tissue organs. It has also been shown that the fetus may be particularly susceptible to thermal damage

during organogenesis.

Organogenesis is the period in the development of the fetus during which cells differentiate and acquire their specialised functions within the body (ICRP, 1986). The main period occurs 12 weeks after conception, except for the brain in which cell multiplication begins at 8 weeks and continues until the 16th week. After the last cell division neurons migrate to their appropriate positions to form the cerebral cortex with some development continuing up to the 25th week. Throughout the whole of this period damage to cells may have a significant effect as the neurons of the central nervous systems are not self renewing. The possibility of malformation of the fetus resulting from ultrasound hyperthermia at this stage exists (Smith *et al.*, 1978) and it is also likely that this is the period when the fetus may be most susceptible to damage resulting from nonthermal ultrasonic interactions.

The results of hyperthermia during pregnancy have been studied in two ways. Animal studies have produced evidence of adverse reactions such as embryonic death, reabsorption, abortion or malformation of offspring (Miller and Ziskin, 1989). It was shown that in the preimplantation stage hyperthermia either killed the embryo outright or it survived and developed normally. In the post implantation stage embryo death could occur resulting from widespread cell death due to severe teratogenic damage to a specific organ. Secondly data relating to human pregnancies has been reported for women who have suffered fever during pregnancy by, for example Smith *et al.* (1978). Conclusions from these studies are presented here although there is controversy over whether the effects were due to hyperthermia and not due to the cause of the fever (Warbany, 1986). An embryo is susceptible to thermal damage from 1–2 days post conception to the end of the period of organogensis. Early embryos are more susceptible to lethal damage whereas teratogenic damage is more likely to occur in the early stages of

organogensis with the central nervous system being most at risk. The temperature elevation required to induce abortion in a human pregnancy at the post implantation stage has been shown to be in the range 1.89 to 2.39 °C (Kline *et al.*, 1985). Similar results have been obtained in monkeys (Hendrickx *et al.*, 1979) and rats (Arora *et al.*, 1979). For a given effect the exposure duration shows an inverse logarithmic relationship with temperature elevation above a threshold (Dickson and Calderwood, 1980) such that the longer a given temperature elevation is maintained the greater is the likelihood of damage. A temperature rise of 1 °C however is below the threshold for damage and can be maintained without restriction.

2.4.3 Temperature elavation due to ultrasound

Temperature elevations in animal fetuses caused by ultrasound exposure have been reported by Sikov *et al.* (1984) using prenatal rats and exteriorising the uterus and by Abraham (1989) in the rat fetus. The latter used a 1 MHz resonant frequency transducer, 2 cm in diameter, operated in continuous mode. The exteriorised fetus was located in water at a distance of 9.5 cm from the transducer. Temperature elevations of 6 °C at 2.6 W cm^{-2} and 11 °C at 4.2 W cm^{-2} were measured after 10 minutes exposure in the ultrasound beam. Most investigations of heating, in common with those reported above, have involved the use of unfocused ultrasound beams operating at intensities typical of physiotherapy units. No experimental evidence is available relating to temperature rises produced *in vivo* by diagnostic imaging equipment or pulsed Doppler beams. This highlights the desirability of modelling temperature elevation in tissue for different intensities and beams patterns. A relatively small number of studies have reported the effects of exposing biological systems to pulsed ultrasound at diagnostic levels. Investigations carried out by Barnett (1983)

on chick embryos, and Child *et al.* (1988) involving over 1500 mice embryos, reported no induced developmental abnormalities.

2.4.4 Heating of Bone

When an ultrasound beam impinges on an interface between soft tissue and bone approximately 40% of the energy is reflected from the bone surface while 60% enters the bone where it is rapidly absorbed. This can result in local heating in soft tissue adjacent to bone. When ultrasonic examination of a fetus is carried out the beam will impinge on bony structures overlayed by a small amount of soft tissue, for example the fetal head, and the concern is that local heating may damage the neurons of the developing brain. No measurement of the absorption of fetal bone has been reported in the literature but it is likely to be relatively low and to depend on gestational age. The absorption of infant bone is reported to be less than a third of adult bone (Fry and Barger, 1978). Local heating may be further enhanced if the beam is focused at or near the tissue/bone interface. In addition shear waves may be generated at the bone surface which will be absorbed very rapidly.

2.5 THERMAL MODELS

2.5.1 Background

The previous section stressed the importance of a knowledge of the temperature rise which may be produced by contemporary diagnostic equipment, in order to ensure that unacceptable temperature elevation does

not occur. This is particularly critical for the situation in which an early fetus is being scanned. However it is generally not possible to obtain measurements of temperature elevation produced *in vivo*. Some information may be obtained from animal experiments but there are difficulties in extrapolating from animal data to human situations. An alternative approach is to predict the temperature elevation to be expected using knowledge of the tissue characteristics and ultrasonic beam parameters. The following sections review a number of models which have been proposed to predict temperature elevation. In the past, models applicable to therapy type fields have been developed since it was generally assumed that heating was not an important consideration at diagnostic intensities. Consequently few theoretical models described to date include the effect of nonlinear propagation and the enhanced absorption of high amplitude beams (Duck and Starritt, 1989). Several reviews of acousto-thermal models have been published including that of Lizzi and Ostromogilsky (1987) and Nyborg (1989).

2.5.2 Basic model

When ultrasound of a given frequency passes through tissue or other absorbing media, some of the acoustic power is converted to heat. Neglecting the effects of shear viscocity the time averaged rate of heat production per unit volume, Q, is given by (Nyborg, 1981)

$$Q = \frac{2\alpha\langle p^2\rangle}{\rho_0 c} \qquad 2.4$$

where α is the absorption coefficient at the transmitted frequency, ρ_0 the density, c the velocity of sound in the medium and $\langle p^2\rangle$ the time average value of the square of acoustic pressure. If linear propagation is assumed, Q is related to the intensity, I, in the beam by the equation

$$Q = 2\alpha I \; . \qquad 2.5$$

This heat causes the tissue temperature to rise to an extent that is controlled by conduction or perfusion.

A simple model which may be considered is that of an absorbing sphere suspended in a larger volume of relatively nonabsorbing material (NCRP, 1974). This situation is commonly encountered in bioeffects experiments in which the 'sphere' may be a tissue sample, in a water-bath. The limiting temperature rise, $\Delta T_{lim,}$ is given by

$$\Delta T_{lim} = \frac{\alpha I r^2}{C_t} \qquad 2.6$$

where α is the absorption of the medium, r is the beam radius and C_t is the thermal conductivity. Two conclusions can be reached from consideration of this model. Firstly the limiting temperature rise will be higher for a larger body, and secondly the time required to reach the limiting temperature will be greater the larger the body.

The analysis can be extended to the situation in which there is a high field intensity within an absorbing medium with a low intensity elsewhere. In this case the limiting temperature rise will be greater for a greater beam width. An estimate of the temperature rise due to a pulsed, focused beam can be obtained using Equation 2.6 and setting I equal to the time average intensity and r equal to the beam width in the focal region. For a spatial average temporal average intensity of 2 W cm^{-2} (typical of the maximum intensities generated by commercial pulsed Doppler units) and a beam radius of 1 mm, a temperature rise of 1.8 ^{0}C would be expected.

2.5.3 Effects of heat transport

Temperatures calculated in this way will overestimate the temperature that may be reached in perfused tissue where blood flow can be regulated to transport heat away. The effects of perfusion in tissue can be taken into

account by use of the bioheat transfer equation initially derived by Pennes (1948) which can be written as

$$\frac{\partial T}{\partial t} = D\nabla^2 T - \frac{T}{\tau} + \frac{Q}{C_v} \qquad 2.7$$

where D, the thermal diffusivity, is equal to C_t/C_v (C_v is the thermal capacity of the medium per unit volume) and τ is the time constant for perfusion. The perfusion constant, τ, is related to the blood perfusion rate, P, by the relationship

$$\tau = \frac{\rho_b C_v}{P C_{vb}} \qquad 2.8$$

where ρ_b is the density of blood and C_{vb} is the specific heat per unit volume for blood.

Nyborg (1988) gives a solution to the bio-heat transfer equation for a point source. Results from this solution indicate that at different perfusion rates the time required to reach 50% of the limiting temperature rise decreases with increasing perfusion rate and, that the final steady-state temperature reached, in a highly perfused medium, is lower than in a less perfused medium.

Another solution is presented by the AIUM (1988) and applies to a steady source of heat in the form of a thin circular disc. This models the situation in which a disc of tissue is heated by a propagating ultrasound field. The results of this solution show (for a heated disc surrounded by tissue with thermal properties similar to water) that the temperature fall-off with distance from the disc is rapid when the diameter of the disc is small and that the temperature elevation is greater the smaller the diameter of the disc for a given heat flow. When the distance is large compared with the diameter of the disc this solution becomes identical to that given by Nyborg (1988).

There is a need to model more complex beam patterns in order to

produce realistic estimates of temperature elevations produced by real beams. It has been suggested (NCRP, 1990 draft) that any circularly symmetric beam pattern can be modelled as a series of thermal discs, since variations in temperature are rapidly smoothed out by thermal diffusion. The effect of beam focusing as well as perfusion may be investigated using this model.

Models are also currently being developed which will predict the effects of nonlinearity and enhanced absorption on heating. Consideration of nonlinear propagation is more important for diagnostic fields than for therapy fields because the acoustic pressure amplitudes generated by diagnostic equipment are generally significantly higher.

2.6 HEATING IN EXCISED TISSUE

Results have been reported (ter Haar *et al.*, 1989) of temperature elevation produced in excised bovine liver due to heating caused by contemporary commercial diagnostic equipment. In order to eliminate the heating effect of the transducer (Duck *et al.*, 1989) the beam was coupled through a water-path into the tissue of interest. It was then found that the maximum observed temperature rise was about 2 °C (unperfused tissue) under pulsed Doppler conditions. The effects of nonlinear propagation on heating in liver were also investigated. Temperature measurements were made under two exposure regimes for which the pulse pressure amplitudes were different but the acoustic power was similar. For a peak positive pressure, $\hat{p}^+$, of 6 MPa and 60 mW total power a temperature rise of 1.9 °C was obtained, while for $\hat{p}^+$ = 3.2 MPa and 76 mW total power the temperature rise at the same location was 1.6 °C (ter Haar *et al.*, 1989). Thus for high amplitude pulses, nonlinear propagation was a more significant factor and resulted in enhanced heating of the tissue.

2.7 SUMMARY

Thermal effects are known to be important in therapy fields but until recently have not been considered to be of significance at diagnostic intensities. An increased awareness of nonlinear propagation and of the circumstances in which it is likely to occur during the clinical use of ultrasound have led to increased interest in the potential of diagnostic ultrasound to heat tissue. Theoretical considerations predict that nonlinear propagation will enhance heating since increased absorption of the higher harmonics will occur. Some experimental evidence is available which shows enhanced heating in tissue mimicking gels (Bacon and Carstensen, 1990) and in excised bovine liver (ter Haar *et al.*, 1989) in nonlinear fields. The experimental situations used, model to some extent a pulsed Doppler investigation being carried out *in vivo* on a fetus. In each case the temperature rise did not exceed 2 ^{0}C. Temperatures rises measured in this way are worst case estimates since they neglect the effects of blood perfusion. Thermal effects in high amplitude diagnostic beams are the subject of work being currently undertaken by a number of research groups and will therefore not be considered further in this thesis.

CHAPTER 3

MECHANICAL EFFECTS OF ULTRASOUND

A number of nonthermal mechanisms for bio-acoustic effects have been identified or postulated in the literature. The most significant of these is cavitation which has received considerable attention in recent years. This mechanism is discussed here in some detail to assess its relevance to acoustic streaming while other mechanisms such as shear stress are discussed more briefly. Effects resulting from nonlinear propagation are described and some experimental measurements of waveform distortion in soft tissue are presented. Acoustic streaming, as a mechanism for bioeffects, is omitted from the discussion here since it is considered more fully in subsequent chapters. Any or all of the mechanisms may be operating simultaneously in an acoustic field and it is possible that synergistic effects may occur between different mechanisms.

3.1 CAVITATION

3.1.1 Physical Aspects

The term cavitation describes the oscillatory behaviour of gas or vapour filled cavities within a fluid in an ultrasound field and is the subject of a recent book by Young (1989). The behaviour of a cavity or bubble can range from regular pulsations, known as stable cavitation, which oscillate for many cycles of the sound field, to the violent collapse of vapour filled voids which is known as transient cavitation (Flynn, 1964). Stable bubbles oscillate in size about an equilibrium position while transient cavities expand

to many times their original size in one cycle of the acoustic wave and then collapse violently, often disintegrating into a mass of smaller bubbles which can act as nuclei for further cavitational activity. On collapse very high temperatures and pressures may be produced resulting in effects such as sonoluminescence and molecular degradation. Cavitation thresholds exist below which no effects are observed. Above the threshold, cavitation bubbles may grow from micronuclei and the occurrence of effects associated with cavitation is critically dependent on the availability of micronuclei within the fluid. Suitable nuclei are thought to occur at solid particles in the liquid which may trap minute gas bubbles or at tiny crevices in the walls of the vessel containing the liquid which may trap gas. Either of these can result in the formation of a cavitation bubble in the fluid when the acoustic pressure falls below the static pressure. Yount *et al.* (1984) identified nuclei in distilled water, which resembled gas bubbles with diameters of 1 μm or less. In theory bubbles of this size would dissolve due to surface tension unless they were stabilised in some way, for example by a skin of organic impurity. A variable permeability model has been proposed to explain how stabilisation may occur.

Stable Cavitation

The most important characteristic of a bubble in a liquid is its compressibility which is likely to be many thousands of times greater than that of water. As a result a bubble will expand and contract in response to the pressure variations in the wave. Bubbles smaller than resonant size grow by a process of rectified diffusion. This process has been described by Crum (1984), who identified two parts to the effect. The first, results from the change in surface area of the bubble. During the positive pressure half-cycle of the sound field the bubble will be compressed and gas will

diffuse outwards from the bubble into the liquid. During the negative half-cycle the bubble will expand and gas will diffuse inwards from the liquid to the bubble. Since the surface area of the bubble is larger during the negative half-cycle than during the compressional half cycle the bubble will gain some gas over a complete cycle and will grow steadily over a number of cycles. The second aspect is a 'shell' effect. The diffusion rate of gas in a liquid is proportional to the gradient of the concentration of dissolved gas. If a spherical shell of liquid surrounding the bubble is considered it can be seen that this shell expands in thickness when the bubble contracts and thus the concentration of gas near the bubble wall is reduced. The concentration gradient between gas in the bubble and gas in the shell is therefore increased and the rate of diffusion of gas away from the bubble is greater than at the equilibrium bubble radius. Conversely as the bubble expands gas diffuses into the bubble and again, since the surface area of the expanded bubble is greater, there is a net flow of gas into the bubble.

The magnitude of bubble oscillation depends on the acoustic pressure and for a given frequency on the bubble size, with the maximum effect occurring when the bubble is at resonant size. At frequencies of interest in medical ultrasound, resonant bubbles are of the order of a few micrometres in diameter.

For small bubbles, at frequencies in the low megahertz range, surface tension effects are important and the resonant frequency, f_r, for a bubble is given by (Young, 1989)

$$f_r = \frac{1}{2\pi r} \left\{ \frac{1}{\rho} \left[3\gamma \left[p_0 + \frac{2\chi}{r} \right] - \frac{2\chi}{r} \right] \right\}^{0.5}. \qquad 3.1$$

Here ρ is the density and χ the surface tension of the medium, γ is the ratio of the specific heats of the gas, p_0 is the hydrostatic pressure and r is the bubble radius.

Transient Cavitation

When the acoustic pressure is increased a sharp transition in behaviour may occur for some bubbles and violent adiabatic collapse may result. During transient collapse local pressures in the gaseous cavities may reach many thousands of atmospheres leading to shock waves and mechanical stress. In addition temperatures of many thousands of degrees may be reached (Young, 1989). These are however very local effects. As a consequence of this behaviour cavitation can be seen as a mechanism by which a bubble transforms the relatively low energy density of a sound field into a very high energy density by absorbing energy from the wave and releasing it over a very short period of time (Flynn, 1964).

3.1.2 Cavitation Thresholds in Water

Thresholds for cavitation depend on acoustic pressure and on frequency. At lower frequencies the thresholds for cavitation are lower, while the likelihood of cavitation occurring increases as the pressure is increased. Peak negative pressure has been suggested as the most relevant parameter for cavitation since bubbles grow during the decompression half cycle. However Aymé and Carstensen (1989a) have shown that for an asymmetrically distorted pulse the peak negative pressure typically underestimates bubble response and a better indicator is the pressure amplitude of the fundamental frequency in a Fourier series expansion of the distorted pulse waveform.

Flynn (1982) predicted the likelihood of transient cavitation occurring at frequencies and intensities used in medical ultrasound and for microsecond pulses which are commonly employed in diagnostic applications. The theory requires the pre-existence of bubbles which are sufficiently large to grow

and cavitate during the time period of a single pulse containing a very small number of acoustic cycles. Predicted thresholds were of the order of 1 W cm^{-2} to 10 W cm^{-2} (Carstensen and Flynn, 1982). As a result of this, considerable experimental work has been carried out in an attempt to detect cavitation in diagnostic fields but generally the results have been negative at short pulse lengths (ter Haar *et al.*, 1989).

Thresholds for bubble formation (but not collapse) in water were measured by Atchley *et al.* (1988) as a function of pulse duration and pulse repetition frequency. Transient cavitation has been observed in water using an extra-corporeal shockwave lithotriptor (Coleman *et al.*, 1987). Despite considerable effort there is no conclusive experimental evidence of transient cavitation occurring in water at diagnostic ultrasound levels.

3.1.3 Detection of Cavitation

In the bio-acoustics literature a number of effects have been observed to occur at pressures above the threshold for cavitation which are absent at lower levels. It is important therefore to identify when cavitation is occurring in an experimental system. Several indirect methods may be employed. Firstly, cavitation results in the formation of subharmonics of the fundamental frequency (Morton *et al.*, 1983) which may be identified in a Fourier series analysis of the pressure waveform. Secondly sonoluminescence may occur in water due to the recombination of free radicals generated by cavitation (Pickworth, 1989). Edmonds and Sancier (1983) and Christman *et al.* (1987) demonstrated the formation of free radicals during transient cavitation using an electron spin resonance technique. Since cavitation may be eliminated by an increase in the ambient pressure, this may also be used as a method of determining whether cavitation is occurring in an experimental system. Daniels *et al.* (1987) produced visible gas bubbles in

agar gels by exposing them to a 0.75 MHz continuous wave ultrasound field, thus providing visual evidence of the existence of cavitation nuclei within the gel.

3.1.4 Biological Aspects

A number of authors have reported detecting either cavitation damage or cavitation indicators such as those defined in the previous section in plant tissue, in insects and in animal tissue. For example ter Haar *et al.* (1982) presented evidence for the appearance of stable cavities *in vivo* in the hind legs of anaesthetised guinea pigs during insonation with 0.75 MHz continuous wave ultrasound. This observation provided indirect evidence that cavitation nuclei existed in the tissues of these animals and could grow by rectified diffusion (Crum and Hansen, 1982) to observable sizes. Useful reviews of bioeffects attributed to mechanisms involving cavitation have been given recently by Carstensen (1987) and Miller (1987).

When transient cavitation is considered as a mechanism for damage in the medical use of ultrasound the question of whether gas bubbles of the correct size exist in tissues and fluids of the body is crucial. A report by a working group of the British Journal of Radiology (Wells, 1987) concluded that with low time average intensities, consistent bioeffects were only observed where stabilised gas bubbles had been introduced deliberately and were therefore unlikely to occur *in vivo*. Two situations in which this could happen in clinical practice are when small gas bubbles are introduced for contrast imaging and when saline is introduced into the body for oocyte collection.

3.2 SHEAR STRESS

Particles in a fluid oscillate in response to an acoustic field. At a boundary the particle velocity is zero under non-slip conditions and a steep velocity gradient is set up in the fluid. The thickness of the boundary layer in which the velocity gradient occurs is given by (Nyborg, 1965)

$$\delta = \left[\frac{2\mu}{\omega \rho_0} \right]^{0.5} \qquad 3.2$$

where μ is the shear viscosity, ω the angular frequency of the ultrasound and ρ_0 is the static fluid density. For a 3.5 MHz field the boundary layer extends 0.3 μm in water. To a first approximation the velocity gradient, du/dr, oscillates at the boundary with an amplitude given by

$$\left[\frac{du}{dr} \right] = \frac{u_1}{\delta} \qquad 3.3$$

where u_1 is the magnitude of the particle velocity oscillation in the free field. The shear stress at the boundary is given by the product of shear viscosity and velocity gradient. Therefore for a 3.5 MHz continuous wave beam, at an intensity of 1 W cm^{-2} in water, the particle velocity is 11.5 cm s^{-1}, the velocity gradient is 3.8 x 10^5 s^{-1} and the oscillating viscous stress in water associated with this velocity gradient is 380 Pa. In a pulsed field with peak positive acoustic pressure of 3 MPa the particle velocity is 2 m s^{-1} and the transient shear stress in water during the pulse is approximately 7 kPa. The ultimate shear stress of soft tissue may be inferred from data on tensile strength (Duck, 1990). For example the maximum shear stress that liver parenchyma can sustain is of the order of 200 kPa which is well above the shear stress predicted above. Applying these considerations to the situation in clinical obstetric scanning it seems reasonable to assume that the viscous stress developed in amniotic fluid will be similar to that in water, while the maximum shear stress that fetal soft

tissue and particularly brain can sustain may be lower than that sustained by liver tissue. Nevertheless damage by this mechanism seems unlikely.

An additional effect can occur where boundaries exist within a sound field. This is acoustic microstreaming which may occur around objects in the field such as bubbles or small particles. Velocity gradients are set up which result in a steady shear stress. It can be shown (Rooney, 1970) that the steady stress, s, exerted on a boundary due to streaming around a spherical object of radius r, vibrating with amplitude A, is given by

$$s = \left[\frac{1}{2} \mu\omega^3 \rho_0 \right]^{0.5} \frac{A^2}{r} \quad . \qquad 3.4$$

If stable cavitation is occurring, the steady state stress around a 2 μm bubble vibrating with a displacement amplitude of 1 μm in a 3.5 MHz field is of the order of 36 kPa. The critical shearing stress of human and canine erythrocytes was given by Nyborg (1971) as 170 Pa although a higher value of 560 Pa was quoted by Williams (1983). It has been shown that lysis of erythrocytes and platelets can occur in a continuous wave field when stabilised gas bubbles are present (for example Williams and Miller, 1980). However Miller *et al.* (1986) failed to show an effect on erythrocytes in pulsed ultrasound fields.

3.3 STANDING WAVE EFFECTS

When an ultrasonic wave is reflected at an interface the incident and reflected waves may interact in such a way that a standing wave is established. Under particular conditions in which a standing wave was deliberately set up, circulating blood cells in chick embryos were shown to clump into static bands at the pressure nodes (Dyson *et al.*, 1974). The effect was usually reversible, although damage to the epithelium sometimes occurred. This effect was obtained in a continuous wave field at an

intensity of 1 W cm^{-2}. One reason for the banding may be simply displacement of the cells to the pressure nodes but in addition acoustic microstreaming occurring at the surfaces of the blood vessel may also have contributed. Nyborg (1965) has shown that small vortices may form at a boundary at half wavelength spacings with stagnant areas occurring in between.

3.4 NONLINEAR PROPAGATION

It has been shown that acoustic shocks may be generated in water in the fields of diagnostic imaging equipment (Duck and Starritt, 1984 and Starritt, 1983). In these cases the degree of nonlinearity was shown to depend on the pulse amplitude and the propagation distance. Nonlinear propagation could result in enhanced effects on tissue if acoustic shocks are formed. The first possiblity is increased absorption of energy from the beam due to the formation of higher harmonics. This may result in enhanced thermal effects in soft tissue as described in Chapter 2 or an increase in the radiation pressure gradient in the field. The significance of the latter is discussed in Chapter 7. The second effect is mechanical and concerns the high accelerations and decelerations experienced by particles at an acoustic shock front. If a 3.5 MHz wave is assumed to be propagating linearly with a peak positive pressure of 3 MPa, the particle acceleration is greater than 10^7 m s^{-2}. However when waveform distortion occurs the leading edge of the waveform steepens and the acceleration experienced by fluid particles as the shock-front passes is much greater. No direct observation of damage attributable to this process has been reported. The significance of both these effects depends on the extent to which nonlinear distortion is occurring in tissue.

3.4.1 Experimental investigations in soft tissue

The results of investigations into the extent of nonlinear distortion occurring in excised bovine liver and human calf muscle are presented. This work is described in detail in two papers contained in Appendix 3 (Starritt *et al.*, 1985 and 1986). The investigations described were carried out using a mechanically scanned pulse-echo imaging unit (Kretzteknik Combison 100) with a 2.5 MHz focused transducer (NR2.5 20-100).

Harmonic generation in calf muscle

Levels of second and third harmonic components in the frequency spectra of detected waveforms following transmission through human calf muscle *in vivo* were measured. The values obtained gave a measure of the degree of nonlinear distortion which had occurred during propagation in the muscle. Only a modest degree of distortion was observed in this investigation with a maximum second harmonic level of 14 dB below the fundamental being generated. However it was likely that the experimental arrangement resulted in an underestimation of the maximum degree of finite amplitude distortion occurring since, due to the thickness of adult human legs, the measurements were made at positions beyond the beam focus, where beam divergence and attenuation could reduce the degree of waveform distortion.

Harmonic generation in liver

The degree of nonlinear distortion occurring during propagation through varying thicknesses of bovine liver *in vitro* was assessed. At maximum the second harmonic was 10.5 dB below the fundamental and the third harmonic

was 19 dB below the fundamental. The levels of second and third harmonic components relative to the fundamental increased as the thickness of liver increased up to a maximum, which occurred on the transducer side of the focus, and then decreased as the propagation distance was extended.

Discussion of experimental results

The results presented for liver indicate that waveform distortion may occur in ultrasound pulses propagating through soft tissue at diagnostic frequencies and intensities. The degree of distortion observed in these experiments was significant but insufficient to constitute an acoustic shock since at maximum the second harmonic component generated in liver was more than 8 dB below the fundamental. This level of second harmonic in a plane wave would indicate the presence of a $\sigma = 1$ shock (Muir and Carstensen, 1980). In the discussion below the problems of extrapolating from measurements made *in vitro* to the clinical situation, together with the limitations of such extrapolations, are discussed.

The degree of distortion which occurs in tissue is dependent on the ultrasonic parameters affecting nonlinear propagation such as focal gain, acoustic frequency and input power, and also on tissue parameters including the nonlinearity parameter, B/A, and the attentuation coefficient and its frequency dependence (Bjørnø, 1976). Differences in morphology are likely to result in changes in B/A and in attenuation. The excised livers used differed from living tissue in that they were not perfused and also because measurements were made at 21 ^{0}C, not at body temperature. This would result in approximately a 10% reduction in B/A and therefore slightly less distortion might be seen due to this change alone. Changes in attenuation due to temperature and after death might also affect the results and such changes are discussed by Duck (1990). There is some evidence that the

attenuation coefficient of soft tissue decreases with temperature (Bamber and Hill, 1979). A temperature dependence of -0.014 dB cm^{-1} $^{0}C^{-1}$ at room temperature was reported for a 2 MHz beam which increased to -0.052 dB cm^{-1} $^{0}C^{-1}$ at 4 MHz. Conversely a reduction in attenuation occurs in the period following death. There is a considerable variation in the measured values of B/A for beef liver reported with values ranging from 6.2 to 8.9 at 30 ^{0}C. Reported values for human liver at 37 ^{0}C are at the lower end of this range. A higher value of B/A would favour harmonic generation.

Harran and Cook (1983) predicted that, for a plane acoustic wave, attenuation would prevent shock formation in a lossy medium. The experimental evidence concerning shock formation in focused fields is inconclusive. The results presented here are the only experimental measurements of finite amplitude distortion occurring in tissue reported in the literature and therefore form an inadequately small basis from which to draw definitive conclusions. The limitations of extrapolating from these results to the *in vivo* situation have been discussed above. It is only possible to speculate therefore whether an increase in pulse amplitude or focusing gain would result in acoustic shock formation in soft tissue, or whether attenuation would dominate and prevent shock formation under any circumstances. Further measurements are needed to resolve this question. One tissue for which the attenuation coefficient is very low is fetal brain and it is therefore less likely to inhibit shock formation. The extent to which this is a serious concern for the clinical use of ultrasound will depend partly on the factors outlined below.

3.4.2 Nonlinearity in clinical situations

In the experiments described above the region between the transmitting

transducer and the receiving hydrophone was entirely filled by tissue and a modest amount of nonlinear distortion was seen to occur as the beam propagated through the tissue. In clinical practice situations exist in which the beam is transmitted partly though a fluid path and partly through tissue. Either a water stand-off is employed before the beam enters the tissue or the beam passes through some thickness of overlying tissue before it traverses a weakly attenuating fluid such as amniotic fluid. In the second case, which corresponds to the more common situation of obstetric scanning, the overlying tissue will attenuate the acoustic beam although, as shown above, nonlinear distortion may also occur in the tissue. When the beam passes into the fluid it will propagate nonlinearly to an extent that depends on the attenuated amplitude. Carson *et al.* (1989) measured minimum thicknesses of overlying tissue in 22 pregnant women between 15 and 20 weeks post conception and calculated a minimum attenuation afforded by the tissue of 0.8 dB MHz^{-1}. At 3.5 MHz this is equivalent to a reduction in intensity of a factor of 2. The location of the focus of the beam with respect to the maternal tissue/fluid interface is of also of major significance. If the location of the focus falls in the fluid path, and particularly if the degree of tissue attenuation is modest, significant waveform distortion and possibly shock formation may occur in the fluid. The beam in question will then be rich in harmonics by the time it is incident on the fetal tissue or bladder wall. Very rapid absorption will occur here. The likelihood of finite amplitude effects occurring in this situation and resulting in enhanced absorption has been discussed by Carstensen *et al.* (1982) while enhanced temperature elevation in gels in the same circumstances has been predicted by Bacon and Carstensen (1990). Similarly in the practical use of ultrasound, the potential for enhanced acoustic streaming to occur due to finite amplitude distortion is greatest when part of the transmission path is through a fluid.

3.5 SUMMARY

After the thermal mechanisms discussed in Chapter 2, cavitation is the second most studied bioeffects mechanism. However there is still uncertainty about whether cavitation can occur *in vivo* and about the thesholds for cavitation in water in pulsed diasgnostic fields. Amyé and Carstensen (1989a) have investigated the significance of nonlinear distortion for cavitational effects. They concluded that a distorted asymmetric pulse was equivalent in its effect on a cavitation bubble to a sinusoidal pulse with an amplitude equal to the fundamental amplitude of the distorted pulse. Experimental results obtained on insects were in agreement with this prediction (Aymé and Carstensen, 1989b). It appears therefore that cavitation is not significantly affected by nonlinear propagation. The mechanism of cavitation is not investigated further in this thesis but continues to be the subject of research work elsewhere.

Nonlinear propagation has been shown to occur in tissue. In particular significant nonlinear distortion may be expected to occur in the situation in which ultrasonic exposure takes place through a water-path. A known nonlinear phenomenon is acoustic streaming. The remainder of this thesis will consider the effects of nonlinear propagation on streaming and particularly the enhancement of streaming in water in diagnostic beams.

CHAPTER 4

THEORY

4.1 NONLINEARITY AND ACOUSTIC SHOCK FORMATION

The propagation of ultrasound is inherently nonlinear and in order to provide an accurate mathematical description of the process the equations describing wave propagation are required to be nonlinear. It has however been common to make the assumption of linearity and this has allowed a comparatively simple mathematical description of the propagation process to be obtained which is adequate in many situations. Linear assumptions becomes less valid for fluids with a high degree of nonlinearity and for ultrasonic waves of high amplitude. In these circumstances an initially sinusoidal wave propagating in a medium undergoes progressive waveform distortion as described in Section 4.1.3. Acoustic streaming is shown to be closely related to waveform distortion. This chapter is divided into two sections. The first deals with nonlinear propagation and waveform distortion and the second section covers the theory of acoustic streaming.

4.1.1 Historical development

The development of nonlinear ultrasound has been reviewed by Bjørnø (1975), Beyer (1984) and Hamilton (1986). The theory of finite amplitude sound propagation can be traced back to Euler's equations of motion and continuity for a fluid from which in 1765 he derived the nonlinear wave

equation for the propagation of finite amplitude waves in a lossless gas. Although Euler did not solve this equation he concluded that the wave propagation velocity would be greater than the isothermal speed of sound. A similar equation led Lagrange (1761) to the conclusion that the propagation velocity of a finite amplitude wave should depend on the original amplitude of the wave. This so shook his confidence in his own calculations that he concluded that the only possible means of wave propagation was the linear one (see Bjørnø, 1975). Poisson in 1808 obtained an exact solution to a one dimensional wave equation for finite amplitude waves in a gas which was later used by Stokes to describe how waveform distortion might occur during propagation. The connection between thermodynamics and kinematics was established by Earnshaw in 1860 enabling the local wave velocity to be expressed in terms of pressure and density variations in a fluid. Rankine and Huganiot went on to formulate the relationship between thermodynamic and kinematic quantities on either side of a shock front which became known as the Rankine–Huganiot equations.

Two Fourier series solutions were published for a plane progressive periodic wave of finite amplitude by Fay (1931) and Fubini (1935). The Fubini solution assumed a sinusoidal wave propagating in a lossless fluid and described how waveform distortion would occur by the generation of higher harmonics during propagation. This solution is only valid in the region close to the transducer and before a shock becomes established. The Fay solution on the other hand is valid for a viscous fluid in the region in which shocks are fully developed and have begun to decay. In the transition region, around the shock front, neither solution is valid but the relationship between them has been established by Blackstock (1966).

While in principle an exact numerical solution of the partial differential equations governing wave propagation is possible, considerable computational

time is involved. As an alternative, reasonable assumptions have been made which simplify the governing equations making exact or approximate analytical solutions easy to obtain. This was the approach adopted by Burgers (1948) who formulated a simple approximate partial differential equation which contained nonlinear and dissipative terms and had the advantage that for plane waves an exact analytical solution was possible. A number of theoretical solutions have been based on Burgers' equation, for example Blackstock (1964). Another approach to the solution of finite amplitude wave propagation has been the so-called weak shock theory which has been shown to be a limiting case of the solution based on Burgers' equation. This theory permits a solution for small amplitude shocks only. Blackstock (1966) made use of this approach to obtain a mathematical model of wave propagation in the region in which shocks are generated within an acoustic field.

A number of workers have addressed the problem of finite amplitude propagation for nonplanar waves. Naugol'nykh *et al.* (1963) and Khokhlov *et al.* (1964) for example modelled spherical and cylindrical waves propagating in an absorbing medium and Blackstock (1964) produced a one dimensional solution to Burgers' equation applicable to finite amplitude cylindrical and spherical waves in lossless fluids.

Focused beams

The problem of finite amplitude propagation for nonplanar waves has been addressed by a number of authors. In general the solutions produced do not apply to conditions in which hard shocks form and commonly they fail to predict behaviour in the focal zone. Naugol'nyky *et al.* (1963) derived a solution for the propagation of converging spherical waves in a viscous medium. This treatment assumed a spherical radiator, and did not consider

a physical source of limited extent for which the presence of source boundaries would lead to diffraction effects similar to those of the infinitesimal amplitude case. Sutin (1978) developed an approximate analysis taking diffraction into account based on the separation of nonlinear and diffraction effects at different locations in the field. Outside the focal zone it was assumed that diffraction could be neglected while within the focal zone linear diffraction theory was applied. An analytical model which predicted levels of second harmonic for a spherically concave source of limited aperture was developed by Lucas and Muir (1983). Their solution applied only to conditions of moderate nonlinearity in which shocks did not form in the focal region. Saito and Kim (1987) used numerical analysis to extend this model to predict the off axis behaviour of the second harmonic. They concluded that the ratio of second harmonic to fundamental amplitude was a maximum at the focus and that the second harmonic component focused more tightly than the fundamental.

Recently the increase in computational power available has led to a renewed interest in numerical solutions of the wave equation. Theoretical work in the Soviet Union by Zabolotskaya and Khokhlov (1969) and Kutznetsov (1971) led to the formulation of a parabolic nonlinear wave equation which contains the effects of diffraction, dissipation and nonlinearity and applies for a quasi-planar wave from a bounded aperture. A number of workers have reported numerical solutions of this equation (for example Aanonsen *et al.*, 1984). Baker *et al.* (1987) obtained a solution for a focused field based on this equation and demonstrated good agreement with experimental results.

4.1.2 Sources of nonlinearity

Wave propagation in a fluid is completely determined through the

following equations:-

(1) The equation of continuity expressing the conservation of mass

(2) The equation of motion expressing conservation of momentum

(3) The equation of state describing the fluid's response to thermal or mechanical stress.

There are two independent sources of nonlinearity inherent in these governing equations which are important in the propagation of finite amplitude waves. One source is inherent in the equation of state for the medium, the other in the equation of motion.

Equation of state

The passage of a sound wave through a medium causes pressure, density and temperature variations in the medium. As a fluid is compressed its stiffness increases and there is a corresponding increase in the speed of sound. This results in the compressional phase of a wave experiencing a higher speed than the decompressional phase. The relationship between pressure and density, ρ, in the medium may be expressed as

$$p = p\ (\rho) \qquad 4.1$$

where p is the sum of the static pressure and the acoustic pressure. The precise form of the equation of state is unknown but it is common to approximate it as a Taylor series expansion of Equation 4.1 to give

$$p = p_0 + \left[\frac{\partial p}{\partial \rho}\right]_{\rho_0} (\rho-\rho_0) + \left[\frac{\partial^2 p}{\partial \rho^2}\right]_{\rho_0} \frac{(\rho-\rho_0)^2}{2!} + \ldots . \qquad 4.2$$

where p_0 and ρ_0 are the equilibrium pressure and density respectively. This can be rewritten as

$$p - p_0 = A\left[\frac{\rho-\rho_0}{\rho_0}\right] + \frac{B}{2}\left[\frac{\rho-\rho_0}{\rho_0}\right]^2 + \ldots . \qquad 4.3a$$

where the coefficients A and B are defined as

$$A = \rho_0 \left[\frac{\partial p}{\partial \rho} \right]_{\rho_0} = \rho_0 c^2 \qquad 4.3b$$

$$B = \rho_0^2 \left[\frac{\partial^2 p}{\partial \rho^2} \right]_{\rho_0} . \qquad 4.3c$$

Here c is the speed of sound for infinitesimal amplitude waves. For very low amplitude waves second and higher order terms can be neglected and in this case the acoustic pressure and density in the medium are linearly related by the following relationship

$$p = c^2 (\rho - \rho_0) \qquad 4.4$$

where $p = p - p_0$. As the wave amplitude becomes larger it is necessary to include higher order terms. Inclusion of the second order term results in the following relationship

$$p \simeq \Delta\rho c^2 + \frac{B}{2A} \Delta\rho^2 \frac{c^2}{\rho_0} \qquad 4.5$$

where B/A is the first order parameter of nonlinearity. This equation describes the nonlinear relationship between changes in pressure and changes in density within the fluid due to finite amplitude wave propagation. The second order term C/A may also be defined, but its contribution is extremely small and it is usual to consider only the first order parameter.

The propagation speed is defined by

$$c^2 = \left[\frac{\partial p}{\partial \rho} \right]_{\rho_0} \qquad 4.6$$

for infinitesimal waves. For waves of finite amplitude the relationship is modified by second order terms in the expansion of the equation of state. Thus nonlinearity inherent in this equation results in a change in propagation velocity in the medium.

Convective nonlinearity

The second source of nonlinearity arises due to the fact that the phase velocity, that is the velocity of a particular point on the waveform, is the sum of the local particle velocity and the local velocity of sound (Earnshaw, 1860). The later is dependent on density as described above and thus is a source of nonlinearity in itself. In addition the local particle velocity can add to or subtract from the local speed of sound producing an effect which becomes more significant as wave amplitude increases. Since pressure and particle velocity in an acoustic wave are in phase with one another the particle velocity adds to the local velocity of sound propagation in the compressional phase and subtracts from it in the decompressional phase. Thus the velocity in the compressional phase is greater than that in the decompressional phase. As a result the compressions travel faster than the troughs and eventually catch up with them forming a shock front.

Combining the effect of convective nonlinearity with that of nonlinearity due to the medium results in the following expression for the velocity $u(x)$, at a point x on an acoustic wavefront (Bjørnø, 1975)

$$u(x) = c + \left[1 + \frac{B}{2A}\right] u(x) \qquad 4.7$$

where u(x), the local particle velocity is positive during the compression phase leading to $u(x)>c$, and negative during the decompressional phase leading to $u(x)<c$. The term in parenthesis is commonly referred to as β. This effect can be seen to increase with increasing particle velocity and with increasing values of B/A.

4.1.3 Waveform distortion

Both sources of nonlinearity lead to cumulative waveform distortion as propagation occurs. The waveform can change shape in two ways. Firstly a steepening of the leading edge occurs as the compressions propagate more quickly than the decompressions due to the nonlinear effects discussed above. Secondly diffraction effects in real acoustic beams result in the waveform becoming asymmetric. This was observed experimentally by Duck and Starritt (1984) and predicted theoretically by (Baker, 1989). Figure 4.1 shows examples of typical pulses.

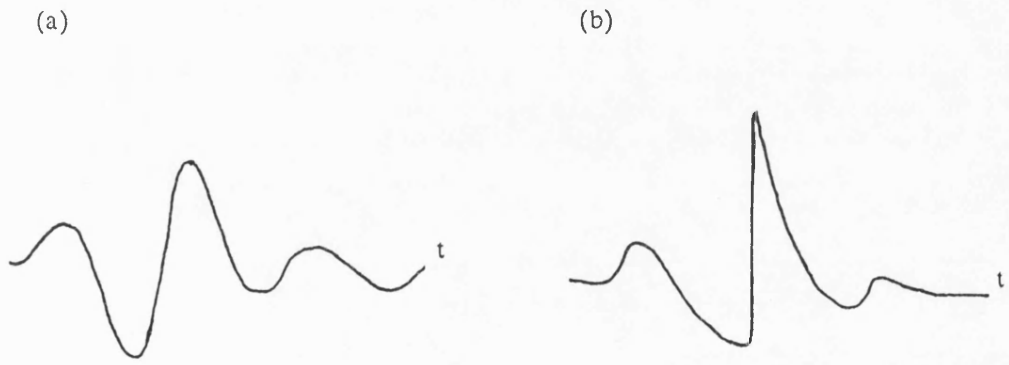

Figure 4.1 Acoustic pulses typical of those measured in water, a) undistorted and b) distorted

It can be seen that as a result of diffraction the compressional half cycle becomes more peaked whilst the decompressional half cycle becomes shallower and more rounded. The peak positive pressure can be a number times greater in magnitude than the peak negative pressure. Distortion in the time domain results in new frequency components in the frequency domain and generates a wave which is rich in harmonics.

The process of nonlinear distortion results in the continual transfer of energy out of the fundamental and into higher frequency harmonics. Since

absorption is frequency dependent, this results in the acoustic wave being absorbed more strongly than predicted by consideration of absorption at the fundamental frequency alone. In water for example, where absorption varies as the square of the acoustic frequency this can be a very significant effect. At frequencies in the low megahertz range water is often considered to be lossless but absorption approaching that of soft tissue has been measured in water in the focal region of a beam where a full shock had formed (see Section 6.7). This process, of energy transfer into higher harmonics and the resulting increase in acoustic absorption, is very important to an understanding of the effects described in this thesis.

In the description of nonlinear propagation given above it was assumed that the wave was propagating through a lossless medium. If instead, propagation is through an attenuating medium, the degree of distortion which occurs depends on two competing processes. One is nonlinearity and the other is attenuation. In an attenuating medium such as soft tissue a mature shock will not form if attenuation dominates over nonlinear effects. Gold'berg (1956) introduced the coefficient, Γ, to describe the ratio between the opposing effects of nonlinear distortion and absorption, α, which is defined as

$$\Gamma = \frac{\beta \epsilon k}{\alpha} . \qquad 4.8$$

In this equation, β is the nonlinearity parameter for the propagating medium, k is the wave number and ϵ is the acoustic Mach number defined for plane waves as the ratio between the particle velocity at the source and the infinitesimal speed of sound.

In practice nonlinear distortion results in there being an upper limit on the amount of sound power that can be transmitted beyond a certain range. The effect, known as acoustic saturation, has been investigated by Shooter *et al.* (1974).

Shock formation

In the absence of strong dissipative effects waveform distortion increases as a finite amplitude wave propagates resulting at some point in an acoustic shock being formed. The degree of shock can be quantified by the shock parameter, σ. Waveform distortion corresponding to a range of values of σ is shown in Figure 4.2. (The effects of diffraction are neglected in this figure.)

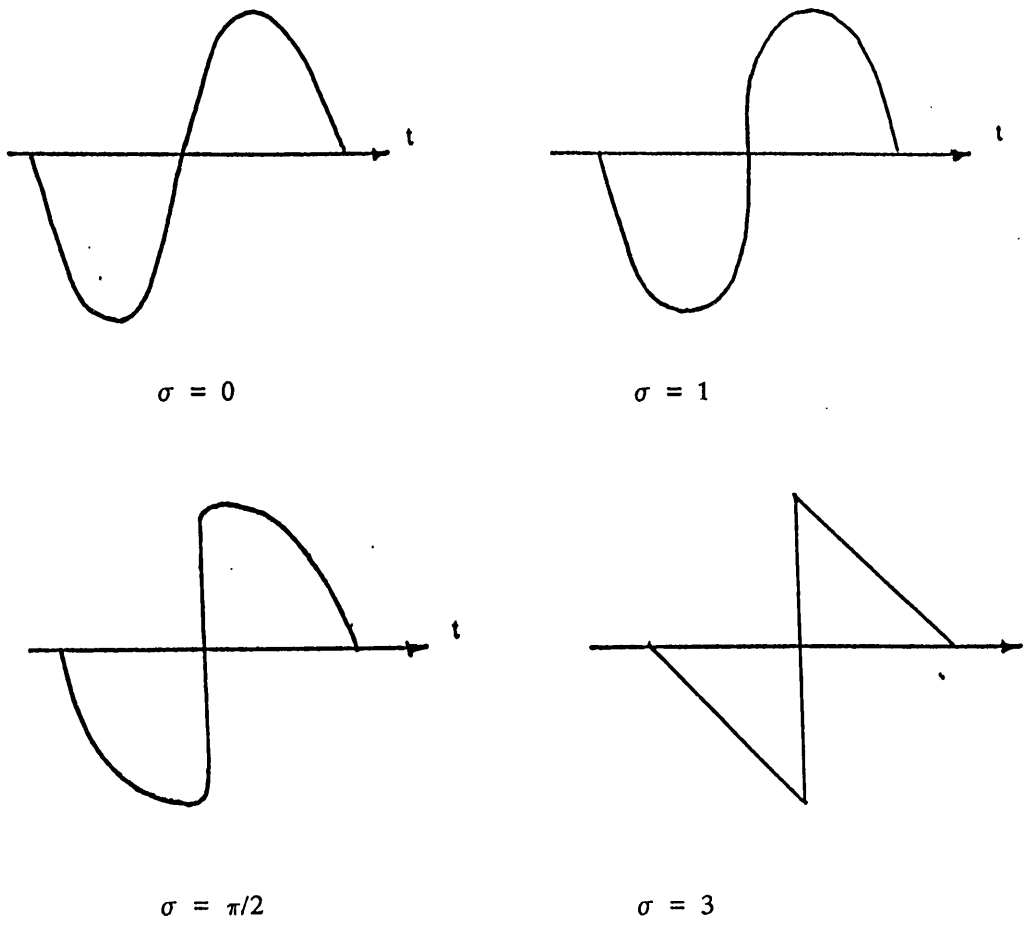

Figure 4.2 Waveform distortion corresponding to different values of σ.

For example a $\sigma = 1$ shock occurs when an originally sinusoidal wave has distorted to the stage of just forming a small discontinuity in pressure close

to the static pressure value. In a plane wave, the fundamental has lost 1 dB due to harmonic generation at this stage. A shock parameter of $\pi/2$ indicates that the peak pressure has moved forward to the location of the zero crossing point of the wave and the peak negative pressure has moved back to the same point. At a shock parameter value $\sigma \geq 3$, a mature shock has formed for a plane wave. At this point, in the absence of diffraction effects, the waveform would be a 'sawtooth' in which the harmonic amplitudes varied as the reciprocal of the harmonic number. Hence the 2nd, 3rd and 4th harmonics would be 6, 10 and 12 dB respectively below the fundamental in amplitude. The waveform can distort no further than this and the tendency to do so results in a reduced amplitude due to loss of energy at the shock front.

For plane waves in the absence of attenuation the shock parameter, σ, may be defined in terms of various wave parameters together with the nonlinearity parameter, β such that

$$\sigma = \beta \epsilon k x \qquad 4.9$$

where x is the propagation distance. The wave number, k, introduces a frequency dependence and, ϵ, the acoustic Mach number introduces an intensity dependence into the equation.

For a focused beam a number of formulae have been proposed to relate σ to the beam parameters in a way analogous to Equation 4.9 above. However most of these are applicable only over a limited region and under conditions of quasilinearity ($\sigma < 1$). In particular they fail to predict σ correctly at the location of the focus. Equations of the form

$$\sigma = \beta \epsilon k f \ln \left[\frac{f}{d} \right] \qquad 4.10$$

have been suggested by a number of authors (for example Sutin (1978), Muir and Carstensen (1980) and Lucas and Muir (1983)). The focal length, f, and the distance d, are defined in Figure 4.3.

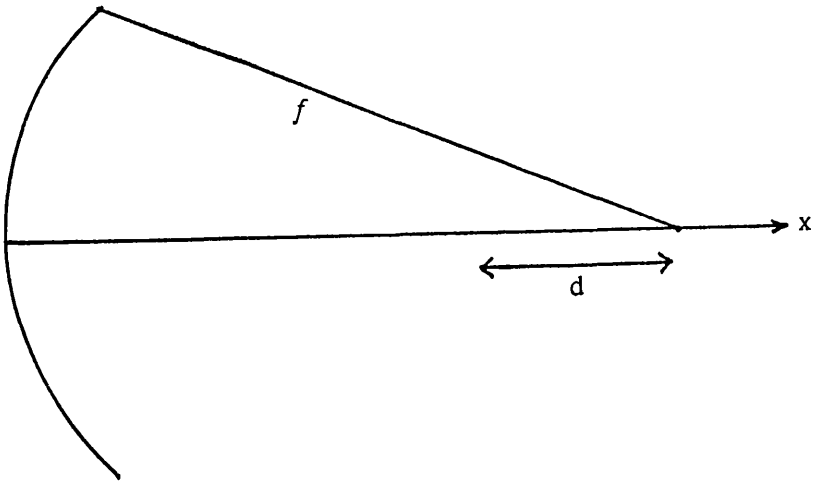

Figure 4.3 Geometry assumed in defining σ for a focused beam

This equation may be used in the region between the transducer and the focus but the solution becomes unbounded when $x = f$ and therefore it cannot be used to predict the degree of shock occurring at the focus.

Lucas and Muir (1983) went on to formulate a relationship between σ at the focus and the acoustic gain, G, defined as the ratio of the pressure amplitude at the transducer and the pressure amplitude at the focus

$$\sigma = \beta \epsilon k f \ln(G) \qquad 4.11$$

The use of this equation is also limited to quasilinear conditions in which $\sigma < 1$ and shocks do not form in the focal region. In effect this equation calculates σ at a distance f from the source for a plane wave and converts it to σ at the focus of a converging field by applying a factor dependent on the gain of the focused system. A similar approach was used by Bjørnø (1976) to produce an equation for a converging spherical wave which relates the distance, l_D, at which a discontinuity occurs (the discontinuity length) to the shock parameter calculated at a distance equal to the focal length, f, but assuming plane wave propagation

$$l_D = f \exp\left[- \frac{1}{\sigma} \right] \qquad 4.12$$

where $\sigma = \beta \epsilon k f$. The term exp $(-1/\sigma)$ is always less than 1.0 ensuring that the pathlength before a discontinuity never exceeds the focal length.

Bacon (1984) derived an expression for a focused field relating, σ, to beam parameters which are easily measured. This model was derived for particular application to the fields of medical ultrasound transducers and a number of assumptions were made which were justified in terms of this application. Firstly, the effects of attenuation at the fundamental frequency were neglected. This is a reasonable assumption at the frequencies used in medical ultrasound. Secondly a Gaussian beam profile was assumed resulting in a model in which diffraction effects were reduced. This may be justified on the grounds that diffraction effects are not significant in the pulsed beams employed in many diagnostic applications. Finally the assumption of symmetrical focusing was made which is true only for a circularly symmetrical transducer. Using this model a shock parameter, σ_m, was obtained which is defined by

$$\sigma_m = \frac{\omega \beta f p_m \ln(G + (G^2-1)^{1/2})}{\rho c^3 (G^2-1)^{1/2}} \qquad 4.13$$

where p_m is half the peak to peak acoustic pressure excursion, f is the focal distance and G is the small amplitude pressure gain, obtained from the ratio of the measured focal area to the radiating area. The result obtained by this method is equal to σ for values of $\sigma_m \leqslant \pi/2$. At shock levels greater than $\pi/2$, the pressure measured at the focus will have been reduced by excess absorption and therefore the calculated value of σ_m will be an underestimate of the true shock parameter.

This equation has been used to assess the degree of shock occurring in the pulsed focused fields investigated in this thesis.

4.1.4 Nonlinearity in diagnostic ultrasound

In recent years a number of authors have considered the relevance of nonlinear propagation in medical ultrasound particularly in its diagnostic use. Most notably Muir and Carstensen (1980) considered nonlinearity and shock formation at biomedical frequencies and intensities both theoretically and experimentally (Carstensen *et al.*, 1980). In formulating solutions for finite amplitude propagation a number of authors have specifically considered propagation in media with properties appropriate to tissue or body fluids. For example Trivett and Van Buren (1981) presented a numerical solution to Burgers equation which is valid for progressive plane, cylindrical and spherical waves and which allows for an arbitrary frequency dependent absorption. Harren and Cook (1983) used a Fourier series expansion of Burgers equation to calculate harmonic content as a function of propagation distance for plane waves in a lossy medium. They carried out calculations for several biological tissues and fluids, for example amniotic fluid and liver, and concluded that for plane waves acoustic shocks were unlikely to occur in soft tissue but could occur in amniotic fluid. Chapter 3 reported experimental investigations of shock formation in soft tissue (Starritt *et al.*, 1985 and 1986)

To accurately model nonlinear distortion in diagnostic beams the effects of focusing and tissue attenuation need to be considered together with nonlinearity. In addition modern diagnostic applications usually employ pulsed ultrasound beams. Numerical solutions for pulsed fields have been obtained by Baker and Humphrey (1990) using a typical pulse spectrum as the starting point for iterative calculations. The solutions considered to date are only applicable to a transducer having circular symmetry and cannot be used to predict the extent of nonlinear distortion occurring in the field of a rectangular transducer array. While it is possible to include focusing for a

single element transducer (Baker *et al.*, 1987) the asymmetric focusing characteristics of an array are more difficult to model. A futher complication arises due to the fact that the human body is not homogenous. A real beam is likely to pass through regions in which the attenuation and nonlinearity parameter are different.

4.2 ACOUSTIC STREAMING

The term streaming has been used to describe two separate phenomena in acoustics. One is the bulk fluid movement which results from the propagation of a high intensity sound wave in a fluid and is associated with forces acting only within the fluid. This effect has been known in the past 'quartz wind'. The second form of streaming, referred to here as microstreaming, occurs near vibrating objects and boundaries and results in the production of small vorticies (Nyborg, 1958). It differs from the quartz wind effect in that it is dependent on the interaction of a sound field with acoustic boundaries. In the bio-acoustics literature microstreaming is commonly associated with cavitation and flow around oscillating bubbles.

This thesis is concerned with the first of these mechanisms, the quartz wind effect, which will be referred to as simply acoustic streaming. The theory developed here relates to this phenomenon in particular.

4.2.1 Historical review

The earliest reported observation of acoustic streaming in a fluid was made by Meissner (1926) who reported that fluid appeared to be sucked into a sound beam at a vibrating quartz crystal and set into motion in the direction of wave propagation. This was followed by the first theoretical analysis of streaming by Eckart (1948). He showed that a stream was

generated by the transfer of momentum from a wave to a fluid which occurred as a result of viscous loss. Extension of the theory was carried out by Markham (1952) who replaced the simple equation of state relating acoustic pressure and density used by Eckart,

$$p = c^2 \rho \ , \qquad 4.14$$

by a more general one taking relaxation effects into account

$$p = c^2\rho + R \frac{\partial \rho}{\partial t} \quad . \qquad 4.15$$

Here R is a relaxation factor which may be a function of frequency. This led to the conclusion (Medwin, 1954) that streaming was proportional not only to viscous loss but to the total attenuation of a sound beam. Fox and Hertzfeld (1950), arguing that all absorption mechanisms for sound waves must lead to attenuation, introduced the concept of radiation pressure to explain acoustic streaming. Based on this suggestion Piercy and Lamb (1954) developed a theory in which time independent gradients of radiation pressure in the direction of propagation acted as the driving force for the stream. Tjøtta (1959) demonstrated that the streaming equations derived using the method of successive approximations (see Section 4.2.3) are the same as those obtained by consideration of radiation pressure.

A number of useful reviews of the development of the theory of acoustic streaming are available, for example Nyborg (1965), Beyer (1974) and Lindsay (1974) although it is notable that the level of interest in this subject has been low over the last twenty years. Several papers by Russian workers in the field have addressed the question of streaming in highly nonlinear fields in which significant waveform distortion occurs during propagation (Naugol'nykh (1958), Ostrovskii and Papilova (1974), Rudenko and Soluyan (1971a)). Stanikov (1967) modified Eckart's analysis to take account of the effect of a sawtooth waveform. More recently Wu and Du (private communication) have developed a general theory which allows axial

streaming velocities to be calculated for nonfocused sawtooth waves and for focused linear Gaussian beams. In this derivation, narrow acoustic beams for which ka $\gg$ 1 (where k is the wave number and a the radius of the transducer) were considered. The effects of boundaries were not included and the results are therefore only valid on axis and when the distance between the edge of the acoustic beam and the tank is large compared with the beam diameter. Analysis of a nonfocused beam of sawtooth waves was carried out by considering the beam as a plane wave when $\sigma < 1$, and as a fully shocked wave when $\sigma > 1$. The predicted axial streaming velocity was expressed as the sum of two components. The first component was the result for a linear plane wave and the second component was the nonlinear enhancement term due to increased absorption of higher frequencies in the sawtooth wave. The analysis was shown to be applicable to a toneburst if the time average intensity was used in the calculation. The enhancement of the streaming velocity in nonlinear beams, predicted by consideration of the effect of attenuation at higher frequencies, is in agreement with the experimental results presented in this thesis.

4.2.2 Basic equations

A theoretical treatment of acoustic streaming requires second order terms to be retained in the wave equation. For a linear beam acoustic variables such as density, pressure and displacement are time dependent, with time averaged values equal to zero and zero streaming is predicted, except in a thin layer near to a solid boundary where vortical flow may occur. Outside the acoustic boundary layer motion is irrotational to the first order and streaming will not occur. When second order terms are considered however a steady second order vorticity and acoustic streaming are predicted.

The theory presented here follows that developed by Nyborg (1965). This approach, involving the method of successive approximations, is a common one generally adopted by many workers in the field. Differences between this derivation and that of other authors are discussed.

Derivation of streaming equations

A homogeneous, isotropic fluid is assumed in which the pressure, density and velocity at any point are given instantaneously by $p(x,y,z)$, $\rho(x,y,z)$ and $\mathbf{u}(x,y,z)$. If a small element of fluid is considered, the net force per unit volume, $\mathbf{F}$, acting on it can be written as

$$\mathbf{F} = \rho \left[\frac{\partial \mathbf{u}}{\partial t} + (\mathbf{u}.\nabla)\mathbf{u} \right]. \qquad 4.16$$

For a fluid subject to both shear and bulk viscosity the force per unit volume is also given by

$$\mathbf{F} = -\nabla p + \left[\mu' + \frac{4}{3}\mu \right] \nabla\nabla.\mathbf{u} - \mu\nabla \times \nabla \times \mathbf{u} \qquad 4.17$$

where μ is the shear viscosity coefficient and μ' is the bulk viscosity coefficient for the fluid. Both are assumed to be constant although the bulk viscosity is a function of frequency. The assumption of constancy is only valid when the level of nonlinear distortion occurring is low.

Equations 4.16 and 4.17 are the Navier–Stokes equations in which the effects of shear stresses resulting from viscosity are combined with the equation of motion. Using the equation of continuity,

$$\frac{\partial \rho}{\partial t} + \nabla.\rho\mathbf{u} = 0 \qquad 4.18$$

it is possible to combine Equation 4.16 and 4.17 as

$$\frac{\partial \rho\mathbf{u}}{\partial t} + \rho(\mathbf{u}.\nabla)\mathbf{u} + \mathbf{u}\nabla.\rho\mathbf{u} = -\nabla p + \left[\mu' + \frac{4}{3}\mu \right] \nabla\nabla.\mathbf{u} - \mu\nabla \times \nabla \times \mathbf{u} \; . \qquad 4.19$$

The term $\rho\mathbf{u}$ is known as the mass transport velocity. The final term in Equation 4.19, $\mu\nabla x\nabla xu$, represents losses from the stream due to streaming and vorticity and is zero for linear fields fulfilling the criterion that $\mathbf{u}$ is irrotational.

Since this equation has no analytical solution the approach followed is to make a series of approximations which are appropriate to the situation in which steady flow is superimposed on a steady state sound field. Firstly the pressure, density and fluid velocity at a point in the fluid are defined by

$$\begin{aligned} p &= p_0 + p_1 + p_2 + \ldots . \\ \rho &= \rho_0 + \rho_1 + \rho_2 + \ldots . \\ \mathbf{u} &= \mathbf{u}_1 + \mathbf{u}_2 + \ldots . \end{aligned} \qquad 4.20$$

where p_0 and ρ_0 are the static pressure and density values. There is no corresponding term for $\mathbf{u}$ in the absence of a sound field. The subscript 1 denotes first order terms which vary sinusoidally in time with frequency, f. Second order time independent terms are denoted by the subscript 2 and the acoustic streaming velocity is represented by $\mathbf{u}_2$. The next stage in the derivation is to assume a first order approximation to $\mathbf{u}_1$ and use this to determine a second order approximation, $\mathbf{u}_2$.

Following Eckart's approach a streaming equation can be obtained from Equation 4.19 by retaining second order terms and taking the time average over a number of cycles to give

$$-\langle F\rangle = -\nabla\langle p_2\rangle + \left[\mu' + \frac{4}{3}\mu \right] \nabla\nabla.\langle \mathbf{u}_2\rangle - \mu\nabla \times \nabla x\langle \mathbf{u}_2\rangle \qquad 4.21a$$

where

$$-\langle F\rangle = 2\rho_0 \langle \mathbf{u}_1(\nabla.\mathbf{u}_1)\rangle \qquad 4.21b$$

(given that the time average of the partial derivative of the mass transport velocity is zero in the steady state). If $\nabla.\langle \mathbf{u}_2\rangle$ is assumed to be negligible Equation 4.21 reduces to

$$\langle F \rangle = \nabla \langle p_2 \rangle + \mu \nabla x \nabla x \langle u_2 \rangle = \nabla \langle p_2 \rangle - \mu \nabla^2 \langle u_2 \rangle . \qquad 4.22$$

The first term in this equation represents compressional stress and the second term represents the viscous stresses in the fluid. From Equation 4.21b it can be seen that **F** may be determined from a knowledge of the first order velocity, $\mathbf{u}_1$. The vector **F** may be interpreted as the time average of the rate of increase of momentum in a fluid element.

It was shown by Markham (1952), who obtained essentially the same results as Eckart from consideration of mass flow rather than particle velocity, that these results could be generalised by assuming an equation of state for which the first order relationship between pressure and density was defined by Equation 4.15. This equation differed from the equation used by Eckart in the inclusion of relaxation effects which could be highly frequency dependent. If the loss of energy from a wave is assumed to be due to shear viscosity, μ, bulk viscosity, μ', and relaxation, R, the absorption coefficient, α, of a fluid is given by the following expression

$$\alpha = \left[\mu' + \frac{4}{3} \mu + R\rho_0 \right] \frac{\omega^2}{2\rho_0 c^3} . \qquad 4.23$$

ω is the angular frequency, ρ_0 the fluid density and c the speed of sound.

When an acoustic beam is propagating in an attenuating medium its intensity decreases with distance from the source resulting in an axial pressure gradient. Provided a return path exists, this constant gradient causes an acceleration of the fluid which results in acoustic streaming. A steady state is reached when viscous forces resisting the stream balance the gradient of radiation pressure.

4.2.3 Solutions of the streaming equation

A number of solutions are developed in the literature which predict

streaming velocities under different conditions. Those discussed below are solutions applicable to situations which most closely resemble the experimental conditions used in this thesis. Their limitations in practical situations are discussed in Section 4.2.6. In all derivations it is assumed that the acoustic wavelength is small compared with the beam width and that the effects of diffraction can therefore be neglected.

In obtaining the solutions described here (Nyborg, 1965) a number of physical assumptions were made and the geometry considered is shown in Figure 4.4.

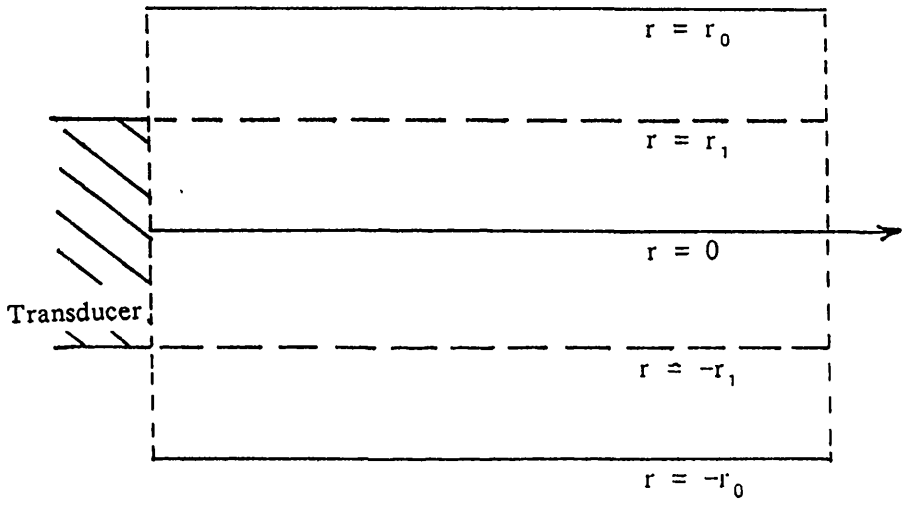

Figure 4.4 Geometry for calculating streaming velocity in a rectangular channel

An attenuated plane wave was assumed to be propagating in the x direction (perpendicular to the face of the transducer), in a rectangular channel of finite length, having parallel sides at $r = r_0$ and $r = -r_0$. The acoustic beam was assumed to be symmetric about the plane $r = 0$ with sharp edges at $r = r_1$ and $r = -r_1$. When $r_1 = r_0$ the beam filled the channel but when r_1 was small the beam was essentially unbounded.

The first order velocity was assumed to be given by the expression for a damped harmonic wave,

$$u_1 = U \exp(-\alpha x) \sin(\omega t - kx) \qquad 4.24$$

in the region $-r_1 < r < r_1$, where U was the particle velocity amplitude. Equation 4.21b reduces to the following expression for **F** in this region,

$$F_x = \rho_0 \alpha U^2 \exp(-2\alpha x) \qquad 4.25$$

or

$$F_x = \frac{\alpha p^2}{\rho_0 c^2} \qquad \text{for } \alpha x \ll 1 \ . \qquad 4.26$$

Since under the conditions described above, **F** was directed along the x axis Equation 4.22 could be written as

$$F_x = - \mu \frac{\partial^2 u_2}{\partial x^2} + \frac{\partial p_2}{\partial x} \qquad 4.27$$

and solved for u_2 given certain boundary conditions. (Here p_2, u_2 and F_x are the time averaged quantities.)

1. Result for an unobstructed channel

For an open ended channel, $\partial p_2/\partial x = 0$, and a solution of Equation 4.27 for streaming in the half channel $0 < r < r_0$ was given by

$$u_2 = \frac{\alpha p^2}{2\mu\rho_0 c^2} \; 2r_1(r_0 - r) \qquad (r_1 < r < r_0) \qquad 4.28a$$

and

$$u_2 = \frac{\alpha p^2}{2\mu\rho_0 c^2} \; 2r_0 r_1 - r^2 - r_1^2 \qquad (0 < r < r_1) \qquad 4.28b$$

The velocity profile predicted by these equations is shown in Figure 4.5 for the condition in which the beam width is equal to half the channel width.

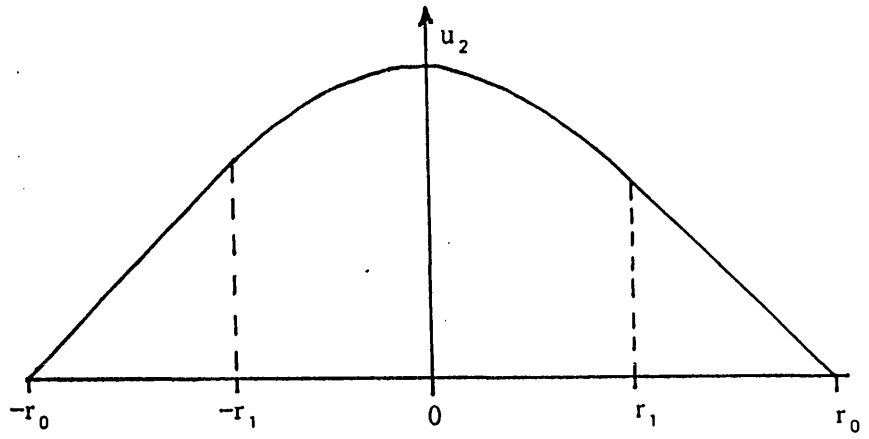

Figure 4.5 Streaming profile in an open channel

Within the channel, predicted fluid flow was always in the direction away from the transducer and reduced to zero at the boundary walls. In practice for an open channel immersed in a volume of fluid identical to that contained within it, a return flow path exists outside the channel in the volume of fluid surrounding it. This is analogous to the situation described in Section 6.5.

2. Result for an obstructed channel

When a channel with closed or partially closed ends was considered, for which $\partial p_2/\partial x \neq 0$, the following solution was obtained (Nyborg, 1965),

$$u_2 = \frac{1}{2\mu}\frac{\partial p_2}{\partial x}(r^2-r_0^2) + \frac{\alpha p^2}{2\mu\rho_0 c^2}(2r_1(r_0-r)) \qquad 4.29a$$

in the region $r_1<r<r_0$, and in the region $0<r<r_1$

$$u_2 = \frac{1}{2\mu}\frac{\partial p_2}{\partial x}(r^2-r_0^2) + \frac{\alpha p^2}{2\mu\rho_0 c^2}(2r_0r_1-r^2-r_1^2). \qquad 4.29b$$

The velocity profile described by these equations is shown in Figure 4.6

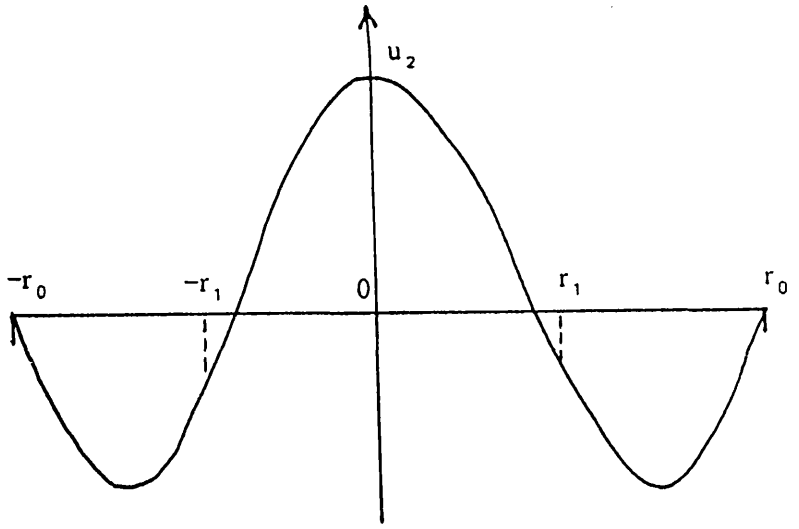

Figure 4.6 Streaming profile in a channel with closed ends

The acoustic beam width is again half the width of the channel. In this case forward flow occurs in the centre of the tube with reverse flow occurring near the walls.

A similar result was reported by Eckart (1948) who considered the propagation of a nondivergent sound beam in a cylindrical tube and imposed the condition of zero mass flow through any cross section. This resulted in the following general expression for the streaming velocity,

$$u_2(r) = k_1(r_0^2-r^2) + k_2 \int_0^{r_0} K(r',r)\, p^2(r')\, dr' \qquad 4.30$$

where r_0 is the radius of the vessel, r and r' are radial parameters and

$$k_2 = \frac{\alpha}{\mu \rho_0 c_0^2}$$

$$K(r',r) = r' \ln(r_0/r) \qquad (r' \leqslant r)$$

$$K(r',r) = r' \ln(r_0/r') \qquad (r' \geqslant r)$$

$$k_1 = -k_2 r_0^{-4} \int_0^{r_0} (r' r_0^2 - r'^3)\, p^2(r')\, dr' \quad .$$

Eckart obtained a specific analytical solution for the axial streaming velocity (r=0) by assuming the simple acoustic pressure field shown in Figure 4.7.

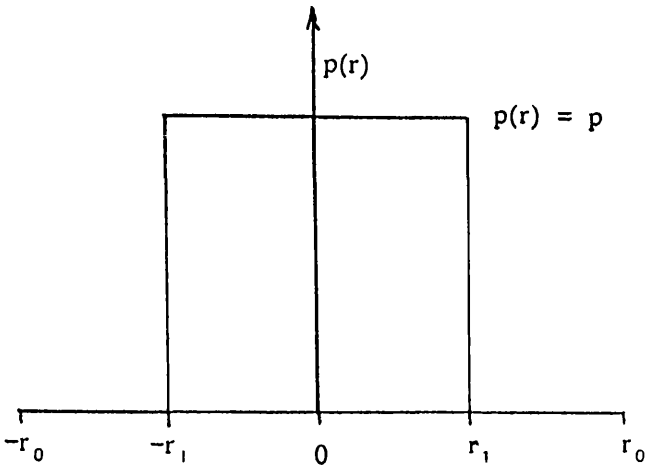

Figure 4.7 Idealised pressure field

In this case the axial streaming velocity was given by the following equation,

$$u_2 = \frac{\alpha p^2}{2\mu\rho_0 c^2} r_1^2 M = \frac{\alpha I}{c\mu} r_1^2 M \qquad 4.31$$

where I (= $p^2/2\rho c$) was the intensity in the acoustic beam and M was a multiplying factor dependent on the radius of the beam, r_1, and of the cylinder, r_0. M was defined as

$$M = \frac{1}{2}\left[\frac{r_1^2}{r_0^2} - 1\right] - \ln\frac{r_1}{r_0} \quad . \qquad 4.32$$

In deriving Equation 4.26 the assumption was made that F was a function only of x and that the streaming velocity was wholly in the x direction. This is not the case near the ends of the cylinder where reversal of the flow direction occurs but is a reasonable assumption if the cylinder is sufficiently long. If the beam radius is small compared to the radius of the cylinder the assumption that there is no radial flow component is no longer

valid and the solution is therefore inappropriate when the beam is effectively unbounded ($r_1 \gg r_0$).

3. Results in a diverging beam

Tjøtta (1959) following a similar analysis to Eckart, obtained a solution for a diverging beam in a tube. This permitted an estimation of the maximum streaming velocity to be made using the following equation,

$$\frac{u_2}{l^3} \simeq \frac{2}{\nu} \alpha k \frac{1}{L} \frac{I}{\rho_0 \omega} \qquad 4.33$$

where ν, the kinematic viscosity, is equal to μ/ρ. l is a geometric factor and L the characteristic length for changes in velocity. This equation can be rewritten as

$$u_2 = \frac{\alpha p^2}{\mu \rho_0 c^2} \frac{l^3}{L} . \qquad 4.34$$

Predicted streaming velocities obtained using this equation are presented in Section 4.2.6

4.2.4 Effect of frequency dependent absorption

Common to all the solutions discussed above is the dependence of streaming velocity on the attenuation coefficient, α, and on the square of the pressure or particle velocity amplitude. Theoretical considerations show that streaming will only occur when the absorption coefficient is non-zero and that the frequency dependence of the streaming velocity is completely determined by the frequency dependence of the coefficient of absorption (Ivanovskii, 1958). An inverse relationship between streaming velocity and the coefficient of shear viscosity is also apparent. The value of the

attenuation coefficient in Equations 4.28, 4.29, 4.31 and 4.34 for predicting streaming velocity, is the attenuation coefficient at the fundamental frequency. Attenuation in water however is strongly frequency dependent and this becomes a significant factor when the acoustic field contains regions in which mature shocks have formed. In the experimental studies reported in Chapters 5 and 6 the degree of waveform distortion occurring was significant and the waveforms were rich in harmonic components. However in the analysis of acoustic streaming to date, although second order nonlinear terms have been taken into account, an assumption has been made that the degree of waveform distortion occurring in the fluid is very low. In real fields this assumption is unlikely to be true. The attenuation coefficient at the fundamental frequency underestimates the acoustic attenuation in a shocked wave (see Appendix 2) and its use in the equations predicting streaming velocity may result in an underestimate of the true streaming velocity. If the degree of nonlinear waveform distortion occurring is significant the simple relationship between streaming velocity and acoustic pressure, predicted by Equation 4.28 for example,

$$u_2 \propto \frac{\alpha p^2}{\mu} ,$$

does not hold because absorption is not constant. Changes in the acoustic pressure and hence the degree of nonlinear distortion result in changes in absorption. Under such conditions the absorption term can be expressed as $(\alpha + \alpha_s)$ where the first term is absorption at the fundamental frequency and the second term represents the excess absorption due to acoustic shock formation or 'shock loss'. The factor α_s is the dominant loss mechanism in a shocked field. It has been suggested that the effective absorption in such a field is approximately constant, irrespective of the propagating fluid and of the value of absorption coefficient at the fundamental frequency within that fluid (Delecki *et al.*, 1990). It depends instead, for a given degree of

nonlinear distortion, on geometrical factors such as focal gain, propagation distance and transducer diameter.

Kubarin and Rudenko (1976) employed numerical methods in the analysis of streaming problems. The technique was used to calculate axial streaming velocity taking into account the effects of nonlinearly enhanced attenuation. In the case of strong attenuation the peak streaming velocity induced in a rectangular channel with a closed end was found to occur nearer to the transducer than in the case of weak attenuation (linear propagation). They attributed this to the fact that an increased fraction of the energy radiated per unit time was absorbed in the medium in the first case. The experimental results shown in Figure 6.5 are in agreement with this prediction.

4.2.5 Time dependent build-up of acoustic streams

The analyses outlined in the previous sections are appropriate for steady state streaming in which the streaming velocity has reached its maximum value. Rudenko and Soluyan (1971a and 1971b) addressed the question of the time dependent build-up of acoustic streams theoretically while Semenova and Statnikov (1968) reported experimental results. In the theoretical analysis, the streaming velocity at a point, x, in the fluid at any time, t, was expressed as the sum of a steady state velocity, u_{ss}, and a transient or build-up term, u_{tr},

$$u(x,t) = u_{ss}(x,\infty) + u_{tr}(x,t) \qquad 4.35$$

where ∞ was the time at which the steady state was reached. A solution was given for this equation in which the transient component of the acoustic streaming velocity was shown to have a time dependence characterised by τ_R where

$$\tau_R \propto r_0^2 \frac{\rho_0}{\mu} \quad . \qquad 4.36$$

Here r_0 was the radius of the cylindrical tube in which the sound beam propagated.

Semenova (1970) reported experimental evidence that the build-up time of the stream reduced as the intensity in the acoustic beam increased. In this thesis streaming velocity build-up times and decay times were investigated as a function of acoustic beam intensity and the results are described in Section 6.10.

4.2.6 Calculation of axial streaming velocities

A number of solutions to the streaming equations are given in the literature and are reviewed above. Essentially these reduce to the same expression but for a multiplying factor determined by the geometry of the system under consideration. In each case streaming velocity is related to acoustic intensity and the radius of the acoustic beam, and to the shear viscosity and absorption of the fluid. Differences in geometrical factors occur due to the different boundary conditions imposed in obtaining the solutions. For example different streaming velocities result from consideration of fluid flow in an open-ended tube and in a tube with closed ends. In particular when the tube is closed, flow velocities are lower and flow ceases when the acoustic beam fills the tube while flow in an open tube does not cease when the beam fills the tube.

In this section values of streaming velocity are calculated using the equations available, for typical values of beam radius and intensity. Despite differences in the derivation of these equations the predicted streaming velocities are in surprisingly good agreement over a limited range of application. For completeness the equations to be used are repeated here.

1. Eckart solution (Equation 4.31)

$$u_2 = \frac{\alpha I}{\mu c} r_1^2 M$$

where M is a geometric factor related to the radius of the tube and the sound beam and I the acoustic intensity. This equation was derived for a nondivergent sound beam in a cylindrical tube of sufficient length for end effects to be neglected. The ends of the tube were considered to be closed so that no fluid could enter or leave the tube but the transmission of acoustic beam was unimpeded and a condition of zero mass flow through any cross section of the tube was applied. Inspection of Equation 4.32 shows that when the radius of the tube is infinite the value of M goes logarithmically to infinity and when the acoustic beam fills the tube ($r_1 = r_0$) M is equal to zero and no flow occurs. A value of $M \simeq 0.3$ is obtained when the radius of the beam is half that of the tube. Eckart obtained an order of magnitude estimate of streaming velocity by setting $M = 1$.

2. Tjøtta solution (Equation 4.34)

$$u_2 = \frac{2\alpha I}{\mu c} \frac{l^3}{L} .$$

The approximations of l = L = radius of the sound beam were suggested by Tjøtta to result in an order of magnitude estimate of the maximum streaming velocity. In this case the equation reduces to

$$u_2 = \frac{2\alpha I}{\mu c} r_1^2 . \qquad 4.37$$

Assuming a circularly symmetric beam, the acoustic power, W, may be substituted for intensity and beam area and the following expression obtained which permits an estimation of the average streaming velocity in the beam to be made from a measurement of total acoustic power

$$u_2 = \frac{W\alpha}{\pi\mu c} . \qquad 4.38$$

3. Nyborg solution

Nyborg (1953) suggested that the streaming velocity in a plane unbounded wave where the attenuation coefficient was $\ll 1$ could be obtained from the following equation

$$u_2 = \frac{(kr_1)^2 cb^*}{4} \left[\frac{U}{c} \right]^2 \qquad 4.39$$

where U was the velocity amplitude of the wave (given by $p/\rho c$) and k was the wave number. The term

$$b^* = \frac{1}{\mu} \left[\mu' + \frac{4}{3}\mu + \rho_0 R \right] ,$$

included relaxation effects. In the derivation of this equation the region considered was a long rectangular space in front of the transducer, equivalent in width to the acoustic beam and bounded at the sides by an acoustically transparent material. The streaming volume was assumed to be unbounded at the ends and surrounded by an infinite volume of identical fluid. Equation 4.28b (Nyborg, 1965) for flow in an open-ended channel can be expressed in the form

$$u_2 = \frac{\alpha I}{\mu c} r_1^2 M' \qquad 4.40$$

to give the streaming velocity on axis. This is identical to Equation 4.39 when M' is equal to 1 and relaxation effects are neglected.

Calculated values of axial streaming velocity for intensity levels and beam widths typical of diagnostic ultrasound applications and therapy ultrasound applications are shown in Table 4.1 and Table 4.2 respectively. In Equation 4.31 the beam radius was assumed to be a) half and b) a tenth of the vessel radius and in Equation 4.40 a) half and b) equal to the vessel radius. None of these solutions accurately model the experimental situation

described in Section 6.5 where the ratio r_1/r_0 was approximately 1/40 and the beam was effectively unbounded.

Solution due to:	Intensity mW cm^{-2}	r_1 mm	Frequency MHz	r_1/r_0	Velociy cm s^{-1}
Tjøtta	2000	1.5	3.5	-	1.9
(4.37)	50	1.5	3.5	-	0.5
Nyborg	2000	1.5	3.5	1.0	1.0
(4.40)	2000	1.5	3.5	0.5	3.0
	50	1.5	3.5	1.0	0.2
Eckart	2000	1.5	3.5	0.5	0.3
(4.31)	2000	1.5	3.5	0.1	1.7
	50	1.5	3.5	0.1	0.4

Table 4.1 Predicted streaming velocities in water in diagnostic ultrasound fields. r_0 is the radius of the vessel and r_1 is the radius of the beam.

Intensity mW cm^{-2}	r_1 mm	Frequency MHz	Velociy cm s^{-1}
5000	5	3	37.5
5000	5	1	4.2

Table 4.2 Predicted maximum streaming velocities (using Equation 4.37) in therapy ultrasound fields in water.

The use of the equations given above to calculate the velocity in diagnostic fields is not strictly valid for two reasons. Firstly no account is taken of beam focusing. To date no theory has been reported in the literature which predicts streaming velocity in a converging acoustic beam although the divergent situation has been considered. Secondly these

equations take no account of enhanced absorption occurring as a result of nonlinear propagation. The implications of this are discussed more fully in Chapter 7. (These limitations are less important for therapy beams which are generally unfocused and of lower amplitude, although some waveform distortion will occur in 3 MHz fields at high intensities.) A general limitation is that all the equations were derived for a diffraction free field although this may not be a significant problem because of the bulk nature of the streaming effect.

The following chapters report an experimental investigation of acoustic streaming in high amplitude, focused fields. In these fields enhanced absorption is shown to occur. This results in higher streaming velocities being generated than those predicted by the conventional theory reviewed in this chapter.

CHAPTER 5

EXPERIMENTAL ARRANGEMENTS

5.1 INTRODUCTION

This chapter deals with the experimental set-up and the equipment used to investigate streaming in water. Two circumstances were studied in which streaming occurred. Firstly a laboratory system was used with a commercial, diagnostic B-scan transducer driven by a radio-frequency power amplifier such that the pulsing regime could be varied systematically. Secondly the streaming produced in water by a number of commercial diagnostic systems was measured. Both of these experimental situations are described in this chapter. The methods used to observe the flow in water directly and to measure the flow velocities accurately are also described.

In addition to the flow measurements, the ultrasonic fields were characterised in terms of their acoustic pressures, intensities and beam widths. The equipment and techniques used to make these measurements are described.

5.2 ULTRASOUND GENERATION

5.2.1 Laboratory arrangement

Most of the experiments used a commercial B-scan transducer (Diagnostic Sonar, MD3483) with a resonant frequency of 3.5 MHz and a diameter of 19 mm. This transducer was weakly focused having a focal pressure gain of about 4 (see Appendix 1 for a definition of focal pressure

gain) and generated a maximum positive pressure in water at a range 9.5 cm from the transducer, at low drive levels. In subsequent discussion this distance is referred to as the focal length although it does not comply with the AIUM/NEMA (American Institute for Ultrasound in Medicine/National Electrical Manufacturers Association) standard definition of focal length (AIUM/NEMA 1983) which is given in Appendix 1. The error introduced by assuming that the focus occurs at the location of the peak positive pressure is discussed by Starritt and Duck (1983).

In the laboratory set-up the transducer was not shock excited but was driven at resonant frequency by an ENI (Electronic Navigation Industries Inc, New York) radio-frequency power amplifier together with a pulse generator (AMF International, model 728) and a gated oscillator (Wavetek 148A) which enabled the pulsing regime to be varied in a controlled fashion. Figure 5.1 shows a block diagram of the experimental arrangement for ultrasound generation.

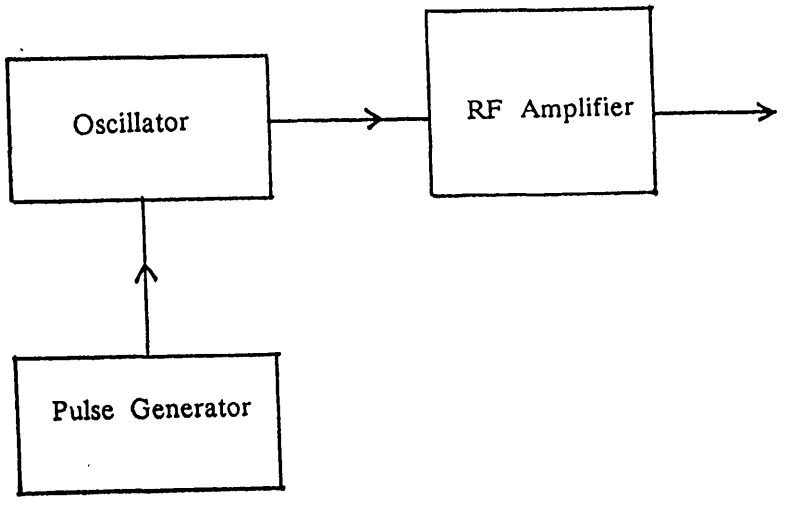

Figure 5.1 Experimental arrangement for generating ultrasound pulses which could be varied in a controlled way.

Control of the pulse repetition frequency and pulse length was provided

by the pulse generator while the frequency and amplitude were controlled by the oscillator. The transducer was coupled into a water-bath 50 cm x 20 cm x 15 cm containing freshly distilled water via a thin polythene end window.

5.2.2 Commercial Equipment

A number of commercial systems employing linear and phased array transducers were investigated in terms of their ultrasonic fields and the consequent streaming that they generated in water. In this case two methods of measuring acoustic beams were available. The first used the water-bath described above with the transducer either coupled through the end window using ultrasonic coupling gel, or where this proved difficult immersed in the water after suitable water-proofing. The second technique used an ultrasound beam calibrator which is described in Section 5.5.

With the commercial equipment, the maximum streaming velocity generated was measured for each unit and where appropriate the equipment was operated in imaging mode, in M-mode and in pulsed Doppler mode. In some instances two modes operated simultaneously and these occasions are indicated in the results. In making the measurements care was taken to ensure that the equipment was operating in such a way as to produce the maximum streaming velocity possible in that mode. In general this involved selecting a combination of the maximum acoustic pressure and the maximum output power. For pulsed Doppler mode it was found that these conditions could best be determined by firstly monitoring the total power using a radiation force balance and observing the effect of controls such as 'sample volume', 'velocity' and 'range gate' and their interaction with one another. Once the settings producing maximum output power were known, the maximum acoustic pressure amplitudes were measured under different

focusing conditions. Streaming velocity measurements were then made under conditions of maximum power, maximum amplitude and the highest combinations of the two available. The axial range and position of the anemometer probe was varied experimentally to find the maximum streaming velocity since the location of maximum velocity did not coincide with the position of maximum positive pressure.

5.3 VELOCITY MEASUREMENT USING DYES

5.3.1 Potassium Permanganate

The first observation of streaming in water due to diagnostic ultrasound beams used potassium permanganate as a dye. Figure 5.2 shows the experimental arrangement used for this investigation.

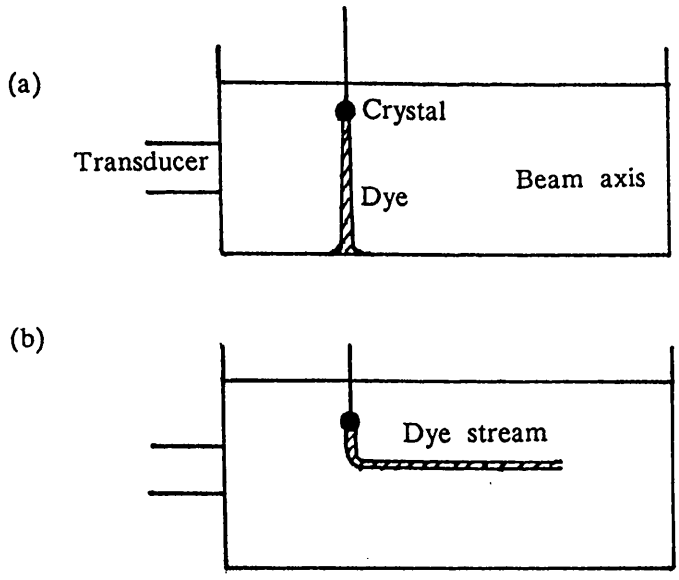

Figure 5.2 Location of a crystal of potassium permanganate in the field of a stationary beam viewed from the front of the water-bath; (a) no ultrasound, (b) ultrasound turned on.

A crystal of potassium permanganate was suspended in water above the beam axis of a 3.5 MHz transducer at approximately the location of the

focus. The ultrasound equipment was a Fisher Diasonograph 4200 static B-scanner and the transducer was a KB-Aerotech transducer (QSB 35DM), 13 mm in diameter. As the potassium permanganate dissolved, a narrow band of colour fell vertically in front of the transducer and was seen to be carried along the beam axis for some distance when the ultrasound beam was switched on.

Two methods were used to measure the streaming velocity using dye. Firstly, the path of the dye stream was timed over set distances using a stop watch. Secondly, a video of the flow against a background scale was made and analysed, using the frame advance facility on the video tape-recorder. The application of both methods was limited to a fairly narrow velocity range, from approximately 0.5 to 10 cm s^{-1}. The first method suffered from large errors at the higher velocities, associated with the use of the stop watch while the second method was slow and labour intensive. Some of these early results are presented in Section 6.3 for comparison with the results obtained subsequently by anemometry. The major usefulness of the dye technique was in providing a visual demonstration of streaming.

5.3.2 Thymol Blue

This provided a second qualitative method of observing flow but with the advantage that the release of colour was controllable and reversible. This technique was described by Quraishi and Fahidy (1982) and Merzbirch (1987) and involves the use of a pH indicator, thymol blue, dissolved in water. The range of colour change for thymol blue is between yellow at pH 8.0 and blue at pH 9.6. Electrolysis of the water was used to control the pH, producing a colour change adjacent to one electrode. Thus a neutral solution would become acidic near the anode and alkaline near the

cathode. In practice a slightly acidic working solution was used which was prepared by dissolving thymol blue (0.04% by weight) in distilled water. In order to increase the concentration of electrolytes a few drops of sodium hydroxide was added to produce a deep blue colour and the solution was then titrated by adding hydrochloric acid until a colour change was produced indicating that a slightly acidic solution had been reached. The colour change produced was deep orange/red rather than yellow due to the considerable volume of solution involved. The end point was not found to be particularly critical.

The experimental arrangement used to demonstrate streaming using thymol blue is shown in Figure 5.3.

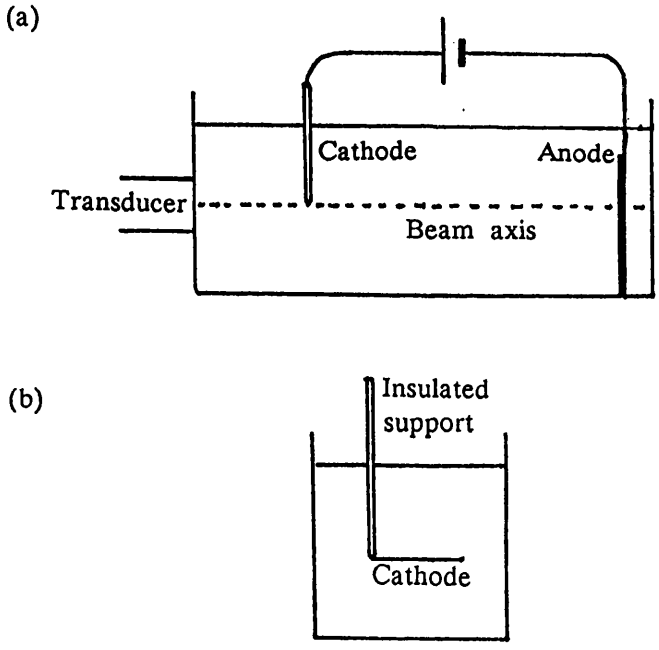

Figure 5.3 Electrodes positioned for demonstrating acoustic streaming using thymol blue indicator; (a) viewed from the front of the water-bath, (b) viewed from the end of the water-bath showing the 'L' shaped cathode.

A 'L' shaped platinum wire was used as the cathode, with the vertical arm of the 'L' being insulated and used as a support, and the horizontal

part positioned across the axis of a beam enabling flow profiles to be observed. The anode was a copper plate positioned at the opposite end of the water-bath from the transducer. Typically voltages of 6 V were applied between the electrodes at steady state currents of a few mA.

This technique was used primarily as a demonstation of flow and of flow profiles produced by different transducers. Results from a single B-scan transducer, a linear array imaging system and a single crystal physiotherapy unit are presented in the next chapter. The advantage of this demonstation was that, because the blue dye consisted of thymol blue ions in solution, the flow was convincingly shown to be fluid flow rather than particle movement within the fluid.

Some measurements of streaming velocities generating in water at 1 MHz and 3 MHz by a Therasonic 1030 physiotherapy unit were attempted. The problems associated with making these measurements are described more fully in Section 6.14.

5.4 VELOCITY MEASUREMENTS USING ANEMOMETRY

The dye techniques described above were useful in demonstrating the presence of streaming in a fluid. However to make accurate measurements of the streaming velocity a different technique was required and quantitative measurements were obtained by anemometry.

5.4.1 Description of the anemometer

The principle of hot wire anemometry measurement is that of measuring heat loss from an electrically heated probe, caused by the flow of fluid surrounding it, in order to estimate the flow velocity (for example Goldstein, 1983). In this investigation a commercial anemometer unit (DISA

type 55DO1) was used in conjunction with a TS1 liquid hot film probe (1210-20w). The probe was connected to the anemometer forming part of a Wheatstone bridge as shown in Figure 5.4.

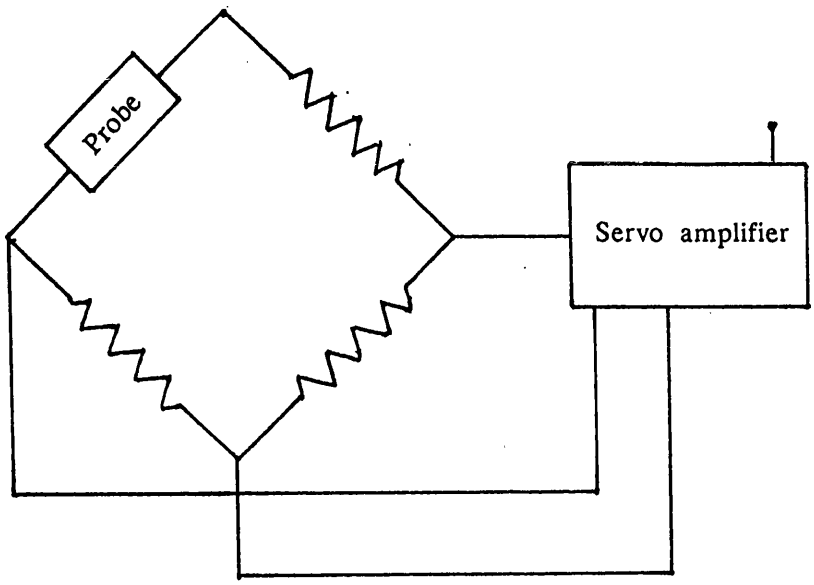

Figure 5.4 Schematic diagram of the basic anemometer circuit.

The probe was operated at a constant temperature using a feedback technique whereby current flowed from a servo amplifier to heat the probe, the amount of current being controlled by the bridge imbalance. This maintained a constant probe temperature and therefore a constant operating resistance. The voltage at the bridge top was proportional to the current flowing and was measured using a digital voltmeter.

The anemometer probe is shown in Figure 5.5. The sensitive tip consisted of a 51 μm diameter platinum wire deposited on a quartz substrate and electrically insulated for use in water by a quartz coating. The active length of the probe was 1 mm.

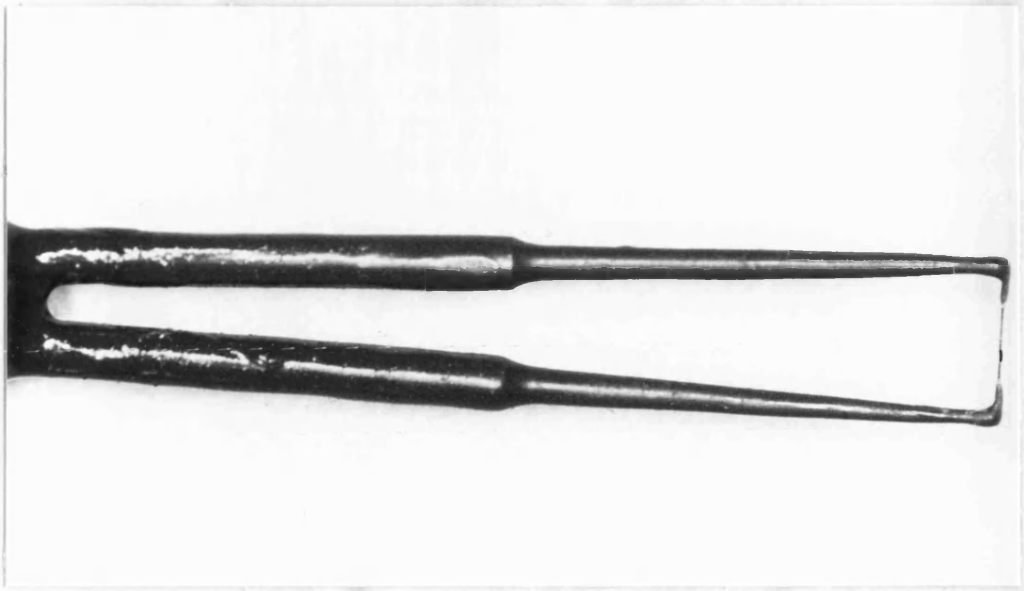

Figure 5.5 Anemometer probe.

Several different probes were used in these experiments but typically the temperature coefficient of resistance was of the order of 0.001 $\Omega\,^{0}C^{-1}$. An operating temperature of 50 ^{0}C was chosen as a compromise between the need for sensitivity and the need to avoid bubbles forming on the probe. Bubbles had a tendency to form even when distilled water was used and was renewed regularly. Their presence on the wire caused the static voltage to rise and the response of the probe to be reduced. At 50 ^{0}C the operating resistance of the probes used was in the range 5.11 Ω to 5.77 Ω. In use the probe support was mounted perpendicular to the beam and the probe tip was aligned with the transverse axis of the beam. The probe support was designed to cause minimal disturbance to the flow. It was important to ensure that no moisture entered the plug and socket connection between the probe support and the probe, since this caused the operating voltage to be unstable. For this reason the probe was mounted in such a way that the connection was clear of the water. Even so the output voltage was occasionally unstable but this could generally be improved by remounting the

probe in the support.

Figure 5.6 shows the complete measurement system.

Figure 5.6 Experimental measurement set-up in use showing anemometer, water-bath and pulse generation system.

5.4.2 Calibration of the anemometer

The relationship between the amount of heat removed per unit time, Q, and the flow velocity, u, was formulated by King (1914),

$$Q = A + B(u)^n \qquad 5.1$$

where A and B are constants. The exponent n was found experimentally to be in the range 0.4 to 0.5 over a wide range of Reynolds' numbers from 0.1 to 10^5. For constant temperature operation the power supplied to the probe is equal to the heat loss and is related to the anemometer output voltage, V, by

$$V^2 = A' + B'(u)^n \qquad 5.2$$

where A' and B' are new constants.

One possible method of calibrating an anemometry system is by measuring a known velocity of flow due to a constant head of water. This method was not suitable for the velocities of interest because a very low pressure head would be needed to produce the required flow. Instead each hot film probe was calibrated in water by mounting it on a micro-computer controlled translation stage and towing it through a tank of distilled water at a range of velocities between 0.3 cm s^{-1} and 11 cm s^{-1}. The tank was 2 m long which allowed the probe to be accelerated to, and remain at, a constant velocity for the duration of the measurement. This method is described by Saunders and Lawrence (1972) for calibration of hot-film probes in water for the velocity range 1 cm s^{-1} to 300 cm s^{-1}.

Three separate readings were recorded at each velocity. For each, the probe was towed in one direction along the tank and then the direction was reversed. Readings were recorded separately in order to check the directional sensitivity of the probes and it was found that the difference between them never exceeded 0.5%. The calibration depends on the viscosity, thermal conductivity, pressure, density and temperature of the calibration fluid. For this reason the water temperature in the tank was monitored throughout the calibration procedure and if it varied, a correction was applied in the way described in Section 5.4.3. Measurements were made alternatively at a high and a low velocity (within the range of interest) so that any drift in the system would be apparent. In addition to minimise the effects of thermal instability the anemometry electonics (but not the probe) were always switched on for half an hour prior to use. The calibration data for a typical probe (serial number 82026) is tabulated in Table 5.1.

u ($cm\ s^{-1}$)	T (^0C)	V^+ (V)	V'^+ (V)	V^- (V)	V'^- (V)
5	20.2	9.64	9.67	9.66	9.69
10	20.0	10.90	10.90	10.90	10.90
2	19.9	8.24	8.22	8.29	8.28
7	19.8	10.30	10.20	10.30	10.20
1	19.7	7.33	7.29	7.43	7.39
9	19.7	10.70	10.60	10.70	10.60
4	19.7	9.34	9.29	9.37	9.32
8	19.6	10.50	10.40	10.60	10.50
3	19.5	8.89	8.83	8.95	8.89
11	19.4	11.10	11.00	11.10	11.00
6	19.4	10.00	9.91	10.10	9.97
0.5	19.4	6.60	6.53	6.67	6.68
1.5	19.3	7.92	7.83	7.96	7.87
2.5	19.3	8.65	8.55	8.70	8.60
3.5	19.2	9.19	9.07	9.19	9.08

Table 5.1 Calibration data for anemometer probe; V^+ and V^- are the mean voltages in the positive and negative direction respectively, V' is the voltage corrected to the reference temperature, u is the velocity and T is the temperature of the fluid at the time of the measurement.

Figure 5.7 shows the calibration curve obtained from this data. This graph was used to convert directly from measured values of anemometer voltage to velocity in the experiments described in Chapter 6. In Figure 5.8 the data is replotted as $u^{0.5}$ verses V^2. A linear regression (Mould, 1989) was performed to obtain the best fit to the data points and this is represented by the solid line. Individual data points were very reproducible and for this reason it was thought that deviations from a linear relationship shown in Figure 5.8 although small, represented the true response of the probe.

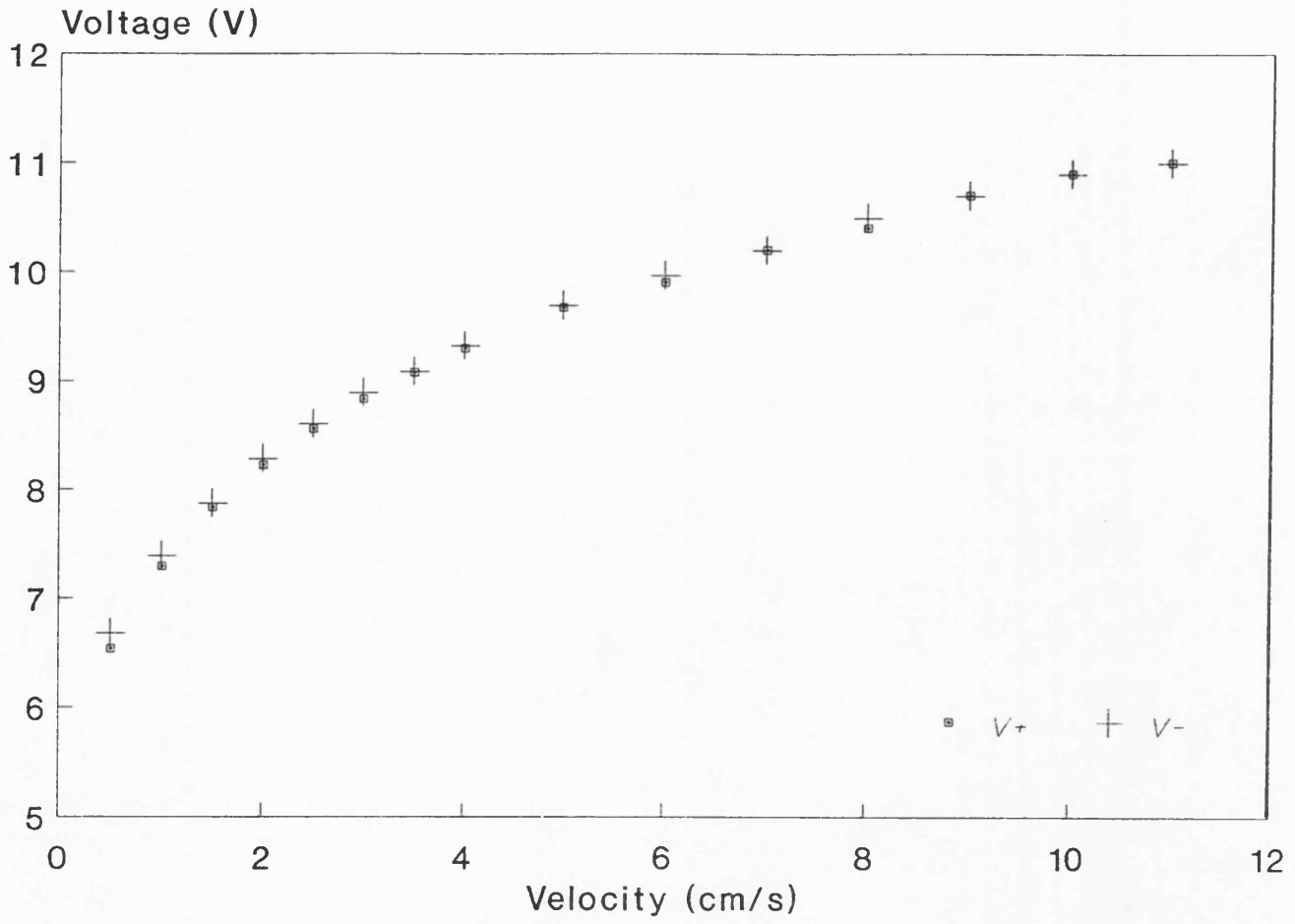

Figure 5.7 Anemometer calibration at 20°C.

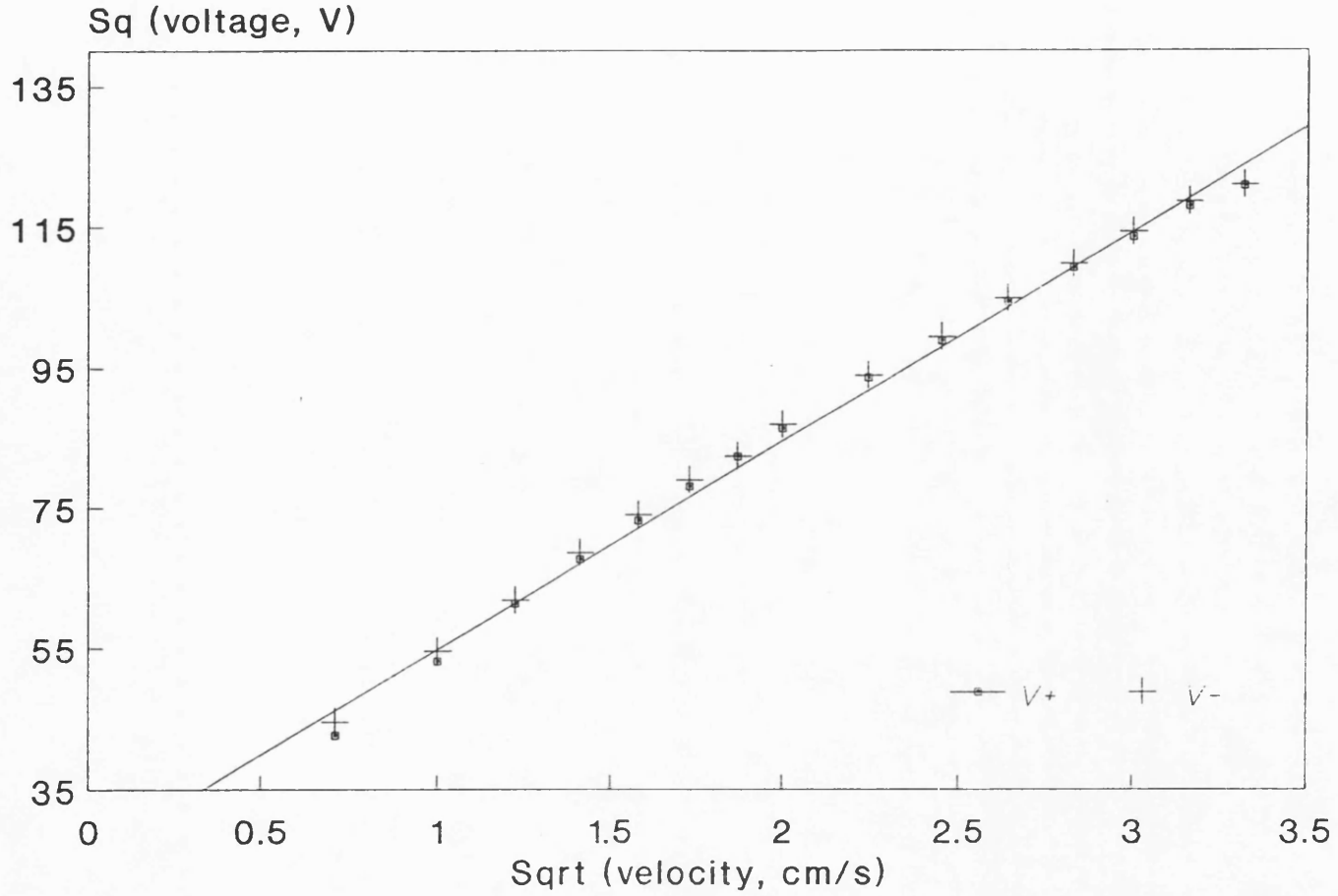

Figure 5.8 Fit of V^2 as a funtion of $u^{0.5}$; regression coefficient 0.997.

Use of Figure 5.7 for converting from voltage to velocity avoided the error introduced by assuming a constant value of 0.5 for n throughout the velocity range of the calibration. Davies and Patrick (1972) have reported a range of values for n required to adequately represent experimental data over various velocity ranges.

In order to ensure that the probe response remained stable following calibration, a set of conditions were established using the laboratory ultrasound exposure arrangement which could be easily reproduced and which generated thereafter a known output voltage for a known acoustic power. This check on the probe calibration was carried out prior to each experiment. If the expected output voltage was not obtained the performance of the ultrasound system was first checked by measuring the acoustic power and if necessary the probe was recalibrated. On one occasion the sensitivity of a probe changed abruptly during use and when recalibration was carried out it was found that the sensitivity was lower than previously measured. This was thought to be due to contaminants adhering to the sensitive portion of the probe thus providing thermal insulation. The probe response was subsequently stable at the new level. The effects of the accumulation of dirt on hot film sensors has been described by Morrow (1972).

5.4.3 Temperature correction of anemometer readings

The voltage measured at the anemometer output at one temperature is related to that at another temperature through the equation (Saunders and Lawrence, 1972),

$$\frac{V(T)}{V(T_0)} = \left[1 - \frac{T - T_0}{T_P - T_0} \right]^{0.5} \qquad 5.3$$

where T_P, the probe temperature was 50 °C in these experiments, T_0 is the

reference temperature of the fluid, and T is the fluid temperature.

For small changes, ΔT, in temperature, the voltage ratio is given approximately by

$$\frac{V(T)}{V(T_0)} = 1 - \Delta T\ M \qquad 5.4$$

where $\Delta T = T - T_0$ and

$$M = 2(T_P - T_0)^{-1} \qquad 5.5$$

is constant for a given probe temperature and reference temperature. Inherent in this equation is the assumption that the term $\Delta T^2 M^2$ may be neglected for small ΔT. In practice this introduced an error in the voltage ratio of 0.5% for a 5°C temperature change. Equation 5.4 may be rearranged to give

$$V(T) = V(T_0) - \Delta T\ M\ V(T_0) \qquad 5.6$$

where the terms $V(T_0)$ and $MV(T_0)$ are constant. This relationship was tested experimentally by measuring the static output voltage as a function of temperature. The probe was positioned in a beaker of degassed water in a water-bath at 25°C. Pairs of temperature and voltage values were recorded as ice was added to the water-bath to reduce the temperature. Table 5.2 contains experimental data which are plotted in Figure 5.9. A linear regression was performed on the data to obtain values for $V(T_0)$ and M. The regression line, for which the correlation coefficient was 0.997 is also shown.

The value of M obtained from this graph was $0.014\,^{\circ}C^{-1}$ whilst the value given by Equation 5.5, assuming $T_P = 50\,^{\circ}C$ and $T_0 = 20\,^{\circ}C$ was $0.0167\,^{\circ}C^{-1}$. To apply a temperature correction to the results obtained with other anemometer probes of the same type it was decided to use the value of M calculated from Equation 5.5 rather than determining M experimentally for each new probe.

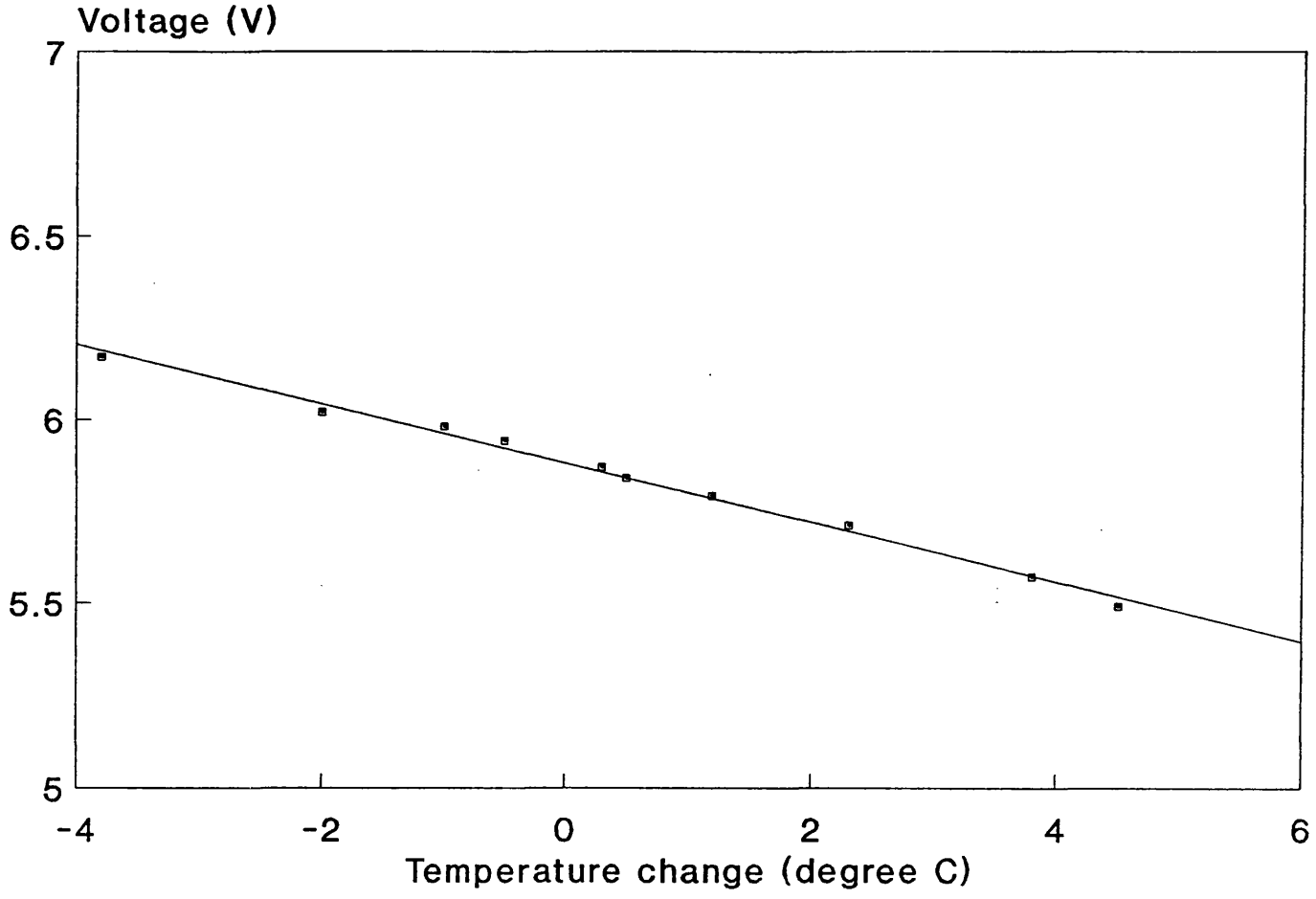

Figure 5.9 Temperature dependance of anemometer output voltage relative to 20°C; operating temperature of probe 50°C.

T (°C)	ΔT (°C)	V (V)
24.5	4.5	5.49
23.8	3.8	5.57
22.3	2.3	5.71
21.2	1.2	5.79
20.5	0.5	5.84
20.3	0.3	5.87
19.5	−0.5	5.94
19.0	−1.0	5.98
19.0	−2.0	6.02
16.2	−3.8	6.17

Table 5.2 Values of output voltage at a range of fluid temperatures (T_0 taken as 20 °C).

Use of a calculated value for M rather than the experimental value introduced an error which was maximal at large values of ΔT and small values of $V(T_0)$. For one probe (serial number 82026), at ΔT = 5 °C and $V(T)$ = 5.5 V, the error in velocity introduced by this was estimated to be approximately 1.5%. However in practice no experimental results were obtained for which the value of ΔT exceeded 2.7 °C.

In the experiments described here, measurements were made at different temperatures depending on the environment, and each voltage measurement was corrected to the voltage at the reference temperature. This was defined as the temperature at which the calibration had been carried out (in general 20 °C). After correction the calibration curve was used to relate voltage to streaming velocity.

5.4.4 Use of a lineariser unit to measure time constants

Measurements of rise times and decay times were made for the streams investigated. For these measurments a lineariser unit (DISA 55D10) was used. This unit electronically corrected for the nonlinear dependence of output voltage on flow velocity and produced an output which was directly proportional to flow velocity. The linearised voltage was displayed on a digital oscilloscope (Gould DSO 1602) and measurements were made from the screen.

Details of the linearisation process are given in DISA Instruction and Service Manual (1970) and are only outlined here. The lineariser functions as an electronic analogue computer which linearises the anemometer output voltage using the function

$$V_l = K(V^2 - A)^m \qquad 5.7$$

where V_l is the linearised voltage, and K and A are constants.
Sustituting this relationship in Equation 5.1 and setting m equal to 1/n gives

$$V_l = ku \qquad 5.8$$

where k is a new constant.

For appropriate selection of the exponent, m, the output voltage is proportional to the flow velocity. An approximate value of m was obtained by calculation based on the calibration data, shown in Table 5.1. A double logarithmic plot of the function $((V/Vs)^2-1)$ against u was used, where V_s was the output voltage at zero velocity obtained by extrapolation from the data points. The slope of the curve was equal to m.

The value of m obtained by this method was optimised by systematically varying the value set by small amounts and checking output voltage linearity at known flow velocities. Once the optimum setting had been found the probe was calibrated by the method described in

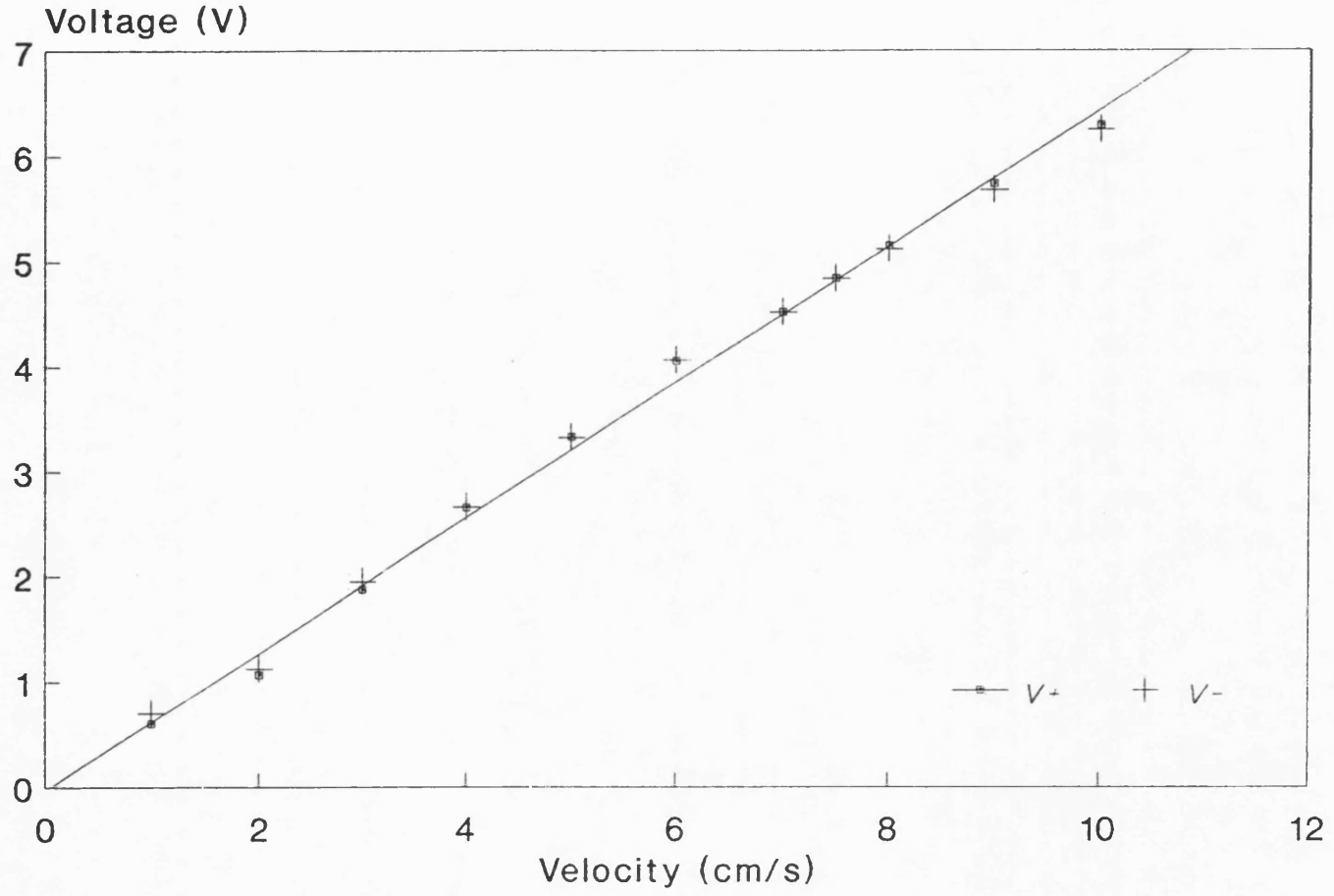

Figure 5.10 Anemometer calibration with lineariser.

Section 5.4.2 with the addition of the lineariser in the circuit. The resulting calibration line is shown in Figure 5.10.

Rise times and decay times were measured for a number of acoustic beams with different beam diameters and generating a range of streaming velocities. The variation in these parameters at differing locations in the acoustic field was also recorded. A single exponential character was assumed for the rise and fall of streaming velocity, and the rise time, τ_R, was defined as the time taken for the velocity to reach a value (1−1/e) of the maximum. Similarly, the decay time, τ_D, was defined as the time taken for the velocity to fall to 1/e of the maximum after the acoustic beam is switched off. Inbuilt cursors on the oscilloscope were used to make direct measurements of rise times and decay times on the stored display of the linearised voltage.

The calibration accuracy of the voltage and time scales on the oscilloscope was estimated to be ±3%. An additional error in the time constant measurement was introduced by the assumption of an exponential increase in velocity. In practice the increase appeared to deviate from an exponential on some occasions (see Figure 6.25). For the rise time measurement, this error was estimated to be about ± 10%.

5.4.5 Frequency response of the system

The frequency response of the electronics was tested by applying a sinusoidally varying test signal. A terminal was available on the anemometer electronics unit for the input of such a signal. This varied the electrical power applied to the probe in order to mimic changes in flow velocity. A signal of constant amplitude, varying in frequency from 1 Hz to 400 kHz was applied and the amplitude of the voltage at the bridge top recorded. The oscilloscope was d.c. coupled throughout. Figure 5.11 shows the

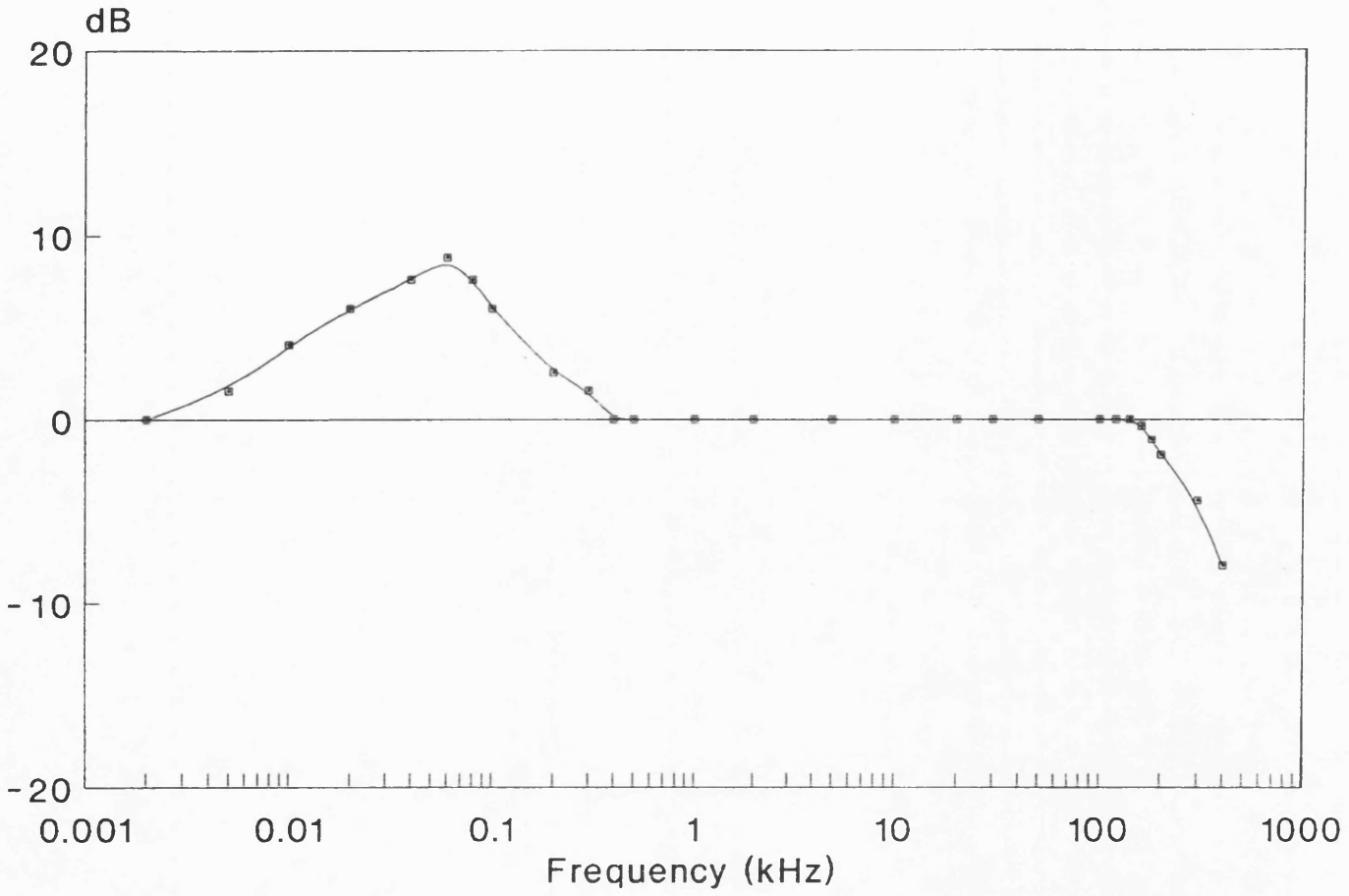

Figure 5.11 Frequency response of anemometer electronics.

variation in the ratio between input and output voltage (in dB) as a function of frequency. The upper frequency limit, at which the output voltage was 3 dB down, was 220 kHz. The upper frequency limit of the hot film probe was quoted by the manufacturers to be 250 kHz which is comparable to the response of the electronics. In the experiments carried out the acoustic beam was pulsed with pulse repetition frequencies of 500 Hz to 20 kHz. These frequencies are clearly within the frequency response of the system but, when the anemometer output voltage was observed on an oscilloscope, no component corresponding to the pulse repetition frequency was observed. A simple calculation based on the time taken for a stream to decay showed that any modulation due to the pulse repetition frequencies used lay within the measurement noise. For example, at a pulse repetition frequency of 500Hz and a decay time of 0.5 s the output voltage will be reduced from 9.3 V to 9.27 V between consecutive pulses. Figure 5.12 shows a simple representation of the situation under consideration. The frequency of the acoustic wave at 3.5 MHz was well beyond the resolution capability of the system.

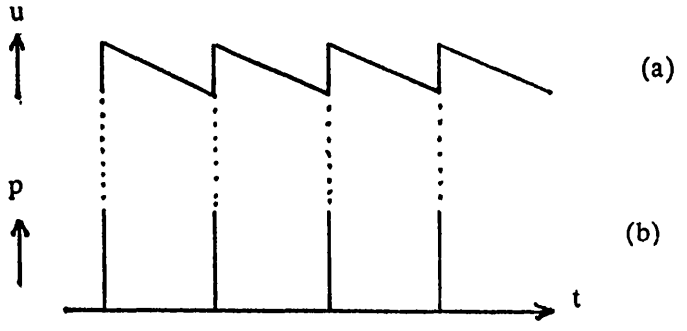

Figure 5.12 Speculated response of the stream to the acoustic pulse repetition frequency; (a) represents the velocity response to the acoustic pulses represented by vertical lines in (b).

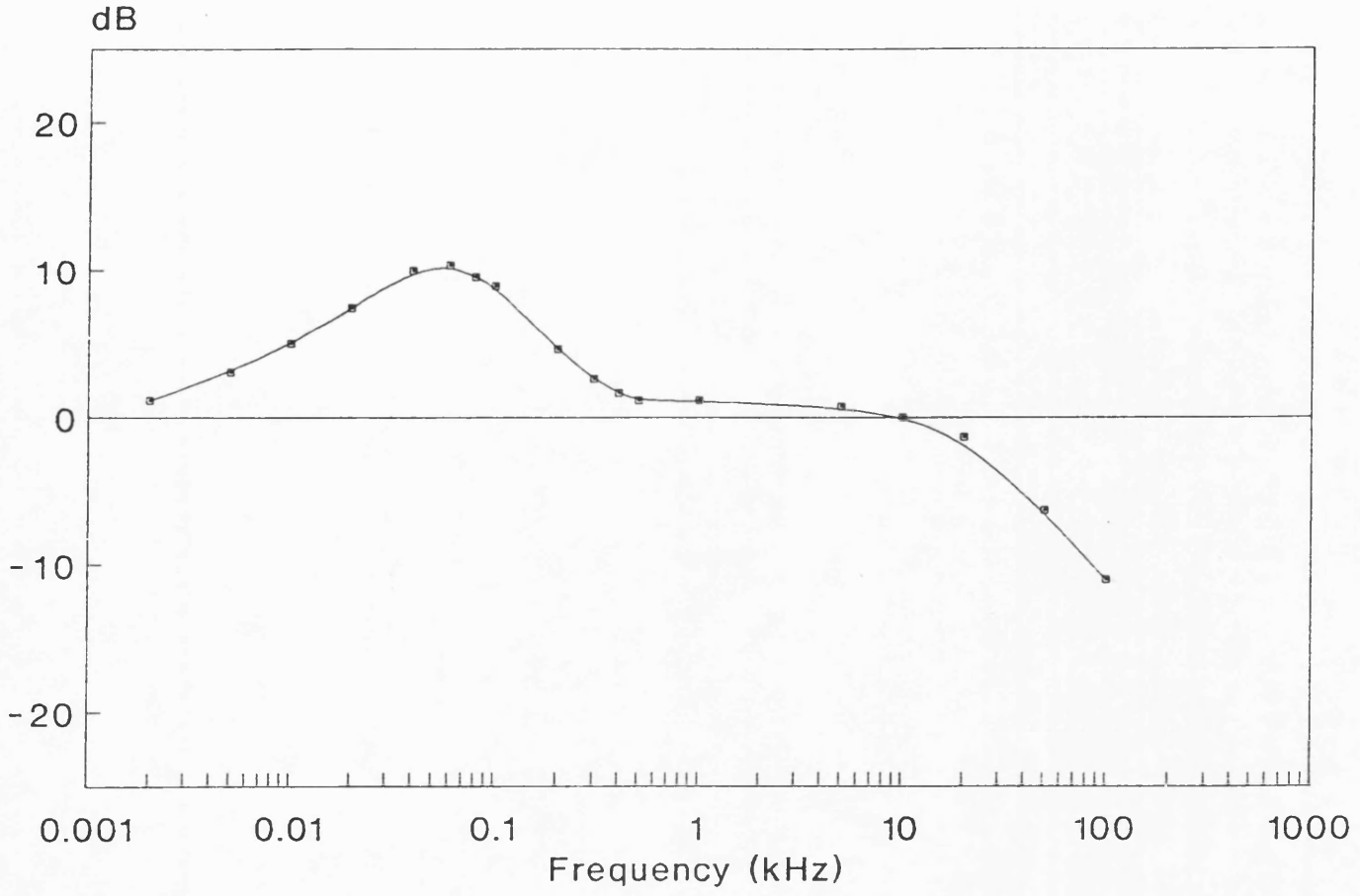

Figure 5.13 Frequency response of anemometer electronics including lineariser.

The frequency response was also measured with the lineariser unit connected. In this case the upper frequency limit of the system was reduced to 30 kHz. The result of this measurement are shown in Figure 5.13.

5.5 ACOUSTIC FIELD MEASUREMENTS USING AN ULTRASOUND BEAM CALIBRATOR

The acoustic beams responsible for generating streaming were characterised using an ultrasound beam calibrator. This system was developed by the National Physical Laboratory and is described in detail by Preston (1988). It enabled fast, accurate measurements to be made on scanning systems such as linear and phased arrays, as well as single element transducers and physiotherapy beams. Although the ultrasound beam calibrator is a commercial system it is felt appropriate to describe it in some detail here.

5.5.1 Description of the ultrasound beam calibrator

The system consists of five parts as shown in the block diagram in Figure 5.14. The components are listed here:-

1. Test Tank
2. Hydrophone Array
3. Digitising unit
4. Computer
5. Printer

The polycarbonate test tank was 30 cm in diameter and 30 cm deep and contained the hydrophone assembly submerged in distilled water which served as the transmission medium. Mounted above the tank, a positioning

rig held the transducer, with the beam pointing vertically down towards the hydrophone, while at the same time allowing horizontal translation in two orthogonal directions in order to maximise the signal from the hydrophone.

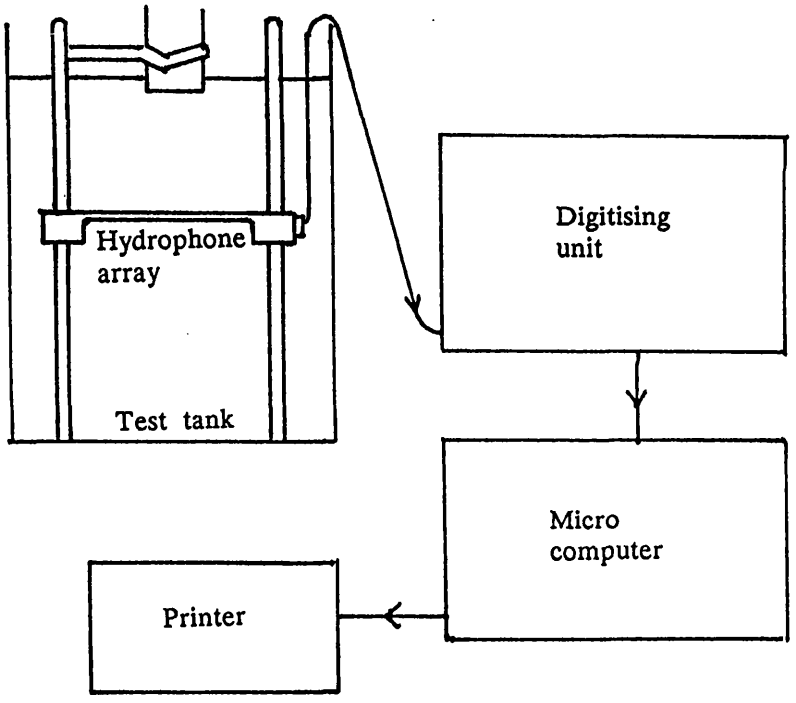

Figure 5.14 Block diagram of the main components of the ultrasound beam calibrator system.

The transducer could be rotated about its central axis and thus about the centre element of the hydrophone array. The distance between the transducer face and the measurement plane of the hydrophone was variable from 0.5 cm to 30 cm. An acoustic absorber was placed in the bottom of the tank to minimise reflections. It was essential that the hydrophone was tilted by more than 90^0 each time the tank was refilled with water in order to allow the air trapped beneath it to escape. The ability to tilt the hydrophone was also important in reducing the effects of reflections from the membrane when continuous wave beams were measured.

The hydrophone assembly consisted of a bilaminar, shielded, polyvinyldene fluoride (pvdf) membrane hydrophone having 21 active

elements. These circular elements were 0.5 mm in diameter and their centres were spaced at distances of 1 mm. Both pvdf layers were 0.025 mm thick. The housing of the hydrophone assembly contained 21 broad-band unity gain amplifiers (band-width >30 MHz) and a multiplexer which enabled a particular channel of interest to be selected. The basic design of the hydrophone array was similar to that described for a single element hydrophone in Section 5.6.1.

The multiplexed analogue signal was fed into an amplifier module contained within the digitising unit. An overall gain of between 0 dB and 59 dB in steps of 1 dB was available at this stage. The response of the individual amplifiers was normalised by the manufacturers using a series of variable gain amplifiers in order to compensate for differences in the overall sensitivities of the hydrophone/amplifier channels. This was necessary for two reasons. Firstly, a difference of up to 20% existed between the hydrophone elements at the centre of the array and those at the ends due to variations in the capacitative loading. The greatest contribution to this was due to the electrode leads on the membrane which were shorter for elements at the edge of the array, resulting in these elements having a higher sensitivity. The second reason was the variation in the input capacitance of preamplifiers and in the gain of amplifiers and multiplexers used in the system.

The acquisition module sampled the analogue data at a rate of 60 MHz with a resolution of 8 bits, although it was possible to reduce the digitisation rate in certain circumstances. Acquisition frame sizes of 128 and 256 were both used as appropriate. A trigger, corresponding to the generation of an ultrasonic pulse by the transducer, was required in order to initiate data acquisition and three different methods of triggering were used. For commercial systems a trigger signal was normally obtained from an electomagnetic pick-up coil positioned close to the transducer. Under

laboratory conditions the trigger was obtained directly from the pulse generator, and for continuous wave beams the calibrator was internally triggered. The signals received from the hydrophone after an appropriate delay, were digitised and stored sequentially in electronic memory. Waveform data corresponding to the largest peak profile was stored in a separate memory of 21 blocks of 128 or 256 bytes and used for determination of the acoustic parameters.

Measurement procedures were controlled through an IBM personal computer and the software, which was supplied as part of the system, used menu-based subroutines. In the display mode, a real-time plot of peak positive or peak negative pressure for each hydrophone element, together with a plot of the pressure-time waveform for one element (normally the centre element), were displayed adjacent to each other on the screen. Digital display of peak acoustic pressure, the integral of the modulus of pressure and the pulse repetition frequency were also available on the screen. Either of the first two could be used to maximise the acoustic signal during the setting-up procedures.

Once acquisition was complete and the peak profile data from a selected element stored in memory, post-processing could be carried out. A range of measured and calculated parameters were displayed and printed, only some of which were relevant to the experiments described here and these are listed below:-

Peak positive acoustic pressure, $\hat{p}^+$

Peak negative acoustic pressure, $\hat{p}^-$

-6 dB beam width

Spatial peak temporal average intensity, I_{spta}

Spatial peak pulse average intensity, I_{sppa}

Definitions of I_{spta}, I_{sppa} and pressure squared integral are given in Appendix 1.

5.5.2 Accuracy

Preston (1988) discussed the accuracies of this system in detail and his conclusions are summarised here. One major source of error was in the calibration of the hydrophone. The system was calibrated at the National Physical Laboratory by comparing its response to that of a single element reference hydrophone over a range of frequencies. For this procedure the amplifier gain was set to 40 dB and a low amplitude wave, $\hat{p}^+ < 100$ kPa, was used to avoid waveform distortion due to non-linear propagation. Any difference between true acoustic pressure and the value indicated was eliminated by adjustment of the amplifier gain. Once the central hydrophone channel had been calibrated all other channels were adjusted to the same sensitivity. The overall uncertainty in the calibration increased with frequency, from ± 8% at 2 MHz to ±17% at 15 MHz. Although slightly lower sensitivity was found at low and high frequencies relative to 10 MHz, the frequency response of the system was flat to ±1 dB up to 20 MHz. A further source of potential error was the band-width of the system. The high frequency response was important for this work because measurement of highly distorted pulses containing high frequency components were commonly made. Further sources of error were hydrophone rotation, spatial averaging over the area of an active element and digitisation resolution. The consequences of spatial averaging caused by finite element size were investigated theoretically by Beissner (1985) who derived formulae for estimating the maximum permissible hydrophone radius as a function of ultrasonic wavelength and the distance from the source. The errors in a number of acoustic parameters due to each of these sources are shown in Table 5.3 taken from Preston (1988) for a 3.5 MHz scanning system. Each of the acoustic parameters in this table was derived from measurements on a single pulse and hence the uncertainties tabulated are also valid for a

stationary beam.

Source of uncertainty	Percentage uncertainty in: $\hat{p}^+$	$\hat{p}^-$	Beam width	I_{sppa}	I_{spta}
Calibration	8.5	8.5	-	17	17
Bandwidth	14	-	13	19	19
Digitisation	2	2	4	4	4
Averaging	5	2	10	8	8
Tilt	0.4	0.4	0.4	0.8	0.8
Gain	7	7	7	14	14
Total	22	13	22	36	30

Table 5.3 Typical values for uncertainties (95% confidence level) in selected acoustic parameters measured using the ultrasound beam calibrator for an automatic scanner operating at 3.5 MHz (Preston 1988).

5.5.3 Use of the beam calibrator with commercial ultrasound systems

The ultrasound beam calibrator was used to measure the acoustic beams from commercial systems in order to predict the control settings and locations in the field which would result in maximum streaming velocity. The procedure is described in Section 5.2.2. Each transducer was fixed in the mounting clamp and moved horizontally in 2 dimensions above the hydrophone array until the pressure signal was maximised. A delay was set which allowed a signal to be received some time after the receipt of a trigger pulse, to allow for transmission of the ultrasound through the water. Pulsed Doppler and M-mode beams were generally easy to measure, although some Doppler systems were found to operate at pulse repetition frequencies greater than 8 kHz, the limit of the system's ability to analyse

every pulse. In this case it was necessary to select a trigger factor greater than 1. For example a factor of 2 was used for a pulse repetition frequency between 8 kHz and 16 kHz and the system then sampled every other pulse but calculated the time average intensity assuming all the pulses were present. Doppler systems were also found commonly to employ long pulses under certain conditions, and in order to measure these it was necessary to use a frame size of 256 and to reduce the digitisation rate to 30 MHz or lower. For example the ATL Ultramark 8 scanner with a PV10 5 MHz Doppler transducer employed a range of pulse repetition frequencies up to 25 kHz, and at 20 mm sample volume the pulse length was 12.5 μs.

For scanning ultrasound systems the ultrasound beam calibrator required the number of lines per frame to be entered. This enabled the system to measure pulses from one transducer element only whilst retaining information about the total number of pulses and the beam overlap factor for calculation of intensity parameters.

5.5.4 Errors in gain settings

It has been stated that adjustable gain was available on the ultrasound beam calibrator, but in fact the system operated with a constant gain amplifier and selection of "gain" on the front panel actually introduced different levels of attenuation. Pushbutton attenuators introduced attenuation in 10 dB steps from 10 dB to 50 dB, and in 1 dB steps from 0 dB to 10 dB with push buttons labelled 1 dB, 2 dB (two of these) and 4 dB. To check the accuracy of these attenuators a sinusoidally varying, continuous wave radio-frequency signal was introduced into the amplifier unit using the socket normally employed for connecting the multiplexed signal from the hydrophone. The calibrator was operated in continuous mode and the peak positive pressure was recorded for different gain settings. It was found that

the error on the set value was cumulative with the number of push buttons used to obtain the required attenuation. For example 15 dB could be entered as 10+4+1 dB, a total of 3 buttons, or as 10+2+2+1 dB requiring 4 buttons. The error was greater in the latter case due to amplifier loading. The excess attenuation introduced by different combinations of push buttons is shown in Table 5.4 In practice the number of pushbuttons selected was limited to two in order to reduce this source of error.

Number of buttons	Loss (dB)
1	0
2	0.37
3	0.65
4	0.93
5	1.15

Table 5.4 Error in attenuation due to the number of gain push buttons selected relative to the selection of a single button.

5.6 ACOUSTIC BEAM MEASUREMENTS USING A HYDROPHONE

A single element hydrophone connected to a Hewlett Packard digitising oscilloscope (54200A) was used to make measurements on the beams generated by the laboratory set–up. The waveforms were analysed using a Hewlett Packard 216 micro–computer and the following parameters were calculated:–

Peak positive pressure,

Peak negative pressure,

Beam radius,

Spatial peak temporal average intensity (I_{spta}),

Spatial peak pulse average intensity (I_{sppa}).

In addition, Fourier analysis of the waveforms was carried out to determine the levels of harmonic components present.

5.6.1 The hydrophone

The pressure waveforms generated in water were measured using a coplanar, screened, polyvinylidene fluoride (pvdf) membrane hydrophone (GEC-Marconi Electronics Ltd). The design and development of polymer hydrophones has been described by Shotton *et al.* (1980) and DeReggi *et al.* (1981). The sensitive area of the hydrophone used in these measurements was 0.5 mm in diameter and the pvdf membrane was 9 μm thick. In the construction of this type of hydrophone the membrane is stretched over an annular frame 100 mm in diameter, which is large enough not to perturb the acoustic field. Gold film electrodes are evaporated onto each surface of the pvdf membrane so that they are overlapped only in a small central area. This area becomes piezoelectrically active when the device is poled at a raised temperature. Electrical radio-frequency pickup is reduced by gold electrodes surrounding the active element which are connected to the screen of the coaxial cable and an earthing pin on the supporting frame. One of the advantages of this type of hydrophone is its broad band frequency response which allows high amplitude distorted pressure waveforms to be measured accurately. Another advantage is that it causes minimal disturbance of the acoustic field. At 10 MHz, 95% of the beam impinging on the membrane is transmitted (Preston *et al.*, 1983).

Hydrophone measurements were made in the perspex tank described in Section 5.2.1 which contained distilled water. Distilled water was essential because tap water provided a conductive path by which charge leakage from the element could occur, resulting in a significantly reduced sensitivity. It

was also necessary to ensure that the hydrophone was submerged to a constant depth in the water since the sensitivity changed if the water did not cover the membrane. This effect occurred due to a change in the capacitative loading associated with the electrode leads which was dependent on the height of the water. The hydrophone was mounted on a micromanipulator which allowed its position to be located in three orthogonal directions to 0.1 mm. No controllable rotational movement was used on either hydrophone or transducer. Great care was taken to ensure that the hydrophone was accurately aligned with the acoustic axis. Firstly the hydrophone and transducer were approximately aligned by eye and the hydrophone position adjusted perpendicular to the beam in order to maximise the received signal. The axial position of maximum positive pressure was then located. By noting this position and also the on–axis location a further 3 cm distant from the transducer, it was possible by iterative adjustment of the respective positions of transducer and hydrophone to achieve accurate alignment.

A preamplifier was attached to the hydrophone cable and this in turn was connected to the oscilloscope. The preamplifier was a vital part of the measurement system. It was designed, built and tested in the Medical Physics Department of the Royal United Hospital by Michael Perkins. The main component is an integrated circuit (National LH0033CG). Dual field effect transistors (U440) provide a high input impedance in excess of 10 MΩ. The amplifier has unity gain and its frequency response is broad–band with a −3 dB reduction occurring at about 80 MHz. In connecting the hydrophone to the amplifier a short cable (15 cm) was used for two reasons. Firstly in order to minimise cable resonances which would be amplified by the broad band response of the 9 μm film. Since the resonant frequency is inversely proportional to the cable length, the resonant frequency will exceed the response of the hydrophone if a short cable is

used. For example, a hydrophone cable 65 cm long shows a broad resonance centred at 70 MHz (Bacon 1982). Secondly, a short cable minimised the reduction in sensitivity due to cable capacitance. Use of the pre-amplifier allowed easy connection between hydrophone and oscilloscope.
A detailed description of the performance characteristics of pvdf membrane hydrophones has been given by Bacon (1982) and Preston *et al.* (1983). Results specific to the 9 μm film are quoted here. Experimental evaluation of the frequency response of this type of hydrophone showed resonances in the sensitivity at 75 MHz and 95 MHz, compared with a resonance at 40 MHz for a 25 μm thick membrane. Hydrophones inevitably show a directional response to incident ultrasound since the element size is finite. This response can be defined in terms of the angle, θ, such that the hydrophone response at θ^0 is reduced to half that at normal incidence. The magnitude of the directional response depends on the size of the hydrophone element and the frequency of the ultrasound incident on the element. For a 0.5 mm element at 10 MHz the response falls to −6 dB at approximately $\pm 30^0$ deviation from normal incidence, this angle being greater the smaller the size of the element. At higher frequencies the directional response becomes increasingly important and this is relevant to the measurement of high amplitude, nonlinear beams.

The hydrophone was calibrated by the National Physical Laboratory by direct comparison with a secondary standard membrane hydrophone positioned at the same location in an acoustic beam. The results were given as an end of cable open-circuit sensitivity over the frequency range 1 MHz to 15 MHz with a maximum variation in sensitivity of ±3% about a mean value of 0.0245×10^{-6} V Pa^{-1}. The overall uncertainties at the 95% confidence level quoted for the calibration increased from ±6% in the range 1 MHz to 4 MHz to ±10% from 13 MHz to 15 MHz.

When a hydrophone is connected to an electrical load such as an

oscilloscope, the sensitivity changes. The sensitivity of a hydrophone connected to any electrical load, M_L, can be calculated from the unloaded sensitivity, M, by combining the impedance of the hydrophone and of the load, assuming that the impedance of both is wholly capacitative, according to the equation

$$M_L = M \frac{C}{C + C_L} \qquad 5.9$$

where C and C_L are the capacitance of the hydrophone and load respectively. For example, for the Hewlett Packard oscilloscope the input impedance was 14 pF and that of the hydrophone 65 pF and the new sensitivity factor at 3.5 MHz was 0.0203×10^{-6} V Pa^{-1}.

However when the pre-amplifier was used, the sensitivity factor could not be calibrated in this way since the capacitance was unknown. Instead it was determined experimentally. In order to obtain a sensitivity factor for the total system, direct comparison was made of the acoustic pressure amplitude measured with the hydrophone connected to the oscilloscope (using the sensitivity value calculated above) and the pressure amplitude measured with the amplifier in the circuit. For the Hewlett Packard oscilloscope and the pre-amplifier, a sensitivity at 3.5 MHz of 0.0189×10^{-6} V Pa^{-1}.

5.6.2 The Hewlett Packard system

The data analysis system consisted of a HP 54200A digitising oscilloscope connected to a HP 216 micro-computer. The oscilloscope was operated at its maximum digitisation rate of 200 MHz for 1001 points with 6 bit resolution. The maximum bandwidth (-3dB) occurs at 50 MHz. The resolution of the system can be increased by data averaging. For each new acquision 1/n times the new data is added to (n-1)/n of the previous data at each time coordinate. Averaging over 16 acquisions increases the

resolution by 4 bits and averaging over 64 acquisions increases the resolution by 6 bits to a total of 12 bits. In acquiring data for pressure and intensity measurements 16 pulse waveforms were acquired and averaged by the oscilloscope before transfer to the computer for calculation of the acoustic parameters listed in Section 5.6.1. This reduced the digitisation noise and improved the signal-to-noise ratio. Data acquired for Fourier analysis were the average of 64 data acquisitions in order to reduce the noise in the signal to the minimum level possible. This was necessary to accurately measure the higher harmonic components in the pulse, which were relatively low in intensity. Discrete Fourier analysis was performed on a single cycle from the centre of each pulse (as shown in Figure 5.15). In order to select the required cycle the time-base of the oscilloscope was chosen such that one cycle of the pulse extended over approximately 70% of the screen. The full display was digitised and transfered to the computer for analysis although only those points corresponding to the peak cycle were analysed.

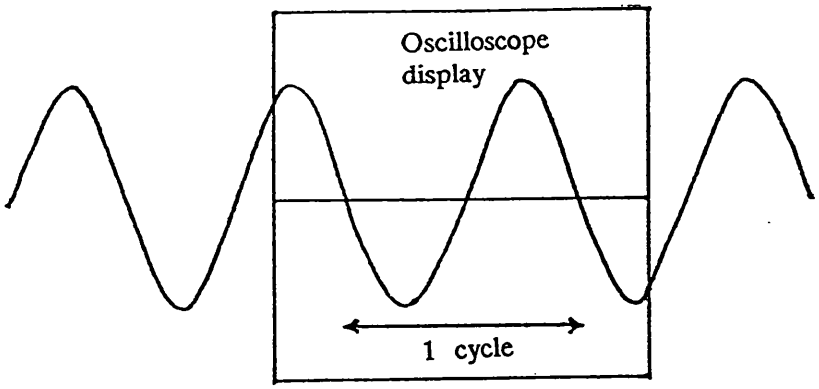

Figure 5.15 Selecting a single cycle for Fourier analysis.

The Fourier coefficients for each harmonic were converted to a power level, in dB, relative to an arbitrary reference level of 80 mV, and in this way a power spectrum was obtained for the first five harmonic components

of the peak cycle in each pulse. The results were restricted to five harmonics by the calibrated range of the hydrophone.

5.7 MEASUREMENT OF ACOUSTIC POWER

Total acoustic power measurements were made using an ultrasonic force balance built in the Medical Physics Department, Royal United Hospital by Michael Perkins, and described by Duck *et al.* (1985). This balance was similar in design to that of Farmary and Whittingham (1978). The basic principle is that of measuring the force, F, exerted by an acoustic beam on a target. For a totally absorbing target or a reflecting target at 45^0 to the beam, the force is related to acoustic power, W,

$$F = \frac{W}{c} \qquad 5.10$$

where c is the acoustic velocity in the transmission medium.

A hollow reflecting target, 48 mm x 34 mm, constructed from 0.05 mm brass shim was used. It was mounted vertically in a small tank of transformer oil at 45^0 to the ultrasound beam such that the transmission path in oil was 21 mm. The transducer was coupled to the oil through a thin plastic membrane and centred by the use of sliding jaws. The reflected wave was absorbed by the tank lining. Coupled opto–diode pairs detected movement of the target which was mounted on the arm of a moving coil meter and a feedback system was employed to measure the current required to hold the target in a null position. The short transmission path employed in this balance reduced the attenuation losses in oil. The balance was calibrated at the National Physical Laboratory. Measurements were made using this balance on the beams generated by the laboratory set–up and by commercial units operating in pulsed Doppler mode or M–mode.

CHAPTER 6

EXPERIMENTAL RESULTS

6.1 INTRODUCTION

This chapter contains the results of experiments conducted to investigate the relationship between streaming velocity in water and a number of ultrasonic parameters. The effects of varying the following parameters were studied:-

pulse amplitude

pulse repetition frequency

pulse length

distance from the tranducer

beam width.

Ideally one parameter was altered while the rest were held constant but this was not always possible. For example changing the distance also changed the beam width and the pulse amplitude. The degree of nonlinear distortion associated with the generation of streaming is discussed and the excess absorption in water due to waveform distortion is quantified. Maximum streaming velocities measured in water for a number of commercial, diagnostic units are also presented. The results of an experimental investigation of rise times and decay times of the fluid streams generated under a variety of conditions are given. In addition the effect on the stream of an acoustically transparent membrane inserted at different locations in the field is described.

6.2 CELLS IN A CONTINUOUS WAVE FIELD

6.2.1 Preliminary observations

The initial observations which led to this investigation of streaming were made using a physiotherapy unit operating in continuous mode. Mouse lymphoma (L1210) cells in suspension were being studied in a cell-holder designed to be positioned on the stage of an inverted phase-contrast microscope. The cross sectional area of the cell holder was 2.5 cm x 1.0 cm, and it was 12 cm in length. The design, shown in Figure 6.1, allowed the behaviour of cells in the ultrasonic field to be observed.

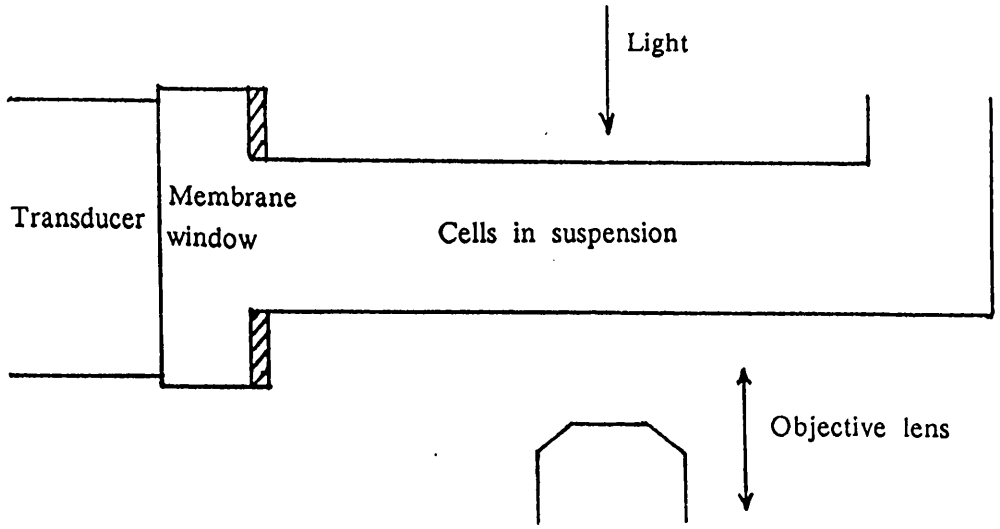

Figure 6.1 Design of cell holder.

When viewed through the microscope, cells on the beam axis, were observed to move away from the transducer during exposure to ultrasound, towards the opposite end of the cell holder, while cells off axis were seen to be in motion in the opposite direction, towards the transducer. This is represented in Figure 6.2. Figure 6.3 represents the form of the velocity

profile across the cell holder. Eckart (1948) predicted streaming profiles of this form for an ultrasonic beam in a tube where the beam width was less than the diameter of the tube.

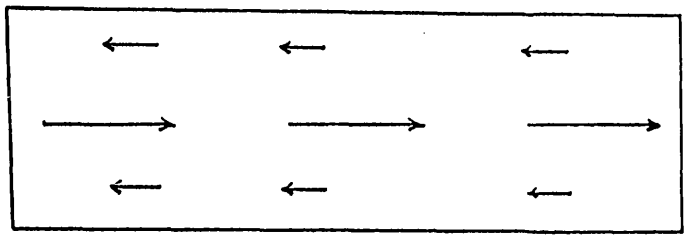

Figure 6.2 Direction of motion observed in cell suspension; viewed from the side.

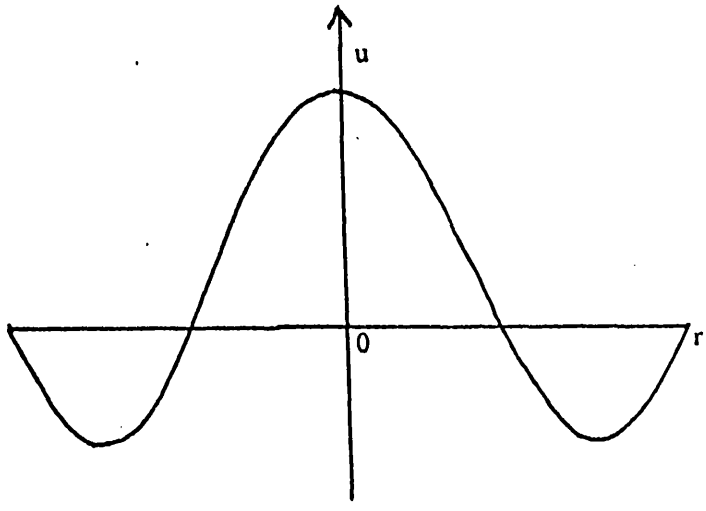

Figure 6.3 Representation of the vertical velocity profile seen in the cell holder.

The end of the cell-holder, made of 6 mm thick perspex, acted as a reflector and it was thought that a standing wave might be set up but in practice this rarely occurred. However at the surface of the cell-holder some cells were observed to clump in bands as shown in Figure 6.4. Bands at drive frequencies of 1 MHz and 3 MHz were observed to be spaced at half-wavelength seperations, that is 0.7 mm and 0.21 mm repectively.

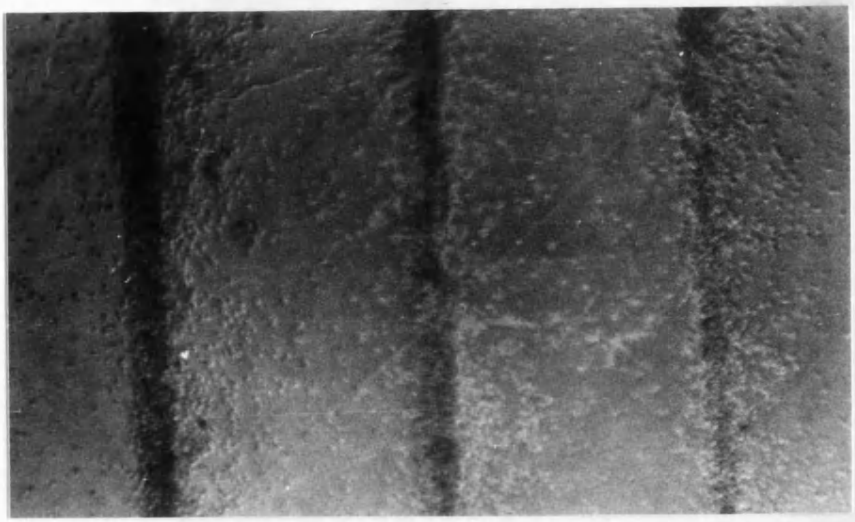

Figure 6.4 Banding of cells at 1 MHz in continuous wave field; band separation 0.7 mm.

The presence of these clumps of cells may be explained if partial reflection of the wave is assumed. A boundary layer exits at the walls of the cell holder in which the flow velocity reduced to zero. This allowed the cells to clump at the pressure nodes or antinodes. This investigation did not distinguish between the two positions although clumping at the nodes was most probable since the particle velocity is zero at these locations. Nyborg (1965) described a similar situation in which eddies, occurring due to streaming in a standing wave field in a channel, created stagnant areas on the channel walls. An effect such as this may have played a part in the banding observed in the cell holder. Band formation was dependent on the input intensity of the ultrasound beam. Above a critical level the streaming was too vigorous and cells were swept away destroying the bands. For example at 1 MHz the bands were stable at 0.5 W cm^{-2} but broke up when the intensity was increased to 1 W cm^{-2}.

In an attempt to make the dimensions of the cell holder more realistic in terms of an experimental bio-effects arrangement, two internal walls of 0.7 mm perspex were inserted at the centre forming a new chamber 1 cm

in length within the large cell holder. Cells were contained in the small chamber and the regions in front and behind were filled with degassed water. Under these circumstances fairly vigorous streaming was still observed but no measurement of the velocity was made.

A separate experiment was carried out to measure the streaming velocity generated by the physiotherapy unit in the large cell holder. The streaming velocity of red blood cells in saline was measured using a commercial continuous wave Doppler unit (Doptek). At 3 W cm^{-2} intensity and 3 MHz drive frequency the measured streaming velocity was 4 cm s^{-1}.

6.3 DEMONSTRATION OF STREAMING USING DYES

Following the observations described above, streaming produced in water by a diagnostic transducer was observed using potassium permanganate as a dye. A typical stream is shown in Figure 6.5.

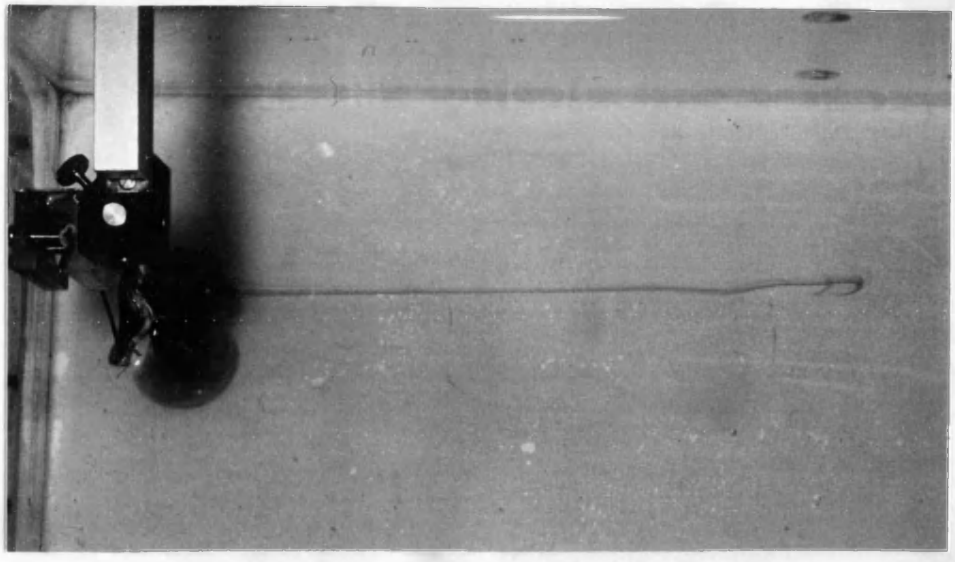

Figure 6.5 Dye stream in diagnostic field; using potassium permanganate.

The transducer, which is not shown in the picture, was located on the left with a crystal of potassium permanganate suspended at its focus. The

stream shown here extended a distance of 15 cm beyond the focus in a time period of about 2 seconds. The width of this stream was estimated to be approximately 2 mm.

6.3.1 Velocity measurements

Streaming velocities generated in diagnostic ultrasound beams produced using a Fisher Diasonograph unit together with a 3.5 MHz transducer (KB–Aerotech QSB 35DM) were measured from video recordings of the dye stream as described in Section 5.3.1. The results are shown in Table 6.1.

Scale lines	Distance (cm)	No. of frames	Time (s)	Σ(time) (s)
5	3.0	18.5	0.76	0.76
10	6.0	16	0.64	1.40
15	9.0	13	0.52	1.92
20	12.0	11	0.44	2.36
25	15.0	11	0.44	2.80
30	18.0	11.5	0.46	3.26
35	21.0	12	0.48	3.74
40	24.0	12	0.48	4.22
45	27.0	12	0.48	4.70
50	30.0	15	0.60	5.30
55	33.0	18	0.72	6.02
60	36.0	15	0.60	6.62

Table 6.1 Measurements taken from a video film of the stream; Fisher Diasonograph, 3.5 MHz transducer (KB–Aerotech QSB 35DB)

The video frame rate was 25 frames per second and the line spacing on the background scale was 0.6 mm. Using the frame advance facility the time taken for the leading edge of the stream to cross every fifth scale line was

recorded. These results are also plotted in Figure 6.6. The peak streaming velocity was calculated from the maximum gradient of the line.

Streaming velocities shown in Table 6.2 were obtained in beams of different amplitudes generated using the transducer described above driven by a ENI power amplifier. These results are included for comparison in magnitude with velocity measurements made using an anemometry system and reported in Section 6.4. Although different transducers were used, the streaming velocities measured by the two techniques were comparable.

I_{spta} ($mW\ cm^{-2}$)	$\hat{p}^-$ (MPa)	Max. velocity ($cm\ s^{-1}$)
834	-1.0	3.0
1200	-1.1	4.8
1477	-1.3	9.0

Table 6.2 Maximum streaming velocities at a range of temporal average intensities (I_{spta}); 3.5 MHz transducer, 5 kHz pulse repetition frequency, 3.4 μs pulse duration; $\hat{p}^-$ is the peak negative pressure.

6.3.2 Velocity profiles using thymol blue

Using thymol blue as an indicator in the way described in Section 5.3.2 pictures of the streams generated by different types of ultrasound equipment were obtained. Shown in Figure 6.7 are: (a) the stream generated by the laboratory set-up (single element pulse-echo transducer), (b) the stream resulting from a commercial real-time scanner operating in imaging mode (ATL Ultramark 9 scanner and LA 5MHz HRS scanhead) and (c) the stream generated in the field of a physiotherapy beam (Therasonic 1030). Significant differences in the streaming profiles can be seen.

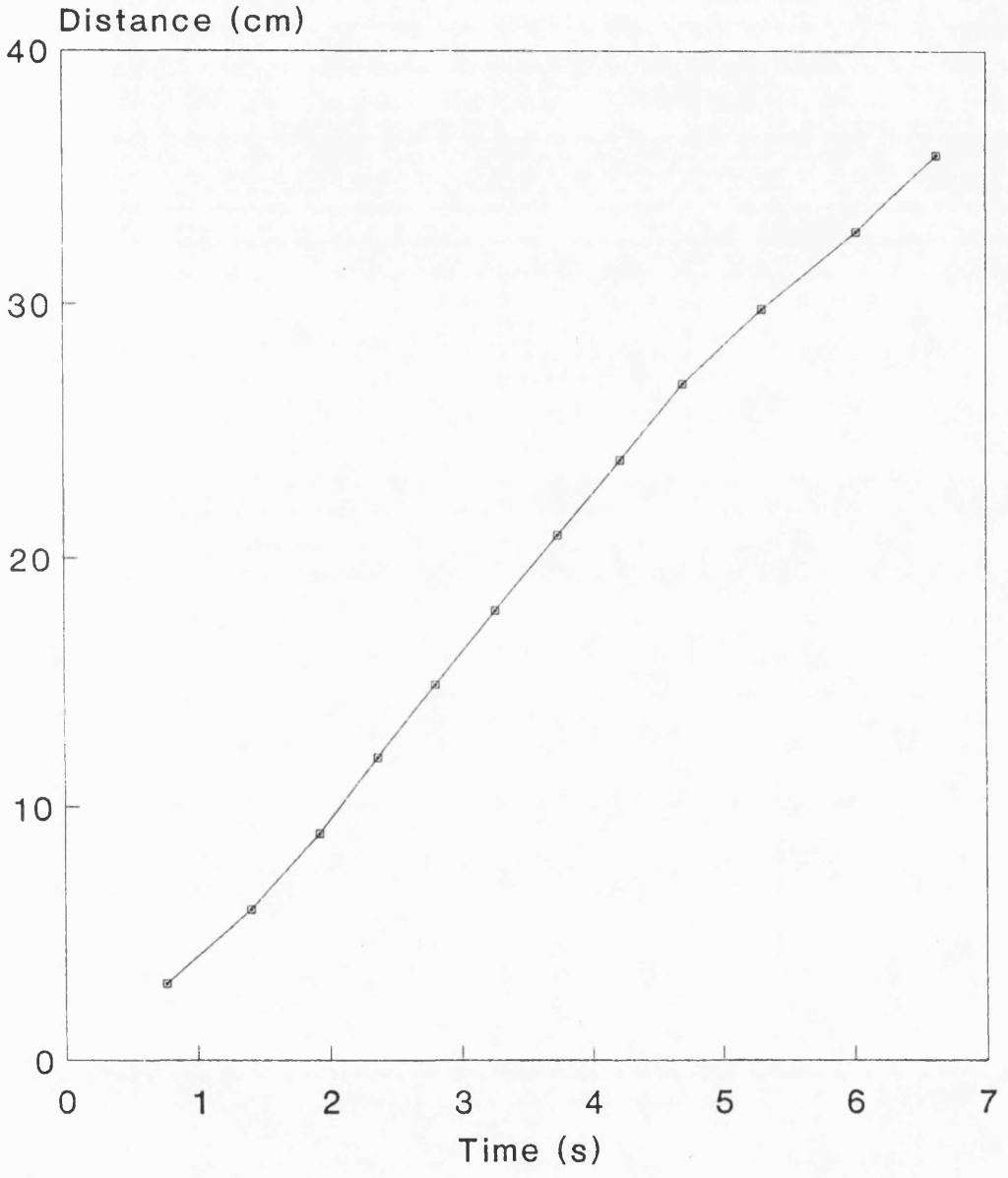

Figure 6.6 Plot of distance travelled by dye stream as a function of time; from video of potassium permanganate stream.

(a)

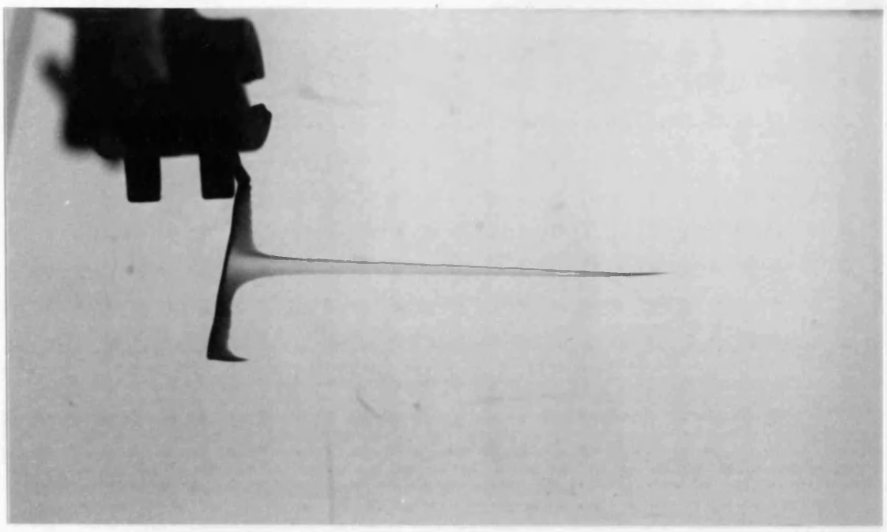

(b)

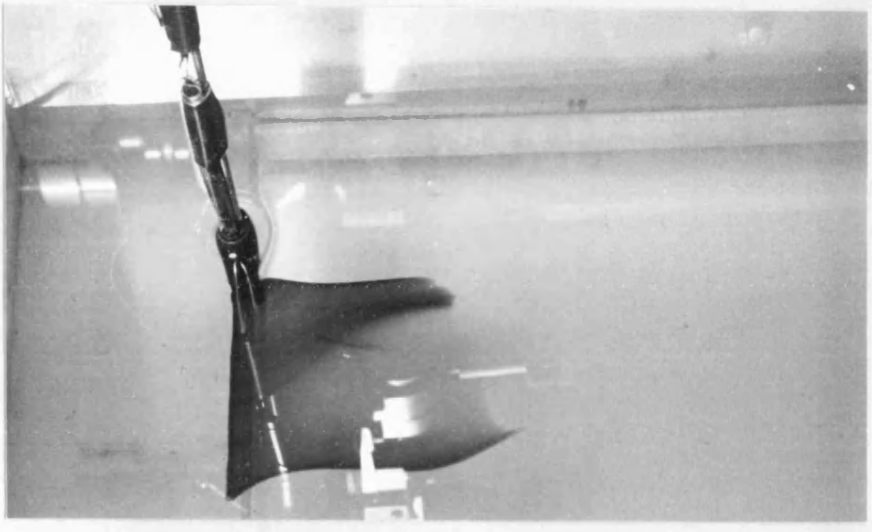

(c)

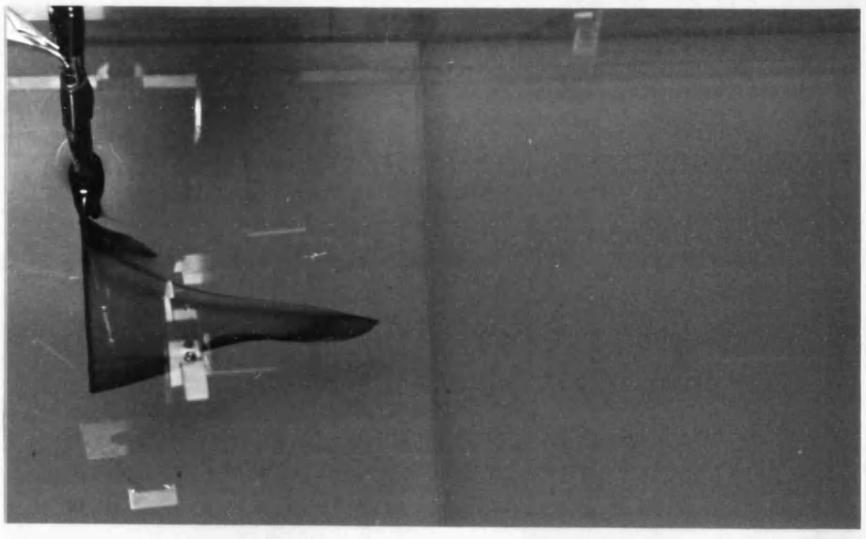

Figure 6.7 Streaming profiles demonstrated using thymol blue as a dye; (a) stationary beam, (b) scanned imaging beam and (c) physiotherapy beam.

The stream generated by the single element diagnostic transducer is narrow and well collimated throughout its length while that generated in the physiotherapy field has a broader profile. The stream generated in the imaging field is a sheet of moving fluid in the scan plane of the transducer.

6.4 ANEMOMETRY MEASUREMENTS

A detailed description of the anemometer, its calibration, use and accuracy was given in Section 5.4. This system was used in a number of investigations of the streaming velocity generated in water and each of the following sections describes one of these experiments in detail. A number of investigations involved measurements of streaming velocity and of related acoustic beam parameters. The significance of the acoustic parameters and particularly pulse pressure amplitude and nonlinear propagation for the generation of acoustic streaming is discussed.

In each experimental determination of velocity the values reported were derived from the average of three voltage measurements. Typically the random variation in voltage was less than 1%. The ultrasound system and the anemometer system were switched off between each reading to allow the streaming to cease. The average voltage measured was temperature corrected to the reference temperature as described in Section 5.4.3 before being converted to velocity using the calibration curve (Figure 5.7). It was estimated that the absolute value of streaming velocity could be measured to better than ± 0.5 cm s^{-1} at the lower end of the velocity range whilst above 10 cm s^{-1} the uncertainty increased to ± 1.5 cm s^{-1} due to the shape of the calibration curve. The minimum velocity that could be measured was taken as 0.5 cm s^{-1}.

6.5 AXIAL VARIATION IN STREAMING VELOCITY AND ACOUSTIC PRESSURE FOR BEAMS OF DIFFERENT AMPLITUDES

The experimental equipment described in Section 5.2 was used to produce three ultrasound beams of differing amplitudes while maintaining a constant average power. Table 6.3 shows the pulsing parameters employed for each beam.

Beam	Power (mW)	$\hat{p}^+$ (MPa)	Prf (kHz)	Pulse (μs)
A	100	3.5	2	3.4
B	100	1.4	20	3.4
C	100	0.2	–	–

Table 6.3 Pulse parameters for three beams of varied amplitudes; for beams A and B, "Prf" is the pulse repetition frequency and "Pulse (μs)" is the pulse duration. Beam C was operated in continuous wave mode.

6.5.1 Streaming velocity measurements

Streaming velocities were measured on axis at 1 cm intervals for each beam in turn, over the range 3.5 cm to 16.5 cm from the transducer. The anemometer probe, mounted on a micromanipulator was initially positioned by eye on axis at about the focus of the transducer. Its height and lateral position were adjusted in order to maximise the output voltage. This adjustment was quite critical because the streams were very narrow (of the order of 3 mm) at this location. A stream could be located with greatest ease when the probe was positioned close to the focus because the streaming velocity was maximal in this region. Nearer to the transducer the velocity reduced to a very low level and positioning was more difficult. Once the

stream had been located, the probe was moved longitudinally along the axis and at each new location the output voltage was again maximised by adjustment of the micromanipulator.

The axial streaming velocities measured for the three beams are plotted against distance in Figure 6.8. Two facts are immediately apparant from this graph. Firstly the streaming velocity beyond the focus was significantly higher in beam A than in the other two beams and secondly, almost no streaming was detected in the near field for any of the beams. In discussing these results more fully three regions in the field will be considered. Firstly in the region close to the transducer, that is between 0 cm and 5 cm, the streaming velocity was low for all beams, less than 0.5 cm s^{-1}. In this region the beam was fairly wide, reducing from 19 mm at the transducer to 11 mm at 5 cm range and therefore the pulse average intensity here was relatively low compared with the focal zone. As the beam became more tightly focused the intensity increased progressively and in the second region, between 5 and 10 cm from the transducer there was an increase in streaming velocity for all beams. This was only partly associated with the increase in intensity due to the focusing effect of the transducer since it was observed that the increase was much more significant for beam A, the high amplitude beam, than for beams B or C. In beam A the streaming velocity increased by approximately a factor of 15, from 0.7 cm s^{-1} to 10.6 cm s^{-1}, while for beam C the corresponding increase in streaming velocity was from 0.6 cm s^{-1} to 2.0 cm s^{-1} a factor of only 3.3. In the region beyond the focus the streaming velocity remained approximately constant at the maximum level over the range of measurement. The maximum velocity generated in the high amplitude beam was therefore approximately 5 times the maximum generated in the low amplitude.

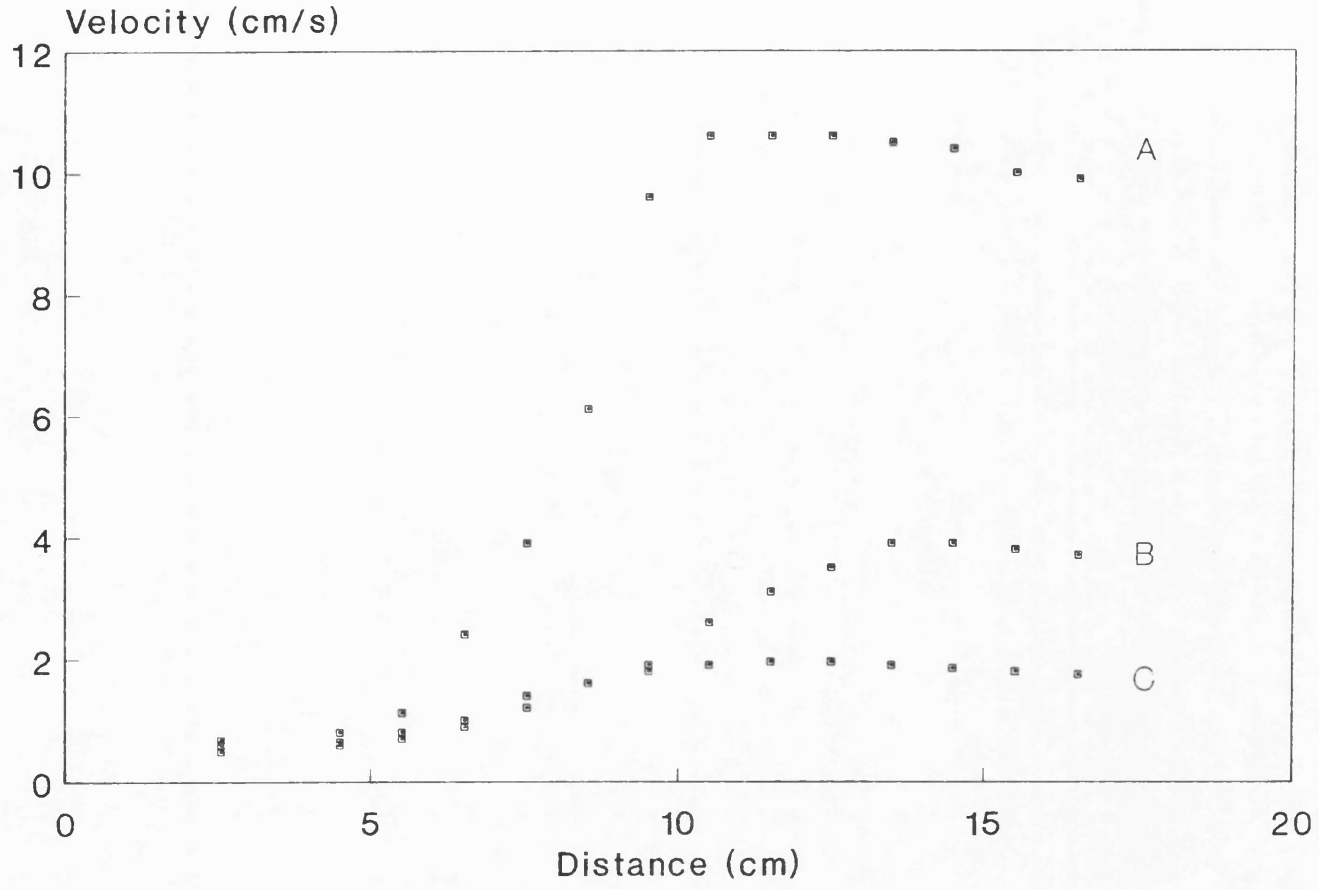

Figure 6.8 Axial streaming velocity in beams of differing pulse amplitudes; A, B and C defined in Table 6.3.

Although the total power was identical for the three beams the differing pulse amplitudes employed resulted in a significant difference in the degree of nonlinear distortion occurring in each beam. Greater nonlinear distortion occurred in the high amplitude beam and this is believed to be the reason for the enhanced streaming velocity generated in this beam. The degree of nonlinear distortion was measured and is discussed fully below. Section 6.7 discusses a potential mechanism by which nonlinear distortion leading to shock formation can result in enhanced streaming.

It was shown in Chapter 4 that streaming velocity is conventionally assumed to be proportional to the (pressure)^2; for examples Equations 4.31 and 4.34. These equations strictly apply only to the situation in which approximately linear propagation is occurring. The work reported here demonstrates that such a relationship does not accurately predict streaming velocity in ultrasound beams which have undergone significant nonlinear distortion.

6.5.2 Measurement of harmonic content

Ultrasound waveforms measured using a single element hydrophone and the Hewlett Packard system were Fourier analysed as described in Section 5.6.2. The levels of the first five harmonic frequency components in the pulses were quantified.

For the three beams defined in Table 6.3, the pulse waveforms were analysed at intervals of 1 cm, on the beam axis, over the range for which streaming velocity measurements had been made. In addition measurements of intensity, acoustic pressure and beam width were made at each location. An axial plot of the level of the second harmonic relative to the fundamental frequency in each beam is shown in Figure 6.9.

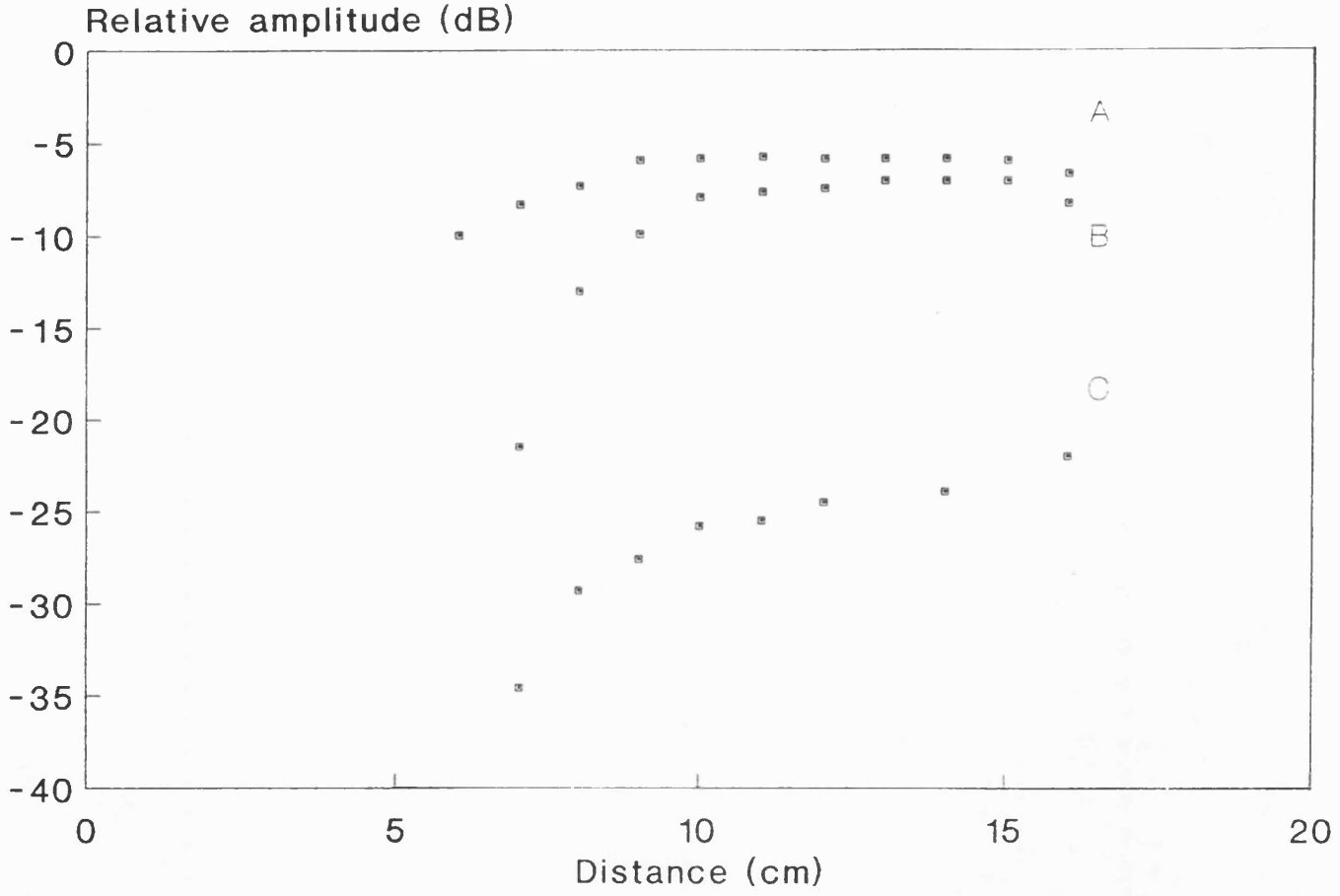

Figure 6.9 Plot of second harmonic amplitude in beams A, B and C relative to the fundamental.

Table 6.4 shows the amplitude of the second harmonic (7 MHz) and third harmonic (10.5 MHz) components relative to the fundamental frequency.

Dist	A_2/A_1 (-dB)			A_3/A_1 (-dB)		
(cm)	A	B	C	A	B	C
6	10.0	18.5	-	16.7	45.1	-
7	8.3	21.5	34.6	13.2	44.5	58.2
8	7.3	13.0	29.3	11.4	23.5	49.6
9	5.9	9.9	27.6	9.6	16.9	48.3
10	5.8	7.9	25.8	9.4	12.7	45.6
11	5.7	7.6	25.5	9.5	12.2	43.7
12	5.8	7.4	24.5	9.6	11.8	43.6
13	5.8	7.0	24.1	9.5	11.1	43.6
14	5.8	7.0	23.9	9.5	11.1	43.5
15	5.9	7.0	23.0	9.6	11.2	42.3
16	6.6	8.2	22.0	10.4	13.4	41.0

Table 6.4 Second and third harmonic amplitudes relative to the fundamental for beams A, B and C (defined in Table 3); 3.5 MHz fundamental frequency.

For a plane wave, a σ = 1 shock is said to have occurred when the second harmonic level is 8 dB below the fundamental: that is when the waveform has distorted sufficiently for a pressure discontinuity to form. (The shock parameter, σ, is defined in Section 4.1.3). A second harmonic level 6 dB below the fundamental corresponds to a σ = 3 shock, or mature shock (Muir and Carstensen, 1980). In beam A, the second harmonic level in the ultrasonic pulse increased rapidly in the region in front of the transducer reaching a level approximately 6 dB below the fundamental at 9 cm as shown in Figure 6.9. In beam B the second harmonic was 7 dB below the fundamental at approximately 13 cm. Both beams had undergone nonlinear distortion and in beam A a mature shock had formed. In

Table 6.4 shows the amplitude of the second harmonic (7 MHz) and third harmonic (10.5 MHz) components relative to the fundamental frequency.

Dist	A_2/A_1 (-dB)			A_3/A_1 (-dB)		
(cm)	A	B	C	A	B	C
6	10.0	18.5	-	16.7	45.1	-
7	8.3	21.5	34.6	13.2	44.5	58.2
8	7.3	13.0	29.3	11.4	23.5	49.6
9	5.9	9.9	27.6	9.6	16.9	48.3
10	5.8	7.9	25.8	9.4	12.7	45.6
11	5.7	7.6	25.5	9.5	12.2	43.7
12	5.8	7.4	24.5	9.6	11.8	43.6
13	5.8	7.0	24.1	9.5	11.1	43.6
14	5.8	7.0	23.9	9.5	11.1	43.5
15	5.9	7.0	23.0	9.6	11.2	42.3
16	6.6	8.2	22.0	10.4	13.4	41.0

Table 6.4 Second and third harmonic amplitudes relative to the fundamental for beams A, B and C (defined in Table 3); 3.5 MHz fundamental frequency.

For a plane wave, a σ = 1 shock is said to have occurred when the second harmonic level is 8 dB below the fundamental: that is when the waveform has distorted sufficiently for a pressure discontinuity to form. (The shock parameter, σ, is defined in Section 4.1.3). A second harmonic level 6 dB below the fundamental corresponds to a σ = 3 shock, or mature shock (Muir and Carstensen, 1980). In beam A, the second harmonic level in the ultrasonic pulse increased rapidly in the region in front of the transducer reaching a level approximately 6 dB below the fundamental at 9 cm as shown in Figure 6.9. In beam B the second harmonic was 7 dB below the fundamental at approximately 13 cm. Both beams had undergone nonlinear distortion and in beam A a mature shock had formed. In

beam C the second harmonic level was very low, at least 20 dB below the fundamental and it was therefore assumed to be propagating linearly.

Table 6.5 shows calculated pressures and intensities in the first five harmonic components of beams A and B. The intensity of each harmonic relative to the fundamental is given for comparison with the theoretical value for a sawtooth wave where the harmonic amplitudes vary as 1/n and the intensities as $1/n^2$. Harmonic intensity in the pulse, I_n, was calculated from the peak acoustic pressure using Equation A1.1.

	$\hat{p}$ (MPa)	I_n (Wcm^{-2})	$\hat{p}$ (MPa)	I_n (Wcm^{-2})	I_n/I_1 saw-		
n	A	A	B	B	tooth	A	B
1	1.34	58.3	0.83	22.0	1.00	1.00	1.00
2	0.70	15.9	0.34	3.7	0.25	0.26	0.17
3	0.46	6.9	0.18	1.0	0.11	0.12	0.05
4	0.35	4.0	0.11	0.4	0.06	0.07	0.02
5	0.28	2.5	0.07	0.2	0.04	0.04	0.01

Table 6.5 Calculated pressures and intensities in the harmonic components of beams A and B compared with theoretical levels for a sawtooth wave; n is the harmonic number.

The intensity ratio for beam A indicated that the pulse cycle analysed had distorted to the stage at which a full shock had formed. The pulses in beams A and B consisted of 12 cycles, most of which distorted identically, and therefore although only one cycle was analysed the results can be applied to the entire pulse with only a small error due to the end effects. Summing the intensities in the first five harmonics (up to 17.5 MHz) for beam A accounted for only 80% of the total intensity indicating that 20% was contained in still higher harmonic components. In beam B, less than 1% of the total intensity was unaccounted for by the same summation. The

parameter, σ_m (Bacon 1984), was calculated in the focal zone of each beam using Equation 4.12. For beam C a value of 0.14 was obtained; for beam B, σ_m = 1.0, and for beam A, σ_m = 2.1.

The results presented here indicate that significant shock formation had occurred in beam A.

6.6 VARIATION IN STREAMING VELOCITY WITH INTENSITY

The effect of the pulse average intensity on the streaming velocity was investigated by varying the pressure amplitude of the acoustic pulse. Temporal average intensity was varied in two further ways; by changing the pulse repetition frequency and by changing the length of each individual pulse.

6.6.1 Streaming velocity measurements

The streaming velocity was measured at the focus of the 3.5 MHz Diagnostic Sonar transducer (MD3483) for a range of peak pulse pressure amplitudes from 1.2 MPa to 3.1 MPa. A pulse repetition frequency of 2 kHz was used together with a pulse length of 3.4 μs. The anemometer probe was located at 9.5 cm. The drive voltage to the transducer was varied in order to change the pulse amplitude in a controlled way. At each drive level measurements of pulse average intensity and peak positive pressure were also made, using the ultrasound beam calibrator described in Section 5.5. These values are tabulated in Table 6.6, together with the corresponding anemometry results for each beam. The raw data presented in this table is typical of the results obtained in the experiments described here. Figure 6.10 shows the variation in streaming velocity with pulse average intensity. Two broad regions can be identified in this graph.

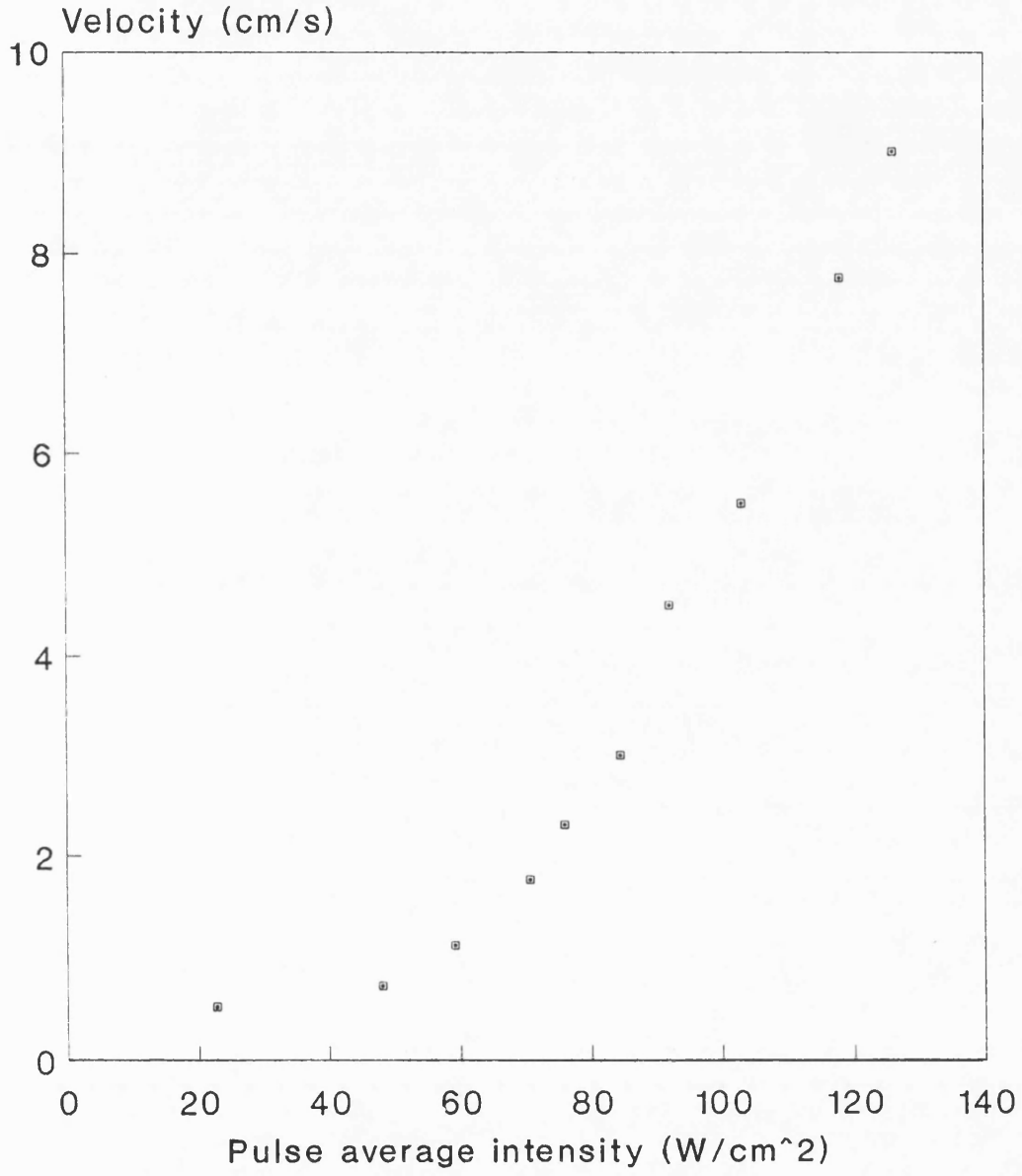

Figure 6.10 Streaming velocity as a function of pulse average intensity.

Initially, at pulse intensity levels up to approximately 60 W cm^{-2}, the streaming velocity increased only slowly with increasing pulse intensity. In the second region, from 70 - 130 W cm^{-2}, the change was much more rapid and a linear relationship was obtained with an increase in streaming velocity of approximately 1.3 cm s^{-1} for every 10 W cm^{-2} rise in pulse average intensity. The significance of nonlinear distortion on these results is discussed in the next section.

$\hat{p}^+$ (MPa)	I_{pa} (W cm^{-2})	V' (V) Mean	SD	Velocity (cm s^{-1})
1.2	22.6	5.95	0.006	0.5
2.0	48.1	6.24	0.006	0.7
2.3	59.1	6.62	0.000	1.1
2.4	70.6	7.07	0.010	1.7
2.5	75.9	7.34	0.006	2.3
2.6	84.3	7.70	0.000	3.0
2.7	92.0	8.06	0.000	4.5
2.8	103.0	8.26	0.015	5.5
2.9	118.0	8.55	0.006	7.8
3.0	126.0	8.75	0.058	9.0
3.1	132.0	8.78	0.006	9.2

Table 6.6 Values of peak positive pressure, $\hat{p}^+$, pulse average intensity, I_{pa}, mean anemometer output voltage, V', and standard deviation (SD), and streaming velocity at 9.5 cm in water; 2 kHz pulse repetition frequency, 3.4 μs pulse length.

This experiment was repeated at a number of pulse repetition frequencies, from 0.5 kHz to 5 kHz and the results are shown in Figure 6.11. An increase in the streaming velocity with increasing pulse average intensity was observed at each pulse repetition frequency. The increase was progressively greater at higher pulse repetition frequencies.

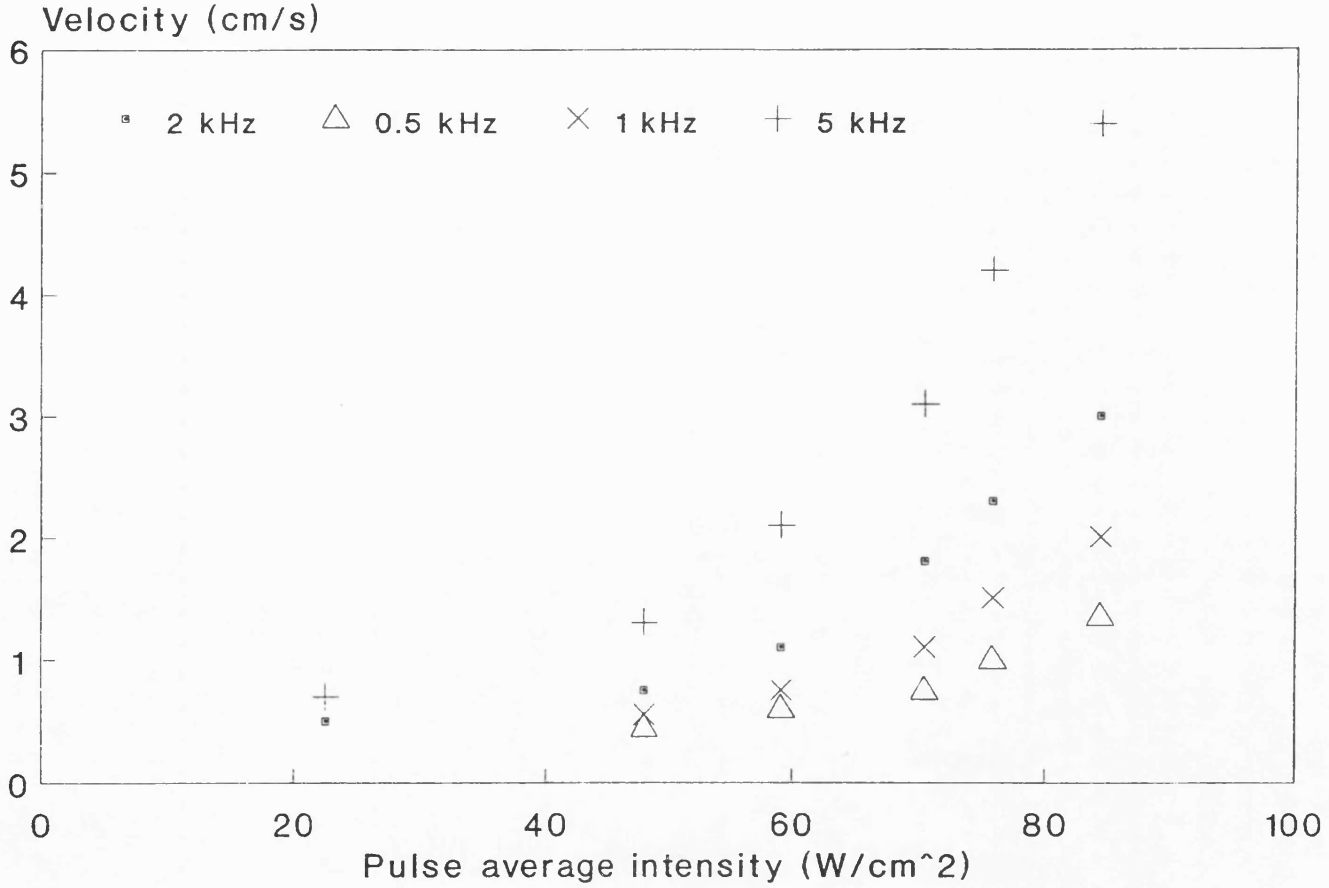

Figure 6.11 Streaming velocity as a function of pulse repetition frequency.

The streaming velocity was also measured at the focus of a transducer as the number of cycles in the pulse was increased. In this case the peak positive pressure was 2.2 MPa. The results, plotted in Figure 6.12, showed an approximately linear increase in streaming velocity with number of cycles in the pulse. Varying the pulse length in this way effectively increased the temporal average intensity while maintaining a constant pulse pressure amplitude. Thus the streaming velocity was seen to be directly related to temporal average intensity at constant pulse amplitude.

6.6.2 Measurement of harmonic content

Pressure waveforms were measured under identical conditions to those used for the streaming velocity measurements at varied pulse pressure amplitudes described in the previous section. Each waveform was Fourier analysed and the level of second and third harmonic components relative to the fundamental are plotted in Figure 6.13. The streaming velocity started to increase rapidly at about 60 W cm^{-2} pulse average intensity and this was associated with a 2nd harmonic level approximately 7 dB below the fundamental. The shock parameter, σ_m (Bacon 1984), was calculated from Equation 4.12 for each waveform, using measured values of focal length, 9.5 cm, focal gain, 4.2, and the average value of the peak to peak pressure amplitude for each waveform. σ_m was 1 at pulse average intensity of 45 W cm^{-2} and $\pi/2$ at 90 W cm^{-2} as shown in Figure 6.14. Thus the streaming velocity started to increase signicantly in the intensity range associated with $1<\sigma<\pi/2$ and with a measured second harmonic level approximately 7dB below the fundamental. (For values of σ_m less than or equal to $\pi/2$, $\sigma_m = \sigma$.)

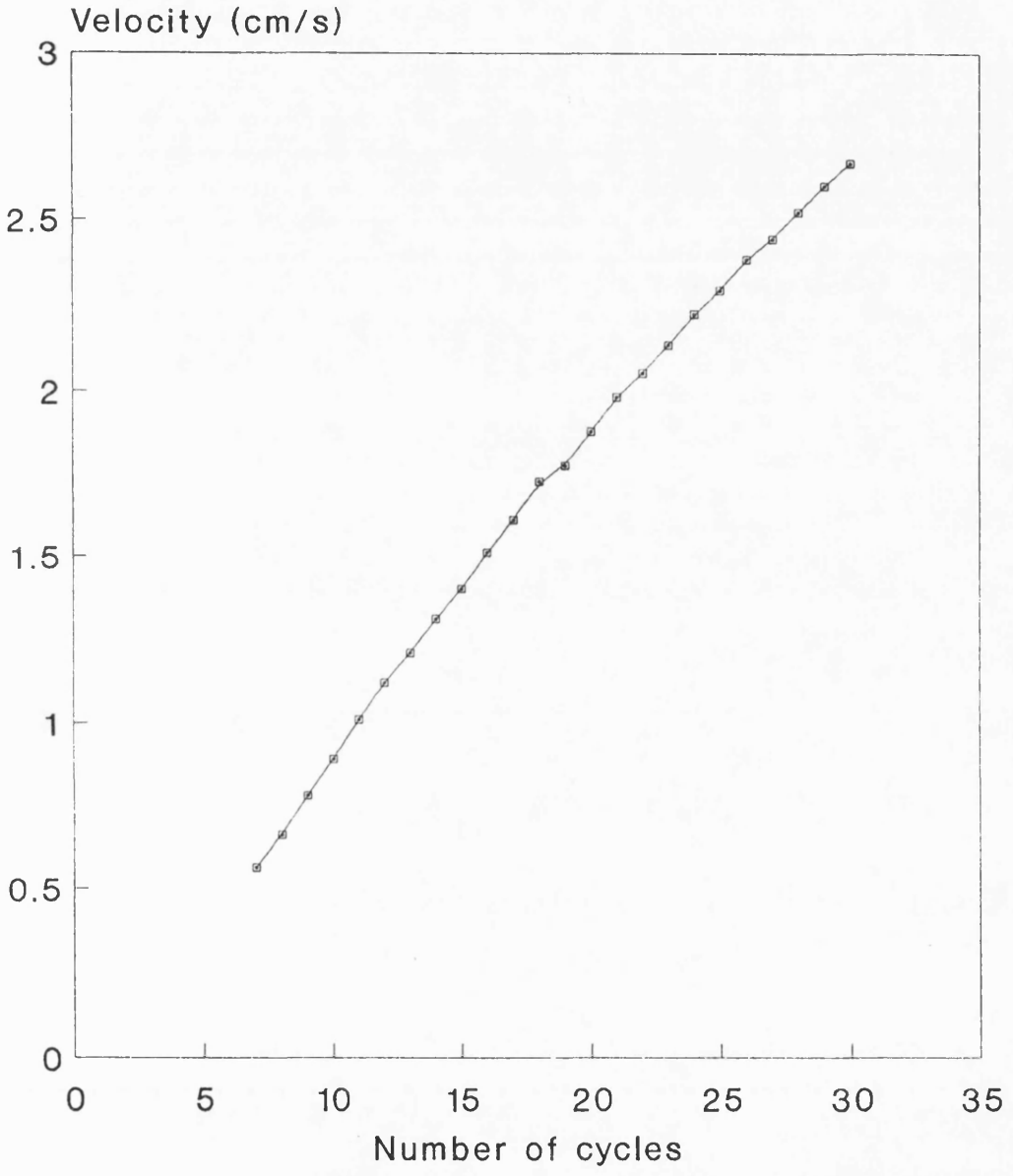

Figure 6.12 Variation in streaming velocity with the number of cycles in the pulse.

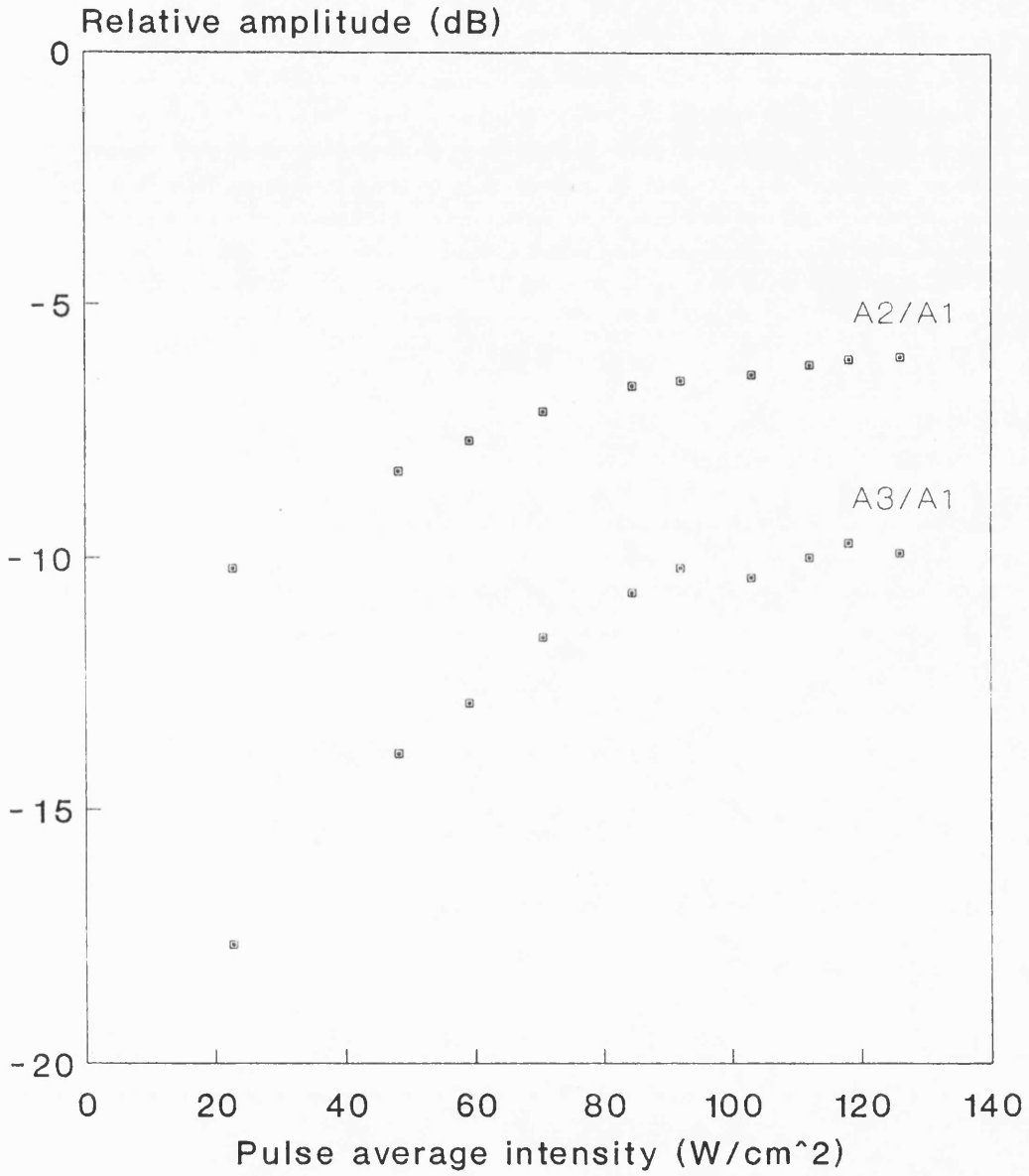

Figure 6.13 Relative second harmonic amplitude as a function of pulse average intensity.

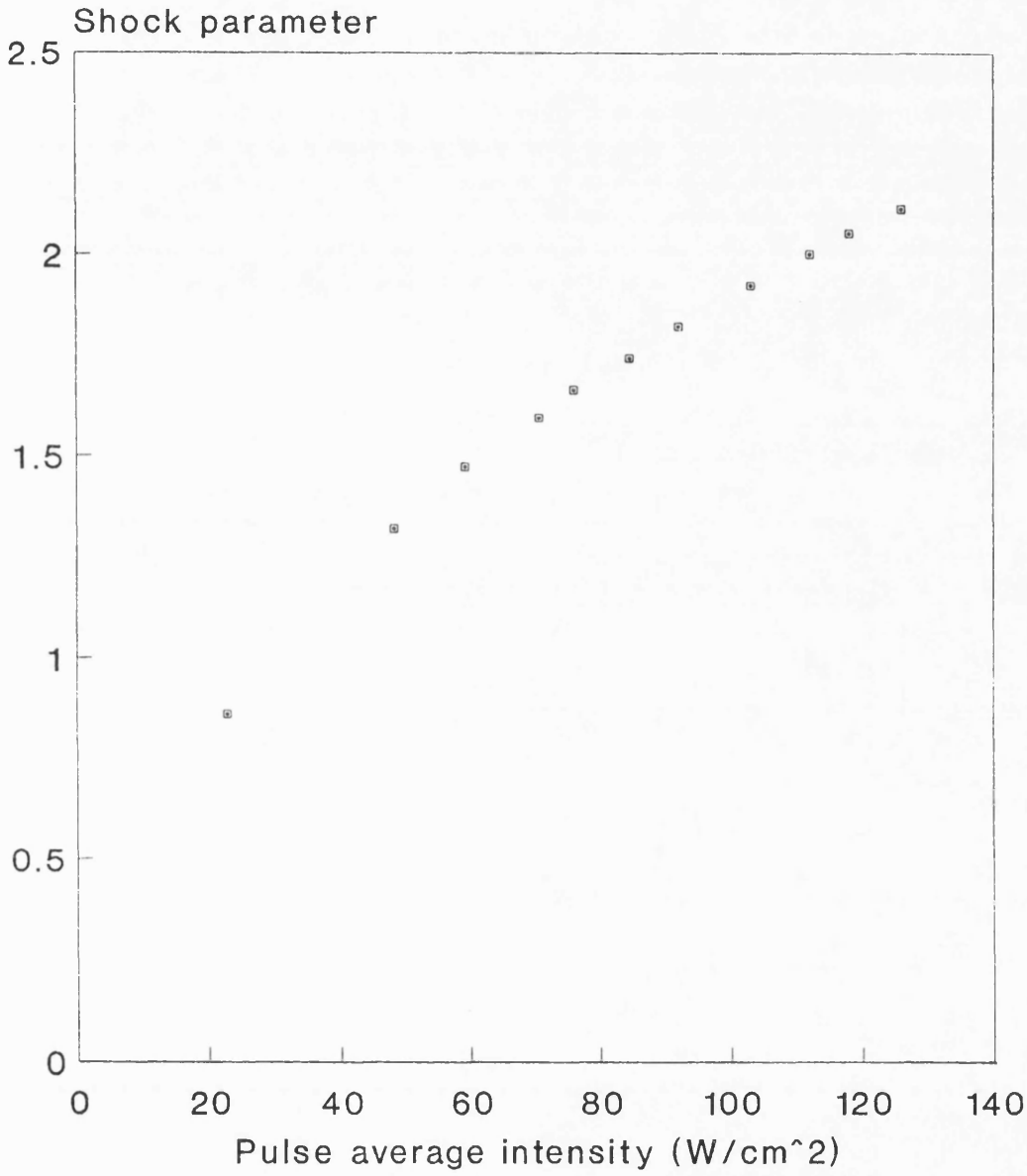

Figure 6.14 Shock parameter, σ_m, with increasing pulse average intensity; 3.5 MHz beam, 2 kHz and 3.4 μs.

6.7 ABSORPTION LOSS IN NONLINEAR BEAMS

The results presented above indicate that the streaming velocity increased more rapidly than would be expected for an undistorted waveform when the acoustic waveform became distorted and therefore rich in harmonic components. This suggests that the increased streaming was associated with nonlinear absorption (Section 2.3) and the increased loss of energy from the beam. In order to investigate this further the relative energy levels in beams A, B and C were measured over the range 1.8 cm to 15 cm from the transducer as the two higher amplidude beams became distorted. The pulse amplitudes were identical to those given in Table 6.3, but for these measurements a constant pulse length of 1.7 μs was used at 1 kHz pulse repetition frequency. The integral of the modulus of acoustic pressure on the beam axis, was recorded for each beam over the measurement range. (This is the square-root of the pressure-squared integral (PSI) defined in Equation A1.4). The distance between measurements was 0.25 cm, 0.5 cm or 1.0 cm depending on the rate of change of pressure-squared integral with distance.

No automatic averaging of the PSI was performed by the beam calibrator and a sample of 10 repeated measurements at a single location showed a standard deviation of 1% about the mean. The major source of error was in the measurement of the distance between the transducer and hydrophone. Scales on the front and back of the measurement tank were used for vertical positioning of the hydrophone. This was accomplished by looking across the top of the hydrophone casing at the required height so that corresponding marks on the two scales were judged to be coincident, and subsequently moving the hydrophone vertically until it was also judged to be in line with the scale marks. In order to improve the accuracy, this series of measurements was repeated three times under identical conditions.

The purpose of this experiment was to investigate the absorption of energy from 'shocked' acoustic beams in water by comparison with that from beams which propagate linearly. Since the maximum level of second harmonic observed for beam C was 20 dB below the fundamental this case was taken as the linear reference. It can be seen from Equations A1.2 and A1.4 that the pressure squared integral on axis, PSI, is proportional to the axial intensity. The intensity in a distorted pulse in beam A, relative to that in an undistorted pulse in beam C, is given by the ratio PSI_A/PSI_C and a similar ratio, PSI_B/PSI_C, can be defined for beam B. Since the intensity in a pulse is proportional to the energy, for particle pressure and velocity in phase (Nyborg 1985), the PSI ratio gives a measure of the relative energy on the beam axes. A comparable experiment carried out on a commercial duplex scanner is described by Duck and Starritt (1989).

Values of the integral of the modulus of acoustic pressure (or the square root of PSI) are plotted in Figure 6.15 for the three beams. Figure 6.16 shows the ratios PSI_A/PSI_C and PSI_B/PSI_C obtained from three separate experiments. At each location this ratio represents the energy flow on axis in the high amplitude beam, either A or B, relative to the low amplitude beam, C. It can be seen that for beam A the ratio decreased with distance from the transducer demonstrating enhanced absorption of the distorted beam relative to the linear beam.

Three regions are apparent in the plot of PSI ratio for beam A. In the near field, from 2 cm to 6 cm, the ratio was constant except for a number of points at about 5 to 6 cm which were very much higher. These high values may be explained by diffraction effects in the near field. In the low amplitude case a minimum of the fundamental occurred on axis at this distance giving a very low PSI value. However in the high amplitude case nonlinear propagation up to this distance resulted in the generation of higher frequency components which were not constrained by the diffraction

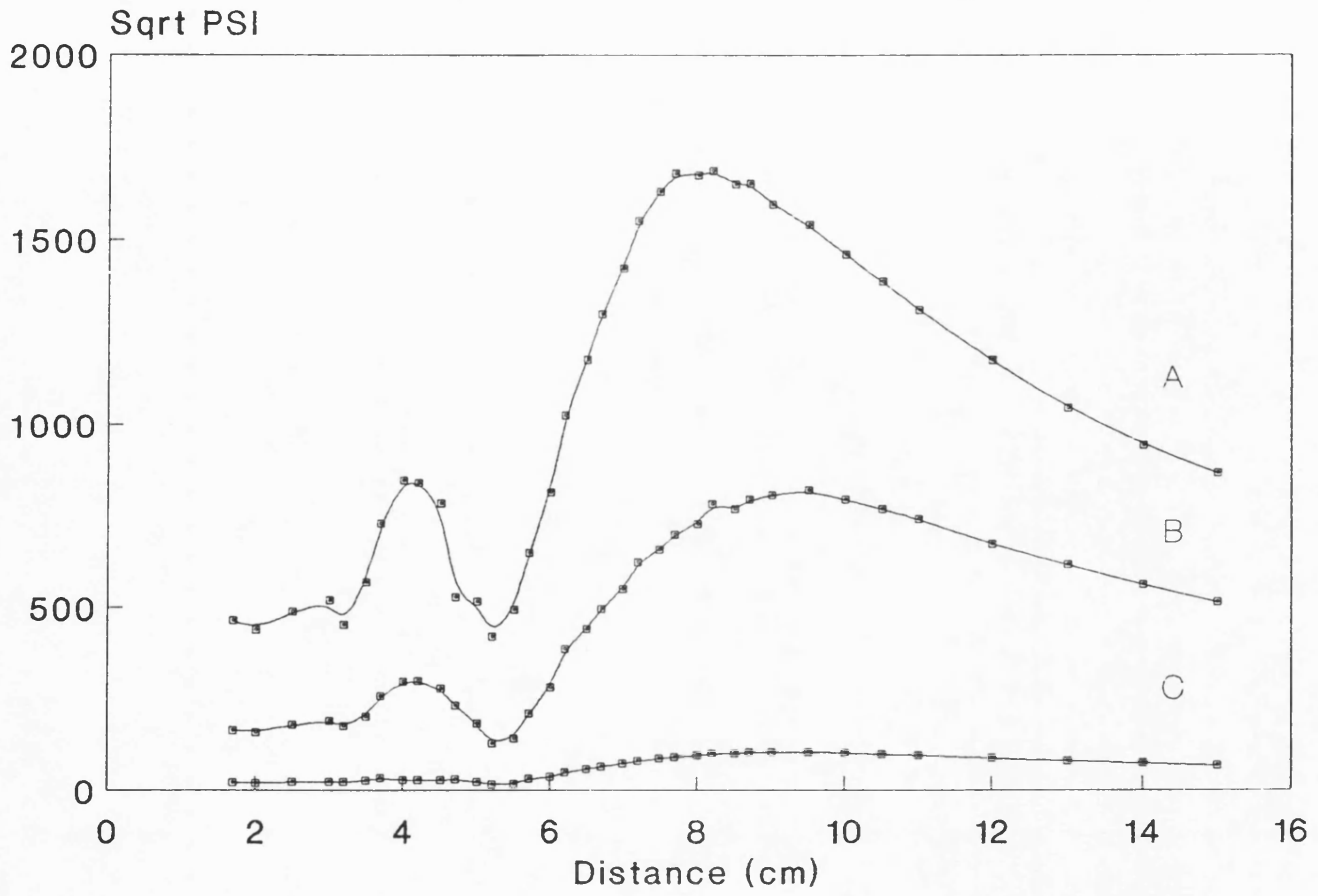

Figure 6.15 Axial plot of PSI^2 or integral of pressure modulus (units: Pa $s^{0.5}$) for beams A, B and C as defined in Table 6.3.

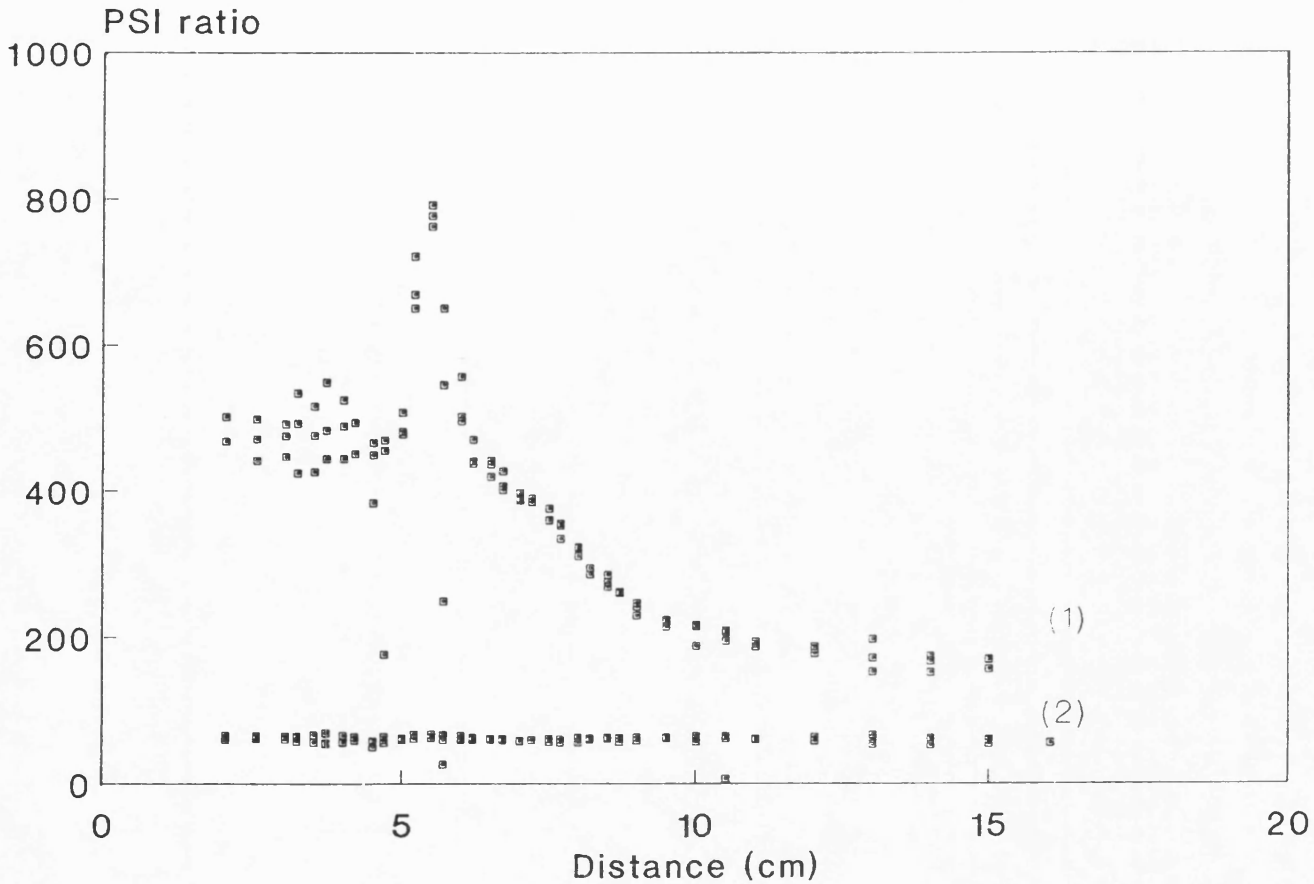

Figure 6.16 Axial variation in the ratios PSI_A/PSI_C and PSI_B/PSI_C in the acoustic field.

pattern of the source. These frequencies did not show a minimum and gave a higher value of PSI than the low amplitude case. In consequence an apparent gain in relative energy was observed on axis at the locations of the diffraction minimum. The second region, from 6 cm to 9.5 cm showed a constant reduction in the PSI ratio. This loss was equivalent to an absorption of 1.1 dB cm^{-1}, or a total enhanced absorption of 3.3 dB from the high amplitude beam, occurring on axis over a 3 cm region immediately in front of transducer focus. In the third region, beyond 9.5 cm the excess absorption was significantly lower, appoximately 0.2 dB cm^{-1}. In a similar investigation of total acoustic power loss in water Duck and Perkins (1988) reported a loss in total energy from a high amplitude, 3.5 MHz beam, of over 3 dB at a range of 12 cm.

For beam B, the PSI ratio was approximately constant demonstrating that no excess absorption was occurring, despite a degree of nonlinear distortion being observed. This suggests that the degree of nonlinearity, $\sigma = 1$, present in beam B was insufficient to generate significant excess absorption in water. For beam A, in which excess absorption was observed, it was shown (Section 6.5.2) that a $\sigma = 3$ shock had been generated.

Transverse profiles were measured at 10.5 cm and 12.5 cm from the transducer for each of the three beams allowing the off-axis enhanced absorption to be studied. Figure 6.17 shows the PSI ratios for beams A and B at 10.5 cm range. The ratios at 12.5 cm range are shown in Figure 6.18. For beam A, at 10.5 cm, the region of loss was seen to extend ±1 mm off axis, and to be bounded by a region in which there was almost no loss. Since the beam was circularly symmetric, this region was an annular ring. At 12.5 cm, the effects of diffraction in the far field of the transducer were seen. An apparent gain in energy occurred in an narrow annular ring approximately ±1.5 mm off axis corresponding to the areas of low intensity between the lobes of beam C. For beam B no significant

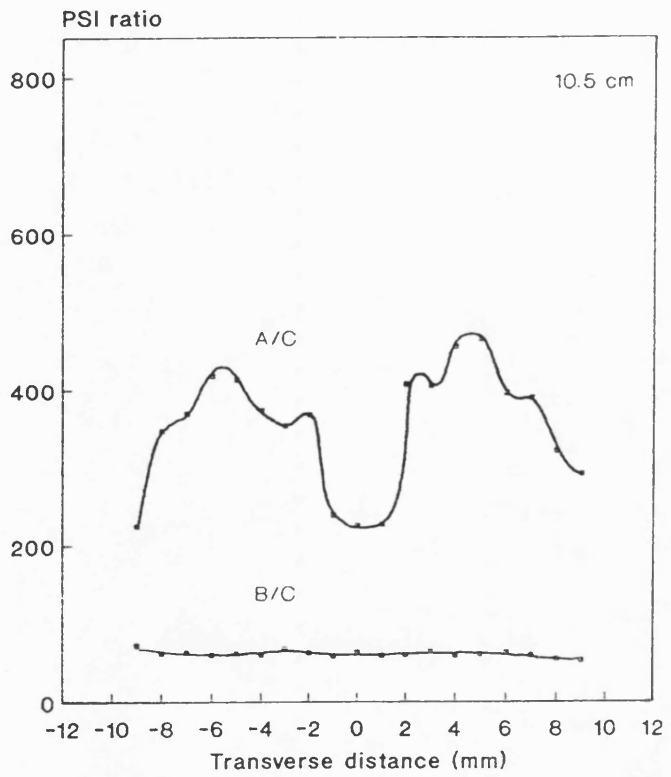

Figure 6.17 Transverse profiles of PSI_A/PSI_C and PSI_B/PSI_C at 10.5 cm range.

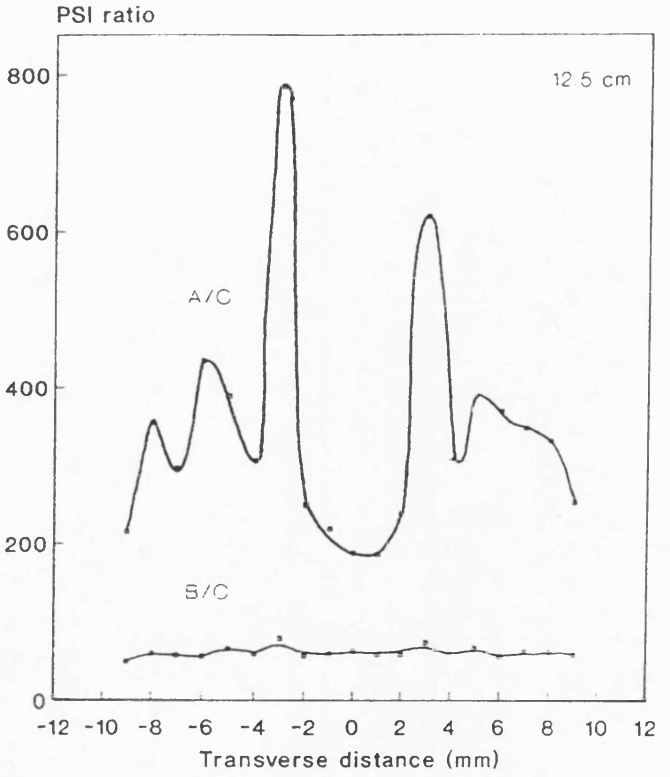

Figure 6.18 Transverse profiles of PSI_A/PSI_C and PSI_B/PSI_C at 12.5 cm range.

enhanced absorption was observed off axis.

The absorption coefficient of ultrasound in water increases as the square of the frequency and example values at 20 °C are tabulated in Table 6.7. Although in the low megahertz range water is generally regarded as lossless, this is not the case at higher frequencies. For example at 25 MHz the absorption of water is almost equivalent to that of liver tissue at 1 MHz (Parker 1988).

Frequency (MHz)	Absorption (dB cm^{-1})
1	0.0022
3.5	0.0266
10	0.217
25	1.356
35	2.67
100	21.70

Table 6.7 Absorption in water at 20 °C.

In the distorted high amplitude pulses of beam A, high frequency harmonic components were present for which the absorption coefficients were considerably higher than the absorption coefficient at the fundamental frequency. These components were therefore absorbed much more strongly. At the same time the intensity in each harmonic was progressively lower as was shown in Table 6.6. (For example assuming the beam was fully shocked, the intensity in the 10th harmonic was only 1/100 that of the fundamental intensity). Due to the process of nonlinear distortion however energy was continuously transferred into higher frequency components as absorption of these components occurred. This was primarily seen in the region in front of the focal zone of the transducer. The situation in beam B was that insufficient energy was being 'pumped' into the higher

frequencies to produce an observable difference in absorption.

Absorption provides a mechanism by which energy is lost from an acoustic wave. In water the transfer of energy by absorption will be greater when higher harmonic components are present in the wave. Although absorption will occur throughout the field, it will be enhanced in the region in front of the focus of the transducer as described above. This will result in enhanced streaming being generated in fields where a high degree of nonlinear distortion has occurred. It is postulated that the excess absorption occurring immediately in front of the focus of the transducer acts as a 'source pump' for the stream.

6.8 STREAMING VELOCITY PROFILES

6.8.1 Velocity measurements

Streaming profiles were measured at a number of axial locations within an acoustic beam. The pulsing conditions were identical to those given in Table 6.3 except that the peak positive pressure was 3.0 MPa in this case. At each location the position of the anemometer probe was adjusted to be on axis in order to maximise the output voltage, and measurements were made at 1.0 mm steps by moving the probe transversely across the acoustic beam. The width of each profile at half maximum was found graphically. Examples of profiles obtained at 8 cm, 9.5 cm and 14.5 cm from the transducer in the field of a high amplitude beam ($\hat{p}^+$ = 3 MPa) are shown in Figure 6.19(a), (b) and (c) respectively. It was estimated that stream widths could be measured to better than 0.5 mm from profiles such as those shown.

Since the active length of the anemometer probe was 1 mm some spatial averaging of streaming velocity occurred at each point of

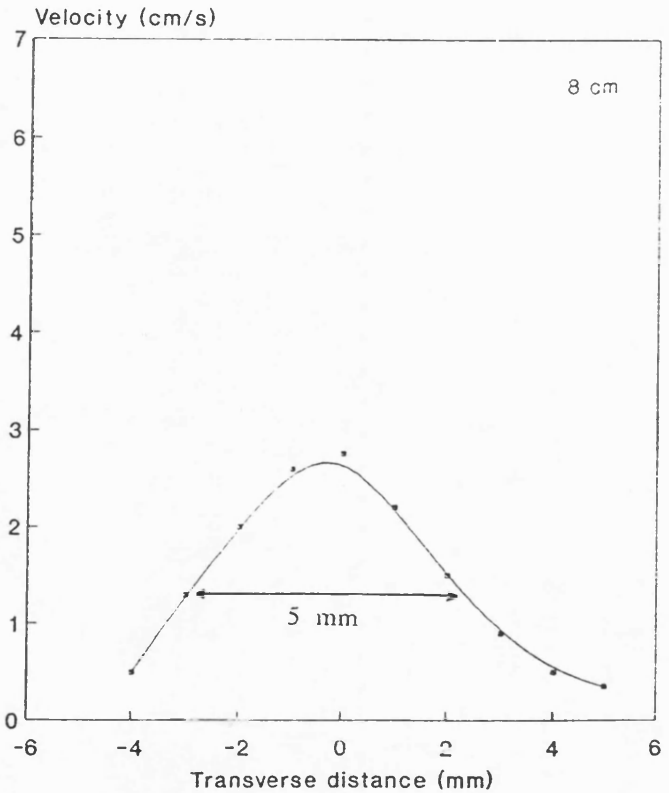

Figure 6.19a Example of streaming profile at 8 cm.

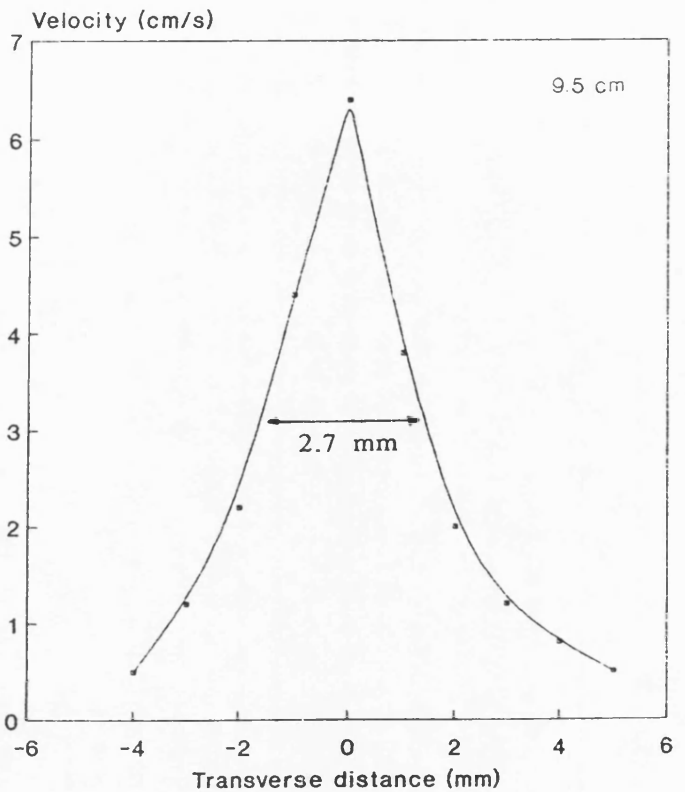

Figure 6.19b Example of streaming profile at 9.5 cm.

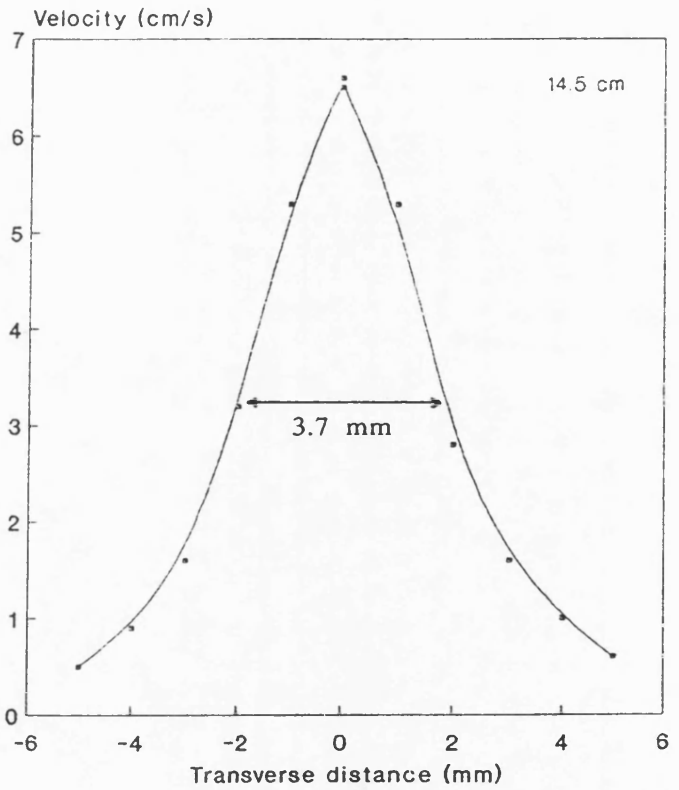

Figure 6.19c Example of streaming profile at 14.5 cm.

measurement. This resulted in an underestimate of the streaming velocity, particularly on or close to the axis where the velocity gradient was steep and near the focus where the profile was narrowest. Initially both horizontal and vertical profiles across circularly symmetric beams were measured but no difference between the two sets of results was observed. In the experiments described above all profiles were measured in the horizontal plane.

6.8.2 Comparison with acoustic measurements

Acoustic beam widths were measured at the −6 dB level using the ultrasound beam calibrator (described in Section 5.5). The axial variation in acoustic beam width is plotted in Figure 6.20 and stream widths measured at corresponding locations are also indicated in this figure. In the focal region the streaming width and the acoustic beam width were of similar magnitudes.

6.9 EFFECT OF A MEMBRANE IN THE STREAM

Membranes of two types were used to investigate streaming in a restricted volume. In a number of experiments, free standing plane membranes formed from "Clingfilm" stretched over a metal frame 10 cm x 10 cm were employed. For a second set of measurements a "clingfilm" membrane formed an end window on a perspex tube 3 cm in length and 1 cm in diameter. A small opening in the centre of the cylinder allowed the anemometer probe to be inserted in order to measure the streaming velocity generated inside the cylinder. The membranes used in these experiment allowed more than 95% transmission of ultrasound. Measured spatial peak intensities with and without a membrane in the beam were the same and similarly the amplitudes of the first 10 harmonic

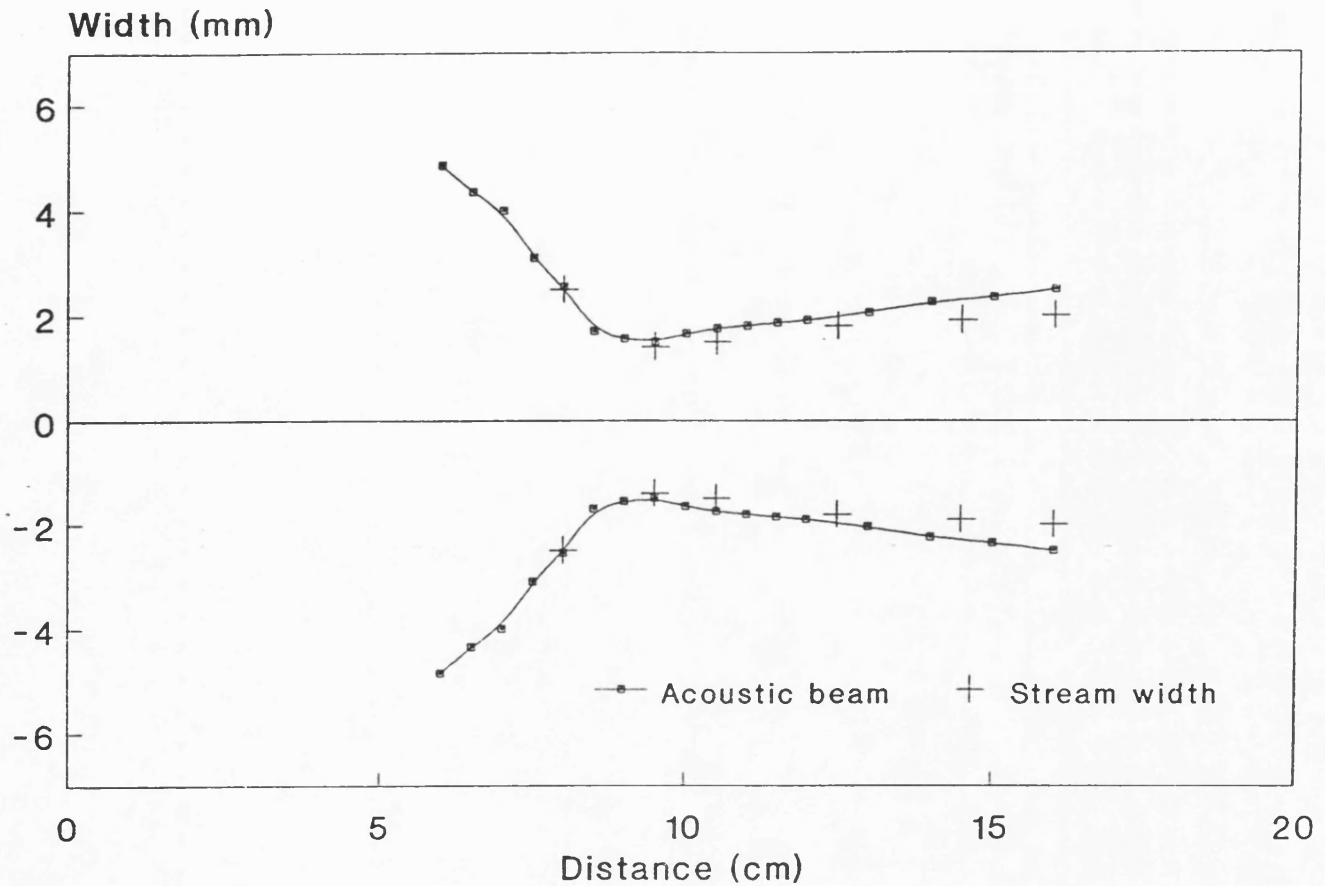

Figure 6.20 Axial variation in acoustic beam width and the stream width.

components obtained by Fourier analysis of the pulse waveforms at 8 cm, 10 cm and 12 cm, with and without a membranes were the same.

For the experiments described in this section, the location of the membranes relative to the location of the beam focus is important. This can be seen by consideration of Figure 6.15 in which the axial profile of the beam used here (beam A) is given.

6.9.1 Free-standing membranes

Using the 10 cm x 10 cm free-standing membranes the effect of obstructing the stream was investigated. Two such membranes were used, one positioned each side of the anemometer probe which was located 10 cm from the transducer. The experimental arrangement is shown in Figure 6.21.

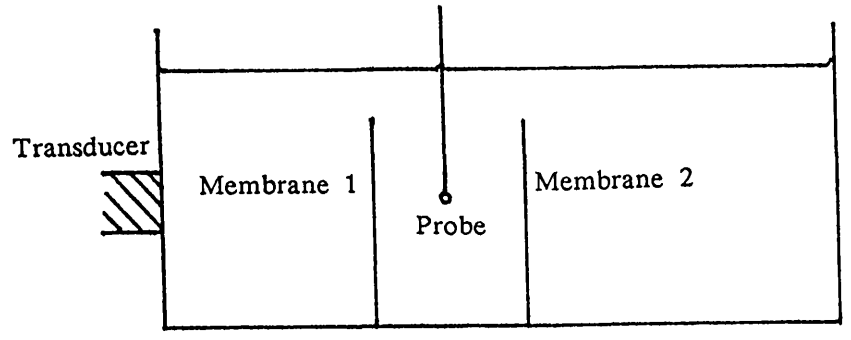

Figure 6.21 Experimental arrangement for membrane investigations showing the locations of the membranes, labelled 1 and 2 relative to the location of the probe; water bath viewed from the side.

The separation of the membranes was varied between 1 cm and 6 cm with the probe positioned centrally between them. Streaming velocities were measured at different separations firstly with both membranes in position and then with each membrane removed in turn. It was found that the velocity

was reduced by the presence of the membranes by an amount which depended on the probe/membrane separation. The velocity measured with a single membrane located at position 1 was identical to that measured with both membranes in position. In contrast, the velocity measured with a single membrane at position 2 was identical to the velocity of the unobstructed flow even at a probe/membrane separation of 0.5 cm. Thus a membrane located 'downstream' from the point of measurement had no effect on the streaming velocity.

The effect of varying the distance between the probe and a membrane located on the transducer side of the probe ('upstream') is shown in Figure 6.22 for measurements made at 10 cm range. In Table 6.8 the flow velocities measured with the probe located 8 cm, 10 cm and 16 cm from the transducer are expressed as a percentage of the unimpeded velocity.

Probe/memb. separation cm	% of maximum streaming velocity measured at: 8 cm	10 cm	16 cm
0.5	50	42	8
1.0	69	63	15
2.0	100	84	28
3.0	100	93	38

Table 6.8 Recovery of streaming velocity beyond a membrane; measurements carried out at 8 cm, 10 cm and 16 cm range.

When the membrane/probe separation was small the flow velocity was reduced, to a degree which depended on the measurement location. For example, for a separation of 1.0 cm the velocity was reduced to 15% of the unimpeded velocity at 16 cm range while at 8 cm range, almost 70% of the flow remained.

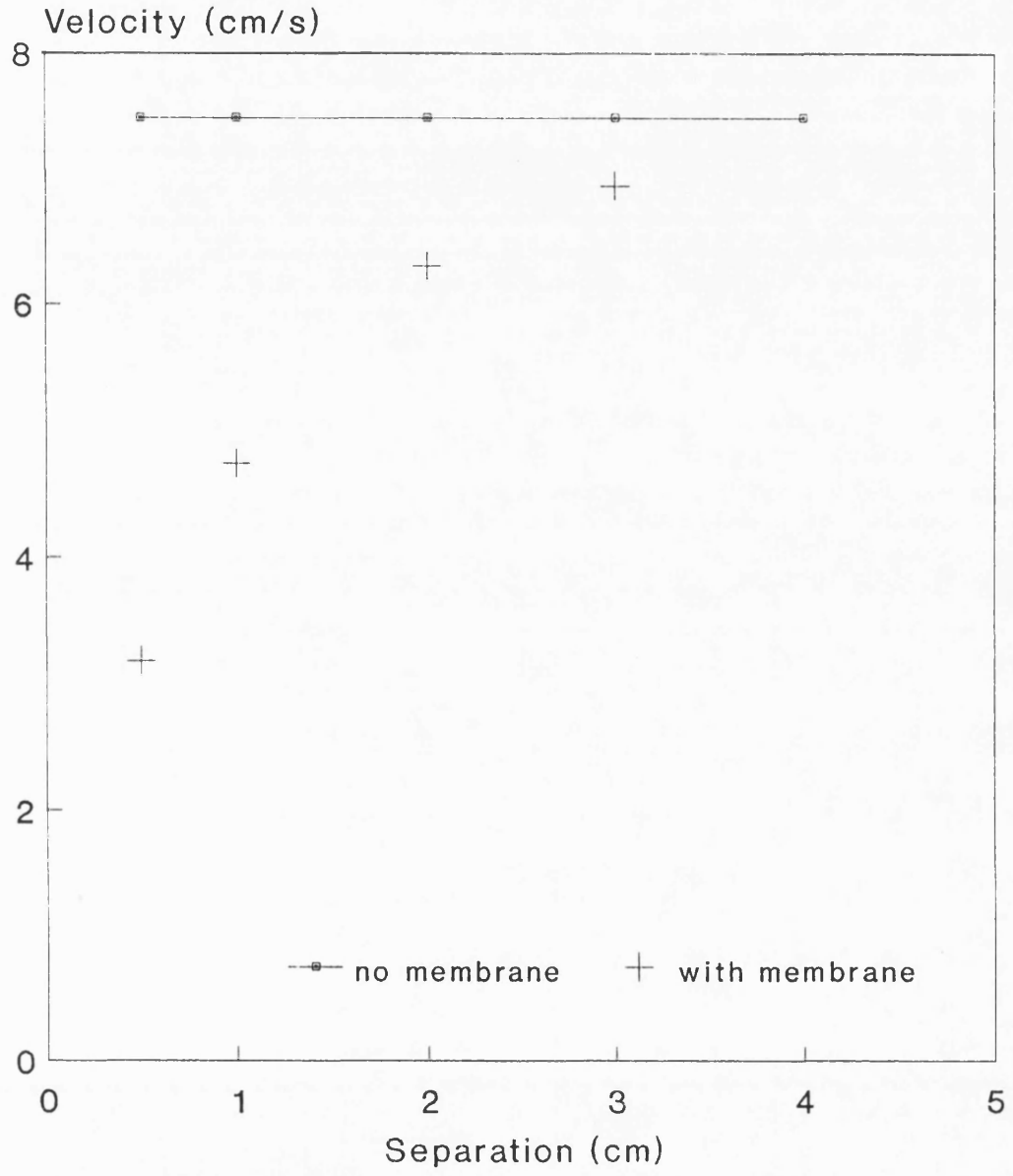

Figure 6.22 Recovery of stream beyond a membrane as a function of probe/membrane separation; measurements at 10 cm.

Manipulation of the anemometer probe closer to the membrane was very difficult experimentally so that, while it is probable that finite flow existed at separations less than 0.5 cm, no experimental evidence is available.

In the region corresponding to maximum absorption, described in Section 6.7, the stream was unaffected by the presence of a membrane more than 2 cm upstream from the point of measurement. In the region beyond the focus, recovery of the stream was significantly poorer even when the probe was positioned 5 cm upstream of the membrane. A possible explanation was that the membrane prevented the flow of fluid generated in the region of maximum absorption near the focus, from moving downstream to the point of measurement and contributing to the total flow. A degree of recovery was still observed which was attributed to local absorption in the region between membrane and probe.

In a separate series of experiments streaming velocity beyond a membrane was measured over the range 4.5 cm to 14 cm from the transducer. Measurements were made for fixed membrane/probe separations of 1 cm and 0.5 cm, for a single membrane at position 1, and for membranes at positions 1 and 2. In this case the probe and membrane were moved together. The results were identical with and without the membrane at position 2, again showing that a membrane located downstream from the point of measurement had no effect on the streaming velocity. A third set of measurements was made without either membrane in the beam. Figure 6.23 shows the resulting streaming velocities measured on axis in all these situations. Two differences are apparent in the curves. Firstly, the streaming velocity at any location in the beam was reduced by the presence of a membrane placed upstream and the reduction is greater for smaller probe/membrane separations. Secondly, whereas the streaming velocity in the unimpeded beam reached a plateau just beyond the focus, when a membrane was inserted the streaming velocity peaked earlier and at

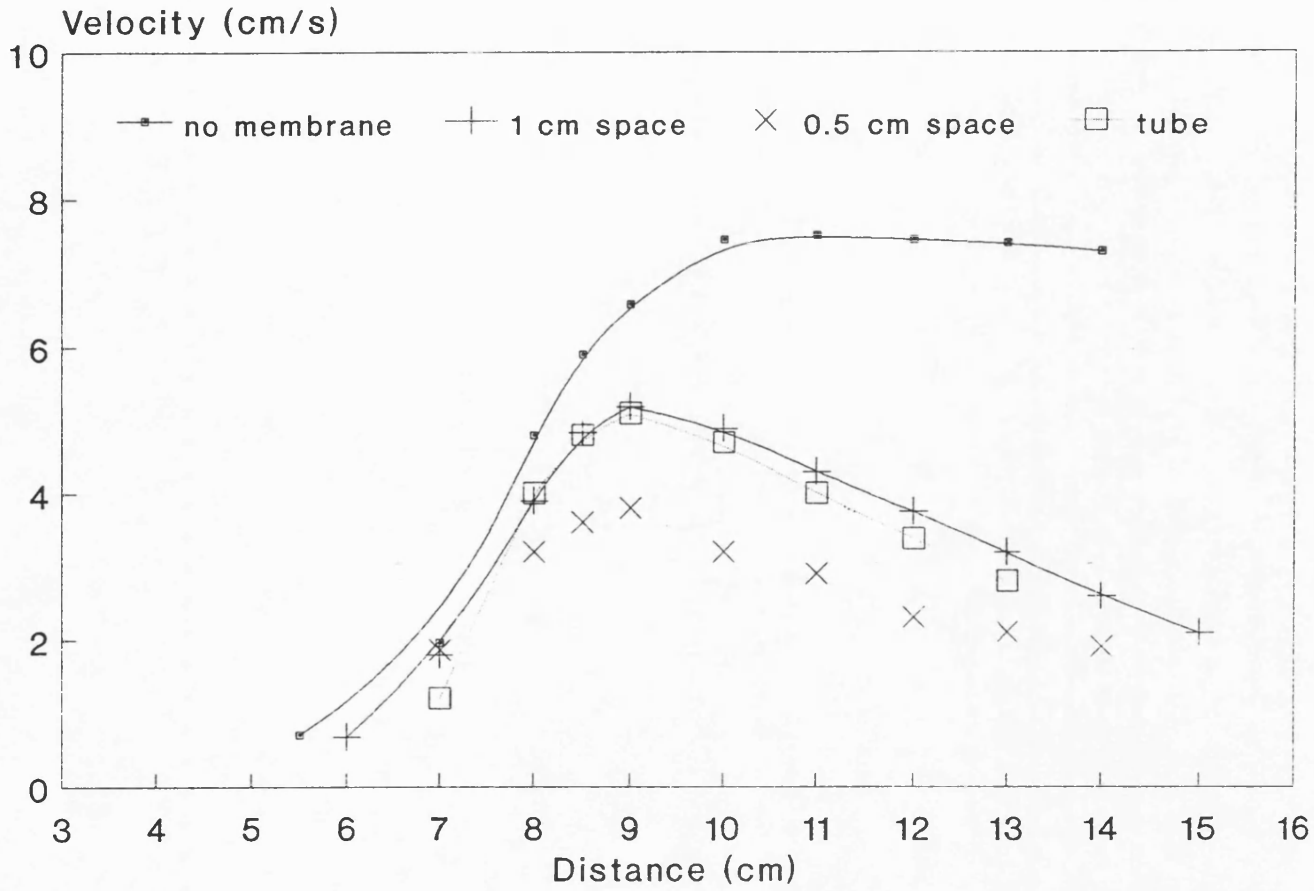

Figure 6.23 Axial plot of streaming velocity for different probe/membrane seperations; seperation with tube 1.25 cm.

lower level, and decreased steadily beyond the focus. This was due to the removal of the flow component generated near the focus.

6.9.2 Streaming velocity in a tube

To investigate the effect of restricting the volume of fluid further a 1 cm diameter tube was used. Initially measurements were made with the tube open at each end and subsequently with a thin "clingfilm" end window fitted over the end corresponding to location 1 in Figure 6.21 above. The tube was secured to the mounting of the anemometer probe so that the probe was located 1.25 cm from each end. The probe and the tube could be moved as a single, rigid assembly throughout the field. Measurements were made at intervals of 1 cm along the beam axis over the range 6 cm to 13 cm from the transducer. The position of the probe/tube assembly was adjusted at each location using the micromanipulator to maximise the anemometer output voltage. The same measurements were repeated without the tube in the beam and the results were identical to those obtained for the open ended tube.

It was found that within experimental error the presence of an open ended 1 cm diameter tube did not impede the flow at any location in the beam at which measurements were made. Over this range the beam width varied, from approximately 5 mm at 6 cm from the tranducer, to less than 3 mm at the focus and increasing again to about 5 mm at 13 cm, and was always less than the diameter of the tube, although not greatly so. Eckart (1948) showed theoretically that the presence of boundary walls results in a reduction in maximum streaming velocity by reducing the space available for the return flow (see Section 4.2.3). However the measurement situation described here differs from that considered by Eckart in that return flow was able to take place in the large fluid volume outside the tube without

without any restriction of the forward flow. With the membrane window on the tube the velocity was slightly lower than that measured with a free standing membrane in the field at a similar probe/membrane separation. The axial variation in streaming velocity in the tube with the end window attached is also indicated in Figure 6.23.

6.9.3 Discussion of membrane results

A major contribution to streaming beyond the focus of the transducer was due to the flow of fluid from upstream. When a membrane was inserted close to the anemometer probe this contribution was removed and the streaming velocity reduced substantially. As the distance between the probe and the membrane was increased the streaming velocity "recovered"; for example in the investigations described above with the probe located at 10 cm and the membrane 3 cm in front, that is at 7 cm from the transducer, absorption of the distorted wave in the region between the probe and the membrane was sufficient to restore the streaming velocity to near the unimpeded level. If the stream was generated locally at the point of measurement and was not influenced by flow from elsewhere in the field the distance between the membrane and the probe would be less unimportant. The region of high absorption in front of the transducer appeared to act as a 'pump' for the stream. In the region beyond the focus, where absorption was shown to be relatively low, streaming was due in part to the forward pressure of flow generated nearer the focus and in part to local absorption. The presence of a membrane reduced the streaming velocity by removing the first of these components, the contribution of the "pump".

6.10 STREAMING TIME CONSTANTS

The time taken for the stream to become established after the ultrasound was turned on, the "rise time", and also the time for the flow to cease after turn-off, the "decay time", were investigated. Measurements were made from an oscilloscope display of the linearised anemometer output voltage as described in Section 5.4.4. A number of pulsing parameters such as amplitude and pulse repetition frequency were varied in order to change the magnitude of the streaming velocity and the effect on the rise times and decay times was investigated. Similar measurements were made at a number of locations in the field. All result quoted were the average of three separate measurements. The time constants measured here relate to the flow of fluid passing a fixed point in the field.

6.10.1 Rise times

For these measurements the anemometer probe was located 10 cm from the 3.5 MHz transducer on the beam axis and the voltage output was maximised. The pulse repetition frequency of the beam was varied from 0.5 kHz to 10 kHz and measurements of streaming velocity and rise times were made. Other acoustic parameters were held constant; the pulse length at 2.8 μs and the peak positive pressure, $\hat{p}^+$, at 3.0 MPa. The results of this investigation are given in Table 6.9 and are also plotted in Figure 6.24. It can be seen that the streams were established very rapidly; in all cases the rise time was less than 1 second. This is short in comparison with the "dwell time" of a pulsed Doppler transducer in clinical use.

Prf (kHz)	I_{spta} (mW cm^{-2})	Velocity (cm s^{-1})	τ_R (s)
10	3615	17.8	0.09
5	1805	13.2	0.14
2	723	8.0	0.26
1	361	5.5	0.39
0.5	180	2.9	0.66

Table 6.9 Measurement of rise times at different pulse repetition rates.

The rise time can be seen to decrease rapidly with increasing pulse repetition frequency between 0.5 kHz and 5 kHz. This can be explained by considering the effect of the acoustic wave on the initally stationary fluid. A given volume of fluid located on the beam axis received a forward impulse due to the wave only during the acoustic pulse, that is for approximately 3 μs. This process was repeated continuously at the pulse repetition frequency of the beam, once every 1 millisecond at a pulse repetition frequency of 1 kHz. The stream became established therefore as the result of the cumulative effect of a series of 'impulses'. The more rapidly these impulses were delivered (increased pulse repetition frequency) the more rapidly the streaming velocity built up and hence the smaller the magnitude of the rise time measured. An upper limit on the streaming velocity resulted from the viscosity of the fluid which acted to oppose the motion of the stream. In the period between acoustic pulses, a degree of slowing down may have occurred due to the viscous drag at the boundary between the moving fluid and the stationary fluid but no modulation corresponding to this frequency was observed in the oscilloscope display of the anemometer output voltage.

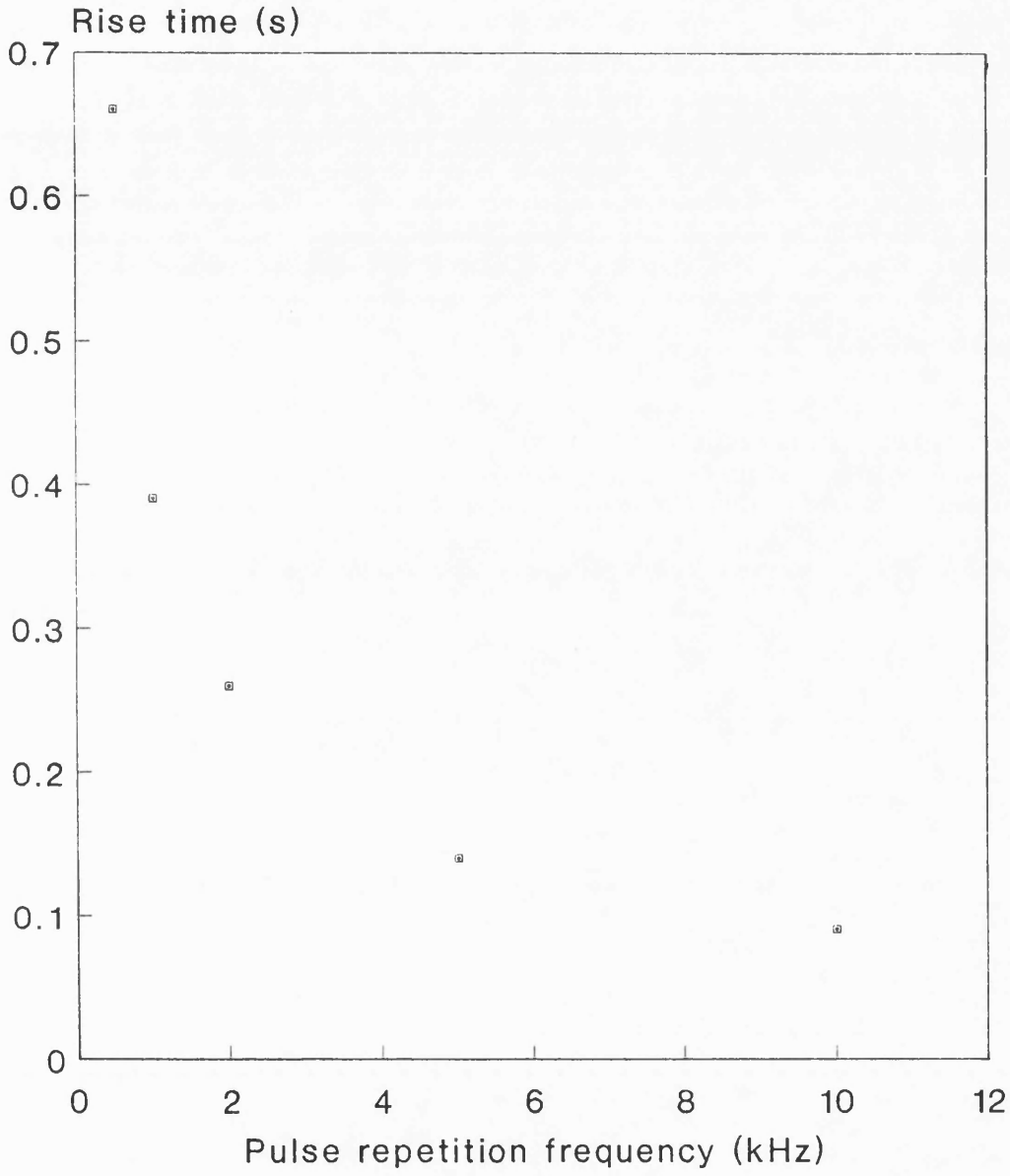

Figure 6.24 Rise time as a function of pulse repetition frequency.

In a separate investigation, streaming velocity and rise time measurements were made at a range of spatial peak temporal average intensities from 300 to 800 mW cm^{-2}, pulse average intensities 71 W cm^{-2} to 126 W cm^{-2}. The results are shown in Table 6.10. An increase in the time taken for the stream to become established was apparent as the intensity in the beam was decreased. In this experiment intensity was varied by varying the pulse amplitude and thus the harmonic content in the beam was different for each measurement. The shock parameter, σ_m, was calculated using Equation 4.12 for the conditions corresponding to each measurement and is also given in Table 6.10.

$\hat{p}^+$ (MPa)	I_{sppa} (W cm^{-2})	Velocity (cm s^{-1})	τ_R (s)	σ_m
3.1	126	8.4	0.25	2.1
3.0	118	7.7	0.26	2.0
2.7	92	5.2	0.28	1.8
2.4	71	2.9	0.30	1.6

Table 6.10 Measurement of rise time at different acoustic intensity (altered pulse amplitude); 10 cm from 3.5 MHz transducer, 2.8 μs pulse length, 2 kHz

It has been reported by a number of authors (for example Carstensen and Muir 1980) that the beam widths of higher harmonic components in an acoustic beam are progressively narrower. Due to this effect the acoustic energy is more tightly concentrated and for this reason, in the experiment described above, greater absorption or energy loss was seen to occur on the beam axis. The volume of fluid absorbing the energy was therefore smaller and the viscous interaction between the cylinder of moving fluid and the surrounding stationary fluid was reduced. This is suggested as the explanation for the observed decrease in rise times in higher amplitude beams.

A third investigation was carried out in which rise times were measured at a number of locations on the beam axis over the range 7 cm to 14 cm from the transducer. A number of parameters varied over this region, for example acoustic beam width and hence spatial average intensity, and also pulse amplitude and harmonic content. Table 6.11 shows the measured values of rise times at each location. It was stated in Section 4.2.5 that rise time varies with the square of acoustic beam width (Rudenko and Soluyan 1971a) but for the reasons discussed above the interpretation of these results was difficult. It was observed however that rise times were shorter in a region just in front of the transducer focus than elsewhere in the field which coincided with the position of minimum acoustic beam width. This was also within the region of maximum shock loss. In the region 10 cm to 14 cm from the transducer the streaming velocity was approximately constant but the rise time increased by a factor of 4. An increase in rise times beyond the focus would be expected due to the time taken for fluid set in motion in the focal region to pass the probe.

Distance (cm)	Velocity (cm s^{-1})	τ_R (s)	Beam width −6 dB (mm)
7	1.4	0.56	4.9
7.5	2.0	0.30	3.8
8	4.4	0.17	3.5
9	7.2	0.18	3.1
10	7.9	0.25	3.3
11	7.9	0.33	3.7
12	7.8	0.48	4.0
14	7.8	1.02	4.2

Table 6.11 Axial variation of rise times; 3.5 MHz transducer, $\hat{p}^+$ = 3.0 MPa, 2 kHz, 2.8 μs pulse length.

Figure 6.25 shows an example of the anemometer output voltage displayed on an oscilloscope as the ultrasound beam was switched on. (The data obtained from this photograph is given in Table 6.9; 2 kHz prf.)

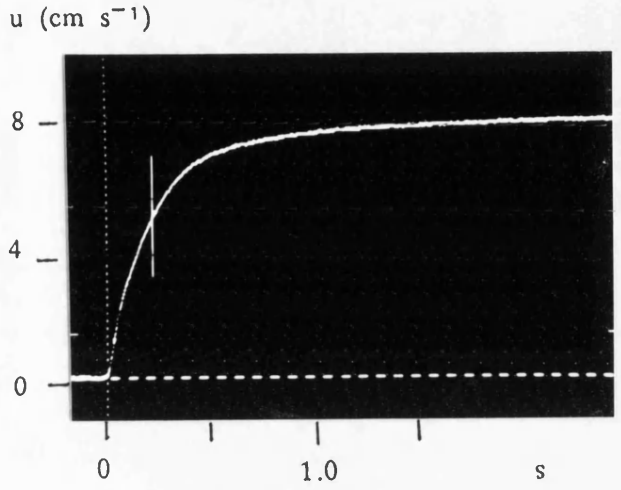

Figure 6.25 Initial increase in anemometer output voltage.

6.10.2 Decay Times

Decay times were measured as a function of pulse repetition frequency in a similar way to that described in Section 6.10.1. The results are shown in Table 6.12.

Prf (kHz)	I_{spta} (mW cm^{-2})	Velocity (cm s^{-1})	τ_D (s)
10	3615	19.1	0.36
5	1805	13.9	0.37
2	723	8.2	0.42
1	361	5.8	0.50
0.5	180	3.3	0.53

Table 6.12 Decay times at different pulse repetition frequencies; 10 cm from 3.5 MHz tranducer; 2.8μs pulse length, $\hat{p}^+$ = 3 MPa

At lower pulse repetition frequencies the streaming velocity was reduced and there was an increase in the time taken for the stream to decay after the beam was turned off. Initially it was thought that the decay constant would be independent of streaming velocity because the viscous force would be constant. However, since the anemometer was fixed at a point in the field 10 cm from the transducer it responded to the passage of fluid passing that point rather than the way in which a given volume of the fluid was slowing down. At 10 cm, the probe was located just beyond the focus and beyond the region in which maximum streaming generation occurred. A high velocity stream generated in this region could be expected to pass the probe more rapidly than one moving more slowly, with the result that the decay time appeared shorter.

If these results are compared with the rise times in Table 6.12 it can be seen that the decay times were consistently longer than the rise times. The rise time of a stream is defined by the cumulative effect of a series of impulses delivered at the pulse repetition rate, balanced by the viscous drag opposing the motion. The decay time depends only on the viscous drag.

Decay times were also measured over a range of intensities from 300 mW cm^{-2} to 800 mW cm^{-2} obtained by varying the pulse amplitude. The results are shown in Table 6.13. In this experiment the measured decay time was longer at high streaming velocities than at lower velocities. This contrasted with the results obtained by changing the pulse repetition rate at constant pulse amplitude. The following explanation is suggested. Increasing the pulse amplitude caused the harmonic content in the pulse to increase and in particular the location of shock formation to move progressively closer to the transducer. In consequence, the region of excess absorption moved towards the transducer and thus a larger volume of fluid was set in motion, at a greater distance from the anemometer probe. When the ultrasound beam was turned off, the time taken for the total

volume of fluid induced to flow in the high amplitude beam to pass the anemometer probe was longer than for the low amplitude beam, resulting in a longer decay time.

$\hat{p}^+$ (MPa)	I_{sppa} (W cm^{-2})	Velocity (cm s^{-1})	τ_D (s)	σ_m
3.1	132	9.2	0.40	2.2
3.0	118	7.9	0.38	2.0
2.8	103	7.0	0.30	1.9
2.6	84	4.4	0.22	1.7
2.4	71	2.5	0.18	1.6

Table 6.13 Decay times at different pulse amplitudes at 10 cm from a 3.5 MHz transducer; 2 kHz pulse repetition frequency.

The results of decay time measurements made on the beam axis over the range 7cm to 12 cm from the transducer are shown in Table 6.14.

Distance (cm)	Velocity (cm s^{-1})	τ_D (s)	Beam width -6dB (mm)
7	1.7	0.35	4.9
8	4.6	0.28	3.5
9	7.3	0.35	3.1
10	8.0	0.43	3.3
11	7.9	0.61	3.7
12	7.8	0.80	4.0

Table 6.14 Decay times on the axis of a 3.5 MHz beam; $\hat{p}^+$ = 3 MPa, 2 kHz pulse repetition frequency.

The decay time in the focal region was shorter than at more distal locations

in the field. This was due, at least in part, to the stream travelling further when the probe was moved downstream from the focal region. A number of parameters varied over this range, for example beam radius and harmonic content, which made the results difficult to interpret fully.

Figure 6.26 shows an example of the anemometer output voltage captured on an oscilloscope as an ultrasound beam was switched off. (The data obtained from this photograph is given in Table 6.12; 1kHz prf.)

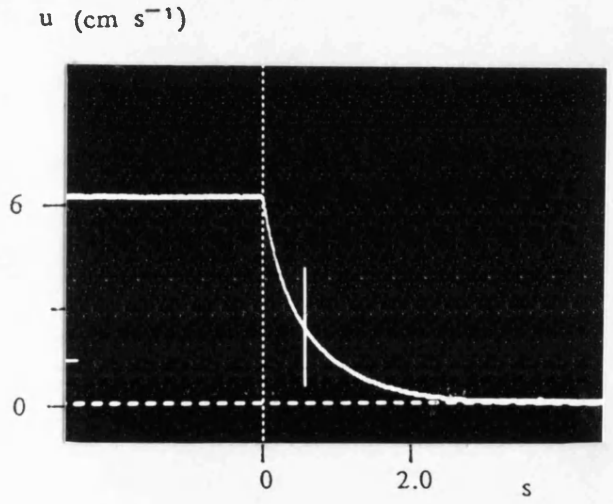

Figure 6.26 Decay of the anemometer output voltage.

6.10.3 Errors in time constant measurements

Linearisation of the output voltage was good over the range 1 cm s^{-1} to 10 cm s^{-1} (see Figure 5.10). No rise time or decay time measurements were made for which the maximum velocity was less than 1.4 cm s^{-1} but in two of the measurement presented above the velocity at 1/e of maximum was less than 1 cm s^{-1}. These results corresponded to the lowest pulse amplitudes and a small systematic error may have been introduced by assuming accurate linearisation of the output voltage below 1 cm s^{-1}. Each

value quoted was the average of three measurements for which the random variation about the mean was commonly less than 5%.

6.11 MEASUREMENT OF THE STREAMING GENERATED BY DIAGNOSTIC ULTRASOUND EQUIPMENT

6.11.1 Streaming measurements

The streaming velocities generated in water by a number of commercial, diagnostic ultrasound units were measured. The anemometer probe was located in the beam at a point where significant streaming was anticipated from measurements of the acoustic field. The position of the probe was then adjusted in order to maximise the voltage output and it was moved along the axis of the transducer to discover the location at which the streaming velocity was highest. The intention was to measure the maximum streaming velocity which could be generated in water by each unit. In order to achieve this a series of measurements were made to find the instrument settings and the location in the field at which the streaming velocity was maximum. Table 6.15 illustrates this with some preliminary measurements made on one scanner. To obtain these results the probe was moved along the longitudinal axis of the transducer and the setting of the range gate was varied in a systemmatic way.

Range gate (mm)	Probe Distance (cm)	Velocity (cm s^{-1})
99	2.5	3.7
99	3.0	5.0
99	4.0	4.7
30	3.0	4.3
30	4.0	5.2
30	5.0	4.3
20	2.5	4.7
20	3.0	5.0
20	3.5	4.3

Table 6.15 Sample measurements made to obtain maximum streaming velocity; Diagnostic Spectra scanner with 7.5 MHz linear array, operating in pulsed Doppler mode at 6 MHz.

A number of scanners operated with more than one scanhead and for these units the maximum streaming velocity for each combination of scanner and scanhead was measured. Three modes of operation were available on many units and maximum velocities were obtained for each mode where appropriate. The results are shown in Table 6.16(a) for pulsed Doppler mode, Table 6.16(b) for M-mode and Table 6.16(c) for imaging mode operation. In each case maximum velocities only are quoted.

The highest streaming velocities were generated in pulsed Doppler mode particularly by equipment with high time average intensities. Some units operating in pulsed Doppler mode employed long pulses, for example pulse durations up to 12.5 μs was observed, compared with imaging pulse durations which are of the order of a microsecond and pulse durations employed in the laboratory set-up of approximately 3 μs.

Scanner	Transducer	Freq (MHz)	Prf (Hz)	$\hat{p}^+$ (MPa)	$\hat{p}^-$ (MPa)	I_{spta} (mW cm^{-2})	u_{max} (cm s^{-1})
ATL Ultramark 8	PV10*	5	11000	3.3	−1.9	6200	14+
	Access C	2.25	3200	2.5	−1.5	320	0.3
Acuson 128	S328*	3.5	6100	3.9	−1.4	4000	14+
	L538	5	6100	3.3	−1.5	1700	3.5
Toshiba Sonolayer	PSE-37L	3.75	4100	5.2	−3.2	1100	3.9
	PSD-73D	3.0	4100	5.8	−2.8	930	1.4
Diasonics Spectra	LA	7.5	14300	5.0	−3.1	2290	5.2
	AA	5	13900	1.9	−0.8	3360	3.7

* Measurement made at higher output than is currently available on this equipment

+ Value from extrapolated calibration curve

Table 6.16(a) Maximum streaming velocities in water generated by commercial equipment; pulsed Doppler mode

Scanner	Transducer	Freq (MHz)	Prf (Hz)	$\hat{p}^+$ (MPa)	$\hat{p}^-$ (Mpa)	I_{spta} (mW cm^{-2})	u_{max} (cm s^{-1})
Acuson 128	S519	5	600	3.0	−2.0	66	0.8
	L382	3.5					1.6'
Kretz Combison 100	NR3.5	3.5	3100	7.4	−2.1	590	5.5
Toshiba Sonolayer	PSE−37L	3.75	860	4.6	−2.3	93	2.5'

' M−mode plus imaging

Table 6.16(b) Maximum streaming velocities in water generated by commercial equipment; M−mode

Scanner	Transducer	Freq (MHz)	Frame rate (Hz)	$\hat{p}^+$ (MPa)	$\hat{p}^-$ (MPa)	I_{spta} (mW cm^{-2})	u_{max} (cm s^{-1})
ATL Ultramark 8	PV10	5	11	3.9	−2.4	3.7	0
Acuson 128	S328	3.5		4.6	−2.6	5.4	1.2
	L558	5	17	2.6	−2.3	2.5	0.3
	L538	5	54.9	3.7	−1.9	29	1.0
	L538	5					1.3'
Kretz Combison 100	NR3.5	3.5	36	7.4	−2.1	21	0.5
Toshiba Sonolayer	PSE−37L	3.75	18	5.3	−3.0	21	0.8
	PSD−73D	7	34.5	4.3	−3.7	31	0.5

'Imaging plus colour flow mapping

Table 6.16(c) Imaging mode

It can be seen in Table 6.16 that higher pulse repetition frequencies were generally observed for pulsed Doppler units whereas pulse amplitudes were comparable in all modes (see also Section 1.4).

The maximum streaming velocity measured in imaging mode was 1.2 cm s^{-1}. This was low in comparison with the Doppler values, mainly due to the low frame repetition frequencies. However this velocity was generated by energy transfered to the fluid from a pulse of approximately 1 μs duration occurring only once every 50 ms, a mark to space ratio of 2 x 10^{-5}. A large volume of fluid in the scan plane of the transducer was set in motion so that the stream profile in the scan plane was many centimetres in width (shown in Figure 6.7), while in the perpendicular direction it was typically a few millimetres wide.

6.11.2 Rise times and decay times

Measurements of rise times and decay times were made on a pulsed Doppler beam generated by an Acuson 128 scanner and a 3.5 MHz transducer (S328). The control settings were adjusted to produce maximum streaming velocity and the anemometer probe was located 10 cm from the transducer in a water-bath. This was the location of maximum streaming velocity. The rise time measured was 86 ms and the decay time was 0.29 s. (The output on this unit has subsequently been reduced with the result that these time constants may no longer be representative.)

Rise times in commercial physiotherapy beams (Therasonic 1030) were observed to be greater than diagnostic rise times and commonly of the order of seconds. This was due to the greater beam width, typically of the order of 1 cm, and the inertia of the larger volume of fluid set in motion.

6.12 STREAMING IN WATER BEYOND A TISSUE SAMPLE

A 2 cm thick sample of bovine liver was immersed in a small quantity of physiological saline and contained in a polythene bag. The saline prevented deterioration of the liver due to dessication and also helped to exclude air within the sample. The bag containing the liver was suspended on the axis of the ultrasound beam at a range of distances from the transducer while the anemometer probe was used to measure the streaming velocity at 12 cm. The experimental arrangement in shown in Figure 6.27.

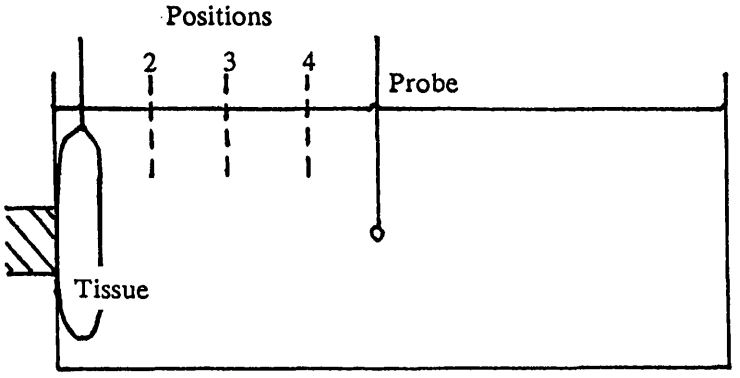

Figure 6.27 Experimental arrangement showing different locations of the tissue sample.

A 3.5 MHz Diagnostic Sonar transducer (MD3483) was operated at 2 kHz pulse repetition frequency, 3.4 μs pulse duration and 3 MPa peak positive pressure. The results of the velocity measurements are shown in Table 6.17 where the distance quoted is the separation between the transducer and the centre of the liver sample.

The results indicated that although the streaming velocity was substantially reduced by the presence of the tissue due to attenuation of the beam it was still possible to generate some streaming in the fluid beyond, particularly with the liver positioned adjacent to the transducer and a relatively long water path to the probe.

Distance (cm)	Velocity (cm s^{-1})
contact	1.6
6	1.3
8	1.2
10	<0.5
no tissue	7.4

Table 6.17 Streaming velocity in water beyond 2 cm of bovine liver.

This experimental arrangement may be assumed to model the clinical situation in which ultrasound passes through the maternal skin and the wall of the uterus into a volume of amniotic fluid or bladder fluid. In a survey of 74 obstetric ultrasound examinations Duck and Perkins (1988) reported abdominal wall thicknesses of 0.7 cm to 6.0 cm with a mean value of 2.1 cm, and bladder path-lengths of 3.0 cm to 10.5 cm. Carson *et al.* (1989), from measurements of 22 patients, reported a mean total thickness of overlying tissues of 2.9 cm and a minimum value of 1.7 cm. The exposure factors used for this investigation were modest in comparison with the maximum settings available on some commmercial pulsed Doppler units and therfore it may very well be possible to generate streaming in amniotic fluid *in vivo* by transcutaneous application of ultrasound. If a vaginal probe is used in pulsed Doppler mode the attenuation of the beam by overlying tissue will be reduced, increasing the likelihood of streaming occurring.

6.13 EFFECT OF STREAMING ON CELL ADHESION

The purpose of the following experiments was to investigate the effects of streaming on cell adhesion. Cells growing on perspex were positioned at

two locations in an ultrasound field in which streaming occurred. One position corresponded to the location of maximum acoustic absorption and one to the location of maximum velocity. The aim was to investigate de-adhesion by the physical interaction of the stream with the cells. Shear forces generated by the stream were thought to be maximal in the region of enhanced acoustic absorption.

Human fibrolast cells were provided, either grown on thin coverslips 2.5 cm in diameter or in flat sided plastic bottles. The cells were long and thin in appearance and were grown to confluency, that is until they formed a single contiguous layer over the supporting plate. When cells were grown in plastic bottles the bottles were cut open paralled to the face on which the cells were growing using a hot wire in order to remove any obstruction to the stream.

The two arrangements were used and are shown diagrammatically in Figure 6.28(a) and (b).

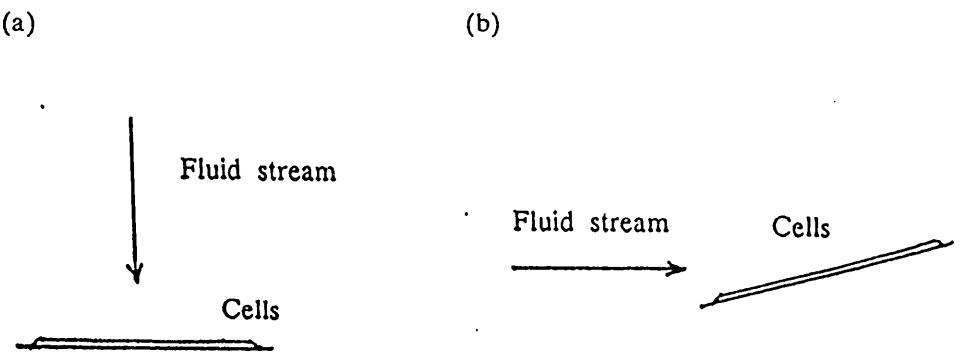

Figure 6.28 Experimental arrangement for cell experiments; fluid flow represented by arrow; (a) flow perpendicular, (b) flow "glancing" cells.

The fluid stream was either directed onto the cells perpendicular to the plane of the supporting plate or the plate was tilted so that the fluid stream hit the cells at a glancing angle, approximately 10°. In each case the plate supporting the cells was immersed in a solution of phosphate buffered saline (PBS) and glucose which kept the cells alive and also provided the transmission fluid for the ultrasound. In the first case the cells were positioned on axis at a distance of either 8 or 10 cm from the transducer. Figure 6.29 shows the detailed experimental arrangement.

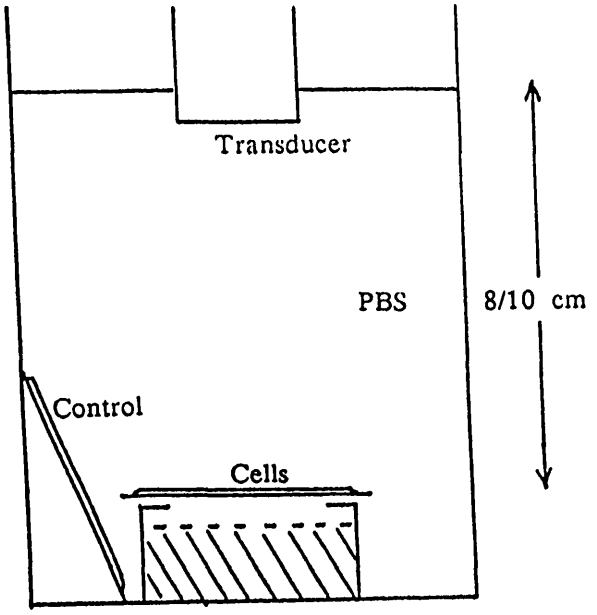

Figure 6.29 Detailed experimental arrangement for cells on a coverslip with the ultrasound beam incident normally.

Care was taken to ensure that the cells were aligned with the beam axis by attaching a plumb line temporarily to the face of the trandsucer using "Plasticine" during the setting up procedure. The transducer was supported in a micromanipulator enabling the ultrasound exposure and the induced stream to be delivered over a matrix of 3 x 3 points at 1 mm spacings.

The exposure at each point was of 5 minutes duration and produced by a Diagnostic Sonar 3.5 MHz transducer (MD3843) operating at 5 kHz pulse repetition frequency and 3 μs pulse duration with a peak positive pressure amplitude in water of 3 MPa. The maximum streaming velocity generated

in water was approximately 13 cm s^{-1}. An identical group of cells formed a 'control' and were also immersed in the PBS in the exposure vessel but were not exposed to the direct stream thoughout the exposure time. Both groups were examined under a microscope both before and after insonation. The experiments were repeated on three separate occasions with five groups of exposed/control cells in total and no de-adhesion of the cells was observed.

In the second arrangement, the plate on which the cells were growing was tilted almost parallel to the stream with the centre of the cell layer approximately 8 cm from the transducer. A matrix of points were exposed to the stream for a duration of 5 minutes as described above and again no de-adhesion of the cells was observed under a microscope.

6.14 STREAMING IN PHYSIOTHERAPY FIELDS

Measurement of the streaming velocities generated in the field physiotherapy equipment is difficult. In an attempt to measure the velocities generated by a Therasonic 1030 commercial physiotherapy unit using hot film anemometry, inconsistent results were obtained due to the growth of bubbles on the probe. The use of a technique involving the timed passage of a dye stream, described in Section 5.3.2, was also attempted but proved difficult. (This method was suggested by Quraishi and Fahidy (1982) for measurement of velocities up to 5 cm s^{-1}). One problem was the long build up time of streams generated in these fields, coupled with the fairly slow rate of dye production. In order to produce a reasonable quantity of dye for each measurement, the current was applied for 30 seconds before the ultrasound was switched on. Production of dye occurred at the cathode which was positioned 10 cm from the transducer and timing was initiated when the dye stream was observed to have travelled 0.5 cm beyond the cathode. The

passage of the dye was then timed over 10 cm or 20 cm. It was likely however that the stream had not reached its maximum velocity at the time of measurement. In addition, at high intensities the flow became very unstable.

Using Equation 4.37 the predicted streaming velocities at 1 MHz and 3 MHz were calculated for an estimated spatial peak temporal average intensity of 5 W cm^{-2} and beam diameter of 1 cm. Values of 4 cm s^{-1} and 37 cm s^{-1} were predicted for the streaming velocities in the 1 MHz and 3 MHz beams respectively. The maximum velocities measured experimentally were 1.4 cm s^{-1} and 7.7 cm s^{-1}. The acoustic power was also measured at each frequency in order to check the efficiency of the transducer.

The values of streaming velocity obtained appear to be significantly lower than predicted values and it seems likely that the reasons outlined above are responsible for this. In addition the validity of the theory, which was largely derived for beams in channels where the acoustic beam width and the stream width were of the same order of magnitude and where end effects in the channel were neglected, may be limited in the real situation.

6.15 SUMMARY

In this chapter it has been shown that streaming can occur in water in the fields of pulsed diagnostic transducers. Hot film anemometry has been used to make consistent measurements of the streaming velocities generated, in the range 0.5 cm s^{-1} to 12 cm s^{-1}. The streaming velocity, generated in a laboratory set up, was shown to increase with pulse amplitude, pulse repetition rate, pulse duration and acoustic power and to be enhanced by nonlinear propagation in high amplitude beams when acoustic shocks formed. Typically a streaming velocity of less than 1 cm s^{-1} in a linear beam was

enhanced, in a shocked beam of the same acoustic power by a factor of approximately 5. The enhanced absorption of higher harmonic components in the distorted pulse was shown to correlate with the onset of significant acoustic streaming. Transverse velocity profiles and acoustic profiles were found to be of similar width in the focal zone.

Measurements were also made on commercial equipment. In this case the maximum streaming velocity, approximately 14 cm s^{-1}, was generated in the field of a pulsed Doppler unit. The maximum velocity seen in water in a scanning field was 1.2 cm s^{-1}.

An investigation of the effect of local absorption on streaming was carried out by inserting a thin membrane into the beam. It was shown that the major component of a stream is generated in the focal region, the "source pump", and that absorption elsewhere in the beam is less significant. At a particular location in the beam, immediately on the transducer side of the focus, the streaming velocity can build up rapidly beyond a membrane. This may be important in bioeffects experiments and is discussed further in the next chapter.

Detailed measurements were made of the streaming time constants under a variety of pulsing regimes. In general rise times in the focal region are shorter than decay times and depend on pulse repetition rate. Typical values for the rise times for stationary beams are hundreds of milliseconds. This means that a stream could be generated very quickly in clinical use. Streaming has also been observed in water beyond 2 cm of excised bovine liver using a 3.5 MHz transducer at intensities similar to those generated by many pulsed Doppler units. The implications of the investigations presented here are discussed in the context of clinical ultrasound usage in the following chapter.

CHAPTER 7

DISCUSSION AND CONCLUSIONS

It has been shown that water may be induced to stream by the passage of an acoustic wave such as typically generated by commercial diagnostic ultrasound equipment. Maximum velocities of approximately 14 cm s^{-1} in pulsed Doppler fields and 1.2 cm s^{-1} in imaging fields have been observed. The velocity of the stream in a particular beam has been shown to be related to the degree of acoustic shock that is generated. If a linearly propagating beam is compared with a high amplitude pulsed beam of the same total power, as described in Section 6.5, two differences are observed. The degree of acoustic shock formation in the high amplitude beam is greater, and also the streaming velocity generated in this beam is higher than in the linear beam. The existing theoretical predictions for streaming velocity reviewed in Section 4.2.3 do not predict this enhancement of streaming velocity in high amplitude pulsed fields. An explanation for the observation is obtained by considering the acoustic absorption of a distorted beam. Consider initially the situation in water. As the waveform propagates harmonic components of the fundamental frequency are generated. These high frequency components are absorbed more strongly in water, which exhibits a quadratic dependence of attenuation coefficient on acoustic frequency, with the result that the acoustic attenuation is higher in such a beam than in a linear beam. More momentum is transferred from the wave to the fluid and hence a higher streaming velocity is generated.

This can be demonstrated by a simple calculation (presented in Appendix 2) which predicts the absorption enhancement factor for a shocked waveform in water. This model assumes a sawtooth waveform and that

only the harmonic levels present initially in the sawtooth wave are available to be absorbed. There is no further pumping of energy from the fundamental frequency into the higher harmonics. The absorption coefficient is predicted to be enhanced by a factor of approximately 10 in this situation. It is likely that the excess absorption or shock loss will manifest itself as enhanced acoustic streaming since according to Medwin (1954) streaming in a fluid is proportional to total absorption by whatever mechanism. In Section 6.7 an experiment to measure the spatial extent of the shock loss in a high amplitude acoustic beam was described. It was found that a region of rapid loss occurred on the beam axis, near to the focus of the transducer. The streaming velocity was also found to increase rapidly in the same region.

Appendix 2 also contains similar calculations of the absorption enhancement factors for a 3.5 MHz sawtooth wave propagating in soft tissue and in amniotic fluid. Absorption coefficients at the fundamental frequency of 0.5 dB MHz^{-1} cm^{-1} and 0.0051 dB $MHz^{-1.6}$ cm^{-1} (Zana and Lang, 1974) were assumed. The first twenty harmonics were considered, up to a maximum frequency of 70 MHz, and the values predicted by these calculations are summarised in Table 7.1 where α_t is the total enhanced absorption coefficient and α_0 is the low amplitude absorption coefficient.

	α_t
Water	$9.5\alpha_0$
Soft tissue	$2.0\alpha_0$
Amniotic fluid	$5.0\alpha_0$

Table 7.1 Total absorption coefficient, α_t, in a sawtooth wave; α_0 is the low amplitude absorption coefficient.

In these calculations, scatter was neglected and attenuation was assumed to be entirely due to absorption. It can be seen that in water and amniotic fluid almost all the absorption occurs as a result of shock loss due to the presence of high frequency components in the sawtooth wave.

7.1 DIRECT EFFECTS OF ACOUSTIC STREAMING

Many bioeffects experiments are conducted using cells in suspension and it is possible that streaming may be generated in some of the experimental arrangements. If streaming occurs it may have a beneficial effect in ensuring that the cells are "stirred" as they move in and out of the acoustic field. However it also has implications for dosimetry because cells are only exposed to ultrasound for the period of time in which they are actually in the beam, which will be some fraction of the total exposure time. Evidence of this stirring action has been obtained in a clinical situation (Meire, 1990) who observed the movement of pus within a testicular abscess when ultrasound imaging was performed using a Diasonics Spectra and 7.5 MHz array. When the acoustic imaging beam was switched on, particulate matter in the pus was observed to be set in motion away from the transducer. This motion ceased rapidly when the acoustic beam was switched off.

The stirring action induced by acoustic streaming may have potential application in processes involving diffusion across membranes or filters in that the layer of fluid next to the filter may be constantly renewed thus maintaining a favourable concentration gradient. It can also be speculated that streaming may affect passive diffusion across semipermeable membranes in the body, for example cell membranes. As discussed in Section 1.5 such an effect could be signicant in the development of the fetus.

Streaming has been shown to build up fairly rapidly beyond a membrane even when the fluid involved is confined to a small volume

(Section 6.9). The streaming velocity can reach approximately 50% of its maximum unimpeded value 0.5 cm beyond such a membrane depending on the location of the membrane relative to the focus of the beam. The possibility of streaming being generated within the cytoplasm of a cell has not been resolved.

7.2 *IN VIVO* STREAMING IN DIAGNOSTIC BEAMS

Within the human body streaming can only be generated in fluid filled spaces such as the eye, the bladder and in amniotic fluid. In ophthalmic scanning the acoustic frequencies employed are generally high, of the order of 10 MHz. The attenuation in the vitreous humour is relatively low and has been reported as 0.6 dB cm^{-1} at 6 MHz (Filipczynski *et al.*, 1967). Both these factors will increase the likelihood of acoustic shock formation. However in view of the low attenuation of the beam path it is unlikely that ophthalmic ultrasound equipment will generate beams of sufficient power to permit acoustic shock formation and generate significant acoustic streaming. Information about the output powers of these devices is scarce in the literature. A fairly old survey (NCRP, 1983) gives spatial peak temporal average intensities of 20 mW cm^{-2} to 34 mW cm^{-2} in A-mode and B-mode and 0.2 mW cm^{-2} to 0.6 mW cm^{-2} for real time imaging. No information about the pressure amplitudes generated is given and so it is not possible to estimate the shock parameter, σ, for these beams. Current equipment may produce higher intensities. If acoustic streaming is likely to occur in the eye its potential for damage to the retina needs to be assessed.

In obstetric scanning the full bladder is used as a low attenuation acoustic pathway through which the fetus is imaged. Section 3.4.2 reviewed the factors which are important in determining whether shock formation is likely to occur in this situation. These include the thickness of overlying

tissue, the focal length of the transducer and the depth of fluid in the bladder. It seems reasonable to assume that acoustic shocks could form and that enhanced streaming may be generated in urine but it is unlikely that any damage to the distal bladder wall would result. A more important situation is the possible generation of streaming within amniotic fluid and the effect this could have on the fetus. There is no direct experimental evidence that streaming occurs *in vivo* in amniotic fluid but it is interesting to speculate on the effects which could result from a stream of fluid impinging on fetal tissue. It can be assumed that there will be some transfer of forward momentum to the fetus, which if the tissue is firmly bound will generally be dissipated. If however the tissue or, in the case of a very early gestational sac, the cells, are loosely bound together it is conceivable that some relative motion may occur within the structure. In general such a fluid stream would be narrow, since it would be generated by a focused stationary beam, and the transfer of momentum resulting in a forward impetus could therefore be a relatively local effect within a part of the fetus.

Another situation in which an acoustic stream may have the potential for causing damage is when shear stresses occur between the edge of the beam and stationary cells of tissue. The shear stress in water associated with the velocity gradient at the edge of a stream of width 0.25 cm, moving at 14 cm s^{-1} is estimated to be of the order of 0.5 kPa, which is below the level at which damage to soft tissue is likely to occur but comparable to the levels at which damage to erythocytes has been reported (Section 3.2). The experimental arrangement described in Section 6.13, in which cells grown on membranes were exposed to an acoustically generated fluid stream, attempted to assess the importance of shear stresses. No de-adhesion of the cells was produced but the bonding forces between cells in an embryo may be quite different from those between the cells and the plastic coverslip. A

particular area of concern here is the period of organogenesis when cells migrate within the developing embryo. Damage to cell membranes through shear forces or changes induced in the relative positions of cells by streaming effects may adversely affect the outcome of the migration process and result in malformation of the fetus. (Damage of this nature due to thermal effects is described in Section 2.4.)

In vaginal scanning the thickness of tissue overlying the fetus can be as little as 0.5 cm, resulting in very little attenuation of the acoustic beam. If the pulse amplitude were sufficiently high, acoustic shock formation would be likely to occur in the amniotic fluid surrounding the fetus. The possibility of streaming would then exist. Vaginal scanning has the potential for increasing the ultrasound exposure to the fetus, and hence the potential for shock formation and acoustic streaming, unless exposure levels are carefully controlled.

7.3 FORCES ASSOCIATED WITH STREAMING

The investigation described in Section 6.9 in which acoustically transparent membranes were inserted in the beam demonstrated that there are two contributions to the stream at any point in the acoustic field on the beam axis. One is the contribution from locally induced streaming due to absorption occurring close to the point of measurement, and the other results from the flow of fluid set in motion nearer to the transducer, passing the point of measurement. It was found that the main impetus for the stream occurred over a small region on the transducer side of the focal zone and that local absorption elsewhere in the beam resulted in a smaller contribution to the stream. In this region energy was continually pumped from the fundamental into the higher frequency harmonics which resulted in enhanced absorption.

Although streaming can only occur in body fluids the volume force or pressure gradient responsible for the generation of streaming will be present whenever absorption produces an energy density gradient in an acoustic field. This will occur in soft tissue as well as in fluids. In fetal tissue the water content is high and enhanced absorption will occur in a shocked wave producing a greater increase in pressure gradient than would be likely in adult tissue. The effect of a pressure gradient in the direction of propagation on the fetus is of some concern for the reasons discussed above.

Equation 4.26 Nyborg (1965) related the volume force responsible for acoustic streaming to acoustic parameters such as the intensity in the beam and the velocity of sound and to the attenuation coefficient of the medium. This equation has been used to calculate the pressure density gradient in an acoustic field under a number of conditions. A linear beam and a fully formed sawtooth waveform propagating through water, soft tissue and amniotic fluid were considered. Each calculation was carried out for intensities and frequencies typical of those available from the higher powered pulsed Doppler units on the market, and produced by extra-corporeal shock wave lithotriptors. In each case for the sawtooth waveforms, the enhanced absorption coefficient was calculated from the frequency dependent absorption of the first twenty harmonics and this value was used in Equation 4.26 to obtain the pressure gradient during the acoustic pulse. For amniotic fluid a frequency exponent of 1.6 was used. The calculations are set out in detail in Appendix 2 and the results are summarised in Table 7.2.

It can be seen that greater pressure gradients are generated in soft tissue than in water or amniotic fluid due to the much higher absorption coefficient of soft tissue at low frequencies. An increase in pressure gradient in water for a sawtooth compared to a linear beam is apparent but the proportional increase in tissue is much lower with a factor of 2 predicted compared with a factor of 8 for water and 7 for amniotic fluid.

	Pressure gradient (Pa mm^{-1})		
	Tissue	Water	Amniotic fluid
		Doppler	
Linear beam	220	4	6
Sawtooth beam	420	38	29
		Lithotripsy	
Linear beam	3700	8	26
Sawtooth beam	6000	75	128

Table 7.2 Calculated pressure gradients during the acoustic pulse in pulsed Doppler and lithotripsy fields for linear and sawtooth waveforms.

In a lithotripsy field the pressure gradients were larger due to the higher value of intensity used in the calculation. The maximum predicted pressure gradient, 6 kPa mm^{-1}, occured for a 0.5 MHz, sawtooth lithotripsy pulse propagating in tissue. It must be stressed that this pressure gradient occurs during the pulse only and any transitory force is likely to be less damaging than a steady force of similar magnitude.

The location of the maximum pressure gradient in an acoustic field will coincide with the location of maximum absorption and in water this will be on the transducer side of the focal zone. A maximum pressure gradient may also occur on the transducer side of the focus in tissue if acoustic shocks are formed. The likelihood of this occurring was discussed in Section 3.4 where evidence of harmonic generation in tissue was presented. Enhanced absorption or shock-loss only becomes significant for $\sigma \geq \pi/2$ in water and significant streaming or pressure gradients are only likely to occur when a shock of this level is generated. In tissue some enhancement of absorption due to the presence of a shock is predicted, but considerably less than occurs in water (see Table 7.2). The calculation assumed a sawtooth

waveform and the circumstances in which this likely to occur are those in which an acoustic beam traverses a fluid path before passing through tissue for example in lithotripsy. If a shock is formed in the fluid, and the focus of the beam is at or close to the interface, higher frequency harmonic components generated in the wave will be transmitted into the tissue where they will be very rapidly absorbed.

7.4 CAVITATION AND STREAMING

In this thesis it has been considered that acoustically generated fluid flow is a genuine bulk movement of the fluid and is not due to cavitational effects. A possible alternative suggestion is that flow occurs due to the fluid being pulled along by viscous drag associated with cavitational bubbles which are themselves moving in the acoustic field. However there are several reasons to doubt this explanation. In the first place bubbles of resonant size or close to resonant size would be required in order to absorb sufficient energy from the field to create a significent energy density gradient and thus be accelerated by the field. It is unlikely that these bubbles pre-exist in sufficient numbers in the water and it is also unlikely that smaller bubbles could grow sufficiently by rectified diffusion during a pulse to reach resonant size. Even for a continuous wave at 3.5 MHz, the frequency used for experiments described in this thesis, cavitation thresholds are higher than at lower frequencies which makes it very unlikely that cavitation would occur in the pulsed field in question. Nyborg (1953) predicted velocities for resonant bubbles in gassy water several orders of magnitude greater than the fluid velocities measured.

Cavitation is essentially a random process which depends on a range of parameters other than the acoustic field (Williams and Millers 1989). For example the temperature and pH of the fluid, dissolved impurities and

mechanical stablility may each effect the occurrence of cavitation. As a consequence the thresholds given in the literature for observed cavitation phenomena show a wide range. In contrast streaming velocities observed have been very reproducible, the same acoustic parameters always resulting in the same measurement of streaming velocity. This suggests that acoustic streaming is not an effect which depends on bubble formation since this would result in a more variable outcome.

Even more significantly, nonlinear theory can predict acoustic streaming without the need to consider cavitation mechanisms. The streaming velocities predicted are somewhat lower than those measured in high amplitude fields. Experimental work presented here has shown that this can be explained by considering enhanced absorption occurring as a result of nonlinear propagation.

7.5 FUTURE WORK

No theoretical model of streaming exists currently in the literature which takes into account the effects of enhanced absorption due to shock formation, or of focusing in a pulsed field. Wu and Du (1990) have attempted to develop such a model based on the results presented in this thesis but have not published their work to date. A model of this nature is essential in order to predict the streaming velocities likely to be generated in clinical situations using ultrasound equipment in current use.

An understanding of the extent to which acoustic shock formation may occur *in vivo* is necessary to predict the extent to which streaming or the forces associated with streaming are important. However existing knowledge of ultrasound exposure *in vivo* is sparse and acoustic shock formation in amniotic fluid needs to be investigated. These measurements may be made using a probe hydrophone (Aindow, 1986) inserted into the uterine contents,

for example during an amniocentesis procedure. Similar *in vitro* measurements are required to determine whether shock formation could occur in fetal brain tissue. In addition the frequency dependence of the attenuation coefficient of amniotic fluid is not accurately known.

Some important biological questions are raised about the strength of the adhesive forces which exist between cells in the developing embryo and whether it is possible to disturb the "programming" of developing cells by applying a local force such as may be generated by streaming or a radiation pressure gradient.

7.6 CONCLUSION

It has been shown that streaming occurs in water in the fields of pulsed diagnostic ultrasound transducers and is enhanced by nonlinear propagation in high amplitude fields. For commercial equipment, the greatest streaming velocities are generated by pulsed Doppler units operating at high pulse average intensities. The rise times of the streams are short in comparison with the "dwell times" of transducers in clinical use. In addition streaming has been shown to be generated in relatively small volumes of fluid and to build up rapidly behind an acoustically transparent membrane if the membrane is located in front of the transducer focus.

Streaming and the forces associated with it provide a potential mechanism of interaction between high amplitude diagnostic ultrasound pulses and tissue. Consideration should be given to the situations described in this thesis in which these effects are likely to occur, both in the design of bioeffects experiments and in the clinical use of diagnostic ultrasound. Further work is required to assess the significance of such effects for biological systems.

APPENDIX 1

DERIVED ULTRASOUND PARAMETERS

In this thesis the derived ultrasonic parameters are those used in the medical ultrasound field. The definitions given below are taken from the AIUM/NEMA (American Institute for Ultrasound in Medicine/National Equipment Manufacturers Association, 1983) standard.

(1) Intensity

For a plane progressive sinusoidal wave the time averaged intensity, I, is given by

$$I = \frac{\hat{p}^2}{2\rho_0 c} \qquad \text{A1.1}$$

where $\hat{p}$ is the peak acoustic pressure, ρ_0 is the density of the medium and c the speed of sound.

In a pulse the intensity is obtained from the pulse intensity integral (see below) averaged over an appropriate time period, t,

$$I = \frac{1}{t} \frac{1}{\rho_0 c} \int_0^{t=t} p^2 \, dt \qquad \text{A1.2}$$

where the limits of integration span one complete period and p is the instantaneous pressure amplitude.

The **spatial peak temporal average intensity**, I_{spta}, is the value of pulse intensity integral averaged over the time period between the beginning of one pulse and the beginning of the next (one pulse repetition period). In

this case $t = t_1$ in Figure A1.1. In scanned beams the frame repetition period defines the averaging time.

The **spatial peak pulse average intensity**, I_{sppa}, is the pulse intensity integral averaged over the duration of a pulse, $t = t_2$ in Figure A1.1.

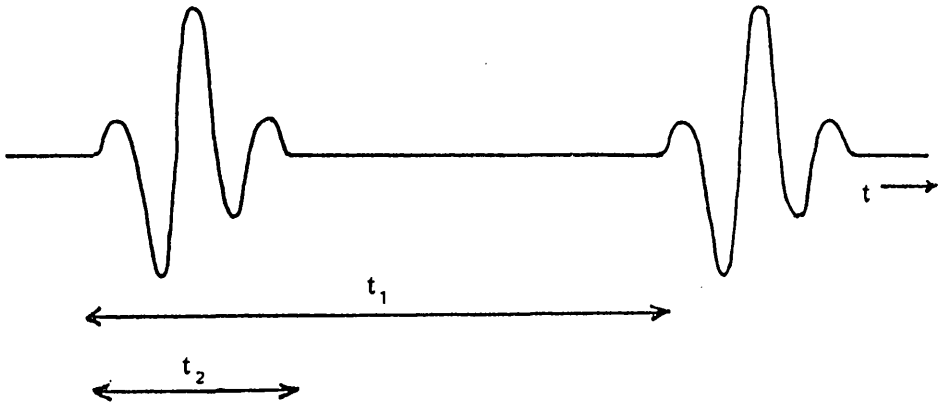

Figure A1.1 Time periods t_1 and t_2 representing one repetition period and the pulse length.

The **spatial average temporal average intensity**, I_{sata}, is defined as the total acoustic power averaged over the beam area. It has a maximum value at the focus, where the beam diameter is minimum. (A definition of the minimum beam area is given below.) Similarly the spatial average temporal average intensity at the transducer is the total acoustic power averaged over the radiating area of the transducer.

(2) Pulse intensity integral

The pulse intensity integral is derived from the value of the integral of (pressure)^2 over a complete pulse and is given by

$$\frac{1}{\rho_0 c} \int_0^{t=t} p^2 \, dt \quad . \qquad \text{A1.3}$$

Figure A1.2 shows the integral as a function of time for a single pulse. The pulse intensity integral has a maximum value when measured in the plane in which the beam is narrowest. The AIUM/NEMA (1983) standard states that the minimum cross-sectional beam area is defined by the pulse intensity integral at the -6 dB level.

(3) Pulse duration

The pulse length is defined (AIUM/NEMA 1983) as the time period when the integral of the pressure squared is between 10% and 90% of its maximum value (indicated as $(t_b - t_a)$ in Figure A1.2), multiplied by a factor of 1.25.

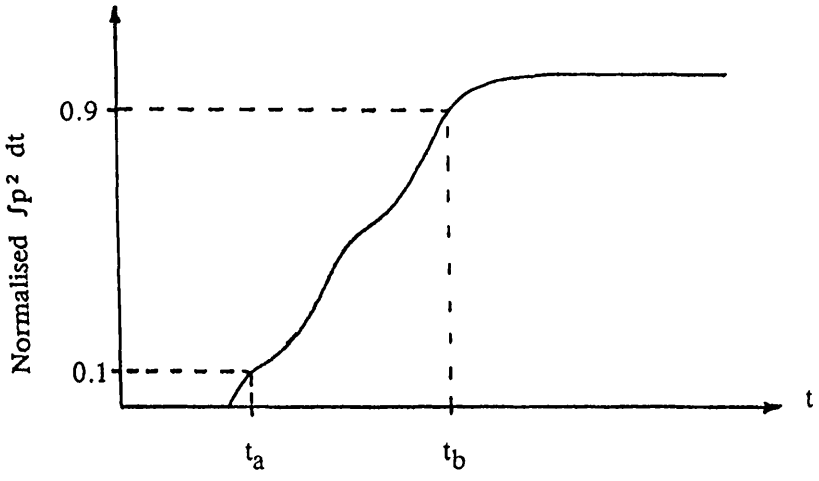

Figure A1.2 Pulse length derived from the integral of p^2; t_b corresponds to 90% of maximum, t_a corresponds to 10% of maximum.

(4) Focal length

This is the axial distance from the transducer to the plane in which the beam area, calculated from consideration of the pulse intensity integral, is a minimum.

(5) Pressure squared integral

For a digitised pulse an approximate value of pressure squared integral is obtained by carrying out the following summation

$$\int_0^{t_2} p^2 \, dt \approx t' \sum_0^m p_n^2 \qquad \text{A1.4}$$

where t' is the sample interval and $m = t_2/t'$ and p is the pressure of the nth sample.

The square root of this parameter, of the modulus of the acoustic pressure, is calculated by the ultrasound beam calibrator.

(6) Focal gain

The intensity gain at the focus can be defined as the ratio of the radiating area to the focal area. The focal pressure gain is the square root of the intensity gain.

APPENDIX 2

CALCULATED VALUES IN A SHOCKED BEAM

The analysis of nonlinear fields in absorbing media is very complex. In the following calculation an extremely simple model is used to attempt to compare the absorption of shocked beams in a number of different situations. For example propagation through water and through tissue is considered. In using this model a number of major assumptions and simplifications have been made. For this reason the results obtained have limited value except as a means of estimating orders of magnitude for enhanced absorption due to nonlinear propagation in different situations.

A2.1 TOTAL ABSORPTION

In the calculation that follows it is assumed that an initially fully developed sawtooth wave propagates 1 cm through fluid or tissue (Figure A2.1). Attenuation of the wave occurs in the medium which is assumed to be entirely due to absorption and no harmonic regeneration takes place. Using the fact that the intensity in a sawtooth waves varies as $1/n^2$, where n is the harmonic number, and calculating the absorption of each harmonic component from the absorption coefficient at 1 MHz and the harmonic frequency, the ratio of the intensity in the unattenuated wave to the intensity in the attenuated wave is obtained. This results in an effective absorption coefficient which is enhanced due to the absorption of high frequencies present in the shocked wave. The calculation is carried out for water, tissue and amniotic fluid.

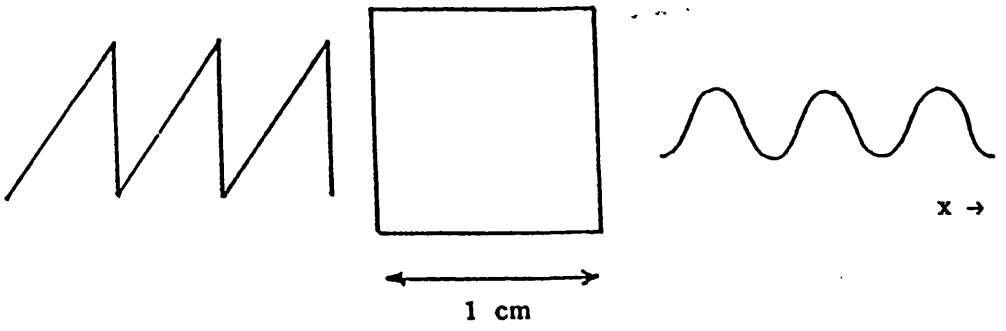

Figure A2.1 Representation of the situation considered in this model.

Water

(1) The relationship between the absorption coefficient of the nth harmonic, α_n, and the absorption coefficient at 1 MHz is given by

$$\alpha_n = \alpha_0 f^2 n^2 \qquad \text{A2.1}$$

where f is the fundamental frequency of the wave.

(2) The value of α_0 used in this calculation is 25×10^{-5} Np MHz^{-2} cm^{-1}.

It is assumed that the reduction in intensity of an ultrasound beam in an attenuating medium can characterised by a single exponential. The intensity is then given by

$$I_x = I_0 e^{-2\alpha x} \qquad \text{A2.2}$$

where x is the distance propagated through the medium, I_x is the intensity at x and I_0 is the initial intensity. In a sawtooth waveform the initial

intensity, I_0', is given by the sum of the intensities in the harmonic components in the wave,

$$I_0' = I_1' + I_2' + I_3' + \ldots$$

where I_1', for example, is the intensity in the fundamental in the sawtooth beam. Thus

$$I_0' = I_1' + \frac{I_1'}{2^2} + \frac{I_1'}{3^2} + \ldots = I_1' \sum_{n=1}^{\infty} \frac{1}{n^2} . \qquad \text{A2.3}$$

At location x, the intensity in an attenuated sawtooth wave is given by

$$I_x' = I_1' \exp(-2\alpha_0 f^2 x) + \frac{I_2'}{2^2} \exp(-2\alpha_0 f^2 2^2 x) + \ldots$$

$$= I_1' \sum_{n=1}^{\infty} \frac{\exp(-2\alpha_0 f^2 n^2 x)}{n^2} . \qquad \text{A2.4}$$

Taking the intensity ratio between the initial wave and the wave at x, where x is a unit length, gives

$$\frac{I_x'}{I_0'} = \frac{\Sigma \exp(-2\alpha_0 f^2 n^2)/n^2}{\Sigma \quad 1/n^2} . \qquad \text{A2.5}$$

The summations in Equation A2.5 are evaluated for the first twenty harmonics in a 3.5 MHz beam and the intensity ratio is obtained. The results of this calculation are given in Table A2.1.

n	$\Sigma 1/n^2$	$\Sigma \exp(X)/n^2$	I_x'/I_0'
1	1	0.9939	0.9939
2	1.2500	1.2378	0.9903
3	1.3611	1.3430	0.9868
4	1.4236	1.3997	0.9857
5	1.4625	1.4340	0.9805
6	1.4903	1.4563	0.9772
7	1.5107	1.4714	0.9740
8	1.5263	1.4820	0.9710
9	1.5386	1.4895	0.9681
10	1.5486	1.4949	0.9653
11	1.5569	1.4988	0.9627
12	1.5638	1.5017	0.9603
13	1.5697	1.5038	0.9580
14	1.5748	1.5053	0.9559
15	1.5792	1.5064	0.9539
16	1.5832	1.5061	0.9513
17	1.5866	1.5059	0.9491
18	1.5897	1.5057	0.9472
19	1.5925	1.5056	0.9454
20	1.5950	1.5055	0.9439

Table A2.1 Calculated factors for predicting the degree of enhanced absorption occurring due to shock loss in 1 cm of water using Equation A2.5. ($X = \exp(-2\alpha_0 f^2 n^2)$ above.)

The total absorption of the sawtooth wave is obtained by comparing the intensity ratio in Table A2.1 with Equation A2.2. For example, consideration of twenty harmonic components gives, $I_x' = 0.9439\ I_0'$. Since, assuming a single exponential relationship, $I_x' = I_0' \exp(-2\alpha x)$, the total effective absorption coefficient, α_T, for a 3.5 MHz shocked beam can be calculated as follows,

$$\alpha_T = \frac{-\ln(0.9439)}{2 \times (3.5)^2} = 2.3 \times 10^{-3} \text{ Np MHz}^{-2} \text{ cm}^{-1} .$$

Under linear conditions (n = 1 in Table A2.1) the absorption coefficient is 2.5×10^{-4} Np MHz^{-2} cm^{-1}. Thus the total predicted absorption coefficient in a sawtooth wave is equal to $9.5\alpha_0$. The proportion of the total absorption due to shock loss, $(\alpha_T-\alpha_0)/\alpha_T$, is also calculated and for water this is 89%.

It can be seen from Table A2.1 however that the ratio I_X'/I_0' does not converge rapidly and therefore consideration of still higher harmonic components will result in a significantly increased total absorption. While in theory a shock will contain an infinite number of harmonics, in practice there will be an upper limit in a real fluid due to absorption. Some limit on the number of harmonics considered is therefore justified but a truncation after 20 harmonics may result in a significant underestimate of the enhanced absorption in water. Experimentally the absorption in water was shown to be enhanced by a factor of approximately 35 in the region in front of the focus of a 3.5 MHz transducer (Section 6.7)

Soft tissue

(1) The relationship between the absorption coefficient of the nth harmonic, α_n, and the absorption coefficient, α_0, at 1 MHz is given by

$$\alpha_n = \alpha_0 fn \qquad \text{A2.6}$$

where f is the fundamental frequency of the wave.

(2) The value of α_0 used in this calculation is 0.057 Np MHz^{-1} cm^{-1}.

In this case the intensity at x in a sawtooth wave is given by

$$I_x' = I_1' \sum_{n=1}^{\infty} \frac{\exp(-2\alpha_0 fnx)}{n^2} \qquad \text{A2.7}$$

while the initial intensity, I_0', is that given in Equation A2.3. Table A2.2 gives the results of the calculation described above for soft tissue.

n	$\Sigma 1/n^2$	$\Sigma \exp(X)/n^2$	I_x'/I_0'
1	1	0.6710	0.6710
2	1.2500	0.7836	0.6269
3	1.3611	0.8172	0.6004
4	1.4236	0.8299	0.5830
5	1.4625	0.8353	0.5711
6	1.4903	0.8378	0.5622
7	1.5107	0.8390	0.5554
8	1.5263	0.8396	0.5501
9	1.5386	0.8399	0.5459
10	1.5486	0.8401	0.5425
11	1.5569	0.8402	0.5397
12	1.5638	0.8402	0.5373
13	1.5697	0.8403	0.5353
14	1.5748	0.8403	0.5336
15	1.5792	0.8403	0.5321
16	1.5832	0.8403	0.5308
17	1.5866	0.8403	0.5296
18	1.5897	0.8403	0.5286
19	1.5925	0.8403	0.5277
20	1.5950	0.8403	0.5268

Table A2.2 Calculated factors for predicting the degree of enhanced absorption occurring due to shock loss in 1 cm of soft tissue. In this case $X = \exp(-2\alpha_0 fn)$.

The ratio, I_x'/I_0', considering the first 20 harmonics only in the shocked wave, is 0.5268. This results in a calculated total absorption coefficient of 0.092 Np MHz^{-1} cm^{-1} compared with the absorption coefficient under linear conditions (neglecting the scatter component) which is 0.057 Np MHz^{-1} cm^{-1}. An enhanced total absorption coefficient for a sawtooth wave propagating in soft tissue of $1.6\alpha_0$ is thus obtained and the proportion of the absorption due to shock loss is 37%. In this case the ratio I_x'/I_0' converges rapidly as can be seen from Table A2.2 with the result that the degree of enhanced absorption predicted is likely to be fairly realistic.

Amniotic fluid

(1) The relationship between the absorption of the nth harmonic, α_n, and the absorption coefficient, α_0, at 1 MHz is given by

$$\alpha_n = \alpha_0 f^{1.6} n^{1.6} \qquad \text{A2.8}$$

where f is the fundamental frequency of the wave.

(2) In this calculation, following Zana and Lang (1974), the value of α_0 used is 59×10^{-5} Np $MHz^{-1.6}$ cm^{-1}.

In this case the intensity at x in a sawtooth wave is given by

$$I_x' = I_1' \sum_{n=1}^{\infty} \frac{\exp(-2\alpha_0 f^{1.6} n^{1.6} x)}{n^2} \qquad \text{A2.9}$$

while the initial intensity is that given be Equation A2.3. The ratio, I_x'/I_0',

considering only the first 20 harmonics in the shocked wave, is 0.9560. This results in a calculated total absorption coefficient of 29×10^{-4} Np $MHz^{1.6}$ cm^{-1}. The attenuation coefficient under linear conditions is 5.9×10^{-4} Np $MHz^{1.6}$ cm^{-1} giving a total effective absorption coefficient for a sawtooth wave in amniotic fluid of $5.0\alpha_0$. The proportion of attenuation resulting from shock loss is 80%. Truncation of the calculation after 20 harmonics may have resulted in an underestimate of the degree of enhancement of absorption occurring.

Limitations of the model

(1) In the model the harmonics are not regenerated as the wave propagates. In reality, near the focus of a beam, energy is continually pumped into the higher harmonics replacing that lost by absorption.

(2) Only 20 harmonic components are retained in these calculations. This may result in an underestimate of enhanced absorption for water and amniotic fluid although the result for tissue is likely to be more reasonable. Nevertheless orders of magnitude predictions of the absorption enhancement due to nonlinear propagation can be made.

(3) A single exponential relationship is used to quantify the reduction in intensity due to attenuation over the distance of interest.

(4) The calculated attenuation coefficients depend on the propagation distance. In the above calculation a distance of 1 cm is assumed. However when the calculation is repeated for tissue, using different propagation distances, the results obtained are not dissimilar.

The model used above is likely to underestimate the degree of enhancement of absorption which occurs as a result of shock loss since it does not consider regeneration of the harmonics and is limited to only 20 harmonics. It is remarkable that even with these limitations, increases in

absorption for water and amniotic fluid, of factors of 9.5 and 5 respectively are predicted due to the formation of a mature shock ($\sigma > 3$) in the acoustic wave. It is unlikely that a sawtooth waveform will be generated in tissue. However, when propagation takes place partly through a low loss fluid, the waveform may have distorted considerably by the time it reaches the tissue interface. This situation is common in the use of extracorporeal shock wave lithotripsy.

A2.2 CALCULATION OF RADIATION PRESSURE GRADIENT

The volume force, F, or radiation pressure gradient during the acoustic pulse is calculated using Equation 4.26 (Nyborg,1965),

$$F = \frac{2\alpha I}{c} \quad . \qquad \text{A2.10}$$

Values of spatial peak temporal average intensities and frequencies typical of those available from commercial pulsed Doppler units and extra-corporeal shock wave lithotriptors are used (Table A2.3). The values of absorption used are those calculated in Section A2.1 which take shock loss into account for the sawtooth beams.

	Doppler	Lithotripsy
I_{spta} ($W\ m^{-2}$)	10^7	10^9
f (MHz)	3.5	0.5

Table A2.3 Spatial peak temporal average intensities, I_{spta}, and acoustic frequencies typical of pulsed Doppler and lithotripsy units.

A number of circumstances are considered:

(1) Linear beam and sawtooth beam in water

(2) Linear beam and sawtooth beam in tissue

(3) Linear beam and sawtooth beam in amniotic fluid.

The pressure gradient predicted by Equation A2.10 in each situation is shown in Table A2.4. The values of absorption coefficient used in the calculations are also shown. For both Doppler and lithotripsy beams the greatest predicted radiation pressure gradient occurs in tissue and is increased when a sawtooth waveform is present.

	Linear tissue	Sawtooth tissue	Linear water	Sawtooth water	Linear amniotic fluid	Sawtooth amniotic fluid
α (dB cm^{-1})	0.5 (MHz^{-1})	0.8 (MHz^{-1})	$2.2x10^{-3}$ (MHz^{-2})	$2.1x10^{-2}$ (MHz^{-2})	$5.0x10^{-3}$ ($MHz^{-1.6}$)	$2.5x10^{-2}$ ($MHz^{-1.6}$)
α (Np m^{-1})	5.7 (MHz^{-1})	9.2 (MHz^{-1})	$2.5x10^{-2}$ (MHz^{-2})	0.2 (MHz^{-2})	$5.8x10^{-2}$ ($MHz^{-1.6}$)	0.3 ($MHz^{-1.6}$)
			Doppler beam			
dP/dx (Pa mm^{-1})	220	420	4	38	6	29
			Lithotripsy beam			
dP/dx (Pa mm^{-1})	3700	6000	8	75	26	128

Table A2.4 Prediction of pressure gradient (dP/dx); absorption parameters and results.

APPENDIX 3

PUBLISHED PAPERS

Copies of three published papers relating to this study are included here. The titles are:

1. An experimental investigation of streaming in pulsed diagnostic ultrasound beams,

2. The development of harmonic distortion in pulsed finite amplitude ultrasound passing through liver,

3. Evidence for ultrasound finite-amplitude distortion in muscle using medical equipment.

A3.1 ACOUSTIC STREAMING IN WATER

Title: An experimental investigation of streaming in pulsed diagnostic ultrasound beams

Authors: Starritt H.C., Duck F.A. and Humphrey V.F.

Sources: Ultrasound in Medicine and Biology, Volume 15

Date: 1989

Pages: 363 - 373

Ultrasound in Med. & Biol. Vol. 15, No. 4, pp. 363–373, 1989
Printed in the U.S.A.

0301-5629/89 $3.00 + .00

●*Original Contribution*

AN EXPERIMENTAL INVESTIGATION OF STREAMING IN PULSED DIAGNOSTIC ULTRASOUND BEAMS

H. C. STARRITT,† F. A. DUCK† and V. F. HUMPHREY‡
†Medical Physics Department, Royal United Hospital, Combe Park, Bath, BA1 3NG, UK.
‡School of Physics, University of Bath, Claverton Down, Bath, BA2 7AY, UK.

(*Received* 16 *August* 1988; *in final form* 17 *November* 1988)

Abstract—Streaming is shown to occur in water in the focused beams produced by a number of medical pulse-echo devices. The use of hot film anemometry to measure the streaming velocity is described and velocities measured in water using commercial equipment are quoted. The highest velocities occur in pulsed Doppler mode with a maximum velocity of 14 cm s^{-1} being observed. An experimental set-up was used to investigate the parameters affecting streaming and it was found that the harmonic content of the pulse waveform had a major effect on the streaming velocity. The time taken for a stream to become established at the focus of the acoustic beams studied was typically approximately 0.5 s.

Key Words: **Ultrasound, Diagnostic ultrasound, Streaming, Nonlinear effects of ultrasound.**

INTRODUCTION

The term "streaming" has been used to describe two separate phenomena in the context of bio-effects mechanisms. Bulk fluid movement which results from the presence of a sound wave in a medium is the subject of the investigation reported here. This is not the same as acoustic microstreaming which has come to be associated with oscillating bubbles or cavitation in a medium. Although bulk streaming is well recognized in continuous wave fields it has not previously been considered to be very significant in diagnostic ultrasound. Thus in a review of mechanisms which could have biological significance, ter Haar (1987) noted that its relevance as a mechanism in diagnostic fields is questionable.

There is a considerable body of literature which develops the theoretical basis of streaming from the nonlinear nature of the wave equation. These analyses are mainly concerned with plane continuous waves or waves within tubes and do not cover the situation in which there is acoustic shock generation. Useful reviews are given by Beyer (1974) and by Tjøtta (1959). In an early theoretical analysis Eckart (1948) concluded that streaming occurred due to the transfer of angular momentum from the wave motion to the fluid. Extension of the theory to include relaxation processes led a number of authors (Markham 1952; Nyborg 1953) to conclude that streaming was in fact due to the loss of acoustic momentum by attenuation of a sound beam. Medwin (1954) in a study of streaming in gases stated that streaming was proportional to attenuation whilst Fox and Herzfeld (1950), arguing that all absorption mechanisms for sound waves must lead to streaming, had introduced the concept of radiation pressure to explain the effect.

For the case of a diverging wave in a tube, Tjøtta (1959) showed that the streaming velocity, v, was related to the intensity in the beam, I, to the beam width, 1, and to the absorption coefficient at the fundamental frequency, α by

$$v = \frac{2\alpha k l^2 I}{\nu \rho \omega} \qquad (1)$$

where k and ω are the wave number and angular frequency of the acoustic wave, ρ is the density of the medium and ν the kinematic viscosity.

Table 1 shows predicted streaming velocities for two "typical" conditions of spatial-average temporal-average intensity and beam width. Significant streaming is only predicted in the second case where the parameters used relate approximately to the maximum intensities generated by some modern commercial duplex scanners in pulsed Doppler mode.

The propagation of a finite amplitude wave results in the generation of harmonics of the funda-

Table 1. Predicted streaming velocities using eq (1).

Spatial-average intensity mW cm $^{-2}$	50	2000
Beam width mm	2.5	2.0
Frequency MHz	3.5	3.5
Calculated streaming velocity cm s $^{-1}$	.12	3.1

mental frequency and the progressive distortion of the wave towards a sawtooth (Muir and Carstensen 1980). The problem of streaming in this situation has received attention from a number of authors (Ostrovskii and Papilova 1974; Rudenko and Soluyan 1971), while Stanikov (1967) modified Eckart's analysis to take account of the effect of a saw-tooth waveform. Experimental studies using a saw-tooth waveform were reported by Romanenko (1960). Propagation of a finite-amplitude wave also results in additional attenuation (Duck and Perkins 1988) by enhanced absorption of the higher harmonics which are generated. In eqn (1) no account was taken of the increase in the absorption coefficient which is to be expected due to the presence of these higher frequency components in the wave. This increase results from the frequency dependence of the absorption coefficient.

This prediction of a modified streaming velocity in a distorted wave is particularly important for diagnostic ultrasound since most commercial devices produce beams in which considerable nonlinear or finite-amplitude distortion does occur. Duck et al. (1985) published a survey of output powers from diagnostic equipment in which the degree of waveform distortion was assessed in terms of the nonlinearity parameter σ (Bacon 1984). In this survey over 70% of the beams had $\sigma > 1.5$ at the focus.

In addition to the problem of finite amplitude propagation, diagnostic ultrasound beams differ in two significant ways from an idealised plane-wave; first, they are generally focused, and second, they are pulsed with a low ratio of on-off time. A complete theory would need to model all these conditions, and has not yet been developed.

METHOD

A simple demonstration of the presence of streaming in water was carried out using coloured dye. Figure 1 shows the stream generated by a pulsed 3.5 MHz transducer using potassium permanganate released in front of the transducer as the dye.

Whilst initial estimates of streaming velocities were obtained using the dye stream, more accurate measurement of streaming velocities and stream dimensions were obtained by hot film anemometry. This investigation of streaming velocities was carried out in two parts. First, streaming was studied under experimentally controlled conditions. A 3.5 MHz transducer, diameter 19 mm, focal length 9.5 cm and focal pressure gain of approximately 6, was driven by an ENI (Electronic Navigation Industries Inc., New York) R.F. power amplifier. The combined use of an R.F. signal generator and a pulse generator enabled the pulsing regime to be varied in a controlled fashion. This transducer was coupled into a water-bath 50 cm × 20 cm × 15 cm containing freshly distilled water. A hot-film anemometer was used to measure the streaming velocities developed in the acoustic beam with different pulsing regimes. The second part of the study consisted of measurements of the

Fig. 1. Demonstration of streaming using coloured dye in water.

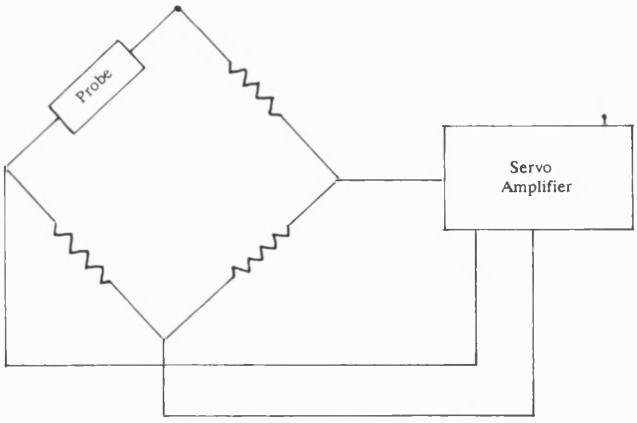

Fig. 2. Schematic representation of basic anemometer circuit.

streaming velocities generated in water by commercial diagnostic equipment in the modes of operation available with each device.

Hot-film anemometry

The principle of hot-wire anemometry measurement is that of measuring heat loss from an electrically heated probe caused by the flow of fluid surrounding it in order to estimate the flow velocity. In this investigation a commercial anemometer unit, DISA type 55DO1 was used with a TSI liquid hot-film probe (1210-20W). The probe was connected to the anemometer forming part of a Wheatstone bridge as shown in Fig. 2. It was then operated at a constant temperature using a feedback technique whereby current flowed from a servo amplifier through the bridge to heat the probe, the amount of current being controlled by the bridge imbalance. This maintained the probe operating resistance and therefore its temperature. The voltage at the bridge top was measured using a digital voltmeter.

The anemometer probe used is shown in Fig. 3. The sensitive tip consisted of a 51 μm diameter platinum wire deposited on a quartz substrate and electrically insulated for use in water by a quartz coating. The active length was 1 mm. The temperature coefficient of resistance of this probe was 0.00114 $\Omega\ °C^{-1}$ and the operating resistance used was 5.77 Ω. The latter was determined by the choice of operating temperature (50°C), a compromise between the need for sensitivity and the need to avoid bubbles forming on the probe. The bubbles had a tendency to form even when distilled water was used and renewed regularly. In use, the probe support was mounted perpendicular to the beam, and the probe tip aligned with the transverse axis of the beam. The probe support was designed to cause minimal disturbance in the flow.

The relationship between the amount of heat removed per unit time, Q, and the flow velocity, U, was formulated by King (1914):

$$Q = A + B(U)^n = P \tag{2}$$

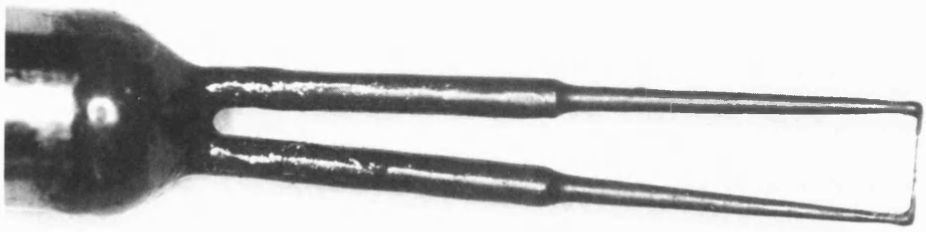

Fig. 3. Anemometer probe.

where A and B are constants and n is a constant in the range 0.4–0.5. For constant temperature operation the power, P, supplied to the probe will be equal to this rate of heat loss.

Since $P \propto V^2$ the form of the equation relating output voltage, V, to flow velocity, U, is

$$V^2 = A' + B'U^n \tag{3}$$

where A' and B' are new constants.

The anemometer probe was calibrated by mounting it on a microcomputer controlled translation stage and towing it through a tank of water at a range of velocities from 5 mm s^{-1} to 10 cm s^{-1}. The water tank was 2 m long which allowed the probe to be accelerated to and remain at a constant velocity for the duration of each measurement. The calibration curve is shown in Fig. 4. Each point is the average of three measurements although the spread on these measurements was insignificant.

The anemometer output is dependent on the fluid temperature in the following way (Saunders and Lawrence 1972):

$$\frac{V(T)}{V(T_0)} = \left[1 - \frac{T - T_0}{T_f - T_0}\right]^{1/2} \tag{4}$$

where T is the fluid temperature, T_0 is the reference temperature and T_f is the the film temperature. $V(T)$ and $V(T_0)$ are the output voltages at T and T_0. Measurements made with the probe subsequent to calibration were corrected to the reference temperature of 20°C. All streaming velocities in this study were derived from the output voltage using the calibration described above.

The frequency response of the anemometer electronics was tested using a sinusoidal test signal which varied the electrical power applied to the probe in order to mimic variations in velocity. The upper frequency limit was 220 kHz (−3 dB level). This is comparable to the upper frequency limit of the hot film probe which is quoted by the manufacturers to be approximately 250 kHz. In the studies described in this paper pulse repetition rates of between 500 Hz and 20 kHz were used. These frequencies were within the frequency response of the system but when the anemometer output voltage was observed on an oscilloscope no component corresponding to the pulse repetition frequency was observed. A simple calculation based on the time taken for a stream to decay showed that any modulation due to the pulse repetition frequencies used lay within the measurement noise. The frequency of the acoustic wave at 3.5 MHz was well beyond the resolution capabilities of the system.

Measurement of the rise times of the streams were made by using in addition, a Lineariser unit (DISA 55DIO). This unit electronically corrects for

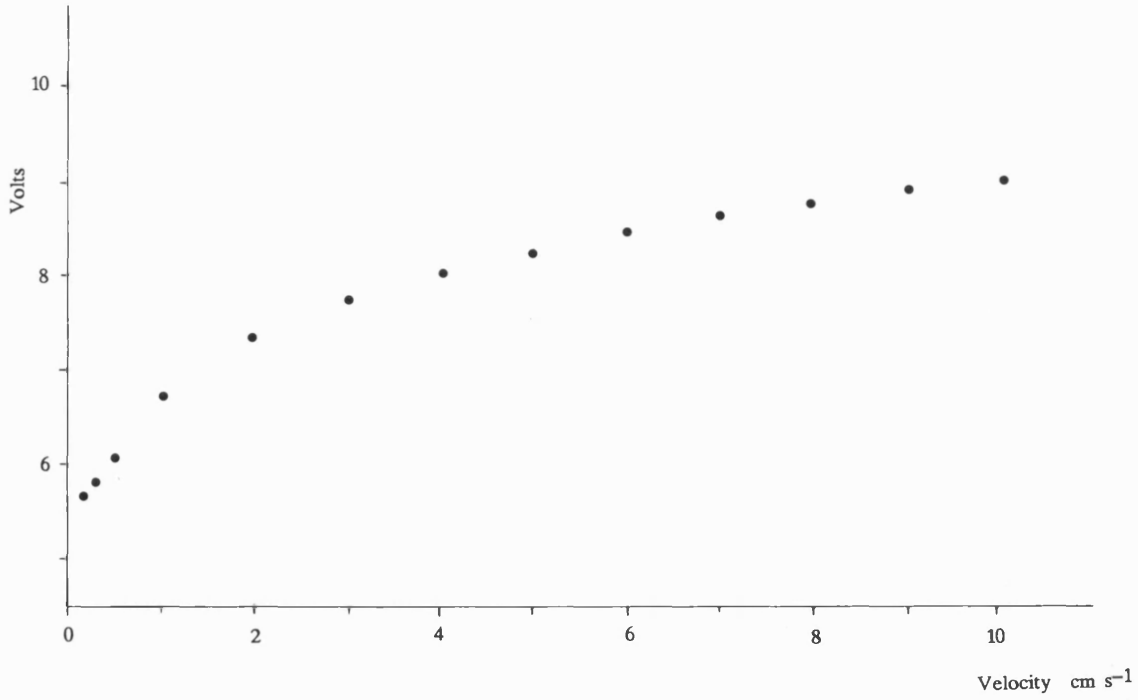

Fig. 4. Calibration curve for anemometer in water at 20°C.

the nonlinear dependence of output voltage on flow velocity and produces an output which is directly proportional to the flow velocity. The linearised velocity-dependent voltage was captured and displayed on a digital oscilloscope (Gould DS0 1602). Use of the Lineariser reduced the upper frequency limit of the system to approximately 30 kHz.

Hydrophone measurements

The acoustic beams causing streaming were also investigated using a PVDF membrane hydrophone to measure acoustic pressure and pulse length. A 9 μm coplanar-screened hydrophone (GEC Marconi Research Centre) with a 0.5 mm diameter sensitive area was used and connected via a unity gain amplifier to a Hewlett Packard digitizing oscilloscope. Details of this experimental arrangement are given elsewhere (Duck et al. 1987).

The primary parameters varied during these investigations were

1. pulse amplitude
2. pulse repetition frequency
3. distance from the transducer

Ideally these would be varied independently while everything else was held constant, however this was not always possible in these particular fields as, for example, changing the distance from the transducer changed the wave amplitude and harmonic content as well as the radius of the beam.

RESULTS

The first investigation carried out demonstrated the variation of streaming velocity along the axis of the transducer. Figure 5 shows how the streaming velocity built up as the distance from the transducer was increased, with no significant streaming being detected close to the transducer. The results for three drive levels are shown. In each case the pulse repetition rate was altered to maintain a total power of approximately 100 mW. The peak positive pressures under these conditions were (a) 3.5 MPa, (b) 1.4 MPa, and (c) 0.16 MPa, and the corresponding pulsing regimes were (a) prf 2 kHz, pulse length 3 μs, (b) prf 20 kHz, pulse length 3 μs, and (c) continuous wave. Measurement of the acoustic power was carried out using a radiation force balance in which the transmission path to the target was through 21 mm of transformer oil (Duck et al. 1985). The use of a lossy coupling medium and a short transmission distance avoided the problems associated with acoustic shock losses described by Duck and Perkins (1988). These problems become significant in a low loss medium such as water when the transmission distance is long, thus allowing an acoustic shock to occur. It can be seen that for the same total acoustic power widely differing streaming velocities were generated, with the highest amplitude waves causing streaming velocities five times greater than the lowest amplitude waves. Digitized waveforms were obtained at 1 cm

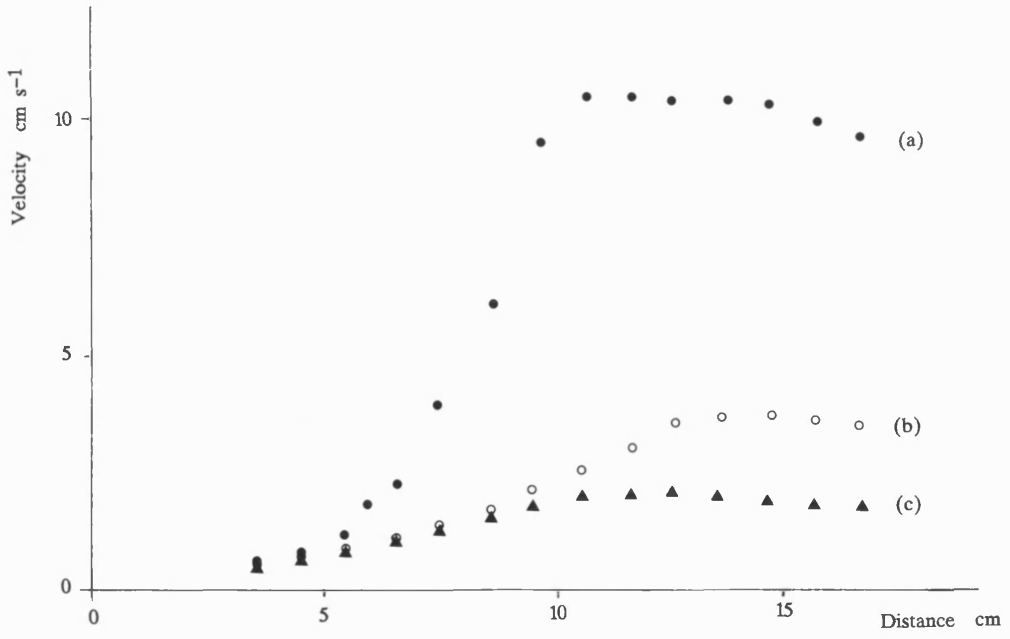

Fig. 5. Variation in streaming velocity with distance from transducer. 3.5 MHz, pulse length 3 μs, total acoustic power 100 mW. (a) peak positive pressure, p^+ 3.4 MPa, prf 2 kHz. (b) p^+ 1.4 MPa, prf 20 kHz. (c) p^+ 0.2 MPa, cw.

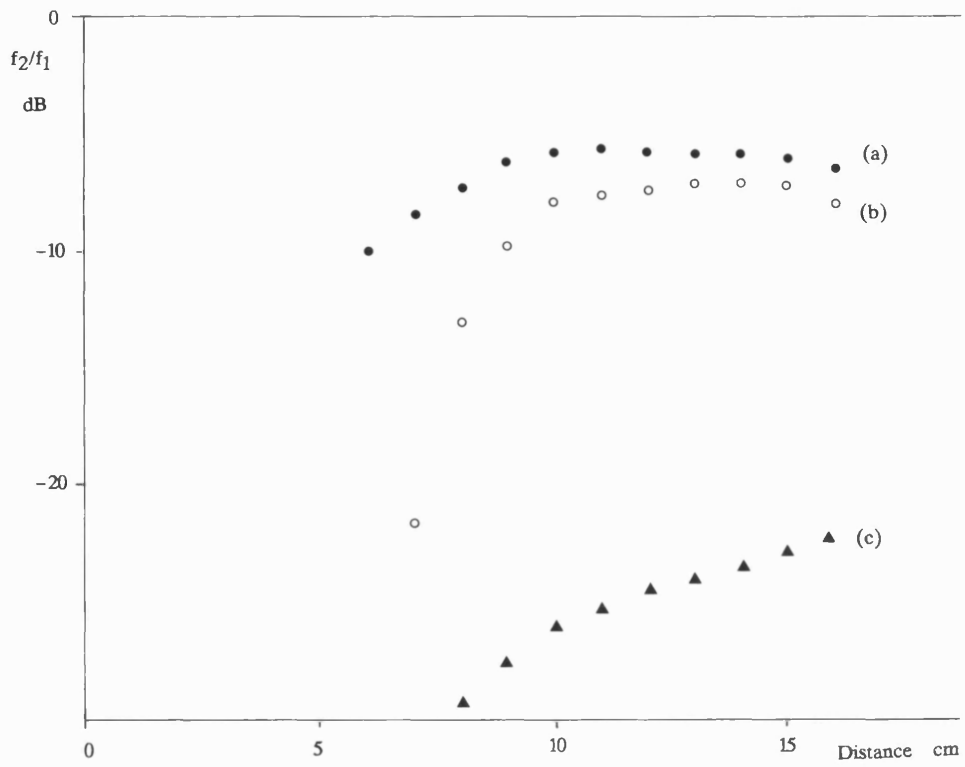

Fig. 6. Variation in second harmonic relative to the fundamental component with distance from the transducer; conditions identical to those of Fig. 5.

intervals along the beam axis and were Fourier analyzed into their harmonic components. The level of the second harmonic component relative to the fundamental frequency is shown in Fig. 6. (The vertical axis in (b) is logarithmic). A significant benchmark is the level at which the 2nd harmonic is 8 dB below the fundamental since this corresponds to a $\sigma = 1$ shock in free field conditions, that is, the waveform has distorted to the stage at which a discontinuity has just occurred (Muir and Carstensen 1980).

The enhanced streaming observed in Fig. 5(a) in comparison with that in Fig. 5(c) may be attributed to the significantly higher level of harmonics present in the pulse as shown in Fig. 6. The build-up of harmonics occurred most rapidly in the region immediately before the transducer focus which corresponds to the region in which the rapid increase in streaming velocity occurred for higher amplitude pulses. The enhanced streaming may be attributed to absorption of the harmonics as they are being generated in the focal zone.

In a separate investigation the streaming velocity was measured at the focus of the transducer, 9.5 cm, for a range of pulse amplitudes from 1.2–3.4 MPa at a pulse repetition rate of 2 kHz. Figure 7 shows the streaming velocity plotted against the pulse-average intensity. For the corresponding pulse waveforms Fig. 8(a) shows the second harmonic component relative to the fundamental and Fig. 8(b) the third harmonic component relative to the fundamental. It can be seen that the streaming velocity increased significantly above a critical pulse amplitude (pulse-average intensity) which again coincided with the development of a wave rich in harmonic components. In

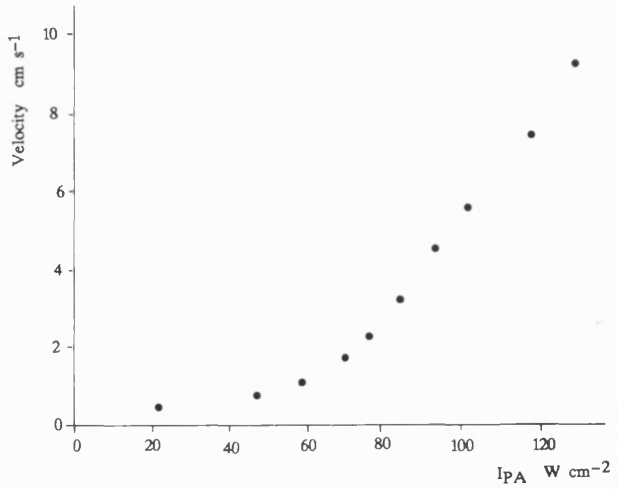

Fig. 7. Variation in streaming velocity with pulse-average intensity at 9.5 cm in water; 3.5 MHz, prf 2 kHz, pulse length 3 μs.

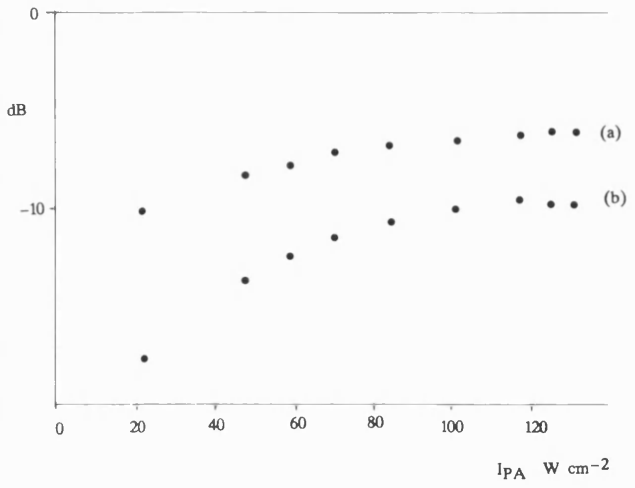

Fig. 8. Variation in (a) second and (b) third harmonic component relative to the fundamental under the conditions of Fig. 7.

addition the shock parameter, σ (Bacon 1984) for a focused field was calculated. σ reached 1.0 at a value of pulse-average intensity of 45 W cm^{-2} and $\pi/2$ at a value of 90 W cm^{-2}. Thus the streaming velocity started to increase significantly in the intensity range associated with $1 < \sigma < \pi/2$.

This experiment was repeated at pulse repetition frequencies from 0.5–5 kHz and the results are shown in Fig. 9. It can be seen that the increase in streaming velocity with increasing pulse amplitude above a certain critical level was more marked at high pulse repetition frequencies.

Streaming velocity profiles were measured at two axial locations in the beam by traversing the anemometer probe across the beam. These profiles are shown in Fig. 10. At the same axial locations the acoustic beam profile was also measured using the membrane hydrophone. Pulse average intensities were calculated from the pressure waveforms and these profiles are shown in Fig. 11. It can be seen that in the region near the focus of the transducer the beam width and streaming width were comparable.

In all the previous experiments each velocity measurement was derived from the average of at least three voltage measurements. Typically the random variation on the velocity was less than 1%. Periods of instability in the anemometer readings did occur but these were overcome by renewing the distilled water and/or remounting the probe. Any moisture entering the joint between the probe and probe support, which was under water, caused instabilities. The greatest problem was that of bubbles forming on the heated wire which caused the static voltage to rise and the response of the probe to be severely depressed. In general it was considered that the streaming velocities could be measured to better than 0.5 cm s^{-1} at the lower end of the velocity range whilst above 10 cm s^{-1} the uncertainty was ±1.5 cm s^{-1}.

The time taken for the stream to become estab-

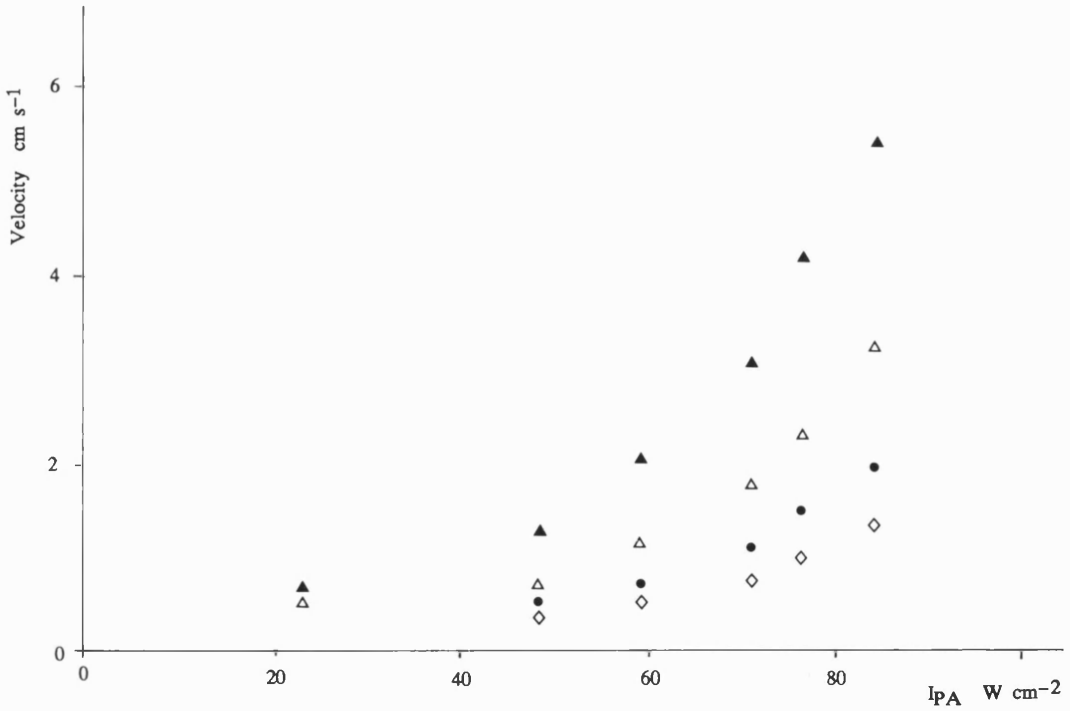

Fig. 9. Variation in streaming velocity with pulse repetition frequency;
◇ = 500 Hz, ● = 1 kHz, △ = 2 kHz, ▲ = 5 kHz.

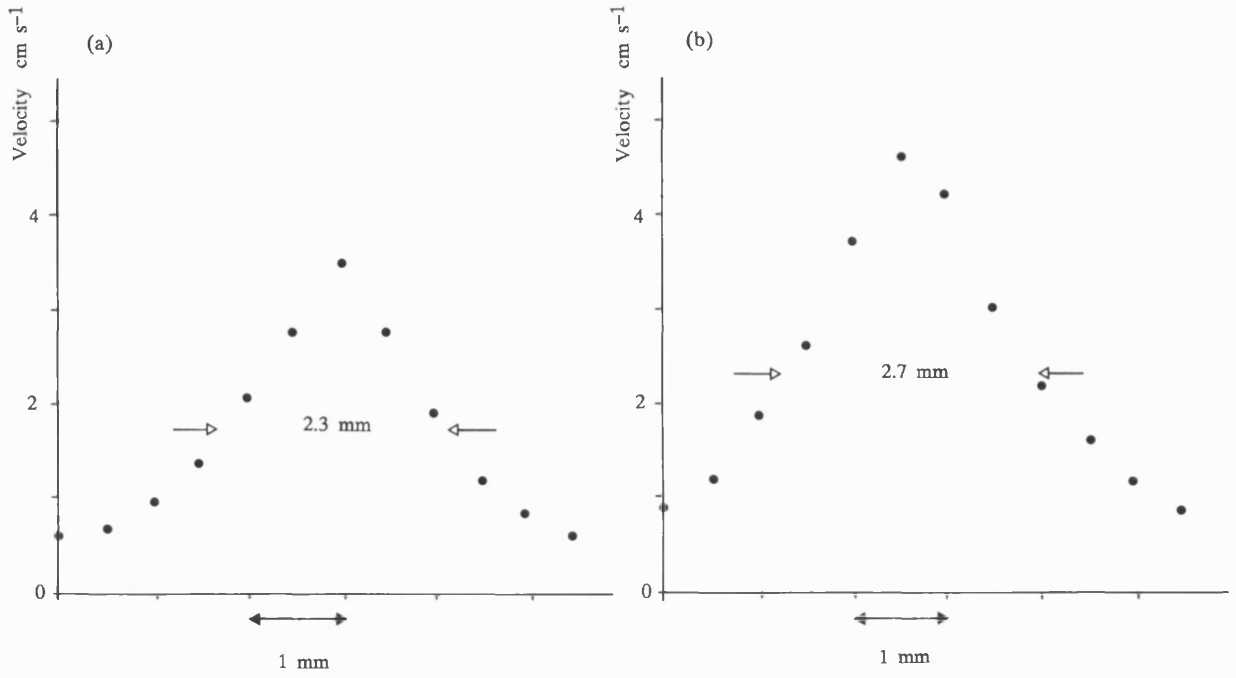

Fig. 10. Streaming velocity profiles at (a) 9.5 cm and (b) 11.5 cm from the transducer.

lished after the acoustic beam was switched on was investigated and for this experiment the Lineariser unit was used. Assuming a single exponential character to the rise or fall of velocity, the rise time, τ_R was defined as the time taken for the velocity to reach (1–1/e) of the maximum velocity and similarly the decay time, τ_D was defined as the time taken for the velocity to fall to 1/e of the maximum velocity after the acoustic beam was switched off. Figures 12(a) and (b) show the build-up of the streaming velocity with time under different conditions and Fig. 12(c) also shows the decay rate of the stream when the acoustic beam was switched off. Values of rise times and decay times at two locations in the field are shown in Table 2. These were measured at a range of drive conditions which resulted in the peak positive pressures given in the table. It can be seen that at a given prf the rise time decreased as the pulse amplitude was increased, that is, the streaming was established more quickly at higher drive levels. The stream decayed more quickly

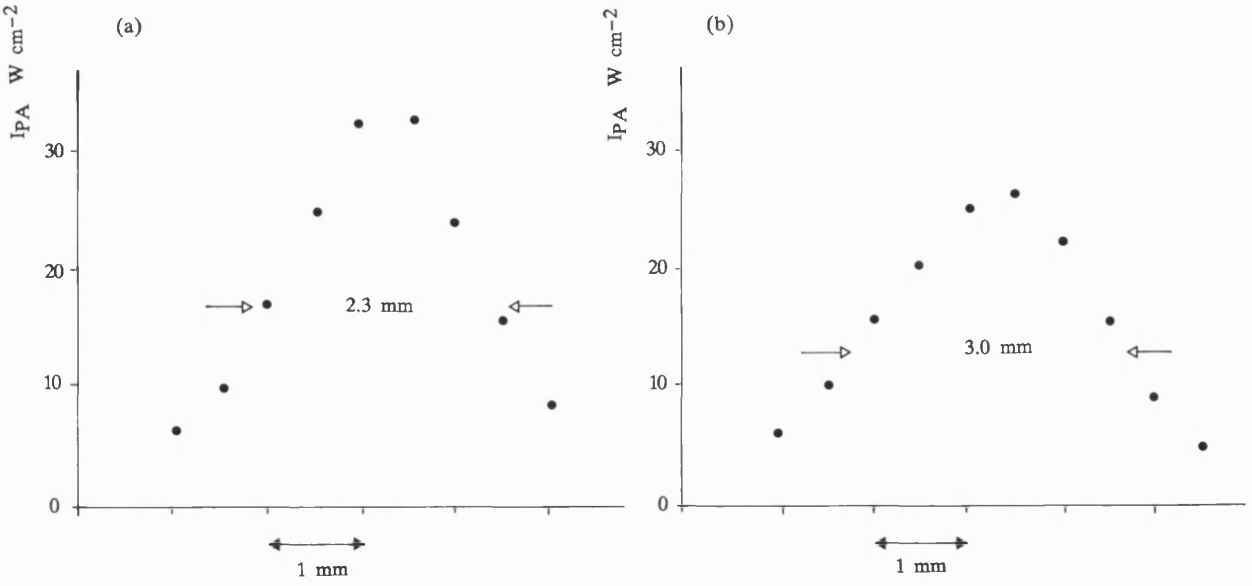

Fig. 11. Pulse-average intensity profiles under identical conditions to Fig. 10.

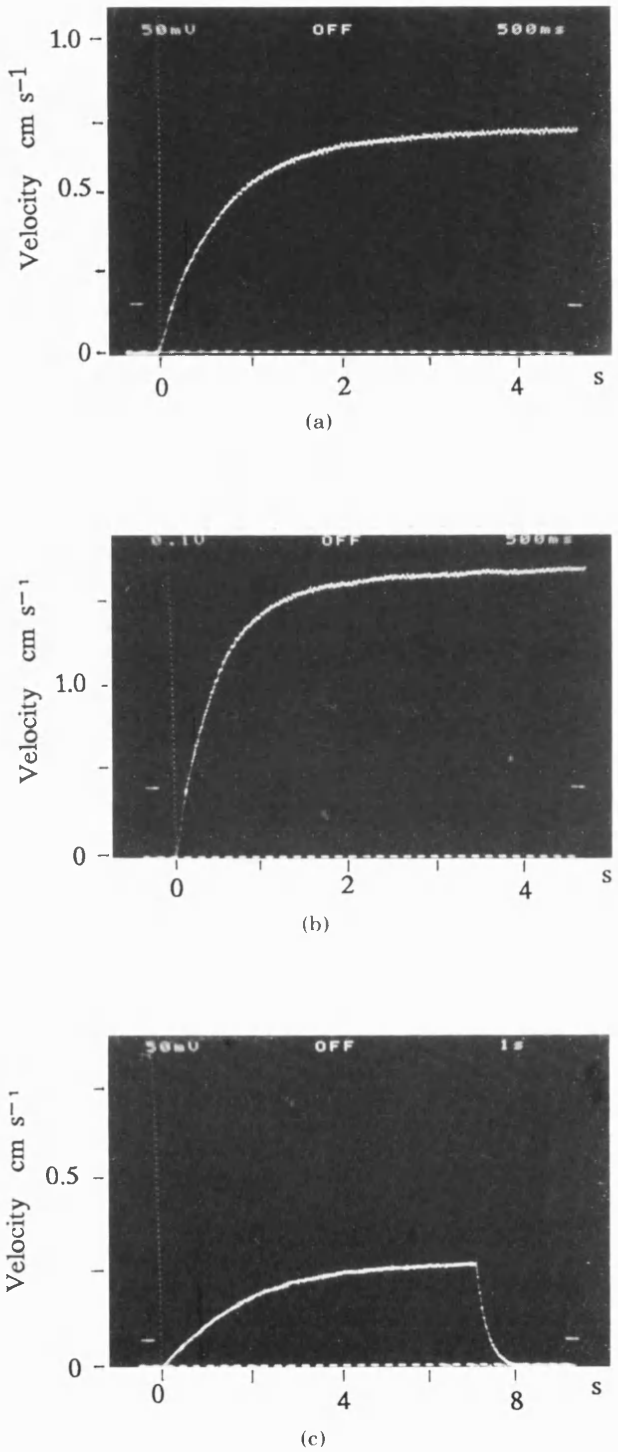

Fig. 12. Streaming velocity build-up (a) $p^+ = 2.2$ MPa and (b) $p^+ = 2.5$ MPa, at 9.5 cm and (c) velocity build-up and decay, $p^+ = 1.9$ MPa, at 11 cm. Prf = 1 kHz.

when the streaming velocity was low, and both rise times and decay times were increased when measurements were made in the diverging part of the beam.

The results of the second part of the study, the measurement of streaming velocities from commercial medical imaging equipment, are shown in Table 3. The velocities given are the maximum measured with each combination of scanner and scanhead in each mode. The highest streaming velocities were developed in pulsed Doppler mode, particularly in equipment which has time-average intensities greatly in excess of 100 mW cm^{-2}. Pulsed Doppler operation uses longer pulse durations and higher pulse repetition frequencies than those used for pulse-echo applications while the pulse amplitudes remain comparable to pulse-echo levels (Duck et al. 1987). The velocities reported in Table 2 are generally higher than those generated by the laboratory experiment, where lower values of these beam parameters were used. It is worth noting that streaming was generated by some scanning equipment operating in imaging mode only. While the highest velocity measured was only 1.2 cm s^{-1}, it is remarkable that this was caused by microsecond pulses at a frame repetition frequency of about 20 Hz and a mark-to-space ratio of about 2×10^{-5}.

DISCUSSION

Absorption in water is related to the square of the frequency, varying from 0.0029 dB cm^{-1} at 1 MHz to 29 dB cm^{-1} at 100 MHz (Kaye and Laby 1973). This means that a wave which has undergone nonlinear distortion and contains significant levels of higher harmonic components will be more strongly absorbed than a sinusoidal wave and, as discussed in the introduction increased absorption, by any mechanism, results in enhanced streaming. Thus the harmonic content in the pulse is an important factor in the prediction of streaming velocities. Temporal-average intensity alone is a poor indicator of streaming velocity since it is possible to locate positions in a field with equivalent intensities, where very different wave distortion and very different streaming velocities may occur. Other factors also affect the streaming velocity, and one obvious parameter is the pulse repetition rate. The highest streaming velocities are produced by high amplitude pulses, in high time-average intensity fields.

Table 2. Rise time τ_R and decay time τ_D at 9.5 and 11 cm from 3.5 MHz transducer; 1 kHz prf, pulse length 1.4 μs.

Peak positive pressure MPa	2.5	2.3	2.2	2.1
Streaming velocity cm s^{-1}	2.8	1.6	1.4	1.1
9.5 cm from the transducer				
Rise time s	0.52	0.54	0.61	0.94
Decay time s	0.39	0.31	0.28	0.26
11 cm from the transducer				
Rise time s	0.96	1.09	1.11	1.40
Decay time s	0.72	—	0.48	—

Table 3. Maximum streaming velocities from diagnostic ultrasound equipment. Measurements made in water.

(a) Pulsed Doppler mode.

Scanner	Transducer	Freq. MHz	Prf Hz	p^+ MPa	p^- MPa	ISPTA mW cm^{-2}	V max cm s^{-1}
ATL Ultramark 8	PV10†	5	11000	3.3	−1.9	6200	14‡
	Access C	2.25	3200	2.5	−1.5	320	0.3
Acuson 128	S328	3.5	6100	3.9	−1.4	4000	14‡
	L538	5	6100	3.3	−1.5	1700	3.5
Toshiba Sonolayer	PSE-37L	3.75	4100	5.2	−3.2	1100	3.9
	PSD73D	3.0	4100	5.8	−2.8	930	1.4

† Measurement made at higher output than is currently available on this equipment.
‡ Value from extrapolated calibration curve.

(b) M-mode.

Scanner	Transducer	Freq. MHz	Prf Hz	p^+ MPa	p^- MPa	ISPTA mW cm^{-2}	V max cm s^{-1}
Acuson 128	S519	5	600	3.0	−2.0	66	0.8
	L382	3.5	—	—	—	—	1.6†
Kretz Combison 100	NR3.5	3.5	3100	7.4	−2.1	590	5.5
Toshiba Sonolayer	PSE-37L	3.75	860	4.6	−2.3	93	2.5†

† M-mode plus imaging.

(c) Imaging mode.

Scanner	Transducer	Freq. MHz	Frame rate Hz	p^+ MPa	p^- MPa	ISPTA mW cm^{-2}	V max cm s^{-1}
ATL Ultramark 8	PV10	5	11	3.9	−2.4	3.7	~0
Acuson 128	SS28	3.5	—	4.6	−2.6	5.4	1.2
	L558	5.0	17	2.6	−2.3	2.5	0.3
	L538	5.0	54.9	3.7	−1.9	29	1.0
	L538	5.0	—	—	—	—	1.3†
Kretz Combison 100	NR3.5	3.5	36	7.4	−2.1	21	0.5
Toshiba Sonolayer	PSE 37L	3.75	17.96	5.3	−3.0	21	0.8
	PSD 73D	7	34.5	4.3	−3.7	31	0.5

† Imaging plus colour mapping.

The results presented in this paper show that streaming is generated by pulsed diagnostic beams. One simple consequence of this to *in vitro* bioeffects experiments is that if cells in suspension are free to move, they will be likely to do so. This may be a desirable effect in that it ensures mixing but it may also complicate the dosimetry. If cells are not free but are fixed in a monolayer, for example, they may experience shear/viscous forces due to the flow of medium past them.

In clinical use, streaming may be set up in any fluid path of a reasonable length *in vivo*. Examples are in urine within the bladder, in amniotic fluid, in blood and possibly in the aqueous humor. As demonstrated above, under some conditions the stream may be established within a few hundred milliseconds.

We have described here another possible mechanism by which ultrasound can interact with tissue. Streaming and the forces causing the movement of fluid must be taken into consideration in the design of new bioeffects experiments and it may be of interest to re-examine the results of previous experiments with streaming in mind. The effects of streaming on tissue, both direct and indirect, remain to be investigated.

CONCLUSION

Streaming velocities in water of up to 14 cm s^{-1} have been measured from some medical ultrasonic equipment operating in pulsed Doppler mode with the streams being established with rise-times less than 0.5 s. In real-time imaging mode velocities may reach 1.2 cm s^{-1}.

Using a single element transducer it has been found that significant streaming is not generally detected close to the transducer or in low amplitude

fields. There appears to be a threshold above which enhanced streaming occurs, and this threshold is related to the harmonic content in the wave. Thus a rapid increase in streaming velocity is observed in a beam which has undergone finite-amplitude distortion and where a $\sigma = 1$ shock has been developed. Temporal average intensity alone is not a good indicator of streaming velocity.

Acknowledgment—This work was supported in part by a grant from the Wellcome Trust. We are indebted to Dr. Derek Tilley of the Mechanical Engineering Department, University of Bath, for the loan of the anemometry system.

REFERENCES

Bacon, D. R. Finite amplitude distortion of the pulsed fields used in diagnostic ultrasound. Ultrasound Med. Biol. 10:189–195; 1984.

Beyer, R. T. Non-linear acoustics. Washington, DC: U.S. Naval Sea Systems, U.S. Government Printing Office; 1974:239–268.

Duck, F. A.; Perkins, M. A. Amplitude dependent losses in ultrasound exposure measurement. IEEE Trans. Ultrason. Ferroelectrics and Frequency Control 35:68–76; 1988.

Duck, F. A.; Starritt, H. C.; Aindow, J. D.; Perkins, M. A.; Hawkins, A. J. The output of pulse echo ultrasound equipment: a survey of powers, pressures and intensities. Br. J. Radiol. 58:989–1001; 1985.

Duck, F. A.; Starritt, H. C.; Anderson, S. P. A survey of the acoustic output of ultrasound Doppler equipment. Clin. Phys. Physiol. Meas. 8:39–49; 1987.

Eckart, C. Vortices and streams caused by sound waves. Phys. Rev. 73:68–76; 1948.

Fox, F. E.; Herzfeld, K. F. On the forces producing the ultrasonic wind. Phys. Rev. 78:156–157; 1950.

Kaye, G. W. C.; Laby, T. H. Tables of physical and chemical constants. New York: Longman; 1973.

King, L. V. On the convection of heat from small cylinders in a stream of fluid: determination of convection constants of small platinum wires with applications to hot-wire anemometry. Philos. Trans. Roy. Soc. Lond. 214:373–432; 1914.

Markham, J. J. Second order acoustic fields: streaming with viscosity and relaxation. Phys. Rev. 86:497–502; 1952.

Medwin, H. An acoustic streaming experiment in gases. J. Acoust. Soc. Am. 26:332–341; 1954.

Muir, T. G.; Carstensen, E. L. Prediction of non-linear acoustic effects at biological frequencies and intensities. Ultrasound Med. Biol. 6:345–356; 1980.

Nyborg, W. L. Acoustic streaming due to attenuating plane waves. J. Acoust. Soc. Am. 25:68–75; 1953.

Ostrovskii, L. A.; Papilova, I. A. Nonlinear acoustic streaming. Sov. Phys. Acoust. 20:45–49; 1974.

Romanenko, E. V. Experimental study of acoustic streaming in water. Sov. Phys. Acoust. 6:87–91; 1960.

Rudenko, O. V.; Soluyan, S. I. Theory of non-stationary acoustic streaming. Sov. Phys. Acoust. 17:97–101; 1971.

Saunders, L. J.; Lawrence, P. Calibration of hot-film anemometers. Cockrell, D. J. ed. Fluid dynamic measurements. Leicester: University Press; 1972:125–130. (Vol. 1).

Stanikov, Yu G. Streaming induced by finite amplitude sound. Sov. Phys. Acoust. 13:122–124; 1967.

ter Haar, G. Interaction mechanisms: non-thermal, non-cavitational effects. Ultrasound, medical applications, biological effects and hazard potential. Repacholi, M. H.; Grandolfo, M.; Rindi, A. eds. New York: Plenum; 1987:105–116.

Tjøtta, S. On some non-linear effects in sound fields, with special emphasis on the generation of vorticity and the formation of streaming patterns. Arch. Math. Naturvidensk. 55:1–68; 1959.

A3.2 NONLINEAR PROPAGATION IN TISSUE

Title: The development of harmonic distortion in pulsed finite amplitude ultrasound passing through liver

Authors: Starritt H.C., Duck F.A. and Hawkins A.J.

Source: Physics in Medicine and Biology, Volume 31

Date: 1986

Pages: 1410 - 1409

Phys. Med. Biol., 1986, Vol. 31, No 12, 1401-1409. Printed in Great Britain

The development of harmonic distortion in pulsed finite-amplitude ultrasound passing through liver

H C Starritt†, F A Duck†, A J Hawkins† and V F Humphrey‡

† Medical Physics Department, Royal United Hospital, Bath, BA1 3NG, England
‡ School of Physics, University of Bath, Claverton Down, Bath, BA2 7AY, England

Received 14 April 1986, in final form 24 June 1986

Abstract. The progressive development of finite-amplitude distortion of ultrasonic pulses has been investigated in excised bovine liver using pulsed focused ultrasonic beams at nominal frequencies of 2.5 and 3.5 MHz. Both the transducers and the powers used were those which may be encountered with clinical imaging equipment. Significant distortion of the waveform was observed to occur, particularly at higher powers. For example, at 2.5 MHz, with a mean input pressure (p_0) of 0.58 MPa, the second harmonic in the pulse spectrum showed a maximum value 10.5 dB below the fundamental and the highest third harmonic component was 19 dB below the fundamental. These particular observations illustrate that finite-amplitude distortion may be of considerable significance in the transmission through tissue of ultrasonic pulses during diagnostic scanning.

1. Introduction

It has been predicted that finite-amplitude effects may be important in the propagation of ultrasound at the power levels commonly used in medical ultrasonic equipment (Muir and Carstensen 1980) and that, in a lossless fluid, this will result in a distortion of the ultrasonic waveform with associated harmonic generation and perhaps acoustic shock generation. Recently, experimental results have been reported which show significant finite-amplitude distortion occurring in water in the fields from focused pulsed ultrasonic transducers used with medical imaging equipment (Duck and Starritt 1984, Bacon 1984). These non-linear propagation effects in water are of significance, particularly in the context of calibration and ultrasonic beam measurement. However, the extent to which such pulse distortion occurs in biological tissue, with its frequency-dependent attenuation, has been relatively unexplored.

The change in pressure Δp in a medium is related to the change in density as follows:

$$\Delta p = c_0^2 \Delta\rho + \frac{1}{2}\frac{c_0^2}{\rho_0}\left(\frac{B}{A}\right)\Delta\rho^2 + \ldots$$

where c_0 is the infinitesimal speed of sound in the medium, ρ_0 is the static density and B/A is the parameter of non-linearity for the medium. If only the first term is considered, the change in pressure is proportional to the change in density. Inclusion of the second-order term describes non-linear propagation. Generally, higher-order terms may be neglected.

0031-9155/86/121401+09$02.25

The importance of the non-linear behaviour of tissue was recognised by Fry and Dunn (1962) who gave an analysis of the loss of energy from the fundamental frequency of an unfocused beam as a result of both absorption and non-linear processes. In a theoretical investigation using published data for ultrasonic absorption and the non-linear parameter B/A Haran and Cook (1983) demonstrated the importance of the frequency-dependent attenuation on the development of finite-amplitude distortion. They predicted that, for unfocused fields, mature shock fronts may form in body fluids at low MHz frequencies with initial pressures around 600 kPa, but that such shocks would not develop in liver tissue. Focused fields were not considered. Swindell (1985) has analysed the potential for enhanced tissue heating due to the absorption of non-linearly generated higher harmonics in tissue concluding that, at 1 MHz, enhancement ratios in the range 1.5–2 may occur near the focus. In a previous paper (Starritt *et al* 1985) we have reported experimental evidence that finite amplitude distortion occurs in human calf muscle *in vivo* using both diagnostic and therapeutic ultrasonic beams. Mean second and third harmonic peaks of up to 17 and 30 dB below the fundamental, respectively, were observed in a clinical pulsed focused beam.

In the present paper, observations of the progression of finite-amplitude distortion in bovine liver are presented. Pulsed focused ultrasonic beams have been used at a range of input pressures and the changes in harmonic content of the wave have been investigated with propagation distance.

2. Experimental method

The experimental arrangement is shown in figure 1. A tank of dimensions 50 cm × 20 cm contained water at room temperature. The transmitting transducer assembly, suitably waterproofed, was rigidly clamped in the water with the hydrophone opposite to it, on a micromanipulator. The hydrophone was aligned so as to maximise the transmitted signal through the water at the focus and beyond. Slices of liver of varying thicknesses were cut in turn from a whole, fresh bovine liver and placed in plastic sample bags, with enough physiological saline in each bag to cover the liver. It was sometimes necessary to build up the larger thicknesses of liver from two or more thinner slices.

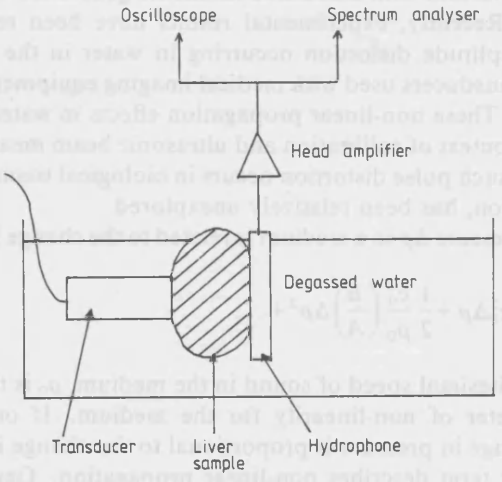

Figure 1. Experimental arrangement.

Each liver sample bag was immersed in the water and suspended in such a way that one side of the bag was in contact with the transducer. The axial position of the hydrophone was adjusted using the micromanipulator until it was in contact with the other side of the liver sample bag and the separation between the hydrophone and the transducer was recorded as the thickness of the liver sample.

The hydrophone used to detect the transmitted signal was a calibrated bilaminar polyvinylidene difluoride (PVDF) membrane hydrophone with a 1 mm diameter sensitive area. The hydrophone signal was amplified using a specially designed head amplifier to provide impedance matching between the hydrophone and the oscilloscope and RF spectrum analyser. Details of this measurement system have been given elsewhere (Starritt *et al* 1985). Two separate pulsed focused transducers were used in this investigation. The first was a mechnically scanned pulse-echo diagnostic unit in which the rotation of the head was stopped. The nominal frequency of the transducer was 2.5 MHz, the diameter was 2 cm and the geometric focus was at 10 cm. The observed peak axial intensity occurred at a range of 58 mm in water and the zero crossing frequency was 2.2 MHz. A series of measurements was made at a range of output powers for which the mean positive input pressures measured adjacent to the transducer, p_0, were in the range 0.08–0.58 MPa. The second unit was a static pulse-echo unit with a nominal 3.5 MHz focused transducer 13 mm in diameter, with maximum pressure in water at 53 mm. One output power only was available on this unit which produced a peak positive input pressure of 1.1 MPa. For this transducer the zero crossing frequency was 3.3 MHz. In order to place these values in context, it is worth summarising the results of a recent survey in which we have reported pressures and intensities from a wide range of commercial pulse-echo equipment in clinical use (Duck *et al* 1985). The range of mean input pressures measured in 38 independent measurements in the survey varied from 0.03 to 1.15 MPa and the mean pressure was 0.53 MPa. Thus, 1.1 MPa is representative of the maximum input pressure observed in the survey whilst the maximum value of p_0 from the 2.5 MHz transducer is close to the survey mean. It can be assumed that the focal gains of the transducers used in the present study are similar to those commonly encountered on clinical equipment.

For each thickness of liver the transmitted positive peak pressure was measured and the relative magnitudes of the fundamental, second and third harmonic components in the pulse spectrum were recorded from the spectrum analyser. For a selection of pulses, the pulse waveform was digitised by hand and the harmonic components of the single cycle of greatest magnitude computed. This analysis enabled the 'worst case' distortion to be evaluated, independent of the diluting effect present by including the spectral content of the beginning, and tail, of the pulse in the total pulse spectrum.

3. Results

The build-up of harmonic content in the pulse waveform with propagation distance in liver was investigated over the range 2.5–9 cm. This was compared with the build-up of harmonic content in water over a similar range. The progressive distortion of an originally sinusoidal wave for $p_0 = 0.58$ MPa is shown at 3, 6 and 8 cm in figure 2. At 3 cm the waveform is still symmetric but by 6 cm it has become noticeably distorted with the maximum compression half cycle becoming narrower and sharper than the decompressional half cycle. The positive peak pressure, $p+$, here is 1.4 MPa and the negative peak pressure, $p-$, 1.1 MPa. At 8 cm the pulse is reduced in amplitude due to attenuation in the tissue and beam divergence but some distortion is maintained.

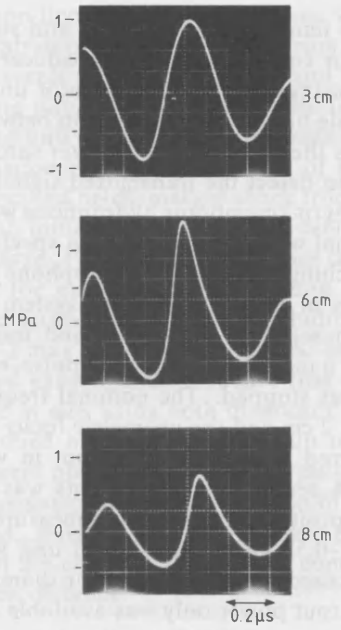

Figure 2. Measured pressure pulse after transmission through 3, 6 and 8 cm of ox liver (2.5 MHz focused transducer, input pressure 0.58 MPa).

The same pattern of distortion may be seen in the pulse in figure 3 which shows a 3.5 MHz pulse ($p_0 = 1.1$ MPa) following transmission through 5 cm of liver. In this case $p+$ is 2.0 MPa and $p-$ is 0.9 MPa.

At each location, on-line analysis of the signal into its frequency components was carried out and a typical frequency spectrum is shown in figure 4, in which second, third and fourth harmonic components can be seen in addition to the fundamental. From spectra such as these the relative contribution to the pulse waveform of each harmonic component was obtained. Figure 5 shows the development of second and

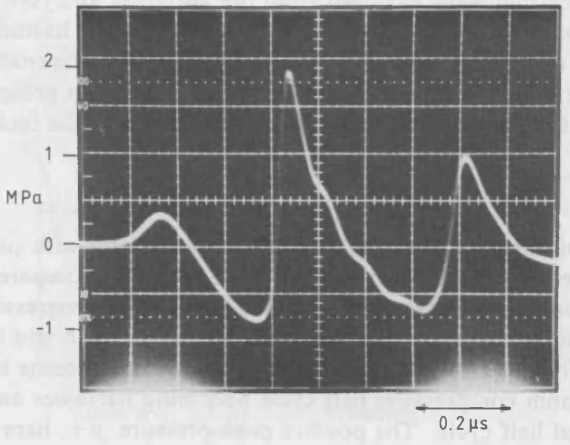

Figure 3. Pulse measured after transmission through 5.0 cm of liver using 3.5 MHz focused transducer (input pressure 1.1 MPa). (The slight ripple on the waveform is caused by the head amplifier.)

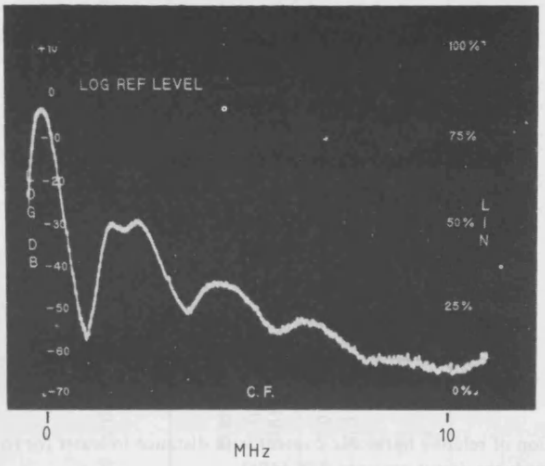

Figure 4. Example of spectrum of 2.5 MHz pulse after transmission through 7.5 cm of liver.

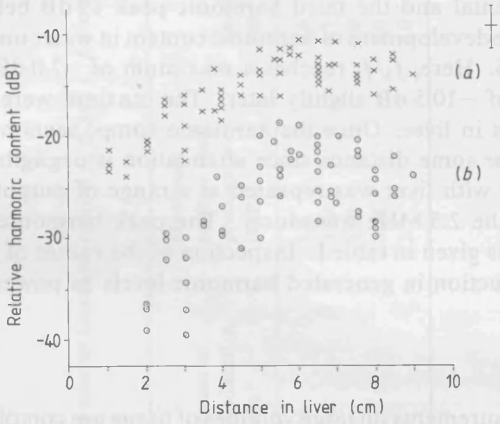

Figure 5. Axial variation of relative harmonic content with distance in liver for $(a) = f_2/f_1$, and $(b) = f_3/f_1$ (2.5 MHz focused transducer, input pressure 0.58 MPa).

third harmonics with propagation distance through liver relative to the fundamental peak. These results were compiled from measurements on five individual ox livers. Multiple measurements were made on a number of occasions on samples from the same liver. As is to be expected, there is a spread in the measurements. For example, at 6.5 cm the second harmonic ranges from 10.5 to 15 dB below the fundamental. These variations are due to inhomogeneity of the liver in the case of samples from the same liver and differences in the physical condition and age of samples from different livers. However, an overall trend is clear. The second and third harmonic components f_2 and f_3 increase relative to the fundamental as the propagation distance increases up to a certain distance and beyond this distance the levels of the harmonics decrease. The distance at which the maximum harmonic content occurs depends on the interaction of two opposing effects, the attenuation in the tissue and the generation of harmonics due to finite-amplitude propagation. The peaks in f_2/f_1 and f_3/f_1 occur at about 6 cm. The pulse recorded with the greatest distortion showed the second harmonic 10.5 dB

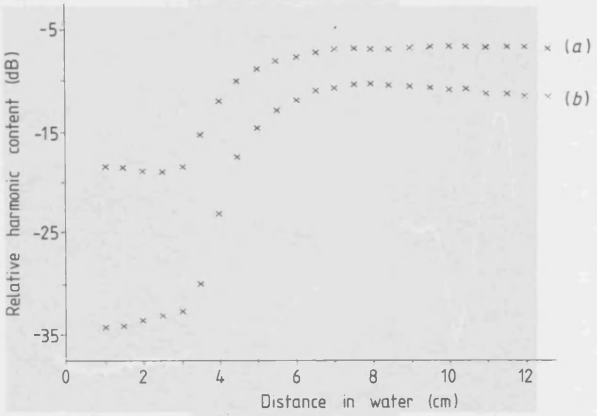

Figure 6. Axial variation of relative harmonic content with distance in water for $(a) = f_2/f_1$, and $(b) = f_3/f_1$ (2.5 MHz focused transducer, input pressure 0.58 MPa).

below the fundamental and the third harmonic peak 19 dB below the fundamental. For comparison, the development of harmonic content in water under similar conditions is shown in figure 6. Here, f_2/f_1 reaches a maximum of -7.0 dB at about 7.5 cm and f_3/f_1 a maximum of -10.5 dB slightly later. The maxima were reached at a greater depth in water than in liver. Once the harmonic components have built up in water they are retained for some distance since attenuation is negligible in this case.

The experiment with liver was repeated at a range of output powers between 0.5 and 64 mW using the 2.5 MHz transducer. The peak harmonic content under these varying conditions is given in table 1. Inspection of the values of f_2/f_1 and f_3/f_1 reveals the progressive reduction in generated harmonic levels as power levels are reduced.

4. Discussion

Any ultrasonic measurements on large volumes of tissue are complicated by the problem of tissue inhomogeneity. These measurements on excised ox liver are no exception resulting in a range of observed values under similar measurement conditions. The situation is further complicated by the fact that the morphology of the liver used will determine the ultrasonic properties on which the passage of ultrasound through tissue depends, such as attenuation and the non-linearity parameter B/A. It must also be remembered that excised liver may differ from living tissue in a number of ways. These experiments were carried out at 21 °C, and non-linear properties are known to be somewhat temperature dependent. For instance, for distilled water, B/A increases by about 10% from 20 to 40 °C. The tissue samples were immersed in physiological saline rather than being fully perfused with blood, in common with the majority of studies reported on tissue measurements *in vitro*. In spite of these conditions the measurements reported here for harmonic content relate smoothly and without an observed discontinuity to those reported before (Starritt *et al* 1985) for measurements through human calf muscle using the same 2.5 MHz beam. Thus we have some confidence that these *in vitro* measurements can provide an insight into the way in which finite-amplitude distortion of pulses may occur during propagation through living tissue. We have shown that progressive harmonic development in the pulse occurs to a certain depth

Table 1. Measured overall maxima of peak pressures and relative harmonic content f_1/f_2 and f_1/f_3 for water and ox liver. There was no measurable harmonic content for $p_0 = 0.08$ MPa (power = 0.5 mW) at 2.5 MHz.

	Nominal frequency (MHz)	Total acoustic power (mW)	Pressure at transducer, p_0 (MPa)	Maximum positive peak pressure, $p+$ (MPa)	Location (cm)	Highest f_2/f_1 (dB)	Location (cm)	Highest f_3/f_1 (dB)	Location (cm)
Water	2.5	64	0.58	5.6	6.6	−7.0	7.5	−10.5	8.0
Liver	2.5	64	0.58	1.69	4.5	−10.5	6.5	−19	5.5
Liver	2.5	27	0.41	1.02	6.0	−13	6.0	−25	6.5
Liver	2.5	9	0.23	0.38	6.0	−18	6.0	—	—
Liver	3.5	11	1.1	2.2	5.0	−9	5.0	−13	5.0

in tissue. This distance depends in varying degrees upon the physical parameters of the ultrasonic field, including frequency, input power and focal gain, and of the ultrasonic properties of liver, including B/A, and attenuation and its frequency dependence. Whilst an increase in frequency will decrease the distance over which a given harmonic content will develop in the absence of attenuation, the harmonics generated will be more strongly attenuated in a medium with frequency-dependent attenuation. The increased distortion which results from increased pressure at the transducer has been demonstrated in this study, but a detailed investigation of the effects of altering all field parameters has yet to be carried out.

A number of measurements of B/A have been reported in the literature both for whole beef liver and for homogenised liver. At 23 °C the values for normal beef liver range from 6.2 to 8.9. Whilst the majority of biological tissues have B/A values in the range 5.5–8.9, Law *et al* (1985) have reported values of 11 and 11.3 for pig fatty tissue. It is possible therefore that the magnitude of finite-amplitude distortion which may occur in fatty tissue could be greater than that observed and reported above.

The pattern of distortion which can be observed in figures 2 and 3 is similar to that following transmission through water, with a peaked positive half cycle of greater peak magnitude than that of the associated negative half cycle. These observations do not accord with predictions of waveform distortion given by Bacon (1986) at the focus of a 3.5 MHz field transmitting through a medium with the acoustic properties of liver. When dispersion of 0.7% per decade was assumed, the asymmetry in the waveform inverted and peak negative pressures up to 15% higher than peak positive pressures were predicted. Furthermore, it was shown that peak negative pressures could exceed those expected from low-amplitude attenuation losses by a factor of up to 1.8. Our observations showed neither asymmetry inversion nor greater than expected peak negative pressures over the range of tissue thicknesses used. It is probable that the disparity between theory and observation arises from an incorrect assumption of the magnitude of the dispersion in liver. The value used by Bacon was obtained from published measurements for haemoglobin solution, in the absence of any direct measurements for liver, and an assumed attenuation of 1 dB cm^{-1} MHz^{-1}. This disparity between prediction and observation requires further investigation and, in particular, careful direct measurements of dispersion in soft tissues will be required before detailed prediction of non-linear waveform distortion will be possible.

The observation that harmonic generation can occur in tissue to measurable and significant levels may have importance beyond that noted above for the enhancement of tissue heating (Swindell 1985). It will be necessary to evaluate whether the very high pressure gradients which occur in the near-shocked conditions demonstrated in figure 3 have biological importance. It is possible in this pulse to observe a pressure increase from 0 to 1 MPa in about 40 ns. In spatial terms this occurs over about 60 μm giving, very approximately, a transient pressure gradient of 0.1 MPa (1 atmosphere) per cell width. Whether considerations such as these are valuable in assessing the real response of cells to ultrasonic fields will have to be investigated, together with associated analyses of accelerative forces, strains, cavitation and non-linear (shock) losses. The potential for improved lateral resolution by the exploitation of finite-amplitude effects has been suggested by several authors (e.g. Muir *et al* 1973, Bjorno and Grinderslev 1979). Some modern imaging systems are capable of generating input pressures at levels equivalent to those studied here. It will therefore be necessary to include some considerations of finite-amplitude effects in a complete discussion of possible mechanisms of cell responses to ultrasound as used for medical imaging applications.

Résumé

Développement des distorsions harmoniques dans les ultrasons pulsés d'amplitude finie se propageant dans le foie.

Les auteurs ont étudié le développement progressif d'une distorsion d'amplitude finie pour des impulsions ultrasonores se propageant dans du foie de bovin excisé, à l'aide de faisceaux ultrasonores focalisés et pulsés, aux fréquences nominales de 2,5 et 3,5 MHz. Les transducteurs et les puissances utilisés sont comparables à ceux qui peuvent être rencontrés sur de l'équipement d'imagerie clinique. Des distorsions significatives de l'onde ont été observées, particulièrement aux plus fortes puissances. A 2,5 MHz, par exemple, avec une pression (p_0) d'entrée moyenne de 0,58 MPa, la seconde harmonique du spectre d'impulsions a présenté une valeur maximale inférieure de 10,5 dB à celle de la fondamentale, et la valeur de la plus haute composante de la troisième harmonique se situait à 19 dB sous celle de la fondamentale. Ces observations particulières montrent que les distorsions d'amplitude finie peuvent présenter une importance significative dans la transmission des impulsions ultrasonores à travers les tissus au cours des examens.

Zusammenfassung

Das Auftreten nicht-linearer Verzerrungen endlicher Amplituden bei gepulstem Ultraschall.

Die fortlaufend entstehende Amplitudenverzerrung von Ultraschallimpulsen wurde an herausgenommener Rinderleber untersucht mit Hilfe eines gepulsten fokusierten Ultraschallstrahls bei Frequenzen von 2.5 und 3.5 MHz. Die verwendeten Wandler und Leistungen können auch für bildgebende Geräte in der Klinik benutzt werden. Eine signifikante Verzerrung der Wellenform wurde beobachtet, besonders bei hohen Leistungen. So zeigt z.B., bei 2.5 MHz und einem mittleren Eingangsdruck (p_0) von 0.58 MPa, die zweite Harmonische im Impulsspektrum einen Maximalwert von 10.5 dB unter der Grundschwingung und der größte dritte Harmonische Komponente wurde 19 dB unter der Grundschwingung. Diese ungewöhnlichen Beobachtungen zeigen, daß die Verzerrung endlicher Amplituden von einiger Bedeutung bei der Transmission von Ultraschallimpulsen durch Gewebe während des Abtastvorgangs in der Diagnostik sein könnte.

References

Bacon D R 1984 *Ultrasound Med. Biol.* **10** 189
——1986 *Proc. Inst. Acoust.* **8** (2) 34
Bjorno L and Grinderslev S 1979 *J Physique* **40** C8-111
Duck F A and Starritt H C 1984 *Br. J. Radiol.* **57** 231
Duck F A, Starritt H C, Aindow J D, Perkins M A and Hawkins A J 1985 *Br. J. Radiol.* **58** 989
Fry F J and Dunn F 1962 *Physical Techniques in Biological Research* Vol 4 (New York: Academic) p 261
Haran M E and Cook B D 1983 *J. Acoust. Soc. Am.* **73** 774
Law W K, Frizzell L A and Dunn F 1985 *Ultrasound Med. Biol.* **11** 307
Muir T G and Carstensen E L 1980 *Ultrasound Med. Biol.* **6** 345
Muir T G, Talkington C M, Shaw B S, Adair R S and Willette J G 1973 *J. Acoust. Soc. Am.* **53** 382
Starritt H C, Perkins M A, Duck F A and Humphrey V F 1985 *J. Acoust. Soc. Am.* **77** 302
Swindell W 1985 *Ultrasound Med. Biol.* **11** 121

Title: Evidence for ultrasound finite-amplitude distortion in muscle using medical equipment

Authors: Starritt H.C., Perkins M.A., Duck F.A. and Humphrey V.F.

Source: Journal of the Acoustical Society America, Volume 77

Date: 1985

Pages: 302 - 306.

Evidence for ultrasonic finite-amplitude distortion in muscle using medical equipment

H. C. Starritt, M. A. Perkins, F. A. Duck, and V. F. Humphrey[a)]
Medical Physics Department, Royal United Hospital, Bath, Avon, England BA1 3NG

(Received 17 April 1984; accepted for publication 8 August 1984)

Finite-amplitude distortion of ultrasonic waves from medical equipment has been observed to occur following transmission through calf muscle in human volunteers. Measurements were made using both dynamic pulse-echo imaging equipment and physiotherapy equipment. In both cases irradiation was carried out under operating conditions commonly used clinically. Pressure waveforms were measured at the skin surface using a broadband polyvinylidene difluoride membrane hydrophone. Using a pulsed, weakly focused 2.5-MHz beam with input peak pressure of 0.8 MPa and a pressure gain of 5.3 at the focus, the mean second harmonic peak magnitude (16 measurements) was 17 dB below the fundamental peak. A 1.1-MHz continuous wave therapy set with input peak pressure of 0.5 MPa showed mean second harmonic magnitude 23 dB below the fundamental.

PACS numbers: 43.80.Cs, 43.25.Cb

INTRODUCTION

The fact that nonlinear propagation of ultrasonic waves is relevant in the context of medical applications has been discussed only relatively recently (see for instance, Muir *et al.*[1]) In this paper we wish to present direct experimental evidence that finite-amplitude distortion of ultrasonic waves occurs in living muscle, and that this is true for beams generated for both pulse–echo diagnosis and for therapeutic applications.

The exact prediction of the magnitude of waveform distortion and harmonic generation in tissue under conditions commonly encountered in the medical use of ultrasound for imaging is difficult. The fields are pulsed and focused, near-field diffraction effects are important, and, perhaps most relevantly the scattering and attenuation properties of tissue, their frequency dependence, and the magnitude of the nonlinearity parameter B/A for all tissue types is still poorly documented. Analysis of focused fields demonstrates the importance of correctly handling the relative phases of the harmonic components in the wave,[2,3] if the true waveform and more particularly the existence and magnitude of a shock is to be correctly predicted. The difficulty of correctly handling the analysis in the focal region where instantaneous pressures can be very high, generally limits the range of shock parameter σ for which any solution applies. With regard to the additional problem of nonlinear propagation in a medium with attenuative losses, Haran and Cook[4] have investigated plane-wave propagation in a lossy medium of tissuelike character where the frequency-dependent attenuation was represented in the form $\alpha(n) = \alpha_0 n^b$. This is in contrast to a situation where the medium is assumed to be a nondispersive viscous fluid with square law frequency dependence. Using reasonable estimates of intensity at source, attenuation and B/A, it was predicted that mature shocks would develop in low-loss fluids within the body (bladder urine or amniotic fluid) but that the higher attenuation of liver tissue would prevent shock generation in spite of some harmonic generation.

A few measurements of the magnitude of the nonlinear parameter B/A for biological tissues have been reported.[5] The values for those tissues that have been investigated have been found to lie in the range 5.5–8.0, but evidence of B/A for muscle is lacking. It can be argued that the parameter of nonlinearity B/A alone is insufficient to characterize nonlinear propagation in inhomogeneous media, and an approach to the theory of nonlinear propagation in mixed media has recently been presented.[6]

We have previously reported that strong nonlinear effects may be observed in water in the beams from focused, pulsed diagnostic imaging equipment.[7] The magnitude of finite-amplitude distortion was shown to increase with propagation distance, frequency, and source amplitude. Peak pressures up to 5 MPa were commonly measured in the focal zones. These pressures suggest spatial peak temporal peak intensities of up to 8.3×10^6 W m^{-2}, in comparison with a maximum of 17×10^6 W m^{-2} given in a survey by Carson *et al.*[8] A measured waveform given in that paper also shows evidence of distortion, perhaps generated by finite-amplitude effects, but with the polarity inverted from that observed in our measurements.

Further experimental work in water using continuous wave unfocused therapy ultrasonic equipment has demonstrated a similar increase in wave distortion with distance, frequency, and source amplitude. The peak pressures measured in these cases are commonly an order of magnitude lower than those encountered in the focal zones of pulsed diagnostic beams.

I. EXPERIMENTAL METHOD

One cause of the slow experimental progress in this area has been the lack of availability of hydrophones whose broadband calibration could be depended upon. The recent

[a)] Also at: School of Physics, University of Bath, Claverton Down, Bath, England BA2 7AY.

 0001-4966/85/010302-05$00.80

availability of such hydrophones using the piezoelectric polymer polyvinylidene difluoride (pvdf) has substantially relieved this problem. We have used a calibrated bilaminar pvdf membrane hydrophone with a 1-mm-diam sensitive area to detect the pressure waveform. This type of hydrophone has been developed by Marconi GEC, Chelmsford, Essex, and the National Physical Laboratory, London and a full description of its design and performance characteristics has been given by Bacon[9] and Preston *et al.*[10] The pulse waveform was displayed on a Tektronix 465 oscilloscope, bandwidth limited to 20 MHz. The pulse spectrum was generated using a Polarad rf spectrum analyzer. A specially designed head amplifier was used to provide impedance matching between the hydrophone and the measurement instruments, and was mounted on the hydrophone itself. This amplifier used a TDA1078 wideband amplifier with a dual cascaded FET front end with very high input impedance giving a voltage gain of about 4. Frequency response measurements showed a -3 dB response at 74 MHz and approximately 1-dB gain and 10° phase shift from low frequencies at 20 MHz.

The experimental arrangement used was as follows: A tank of dimensions 75 × 75 cm was filled to a depth of 40 cm with tap water which was allowed to degas naturally. The hydrophone, mounted on a micromanipulator, and the transmitting transducer were clamped in position in the water, allowing a gap of approximately 15 cm for the insertion of a leg between them, at approximately midcalf level. The hydrophone was positioned and aligned to maximize the signal received. The leg was immersed in the water and positioned so that the transmitting transducer was in contact with one side of the calf. The hydrophone position was adjusted along the axis until it was in contact with the opposite side of the calf, ensuring that the entire transmission path was through tissue, and that no water was included in this path. Care was taken when positioning the leg to ensure that the ultrasound beam passed entirely through soft tissue and was well clear of the tibia. The separation between the hydrophone and transducer was recorded as the leg thickness. A final minor adjustment in the position and height of the hydrophone to maximize the signal was occasionally necessary to correct for refraction.

Normal volunteers of both sexes in the age range 20–45 years were used and a total of 16 legs were investigated. Two separate clinical ultrasonic units were used. The first was a mechanically scanned pulse–echo imaging unit with a focused transducer. The nominal frequency was 2.5 MHz, the diameter was 20 mm, and the geometric focus was at 100 mm. At minimum output powers (peak axial pressure at 1 cm of 122 kPa) the location of the last axial pressure maximum was at 58 mm. Using equations given by Lucas and Muir[11] the focal pressure gain of this transducer has been calculated as 5.3 and the location of the last maximum at 56.7 mm. All experiments were carried out using the equipment at maximum output power and with the rotation of the scanning head arrested. The second unit was a physiotherapy unit operating continuously at 1.1 MHz using an unfocused transducer of 2.5 cm diam. The source peak pressure was 0.5 MPa.

II. RESULTS

Leg thicknesses were in the range 9–12 cm. Thus for the focused field the point of measurement was beyond the focal zone, where the beam is diverging. For comparison with the tissue measurements, the pressure waveforms and harmonic amplitudes in water were measured at a 10-cm range. The finite amplitude distortion of the pulse in water is shown in Fig. 1. The peak positive pressure is 3.8 MPa. There is asymmetry of the compression and rarefaction half cycles which is characteristic of nonlinear distortion in a diffracting field, and considerable steepening of the rising edges. The spectrum of this waveform also is shown with 2nd, 3rd, and 4th harmonic spectral peaks only displayed. The second harmonic peak is 11 dB below the fundamental pulse spectral peak. (Value corrected for analyzer nonlinear response.)

Similarly Fig. 2 shows the pressure waveform and corresponding spectrum for the 1.1-MHz physiotherapy unit at 10 cm and irradiating continuously into water. Up to seven harmonic components are displayed in this case and the second harmonic is 15 dB below the fundamental. The peak positive pressure measured was 0.45 MPa. For these conditions, the shock parameter σ is 0.35 if a free field is assumed.

A typical example of the pulse waveform after transmission through 10 cm of calf tissue is shown in Fig. 3; the

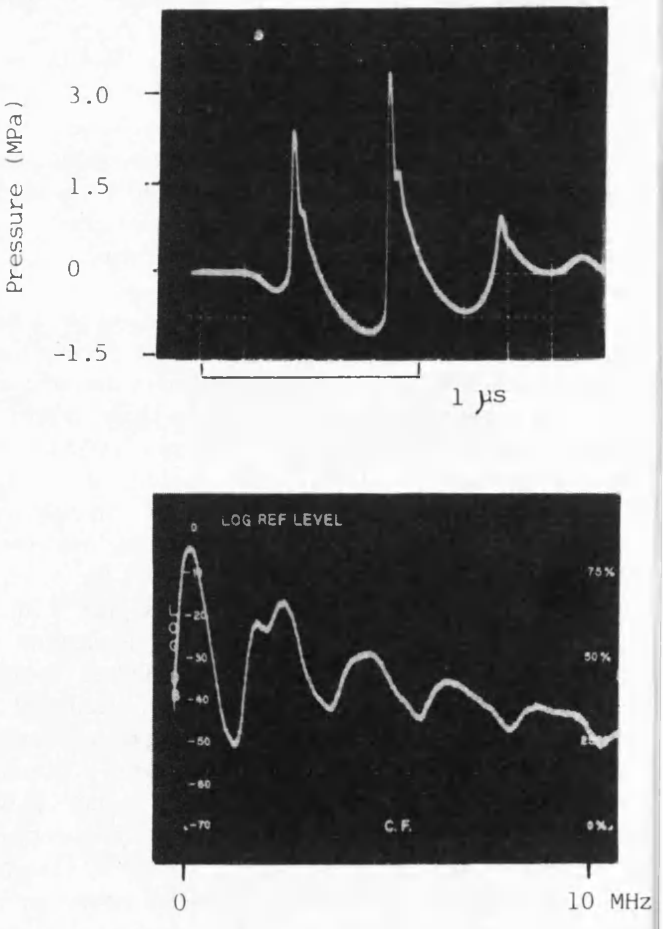

FIG. 1. Measured pressure pulse and associated spectrum from a 2.5-MHz focused medical pulse–echo transducer. Measurement at 10-cm range in water.

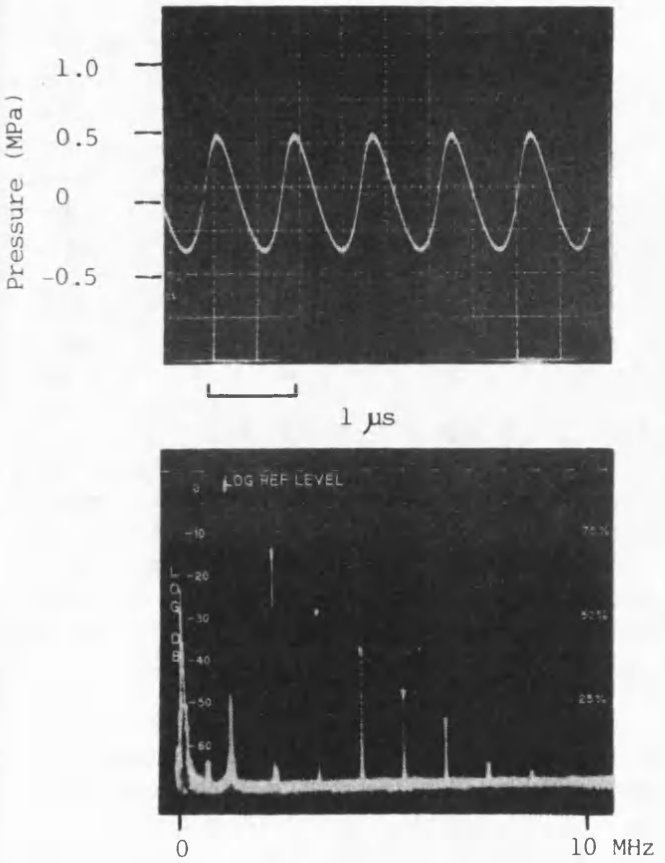

FIG. 2. Measured pressure wave and associated spectrum from a 1.1-MHz continuous wave physiotherapy transducer at 3 W cm^{-2} nominal output intensity. Measurement at 10-cm range in water.

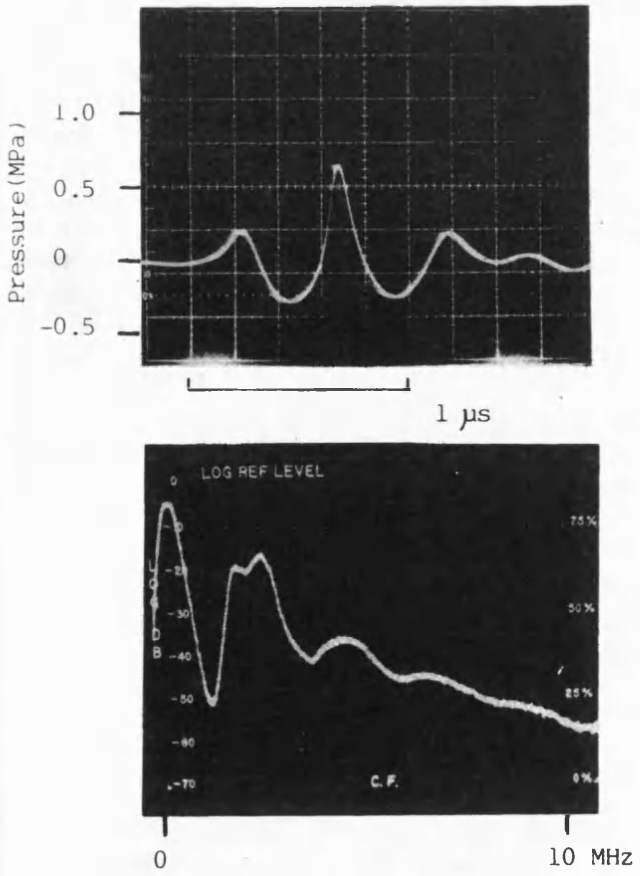

FIG. 3. Measured pressure pulse and associated spectrum, as Fig. 1, but through calf muscle.

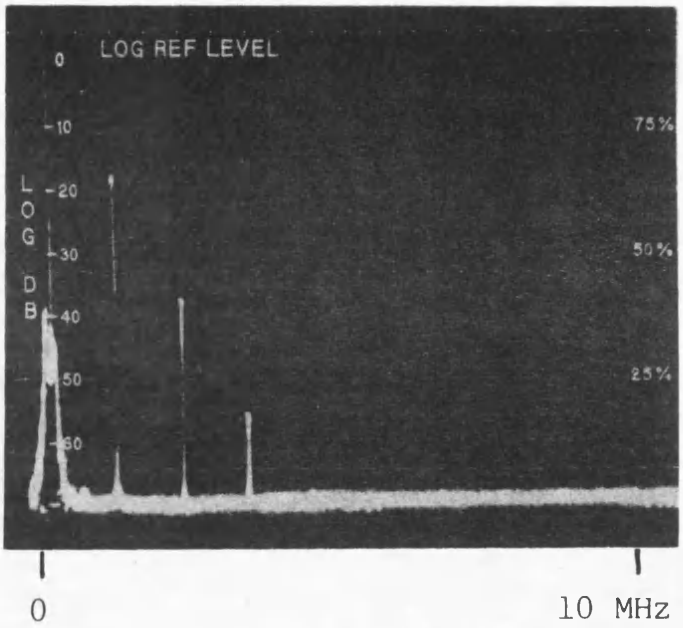

FIG. 4. Spectrum of 1.1-MHz wave as Fig. 2 but through calf muscle. The waveform appeared sinusoidal.

peak positive pressure is 0.64 MPa. The waveform distortion is clearly less in this case than that which occurs in water at the same propagation distance but it can be seen from the spectrum of this waveform that pulse distortion has taken place; 2nd and 3rd harmonic components are present in the spectrum at 17 dB and 25 dB below the fundamental peak. Figure 4 shows the spectrum of a transmitted 1.1-MHz wave through calf muscle, and again 2nd and 3rd harmonic components have been generated during propagation through the tissue.

The amplitudes of the second and third harmonics relative to the fundamental are tabulated from the series of measurements on each of the ultrasonic units. Table I shows the results from 16 legs investigated in the pulsed field and Table II contains the results from 16 legs investigated in the 1.1-

TABLE I. Transmitted harmonic amplitudes through calf muscle relative to the fundamental peak; pulsed, focused, 2.5 MHz (missing values were below detectable limit).

2nd harmonic (dB)	3rd harmonic (dB)
− 14.5	− 24.5
− 18.5	− 32.5
− 20.0	− 33.0
− 18.5	− 33.5
− 20.0	...
− 20.5	− 36.5
− 14.0	− 25.0
− 17.0	− 28.0
− 15.0	− 24.0
− 15.0	− 25.0
− 20.5	− 34.5
− 19.0	− 34.0
− 16.5	...
− 19.5	− 34.5
− 16.0	− 29.0

TABLE II. Transmitted amplitude through calf muscle relative to fundamental; 1.1-MHz physiotherapy unit at nominal 3 W cm^{-1} output intensity (missing values were below detectable limits).

2nd harmonic (dB)	3rd harmonic (dB)
−22	−37
−24	−37
−27	−51
−23	−45
−22	−38
−17	−30
−22	−32
−18	−40
−27	...
−35	...
−23	−38
−25	−42
−23	−32
−19	−40
−30	−31
−27	−46

MHz cw field. These values were obtained directly from the spectral display with a correction applied for the response of the spectrum analyzer in pulsed operation. No attempt has been made to relate harmonic amplitude to calf thickness, age, etc. In spite of the variation of magnitude in the second harmonic peaks their presence was always noted. Measurements in water close to both transducers indicated that the magnitude of second harmonic contamination at the source was in both cases less than −30 dB.

III. DISCUSSION

In order to quantify the extent to which finite-amplitude distortion occurs in ultrasonic waves used clinically, *in-vivo* measurements have been made to complement theoretical and laboratory evaluations. It is clearly difficult to measure pulse distortion *in vivo*, involving as it would implantable hydrophones. Calf muscle gives a useful tissue mass to enable some direct measurements to be made. As indicated above both for the weakly focused pulsed beam at 2.5 MHz and the unfocused continuous wave beam at 1.1 MHz, measurable finite-amplitude distortion has been demonstrated. Under the conditions used the mean second and third harmonic peaks were 17 and 30 dB below the fundamental in the pulsed focused case, and 23 and 37 dB below the fundamental for continuous 1.1-MHz irradiation.

It is worth noting that the pulse distortion through muscle is of a different character than that seen through water. In both cases the decompression half-cycle is characteristically rounded and the compressional half-cycle peaked. However, in water, the compressional peak tends to occur early in the trough-to-trough period, whereas through tissue there is less tendency for this shift to occur. Such waveform variations may be explained purely on the basis of the relative phases of the harmonic components.[2] Harmonic analysis of the single cycle of maximum amplitude (rarefraction followed by compression) was carried on the waveforms shown in Figs. 1 and 3. In water there is a phase lag of 41° of the second harmonic with respect to the fundamental, and in muscle this lag is 73°. The analysis used a Fourier sine series.

These measured phase shifts at one location indicate the need to investigate more fully the progressive distortion of these waves through tissue in terms of both amplitude and phase. Diffraction, focusing, and possibly, dispersive attenuation may all play a part in affecting the distortion. In addition a process of undistortion may be occurring in which energy stored in the harmonics returns to the fundamental, as described by Muir *et al.*[12]

It is reasonable to assume that these observations of finite-amplitude distortion underestimate the extent to which such distortion may occur in soft tissue, under some clinical circumstances. It is established that the attenuation due to muscle is at the upper end of the range of attenuation of soft tissues, with measured attenuation coefficient values commonly quoted in excess of 1 dB cm^{-1} MHz^{-1} whereas the mean for soft tissue is about 0.5 dB cm^{-1} MHz^{-1} (Ref. 13). Since the nonlinear generation of harmonics is in part controlled by the magnitude of the attenuation coefficient of the medium, it must be concluded that in tissues other than muscle (for instance liver, spleen, brain) the finite-amplitude distortion would be greater than that demonstrated here, given comparable nonlinear properties. Furthermore, the measurements on the pulsed focused field were made at positions beyond the focus where the reduction of beam intensity due to beam divergence, together with attenuation, would probably reduce the likelihood of further strong finite-amplitude distortion. In preliminary measurements on distortion through ox liver of varying thicknesses we have confirmed the presence of harmonic components in excess of those reported above. Detailed measurements will be the subject of a later publication.

For these reasons it seems safe to assume that when, for instance, the liver or other viscera are examined using commercial equipment under its normal operating conditions, the acoustic pulses will suffer finite-amplitude distortion and harmonic generation similar to, or greater than that described here, particularly in the focal zone. As the quest for improved image quality and resolution continues, the trend towards tighter foci, and beams of higher intensity must result in even greater nonlinear distortion occurring.

These observations reinforce the need for significantly greater effort to be placed in the fundamental investigation of the nonlinear properties of tissues, of finite-amplitude distortion in focused fields, and of pulse propagation through inhomogenous, nonlinear media.

ACKNOWLEDGMENTS

We are most grateful for the assistance given by D. Taylor with some of the measurements, and to O. Berktay for his continued interest and encouragement.

[1]T. G. Muir and E. L. Carstensen, "Prediction of non-linear acoustic effects at biological frequencies and intensities," Ultrasound Med. Biol. 6, 345–357 (1980).
[2]B. G. Lucas and T. G. Muir, "Field of a finite-amplitude focusing source," J. Acoust. Soc. Am. 74, 1522–1528 (1983).
[3]N. S. Bakhvalov, Ya. M. Zhileiken, E. A. Zabolotskaya, and R. V. Khokh-

lov, "Focused high amplitude sound beams," Sov. Phys. Acoust. **24**, 10–15 (1978).
[4]M. E. Haran and B. D. Cook, "Distortion of finite amplitude ultrasound in lossy media," J. Acoust. Soc. Am. **73**, 774–779 (1983).
[5]W. K. Law, L. A. Frizzell, and F. Dunn, "Ultrasonic determination of the nonlinearity parameter B/A for biological media," J. Acoust. Soc. Am. **69**, 1210–1212 (1981).
[6]R. E. Apfel, "The effective nonlinearity parameter for immiscible liquid mixtures," J. Acoust. Soc. Am. **74**, 1866–68 (1983).
[7]F. A. Duck and H. C. Starritt, "Acoustic shock generation by ultrasonic imaging equipment," Brit. J. Radiol. **57**, 231–240 (1984).
[8]P. L. Carson, P. R. Fischella, and T. V. Oughton, "Ultrasonic power and intensities produced by diagnostic ultrasound equipment," Ultrasound Med. Biol. **3**, 341–350 (1978).
[9]D. R. Bacon, "Characteristics of a pvdf membrane hydrophone for use in the range 1–100 MHz," IEEE Trans. Sonics Ultrason. **SU-29**, 18–25 (1982).
[10]R. C. Preston, D. R. Bacon, A. J. Livett, and K. Rajendran, "PVDF membrane hydrophone performance properties and their relevance to the measurement of the acoustic output of medical ultrasonic equipment," J. Phys. E: Sci. Instrum. **16**, 787-796 (1983).
[11]B. G. Lucas and T. G. Muir, "The field of a focusing source," J. Acoust. Soc. Am. **72**, 1289–1296 (1982).
[12]T. G. Muir, L. L. Mellenbruch, and J. C. Lockwood, "Reflection of finite-amplitude waves in a parametric array," J. Acoust. Soc. Am. **62**, 271–276 (1977).
[13]S. A. Goss, R. L. Johnstone, and F. Dunn, "Comprehensive compilation of empirical ultrasonic properties of mammalian tissue," J. Acoust. Soc. Am. **64**, 423–457 (1978).

REFERENCES

Aanansen S.I., Barkve T., Tjøtta N.J. and Tjøtta S., 1984, Distortion and harmonic generation in the nearfield of a finite amplitude sound beam, J Acoust Soc Am, 75, 749–766.

Abraham V., Ziskin M. and Heyner S., 1989, Temperature elevation in the rat fetus due to ultrasound exposure, Ultrasound Med Biol, 15, 443–449.

Aindow J.D., Robins P.A. and Deogan D.S., 1986, A pvdf membrane hydrophone for *in vivo* tissue measurements, Proceedings of 18th annual meeting of British Medical Ultrasound Society, 16th – 18th Dec 1986, University of Warwick, p 110.

AIUM/NEMA (American Institute of Ultrasound in Medicine/National Electrical Manufacturers Association), 1983, Safety standard for diagnostic ultrasound equipment, UL1–1981, J Ultrasound Med, 2 (Suppl).

AIUM (American Institute of Ultrasound in Medicine), 1988, Bioeffects considerations for the safety of diagnostic ultrasound, American Institute for Ultrasound in Medicine (AIUM) bioeffects committee, J Ultrasound Med, 7.

Arora K.L., Cohen B.J. and Beaudoin A.R., 1979, Fetal and placental responses to artificially induced hyperthermia in rats, Teratology, 19, 251–260.

Atchley A.A., Frizzell, L.A., Apfel R.E., Holland C.K., Madanshetty S. and Roy R.A., 1988, Thresholds for cavitation produced in water by pulsed ultrasound, Ultrasonics, 26, 280–285.

Aymé E.J. and Carstensen E.L., 1989a, Cavitation induced by asymmetric distorted pulses of ultrasound: theoretical predictions, IEEE Trans Ultrason Ferroelec Freq Contr, 36, 32–40.

Aymé E.J. and Carstensen E.L., 1989b, Cavitation induced by asymmetric distorted pulses of ultrasound: a biological test, Ultrasound Med Biol, 15, 61–66.

Bacon D.R., 1982, Characteristics of a pvdf membrane hydrophone for use in the range 1–100 MHz, IEEE Trans Sonics and Ultrason, SU–29, 8–25.

Bacon D.R., 1984, Finite amplitude distortion of the pulsed fields used in diagnostic ultrasound, Ultrasound Med Biol, 10, 189–195.

Bacon D.R. and Carstensen E.L., 1990, Increased heating by diagnostic ultrasound due to nonlinear propagation, J Acoust Soc Am, 88, 26–34.

Baker A.C., 1989, Finite amplitude propagation of focused ultrasonic waves in water, PhD thesis, University of Bath.

Baker A.C. and Humphrey V.F., 1990, Nonlinear propagation of short ultrasonic pulses in focused fields. In *Frontiers of Nonlinear Acoustics: ISNA*, M.F. Hamilton and D.T. Blackstock (eds), Elsevier, London, pp 185–190.

Baker A.C., Anastasiadis K. and Humphrey V.F., 1987, Nonlinear propagation in focused fields: experiment and theory. In *Proceedings of*

Ultrasonics International '87, Butterworth, London, pp 184–189.

Bamber J.C., 1981, Ultrasonic attenuation in fresh human tissues, Ultrasonics, 19, 187–188.

Bamber J.C, and Hill C.R., 1979, Ultrasonic attenuation and propagation speed in mammalian tissue as a function of temperature, Ultrasound Med Biol, 5, 149–157.

Barnett S.B., 1983, The influence of ultrasound on embryonic development, Ultrasound Med Biol, 9, 19–24.

Barnett S.B., Walsh D.A. and Angles J.A., 1990, Novel approach to evaluate the interaction of pulsed ultrasound with embryo development, Ultrasound Med Biol, 28, 166–170.

Beissner K., (1985), Maximum hydrophone size in ultrasound field measurements, Acustica, 59, 61–66.

Beyer R.T., 1974, Streaming. In *Nonlinear Acoustics*, R.T.Beyer (ed), US Navel Sea Systems, US Government Printing Office, Washington DC, pp 239–268.

Beyer R.T., 1984, *Nonlinear Acoustics in Fluids*, Benchmark Papers in Acoustics Volume 18, Van Nostrand Reinhold, New York.

Bjørnø L., 1975, Nonlinear ultrasound – a review. In *Conference Proceedings Ultrasonics International 1975*, pp 110–115.

Bjørnø L., 1976, Nonlinear acoustics. In *Acoustics and Vibration Progress*, Volume 2, R.W.B. Stevens and H.G. Leventhall (eds), Chapman and Hall, London, pp 103–203.

Blackstock D.J., 1964, On plane, spherical and cylindrical sound waves of finite amplitude in lossless fluids, J Acoust Soc Am, 36, 217–219.

Blackstock D.J., 1966, Connection between Fay and Fubini solutions for sound waves of finite amplitude, J Acoust Soc Am, 39, 1019–1026.

Burgers J.M., 1948, A mathematical model illustrating the theory of turbulence. In *Advances in Applied Mechanics*, Volume 1, Academic Press, New York, pp 171–199.

Burgess S.E.P., Silverman R.H., Coleman D.J., Yablonski M.E., Lizzi F.L., Driller J., Rosado A.L. and Denis P.H., 1986, Treatment of glaucoma with high intensity focused ultrasound, Ophthalmol, 93, 831–838.

Carson P.L., Rubin J.L. and Chiang E.H., 1989, Fetal depth and ultrasound path lengths through overlying tissues, Ultrasound Med Phys, 15, 629–639.

Carstensen E.L., 1987, Acoustic cavitation and the safety of diagnostic ultrasound, Ultrasound Med Biol, 13, 597–606.

Carstensen E.L., 1989, NCRP/AIUM Absorption models, 2nd World Federation of Ultrasound in Medicine and Biology Symposium in Medical Ultrasound, G. Kossoff and W. Nyborg (eds), Ultrasound Med Biol, 15 Suppl 1, pp.31–34.

Carstensen E.L. and Flynn H.G., 1982, Generation of transient cavities in liquids by microsecond pulses of ultrasound, Ultrasound Med Biol, 8, 720–724.

Carstensen E.L., Law W.K., McKay N.D. and Muir T.G., 1980, Demonstration of nonlinear acoustical effects at biomedical frequencies and intensities, Ultrasound Med Biol, 6, 345–357.

Carstensen E.L., Mckay N.D., Delecki D. and Muir T.G., 1982, Absorption of finite amplitude ultrasound in tissues, Acustica, 15, 116–123.

Carstensen E.L. and Schwan H.P., 1959, Absorption of sound arising from the presence of intact cells in blood, J Acoust Soc Am, 31, 185–189.

Chaussy Ch., Schmiedt E., Jocham D., Fuchs G., Brendel W., Forssman B. and Hepp W., 1986, *Extracorporeal shock wave lithotripsy*, Ch. Chaussy (ed), Karger, Basel.

Child S.A., Carstensen E.L., Gates A.H. and Hall W.J., 1988, Testing for teratogenecity of pulsed ultrasound in mice, Ultrasound Med Biol, 14, 493–498.

Christman C.L., Carmichael A.J., Mossaba M.M. and Riesz P., 1987, Evidence for free radicals produced in aqueous solutions by diagnostic ultrasound, Ultrasonics, 25, 31–34.

Coleman A.J. and Saunders J.E., 1989, A survey of acoustic output of commercial extra–corporeal shock–wave lithotripsy, Ultrasound Med Biol, 15, 213–227.

Coleman A.J., Saunders J.E., Crum L.A. and Dyson M., 1987, Acoustic cavitation generated by an extra–corporeal shock–wave lithotriptor, Ultrasound Med Biol, 13, 69–72.

Creasy R.K. and Resnik R., 1984, *Maternal–fetal Medicine: principles and practice*, W.B. Saunders, Philadelphia.

Crum L.A., 1984, Rectified diffusion, Ultrasonics, 22, 215–223.

Crum L.A. and Hansen G.M., 1982, Growth of air bubbles in tissue by rectified diffusion, Phys Med Biol, 27, 412–417.

Daniels S., Blondel D., Crum L.A. and Dyson M., 1987, Ultrasonically induced gas bubble production in agar based gels: Part 1 Experimental investigation, Ultrasound Med Biol, 13, 527–539.

Davies T.W. and Patrick M.A., 1972, A simplified method of improving the accuracy of hot film anemometry. In *Fluid Dynamic Measurements in the Industrial and Medical Environments*, D.J. Cockrell (ed), Leicester University Press, Leicester, pp 152–154.

Delecki D., Carstensen E.L., Parker K.J. and Bacon D.R., Overview of absorption of finite amplitude focused ultrasound. In *Frontiers of Nonlinear Acoustics: ISNA*, M.F. Hamilton and D.T. Blackstock (eds), Elsevier, London, pp 125–130.

DeReggi A.S., Roth S.C., Kenny J.M. and Edelman S., 1981, Piezoelectric polymer probe for ultrasonic applications, J Acoust Soc Am, 69, 853–859.

DHSS, 1977, Evaluation of four ultrasonic therapy units, K.G.R. Allen and C.K. Battye, DHSS STB/16/77.

Dickson J.A. and Calderwood S.K., 1980, Temperature range and selection and sensitivity of tumours to hyperthermia: a critical review. In *Thermal Characteristics of Tumours: Applications in detection and treatment*, R.K. Jain and P.M. Gullino (eds), Ann of N.Y. Acad Sci, New York.

Dinno M.A., Dyson M., Young S.R., Mortimer A.J., Hart J and Crum L.A., 1989, The significance of membrane changes in safe and effective use of therapeutic and diagnostic ultrasound, Phys Med Biol, 34, 1543–1552.

DISA, 1970, *Instruction and Service Manual for Type 55D10 Lineariser*, DISA Elektronik, Denmark.

Duck F.A., 1989, Output data from european studies, Ultrasound Med Biol, 15, Suppl 1, 61–64.

Duck F.A., 1990, *Physical properties of tissue, a comprehensive review*, Academic Press, London.

Duck F.A. and Martin K., 1986, Acoustic output from commercial diagnostic ultrasound equipment, British Medical Ultrasound Bulletin, No.40, 12–14.

Duck F.A. and Perkins M.A., 1988, Amplitude dependent losses in ultrasound exposure measurement, IEEE Trans Ultrason Ferroelec Freq Contr, 35, 232–241.

Duck F.A. and Starritt H.C., 1984, Acoustic shock generation by ultrasonic imaging equipment, Br J Radiol, 57, 231–240.

Duck F.A. and Starritt H.C., 1989, The spatial distribution of excess absorption in water due to shock transmission, Phys Med Biol, 34, 1623–1631.

Duck F.A., Starritt H.C. and Anderson S.P., 1987, A survey of the acoustic output of ultrasound Doppler equipment, Clin Phys Physiol Meas, 8, 39–49.

Duck F.A., Starritt H.C., ter Haar G.R. and Lunt M.J., 1989, Surface heating of diagnostic ultrasound transducers, Br J Radiol, 62, 1005–1013.

Duck F.A., Starritt H.C., Aindow J.D., Perkins M.A. and Hawkins A.J., 1985, The output of pulse–echo ultrasound equipment: a survey of powers, pressures and intensities, Brit J Radiol, 58, 989–1001.

Dyson M., 1985, Therapeutic Applications of Ultrasound, in *Biological Effects of Ultrasound*, W.L. Nyborg and M.C. Ziskin (eds.), Churchill Livingstone, New York.

Dyson M., and Brooks M., 1982, Stimulation of bone repair by ultrasound, Fifth World Congress of Ultrasound in Medicine Biology, Ultrasound Med Phys, 8 Supp 1, 50.

Dyson M., Pond J.B., Woodward B. and Broadbent J., 1974, The production of blood cell stasis and endothelial damage in the blood vessels of chick embryos treated with ultrasound in a stationary wave field, Ultrasound Med Phys, 1, 133–148.

Earnshaw S., 1860, On the mathematical theory of sound, Philos Trans R Soc London, 150, 133–148.

Eckart C, 1948, Vorticies and streams caused by sound waves, Physical Review, 73, 68–76.

Edwards M.J., 1986, Hyperthermia as a teratogen: a review of experimental studies and their clinical significance, Teratogenesis, Carcinogensis and Mutagenesis, 6, 563–582.

Edwards P.D. and Sancier K.M., 1983, Evidence for free radical production by ultrasonic cavitation in biological media, Ultrasound Med Biol, 9, 635–639.

Farmary M.J. and Whittingham T.A., 1978, A portable radiation force balance for use with diagnostic ultrasound equipment, Ultrasound Med, 3, 373–379.

Fay R.D., 1931, Plane sound waves of finite amplitude, J Acoust Soc Am, 3, 222–241.

Filipczynski L., Etienne J., Lypacewicz G. and Salkowski J., 1967, Visualising internal structures of the eye by means of ultrasonics, Proc Vib Probl Warsaw, 8, 357–368.

Flynn H.C., 1964, Physics of acoustic cavitation in liquids. In *Physical Acoustics*, W.P.Mason (ed), Academic Press, New York, pp 57–171.

Flynn H.G., 1982, Generation of transient cavities in liquids by microsecond pulses of ultrasound, J Acoust Soc Am, 72, 1926–1932.

Fox F.E. and Hertzfeld K.F., 1950, On the forces producing the ultrasonic wind, Physical Review, 78, 156–157.

Fry F.J. and Barger J.E., 1978, Acoustical properties of the human skull, J Acoust Soc Am, 63, 1576–1590.

Fubini G.E., 1935, Anomalies in the propagation of an acoustic wave of large amplitude, Altra Freq, 4, 173–180.

Gold'berg Z.A., 1956, On the propagation of plane waves of finite amplitude, Sov Phys Acoust, 3, 340–347.

Goldstein R.J., 1983, *Fluid Mechanics Measurements*, Hemisphere Publishing Corporation, Washington, pp 99–151.

ter Haar G., 1987, Recent advances and techniques in therapeutic ultrasound. In *Ultrasound Medical Applications, Biological Effects and Hazard Potential*, M.H. Repacholi, M. Grandolfo and A. Rindi (eds), Plenum Press, New York, pp 333–342.

ter Haar G.R., Daniels S., Eastaugh K.C. and Hill C.R., 1982, Ultrasonically induced cavitatin *in vivo*, Br J Cancer, 45 Suppl V, 151–155.

ter Haar G. R., Duck F.D., Starritt H.C. and Daniels S., 1989, Biophysical characterisation of diagnostic ultrasound equipment – preliminary results, Phys Med Biol, 34, 1533–1542

ter Haar G., Sinnett D. and Rivens I., 1989, High intensity focused ultrasound – a surgical technique for the treatment of discrete liver tumours, Phys Med Biol, 34, 1743–1750.

Hamilton M.F., 1986, *Nonlinear Wave Propagation in Mechanics*, AMD–Vol 77, T.W. Wright (ed), The American Society of Mechanical Engineers, New York.

Harran M.E. and Cook B.D., 1983, Distortion of finite amplitude ultrasound in lossy media, J Acoust Soc Am, 73, 774–779.

Hendrickx A.G., Stone G.W., Hendrickson R.V. and Matayoshi K., 1979, Teratogenic effects of hyperthermia in the bonnet monkey (Macaca radiata), Teratology, 19, 177–182.

ICRP, 1976, *Report of the task group on reference man*, ICRP Report 23, International Commission on Radiological Protection Report 49, Pergamon Press, Oxford.

ICRP, 1986, *Developmental effects of irradiation on the brain of the embryo and fetus*, ICRP Report 49, International Commission on Radiological Protection Report 49, Pergamon Press, Oxford.

ICRU, 1989, *Tissue substitutes in Radiation Dosimetry and Measurement*, ICRU Report 44, International Commission on Radiological Units and Measurement, Bethesda MD, USA.

Ivanovskii A.I., 1958, The connection of acoustic streaming with absorption, Sov Phys Acoust, 4, 142–152.

Kelman K.A., 1964, Phaco–emulsification and aspiration, Am J Ophthalmol, 67, 464–477.

Khokhlov R.D., Naugol'nykh K.A. and Soluyan S.I., Waves of moderate amplitudes in absorbing media, Acustica, 14, 248–253.

King L.V., 1914, On the convection of heat from small cylinders in a stream of fluid: determination of convection constants of small platinum wires with applications to hot–film anemometry, Philos Trans R Soc London, 214, 373–432.

Kinsler L.E., Austin R.F., Coppens A.B. and Sanders J.V., 1982, *Fundamentals of Acoustics*, Wiley, New York.

Kline J., Stein Z., Susser M., and Warburton D., 1985, Fever during pregnancy and spontaneous abortion, Am J Epidemiol, 121, 832–842.

Kremkau F.W., Barnes R.W. and McGraw C.P., 1981, Ultrasonic attenuation and propagation speed in normal human brain, J Acoust Soc, 70, 29–38.

Kubarin A.B. and Rudenko O.V., 1976, Numerical analysis of multi–dimensional acoustic streaming, 22, 75–76.

Kutznetsov V.P., 1971, Equations of nonlinear acoustics, Sov Phys Acoust, 16, 467–470.

Lagrange J., 1761, New researches on the nature and propagation of sound, Misc Taur, 2, 11–172.

Lele P.P., 1979, Safety and Potential Hazards in the current applications of ultrasound in obstetrics and gynecology, Ultrasound Med Biol, 5, 307–320.

Lele P.P., 1987, Ultrasound: synergistic effects and application in cancer therapy by hyperthermia, In *Ultrasound Medical Applications, Biological Effects and Hazard Potential*, M.H. Repacholi, M. Grandolfo and A. Rindi (eds), Plenum Press, New York, pp 307–332.

Lindsay R.B., 1974, *Physical Acoustics*, R.B. Lindsay (ed), Dowden, Hutchinson and Ross, Stroudsburg.

Lizzi F.L. and Ostromogilsky M., 1987, Analytical modelling of ultrasonically induced tissue heating, Ultrasound Med Biol, 13, 607–618.

Lucas B.G. and Muir T.G., 1983, Field of a finite amplitude focusing source, J Acoust Soc Am, 74, 1522–1528.

Markham J.J., 1952, Second–order acoustic fields: Streaming with viscosity and relaxation, Physical Review, 86, 497–502.

Masaoka H., Akamatsu N. and Numato A., 1987, Ultrasonic attenuation coefficient of uterine myomas, Euroson '87, Finnish Soc for Ultrasound in Med Biol, p 309.

Medwin M., 1954, An acoustic streaming experiment in gases, J Acoust Soc Am, 26, 332–341.

Meire H.B., 1990, Private communication.

Meissner A., 1926, Uber piezo–elektrische Kristalle bei hochfrequenz, Zeitschr. f. techn. Physik, 12, 585–594.

Mellette H.C., Hutt B.K., Askovitz S.I. and Hovarth B.M., 1951, Diurnal variations in body temperature, J Appl Physiol, 3, 665–675.

Merzkirch W., 1987, *Flow Visualization*, Academic Press, London.

Miller D.L., 1987, A review of the ultrasonic bioeffects of microsonation, gas body activation and related cavitation–like phenomena, Ultrasound Med Biol, 13, 443–470.

Miller D.L., Lamore B.J. and Boraker D.K., 1986, Lack of effect of pulse ultrasound on ABO antigens of human erythrocyes *in vitro*, Ultrasound Med Biol, 12, 209–216.

Miller M.W. and Ziskin M.C., 1989, Biological consequences of hyperthermia, Ultrasound Med Biol, 15, 707–722.

Morrow T.B., (1972), Effects of dirt accumulation of hot wire and hot film sensors. In *Fluid Dynamic Measurements in the Industrial and Medical Environments*, D.J. Cockrell (ed), Leicester University Press, Leicester, pp 122–124.

Morton K.I., ter Haar G.R., Strarford I.J. and Hill C.R., 1983, Subharmonic emmission as an indicaltor of ultrasonically induced biological

damage, Ultrasound Med Biol, 9, 629–633.

Mould R.F., 1989, *Introductory Medical Statistics,* Adam Hilger, Bristol, pp 165–179.

Muir T.G. and Carstensen E.L., 1980, Prediction of nonlinear acoustic effects at biomedical frequencies and intensities, Ultrasound Med Biol, 6, 345–357.

Naugol'nykh K.A., 1958, On the question of flows excited by sound, Sov Phys Doklady, 3, 1230–1232.

Naugol'nykh K.A., Soluyan S.I. and Khokhlov R.V., 1963, Spherical waves of finite amplitude in a viscous thermally conducting medium, Sov Phys Acoust, 9, 42–46.

NCRP, 1983, *Biological effects of ultrasound: mechanisms and clinical implications,* National research council on radiation protection and measurement (NCRP), Report No. 74, Betheseda M.D.

NCRP, 1990 (draft), Exposure criteria for medical diagnostic ultrasound Part 1: Criteria based on thermal mechanisms.

Nyborg W., 1953, Acoustic streaming due to attenuated plane waves, J Acoust Soc Am, 25, 68–75.

Nyborg W., 1958, Acoustic streaming near a boundary, J Acoust Soc Am, 30, 329–339.

Nyborg W., 1965, Acoustic streaming. In *Physical Acoustics*, Volume II, W.P. Mason (ed), Academic Press, New York.

Nyborg W., 1971, Interaction of ultrasound and biological tissues, Workshop procedings, DHEW (FDA)73–8008, Washington.

Nyborg W., 1981, Heat generation by ultrasound in a relaxing medium, J Acoust Soc Am, 70, 310–312.

Nyborg W., 1985, Optimisation of exposure conditions for medical ultrasound, Ultrasound Med Biol, 11, 245–260.

Nyborg W., 1988, Solutions of the bio–heat transfer equation, Phys Med Biol, 33, 785–792.

Nyborg W., 1989, NCRP/AIUM Models for temperature calculations, 2nd World Federation of Ultrasound in Medicine and Biology Symposium in Medical Ultrasound, G. Kossoff and W. Nyborg (eds), Ultrasound Med Biol, 15 Suppl 1, pp.37–40.

Ostrovskii L.A. and Papilova I.A., 1974, Nonlinear acoustic streaming, Sov Phys Acoust, 20, 45–49.

Parker K.J., 1983, Ultrsonic attenuation and absorption in liver tissues, Ultrasound Med Biol, 9, 363–369.

Parker K.J., Asztely M.S., Lerner R.M., Schenk E.A. and Waag R.C., 1988, *In vivo* measurements of ultrasound attenuation in normal or diseased liver, Ultrasound Med Biol, 14, 127–136.

Pauli H. and Schwan H.P., 1971, Mechanisms of absorption of ultrasound in liver tissue, J Acoust Soc Am, 50, 692–699.

Pennes H.H., 1948, Analysis of tissue and arterial blood temperatures in the resting human forearm, J Appl Pysiol, 1, 93–122.

Pickworth M.J.W., Dendy P.P., Leighton T.G., Worpe E. and Chivers R.C., 1989, Studies of cavitational effects of clinical ultrasound by somoluminescence: 3 Cavitation from pulses a few microseconds in length, Phys Med Biol, 34, 1139–1151.

Piercy J.E. and Lamb J., 1954, Acoustic streaming in liquids, Proc R Soc, A229, 43–50.

Pinamonti S., Gallenga P.E. and Mazzeo V., 1982, Effects of pulsed ultrasound on human erythrocytes *in vitro*, Ultrasound Med Biol, 8, 631–638.

Preston R.C., 1988, The ultrasound beam calibrator, IEEE Trans Ultrason Ferroelec Freq Contr, 35, 122–139.

Preston R.C., Bacon D.R., Livett A.J. and Ragendran K., 1983, Pvdf membrane hydrophone performance properties and their relevance to the measurement of the acoustic output of medical ultrasonic equipment, J Phys E: Sci Intrum, 16, 786–796.

Quraishi M.S. and Fahidy T.Z., 1982, A flow visualisation technique using analytical indicators: theory and some applications, Chem Eng Sci, 37, 775–780.

Repacholi M.H., Grandolfo M. and Rindi A, 1987, *Ultrasound Medical Applications, Biological Effects and Hazard Potential*, M.H. Repacholi, M. Grandolfo and A. Rindi (eds), Plenum Press, New York.

Rooney J.A., 1970, Hemolysis near an ultrasonically pulsating gas bubble, Science, 169, 869–871.

Rudenko O.V. and Soluyan S.I., 1971a, Theory of nonstationary streaming, Sov Phys Acoust, 17, 97–101.

Rudenko O.V. and Soluyan S.I., 1971b, Nonmonotonicity of the build–up of acoustic streaming, Sov Phys Acoust, 17, 228–232.

Saito S. and Kim B.C., Second harmonic component of a nonlinearly distorted wave in a focused field, 1987, J Acoust Soc Am, 82, 621–628.

Saunders L.J. and Lawrence P., 1972, Calibration of hot film anemometers. In *Fluid Dynamic Measurements in the Industrial and Medical Environments*, D.J. Cockrell (ed), Leicester University Press, Leicester, pp 125–130.

Semenova N.G., 1970, Build–up of acoustic streaming at various intensities of the sound field, Sov Phys Acoust, 15, 412–413.

Semenova N.G. and Statnikov Y.G., 1968, Build–up of acoustic streaming, Sov Phys Acoust, 14, 251–252.

Shooter J.A., Muir T.G. and Blackstock D.T., 1974, Acoustic saturation of

spherical waves in water, J Acoust Soc Am, 55, 54–62.

Shotton K.C., Bacon D.R. and Quilliam R.M., 1980, A pvdf membrane hydrophone for operation in the range 0.5 MHz to 15 MHz, Ultrasonics, 123–126.

Siegel E., Goddard J., James A.E. and Siegel E.P., 1979, Cellular attachment as a sensitive indicator of the effects of diagnostic ultrasound exposure on cultured human cells, Radiology, 133, 175–179.

Sikov M.R., Collins D.H. and Carr D.B., 1984, Measurement of temperature rise in prenatal rats during exposure of the exteriorised uterus to ultrasound, IEEE Trans Sonics Ultrason, SU–31, 497–503.

Smith D.W., Clarren J.K. and Harvey M.A.S., 1978, Hyperthermia as a possible teratogenic agent, J Paediatrics, 92, 878–883.

Stanikov Y.G., 1967, Streaming induced by finite amplitude sound, Sov Phys Acoust, 13, 122–124.

Starritt H.C., 1983, Nonlinear propagation of ultrasound pulses in medical diagnosis, MSc Thesis, University of London.

Starritt H.C. and Duck F.A., 1983, The dependance of measured beam parameters on power. In *Physics in Medical Ultrasound*, IPSM Report 47, 60–66.

Starritt H.C., Duck F.A and Hawkins A.J., 1986, The development of harmonic distortion in pulsed finite amplitude ultrasound passing through liver, Phys Med Biol, 31, 1401–1409.

Starritt H.C., Perkins M.A., F.A. Duck and Humphrey V.F., 1985, Evidence for ultrasound finite–amplitude distortion in muscle using medical equipment, J Acoust Soc Am, 77, 302–306.

Starritt H.C., Duck F.A. and Humphrey V.F., 1989, An experimental envestigation of streaming in pulsed diagnostic ultrasound beams, Ultrasound Med Biol, 15, 363–373.

Sutin A.M., 1978, Influence of nonlinear effects on the properties of acoustic focusing systems, Sov Phys Acoust 24, 334–339.

Swindell W., 1985, A theoretical study of nonlinear effects with focused ultrasound in tissue: an "acoustic Bragg peak", Ultrasound Med Biol, 11, 121–130.

Tjøtta S., 1959, On some nonlinear effects in sound fields with special emphasis on the generation of vorticity and the formation of streaming patterns, Archiv Math Naturvidensk, 55, 1–68.

Trivett D.H. and Van Buren A.L., 1981, Propagation of plane, cylindrical and spherical finite amplitude waves, J Acoust Soc Am, 69, 943–949.

Walmsley A.D., 1988, Applications of ultrasound in dentistry, Ultrasound in Med Biol, 14, 7–14.

Warkany J., 1986, Teratology update: hyperthermia, Teratology, 33, 365–371.

Wells P.N.T., 1977, *Biomedical Ultrasonics*, Academic Press, London.

Wells P.N.T., 1987, The Safety of Diagnostic Ultrasound, Br J Radiol, Suppl 20, P.N.T. Wells (ed).

Williams A.R., 1983, *Ultrasound: Biological Effects and Potential Hazards*, Academic Press, London.

Williams A.R. and Miller D.L., 1980, Photometric detection of ATP release from human erythrocytes exposed to ultrasonically activated gas filled pores, Ultrasound Med Biol, 6, 251–256.

Williams A.R. and Miller D.L., 1989, The role of nonacoustic factors in the induction and proliferation of cavitational activity *in vitro*, Phys Med Biol, 34, 1561–1569.

Wu J. and Du G., 1989, private communication.

Young F.R., 1989, *Cavitation*, McGraw–Hill, London.

Yount D.E., Gillary E.W. and Hoffmann D.C., 1984, A microscopic investigation of bubble formation nuclei, J Acoust Soc Am, 76, 1511–1521.

Zabolotskaya E.A. and Khokhlov R.V., 1969, Quasi–plane waves in the nonlinear acoustics of confined beams, Sov Phys Acoust, 15, 35–40.

Zana R. and Lang J., 1974, Interaction of ultrasound and amniotic liquid, Ultrasound Med Biol, 1, 253–258.

Ziskin M.C. and Petitti D.B., 1988, Epidemiology of human exposure to ultrasound: a critical review, Ultrasound Med Biol, 14, 91–96.

The help and support of the following people are gratefully acknowledged; Dr Victor Humphrey of Bath University, Dr Francis Duck and Professor Stephen Lillicrap of the Medical Physics Department of the Royal United Hospital in Bath, and my family. The following contributions are also acknowledged; Mike Perkins (Medical Physics Department) for the design, building and testing of the amplifiers and power balance, Dr Derek Tilley (University of Bath) for the loan of the anemometry system, Dr Valerie Shakespeare (Lang Laboratory, Odstock Hospital) for culturing and supplying the cells, Mike Tyszka and Stephen Anderson for software development and the Wellcome Foundation for their support.